



Nitrogen conversions in wastewater treatment:
from microbial interactions to process evaluations

Mingsheng Jia

2019

Nitrogen conversions in wastewater treatment: from microbial interactions to process evaluations

$$\mu = \mu_{max} \frac{S}{K_s + S}$$

Mingsheng Jia
贾明升

The important thing is not to stop questioning.

Albert Einstein

Promotors:

Prof. dr. ir. Eveline Volcke

Department of Green Chemistry and Technology, Faculty of Bioscience Engineering
Ghent University, Belgium

Prof. dr. ir. Mari Winkler

Department of Civil and Environmental Engineering,
University of Washington, USA

Examination committee:

Prof. dr. ir. Nico Boon

Chairman

Department of Biotechnology, Faculty of Bioscience Engineering
Ghent University, Belgium

Prof. dr. ir. Diederik Rousseau

Secretary

Department of Green Chemistry and Technology, Faculty of Bioscience Engineering
Ghent University, Belgium

Prof. dr. Dana Ofiteru

School of Engineering
Newcastle University, UK

Prof. dr. Mathieu Sperandio

Department of Chemical and Environmental Engineering
National Institute of Applied Sciences (INSA Toulouse), France

Dr. Michele Laurenzi

Department of Biotechnology
Delft University of Technology The Netherlands

Dr. Jose Maria Carvajal Arroyo

Department of Biotechnology, Faculty of Bioscience Engineering
Ghent University, Belgium

Dean: Prof. dr. ir. Marc Van Meirvenne

Rector: Prof. dr. ir. Rik Van de Walle

Mingsheng Jia

**Nitrogen conversions in wastewater treatment:
from microbial interactions to process evaluations**

Thesis submitted in fulfillment of the requirements for the degree of
Doctor (PhD) in Bioscience Engineering:
Environmental Science & Technology

Dutch translation of the title:

Stikstofomzettingen bij afvalwaterzuivering: van microbiële interacties tot procesevaluaties

Cover illustration:

Front: Anammox granules and Monod Kinetics. Back: St Michael's Bridge (Gent) and Me. Credit to Lingshan Ma.

Mingsheng Jia was supported by the China scholarship Council (CSC) and the Special Research Fund (BOF) in Ghent University.

Please refer to this work as follows:

Jia, M. (2019). Nitrogen conversions in wastewater treatment: from microbial interactions to process evaluations, PhD Thesis, Ghent University, Belgium.

ISBN: 978-94-6357-268-2

All rights reserved. No part of this document may be reproduced or transmitted in any form or by any means, electronic, mechanical, photocopying, scanning, recording, or otherwise, without prior written permission of the author and/or dissertation promoter(s). A written permission of the author is also required to use the methods, products, schematics and programs described in this work for industrial or commercial use, and for submitting any part of this dissertation in scientific contests. Every other use is subjected to the copyright laws.

Table of Contents

Notation index	V
Summary	VII
Samenvatting.....	XI
Chapter 1 General introduction.....	1
1.1 A brief history of biological nitrogen removal from wastewater	2
1.1.1 N1.0: Nitrification-based ammonium removal	2
1.1.2 N2.0: Heterotrophic denitrification-based nitrogen removal	4
1.1.3 N3.0: Autotrophic anammox-based nitrogen removal	9
1.1.4 Interactions between biological nitrogen and carbon removal.....	10
1.2 A few challenges and research objectives.....	11
1.2.1 N ₂ O emission from biological nitrogen removal (Chapter 2).....	11
1.2.2 Providing nitrite for the anammox reaction (Chapter 2-4).....	12
1.2.2.1 Aerobic ammonium oxidation to nitrite	12
1.2.2.2 Nitrate reduction to nitrite	14
1.2.3 Factors governing the competition between denitrification and DNRA (Chapter 3).....	17
1.2.4 Feasibility of the integrated HRAS-PNA system (Chapter 4)	17
1.3 Outline of the thesis	18
Chapter 2 Impact of organic matter on the performance and N₂O emission of a granular sludge anammox reactor.....	21
2.0 Abstract.....	22
2.1 Introduction	23
2.2 Materials and methods.....	25
2.2.1 Reactor setup and operation	25
2.2.2 Analytical procedures.....	27
2.2.3 Calculation of the anammox reaction stoichiometry	28

2.2.4 Mass balance for process rate estimation	29
2.3 Results and discussion.....	29
2.3.1 Reactor performance without and with influent organic carbon	29
2.3.2 Stoichiometry of the Anammox process	32
2.3.2.1 Application of general procedure – verification to literature reports	32
2.3.2.2 Anammox stoichiometry expressed in ASM format	34
2.3.3 Process identification and quantification using mass balances	37
2.3.4 Impact of influent organic matter on N ₂ O emission.....	41
2.4 Conclusions	43
Acknowledgements	44
Appendix	45
Chapter 3 Elucidating the competition between heterotrophic denitrification and DNRA using the resource-ratio theory	59
3.0 Abstract	60
3.1 Introduction.....	61
3.2 Materials and methods	63
3.2.1 Resource-ratio theory	63
3.2.2 Application of the theory for denitrification and DNRA	66
3.2.3 Experimental cases for theory verification	67
3.3 Results and discussion.....	68
3.3.1 Verification of the resource-ratio theory	68
3.3.2 Impact of resource concentration on competition outcomes.....	70
3.3.3 Impact of dilution rate on competition outcomes.....	74
3.3.4 Impact of kinetic and stoichiometric parameters on competition outcome....	76
3.3.5 Dynamic system behaviour.....	80
3.3.6 Model limitations and their implications	81
3.3.7 Potential application of the resource-ratio theory in other studies	83

3.4 Conclusions	84
Acknowledgments	85
Appendix	86
Chapter 4 Model-based evaluation of an integrated high-rate activated sludge and mainstream anammox system	101
4.0 Abstract	102
4.1 Introduction	103
4.2 Materials and methods	105
4.2.1 The integrated HRAS-PNA system	105
4.2.2 High-rate activated sludge (HRAS) stage model.....	106
4.2.3 Partial nitrification-anammox (PNA) model	107
4.2.4 Plant-wide comparison with conventional activated sludge (CAS) system..	108
4.2.5 Evaluation criteria for plant-wide comparison.....	108
4.2.6 Simulation strategies.....	108
4.3 Results and discussion	110
4.3.1 HRAS stage for COD redirection.....	110
4.3.1.1 Modelling the HRAS stage	110
4.3.1.2 Factors influencing COD redirection	112
4.3.2 The partial nitrification anammox (PNA) stage for nitrogen removal.....	115
4.3.2.1 Factors influencing nitrogen removal	115
4.3.2.2 Effect of biomass concentration	118
4.3.3 Plant-wide comparison of the HRAS-HRAS and CAS system	120
4.3.3.1 Steady-state COD and N mass balances	120
4.3.3.2 Dynamic performance – overall effluent quality and operational costs .	122
4.3.3.3 Dynamic performance- feasibility of PNA process under dynamic mainstream conditions.....	124
4.3.4 Model limitations and their implications.....	127
4.4 Conclusions	128

Acknowledgements	129
Appendix	130
Chapter 5 General conclusions and perspectives	151
5.1 Methodology	152
5.1.1 Stoichiometry matters	152
5.1.1.1 Mass balance and modelling of anammox process	152
5.1.1.2 Microbial competition for shared resources	153
5.1.2 Resource-ratio theory for interspecies competition studies	154
5.2 Fate of nitrate during biological nitrogen conversions	154
5.3 Process evaluation	157
5.3.1 N ₂ O emission from anammox reactors	157
5.3.2 Feasibility of mainstream anammox	158
5.3.2.1 Integrated HRAS-PNA system	158
5.3.2.2 Moving forward	160
Bibliography	162
Curriculum Vitae	175
Acknowledgement	179

Notation index

Abbreviation	Description
ANAMMOX	ANAerobic AMMonium OXidation
AOA	Ammonia-Oxidizing Archaea
AOB	Ammonia-Oxidizing Bacteria
ASM	Activated Sludge Model
BNR	Biological Nitrogen Removal
BOD	Biochemical Oxygen Demand
BSM2	Benchmarking Simulation Model no. 2
CAS	Conventional Activated Sludge
COD	Chemical Oxygen Demand
CSTR	Continuous Stirred Tank Reactor
DEN	Denitrifying bacteria
DNRA	Dissimilatory Nitrate Reduction to Ammonium
DO	Dissolved Oxygen
FISH	Fluorescence In Situ Hybridization
FNA	Free Nitrous Acid
GHG	Greenhouse Gas
HET	Heterotrophs
HRAS	High-Rate Activated Sludge
HRT	Hydraulic Retention Time
MLSS	Mixed Liquor Suspended Solid
NLR	Nitrogen Loading Rate
NOB	Nitrite-Oxidizing Bacteria
ODE	Ordinary Differential Equation
OLR	Organic Loading Rate
PDA	Partial Denitrification/DNRA-Anammox
PNA	Partial Nitritation-Anammox
SRT	Solids Retention Time
TN	Total Nitrogen
TSS	Total Suspended Solid
WWTP	Wastewater Treatment Plant
WRRF	Water Resource Recovery Facility

Notation index

Symbols	Characterization	Unit
b	Decay rate	d ⁻¹
COD/N	The ratio of COD to nitrogen	g COD.g N ⁻¹
D _{NH4}	Diffusion coefficient of NH ₄ ⁺	m ² .d ⁻¹
D _{NO2}	Diffusion coefficient of NO ₂ ⁻	m ² .d ⁻¹
D _{NO3}	Diffusion coefficient of NO ₃ ⁻	m ² .d ⁻¹
D _{O2}	Diffusion coefficient of O ₂	m ² .d ⁻¹
D _S	Diffusion coefficient of COD	m ² .d ⁻¹
E _a	Activation energy	kJ.(mol) ⁻¹
ε _{Xi}	Volume fraction of particulate component X _i	-
f _{XI}	Inert fraction in biomass	g COD.g COD ⁻¹
i _{NXB}	Nitrogen fraction in biomass	g N.g COD ⁻¹
i _{NXI}	Nitrogen fraction in particulate inert components	g N.g COD ⁻¹
J	Subsistence concentration of limiting resource	g .m ⁻³
K _{NH}	Affinity constant for total ammonium	g NH-N.m ⁻³
K _{NO2}	Affinity constant for nitrite	g NO ₂ -N.m ⁻³
K _{NO3}	Affinity constant for nitrate	g N.m ⁻³
K _{O2}	Affinity constant for oxygen	g O ₂ .m ⁻³
K _S	Affinity constant for COD	g COD.m ⁻³
L _F	Biofilm thickness	m
μ _{max}	Maximum growth rate	d ⁻¹
η	Anoxic reduction factor	-
n _p	Number of granules	-
Q _{in}	Inflow rate	m ³ .d ⁻¹
ρ	Process rate (Growth or Decay)	g COD.m ⁻³ .d ⁻¹
r	Pearson correlation coefficient	-
r _i	Conversion rate of component i	g.m ⁻³ .d ⁻¹
S _{N2}	N ₂ concentration	g N.m ⁻³
S _{NH}	Ammonium concentration	g N.m ⁻³
S _{NO2}	Nitrite concentration	g N.m ⁻³
S _{NO3}	Nitrate concentration	g N.m ⁻³
S _{O2}	Oxygen concentration (DO)	g O ₂ .m ⁻³
S _S	Soluble organic substrate concentration	g COD.m ⁻³
V	Volume	m ³
X _i	Particulate component i	g COD.m ⁻³
X _I	Inert particulate components	g COD.m ⁻³
X _S	Particulate biodegradable organic substrate	g COD.m ⁻³
Y	Yield coefficient	g COD.g N ⁻¹ or COD ⁻¹
z	Spatial coordinate in Aquasim	m

Summary

The global water demand is predicted to increase significantly over the coming decades, which also implies increased freshwater withdrawals (WWAP, 2017). An estimated 56% of the global freshwater withdrawals are released into the environment as wastewater, over 80% of which is released without adequate treatment (WWAP, 2017). Pollution from untreated wastewater has adverse effects on human health and the environment and reduces freshwater availability. In 2015, 29% of the global population still failed to safely manage drinking water supplies. Among the Sustainable Development Goals (SDGs) set by the United Nations, goal 6 concerns “*Ensure availability and sustainable management of water and sanitation for all*”. In this context, more sustainable wastewater treatment is needed.

Conventional municipal wastewater treatment plants (WWTPs) are typically designed to obtain a high degree removal of organic carbon (expressed as COD) and nitrogen, which are mainly eliminated by oxidation. This does not only require a large amount of aeration energy but also causes the loss of the energy present in COD (14 MJ.kg COD⁻¹) (Jetten et al., 1997). Conventional WWTPs, like activated sludge systems, consume about 0.6 kWh per m³ of wastewater treated, accounting for about 3% of electrical energy load in developed countries (McCarty et al., 2011). To shift from the current energy-inefficient WWTPs towards energy-neutral (even energy-positive) ones, maximization of energy recovery and minimization of energy consumption are necessary. The innovative autotrophic partial nitrification-anammox (PNA) process decouples biological nitrogen and carbon removal, allowing for potentially maximizing energy recovery from organic carbon contained in wastewater and substantial saving in aeration energy for nitrogen removal. A two-stage scheme based on PNA process has been proposed in the literature (Jetten et al., 1997; Kartal et al., 2010; Verstraete and Vlaeminck, 2011), featuring an high-rate activated sludge (HRAS) process in the first stage for COD direction to anaerobic digester for energy recovery and a mainstream PNA process in the second stage for nitrogen removal. This thesis focuses on microbial interactions in anammox-based biological nitrogen removal processes and assesses these systems experimentally (*via* lab-scale studies) and theoretically (*via* mathematical modelling and simulations).

Chapter 1 presents a brief history of biological nitrogen removal from wastewater, highlighting the main biological nitrogen transformations as well as the interactions between nitrogen and carbon removal processes. An overview of anammox-based processes is given as well, comprising different pathways to provide nitrite for the anammox conversion. Moreover, a few challenges in innovative biological nitrogen removal processes are detailed, highlighting the research gaps and objectives of this thesis.

The carbon footprint, i.e., greenhouse gas emission, is an important sustainability aspect of wastewater treatment. One unignorable concern for biological nitrogen removal is the emission of nitrous dioxide (N_2O). With 297 times stronger global warming potential than CO_2 (IPCC, 2014), even small amounts of N_2O emission can contribute significantly to the carbon footprint of WWTPs. Moreover, both N_2O and its precursor nitric oxide (NO) are substances involved in the ozone depletion (Ravishankara et al., 2009). **Chapter 2** is dedicated to the impact of influent organic matter on the reactor performance and N_2O emission of a standalone granular sludge anammox reactor, mimicking the scenario where two-stage PNA process is applied for sidestream nitrogen removal. A continuously fed bubble column granular sludge anammox reactor was operated for 405 days. Results show that low influent COD could slightly improve the nitrogen removal of the anammox reactor (ca. influent COD/TN ratios = $0.1 \text{ g COD.g N}^{-1}$), at the cost of a concurrent significant increase in N_2O emission. The average N_2O emission increased by 2.5 times ($p < 0.05$) with increasing influent COD concentration, accounting for up to 0.46% of the incoming nitrogen load. In addition, the substantial differences in anammox stoichiometry reported in the literature were highlighted. A generalized method was thus applied to derive the anammox stoichiometry from experimental data for improved mass balance and demonstrated to ease the application for other experimental studies. Moreover, it was found that the experimentally measured anammox biomass yield in the overall metabolic reaction has been mistakenly used as the catabolic yield in many modelling studies. Solutions were proposed to address this and similar modelling issue.

Denitrification and dissimilatory nitrate reduction to ammonium (DNRA) are two microbial processes competing for nitrate and organic carbon (COD). Their competition has great implications for the fate of nitrogen and greenhouse gas (i.e., N_2O) emissions. Moreover, partial denitrification and/or partial DNRA (nitrate to nitrite) can

service for nitrite supply for anammox as an alternative to nitrification (ammonium to nitrite). **Chapter 3** elucidates the competition between denitrification and DNRA for nitrate and organic carbon in continuous cultures using the resource-ratio theory. This theory describes the interactions between competing species based on the use of shared resources and enables to mechanistically predict the outcomes of multispecies competition. Firstly, the resource-ratio theory was proven valid with experimental data from the literature on the competition outcome of heterotrophic denitrification and DNRA. Based on this theory, the impact of resource concentrations, COD/N ratio, dilution rate and microbial physiological features on the competition outcome was highlighted. In particular, the collective impact of these factors on competition outcomes was revealed. The results show that the influent COD/N ratio was determinative but not sufficient for prediction, as the competition outcome could change significantly with influent resource (i.e., nitrate and/or COD) concentrations. The boundary influent COD/N ratios for different competition outcomes at high influent resource concentrations were mainly determined by the stoichiometry (i.e., consumption of COD per nitrate) of the two competing processes, whereas kinetic parameters (namely, affinity for the resources (K_S) and maximum specific growth rate (μ_{max})) and dilution rate became important as well at low influent resource concentrations (e.g., $<100 \mu\text{M}$). The impact of resource concentrations on the competition outcomes has great implications, as different ecosystems have various nitrate availability and therefore possibly different boundary COD/N ratios for nitrate partitioning. The nitrate concentration in natural aquatic and terrestrial ecosystems are usually low ($<100 \mu\text{M}$) at which the boundaries of different competition outcomes changed dramatically. Nonetheless, lab-scale competition studies often supply high concentration of nitrate at which the boundaries were rather stable and mainly defined by the stoichiometries of denitrifiers and DNRA bacteria. Noteworthy, the implications of the results are not limited to denitrification and DNRA but may hold for other cases where multispecies exploitatively compete for two potentially limiting resources. Overall, the results shed light on the understanding and management of the fate of nitrate in both natural and engineered (e.g., WWTPs) ecosystems and provide testable hypotheses and tools for further research.

The promising HRAS-PNA system was evaluated in **Chapter 4**, through modelling and simulations under both steady-state and dynamic conditions. The impact of operating

conditions on the unit processes was investigated first, followed by a plant-wide assessment of the combined HRAS-PNA system. Simulation results showed that the operation of an HRAS stage often implies a trade-off between maximizing the COD capture in the sludge for energy recovery and minimizing the effluent COD for the subsequent PNA process. For this purpose, moderate DO concentrations (0.3-0.5 g O₂.m⁻³) and SRT values (0.3-0.5 d) were recommended. For granular sludge PNA reactors, a higher biomass concentration would allow a lower DO set point for maximum nitrogen removal. The anammox process remained the dominant process for nitrogen removal throughout the one-year evaluation period with varying influent COD/N (1.3-4.3) and temperature (10-20 °C), indicating the resilience of the PNA system at mainstream conditions. However, both COD removal (in HRAS) and N removal (in PNA) decreased at low temperatures and dynamic conditions. Overall, steady-state and dynamic simulations showed that the integrated HRAS-PNA system could achieve an effluent quality that complies with EU regulations with a significantly lower operational cost, compared to the conventional activated sludge system.

Chapter 5 summarizes the main conclusions from this thesis and gives perspectives for future research. In conclusion, it can be summarized that stoichiometry sets the basis for mass balance, modelling and process design, and plays an important role in microbial competitions for shared resources (i.e., denitrification and DNRA for nitrate and COD). Caution is needed when choosing anammox stoichiometry and further research is required to determine the stoichiometry of DNRA. The resource-ratio theory applied in this study can be more broadly applied to multispecies competition studies. Concerning the integrated HRAS-PNA system, future research should target the understanding of bioflocculation process and thereby the development of control strategies of the effluent COD/N of the HRAS stage. The further integration of engineering, microbiological and modelling insights is needed for the implementation of mainstream anammox. Alternative anammox-based processes (e.g., partial DNRA-anammox) and anammox-assisted systems (i.e., where anammox contributes significantly but not necessarily dominant in nitrogen removal of the mainstream) should be further explored.

Samenvatting

Er wordt in de komende decennia wereldwijd een aanzienlijke toename voorspeld in de vraag naar water (en dus de onttrekking van zoet water) (WWAP, 2017). Naar schatting komt 56% van de wereldwijde zoetwateronttrekkingen als afvalwater in het milieu terecht, waarvan meer dan 80% zonder adequate behandeling (WWAP, 2017). Vervuiling door onbehandeld afvalwater heeft negatieve effecten op de menselijke gezondheid en het milieu en vermindert de beschikbaarheid van zoet water. In 2015 slaagde 29% van de wereldbevolking er nog steeds niet in om drinkwatervoorraden veilig te beheren. Onder de Duurzame Ontwikkelingsdoelen (SDG's) van de Verenigde Naties, heeft doel 6 betrekking op "*Zorg voor beschikbaarheid en duurzaam beheer van water en sanitaire voorzieningen voor iedereen*". In deze context is een duurzamere afvalwaterzuivering nodig.

Gewoonlijk zijn gemeentelijke rioolwaterwaterzuiveringsinstallaties (RWZI's) ontworpen om een hoge mate van verwijdering van organische koolstof (uitgedrukt als CZV) en stikstof te verkrijgen, die hoofdzakelijk worden geëlimineerd door oxidatie. Dit vereist niet alleen een grote hoeveelheid beluchtingsenergie, maar veroorzaakt ook het verlies van de aanwezige energie in CZV ($14 \text{ MJ.kg COD}^{-1}$) (Jetten et al., 1997). Conventionele RWZI's, zoals actiefslibsystemen, vertegenwoordigen ongeveer 3% van de elektrische energievraag in ontwikkelde landen (ca. $0,6 \text{ kWh.m}^{-3}$ gezuiverd afvalwater) (McCarty et al., 2011). Om van de huidige energie inefficiënte RWZI's naar energieneutrale (of zelfs energiepositieve) RWZI's te gaan, is een maximalisatie van energierterugwinning en minimalisatie van energieverbruik nodig. Het innovatieve autotrofe partiële nitritatie-anammox (PNA) proces ontkoppelt biologische stikstof- en koolstofverwijdering, waardoor meer energierterugwinning uit organische koolstof in afvalwater en substantiële besparingen in beluchtingsenergie voor stikstofverwijdering mogelijk worden. In de literatuur (Jetten et al., 1997; Kartal et al., 2010; Verstraete and Vlaeminck, 2011) wordt een tweetrapschema op basis van het PNA-proces voorgesteld, met een hoge snelheid actief slibproces (HRAS) in de eerste fase om CZV naar een anaërobe vergister te sturen voor energierterugwinning en een mainstream PNA-proces in de tweede fase voor stikstofverwijdering. Dit proefschrift richt zich op microbiële interacties in op anammox gebaseerde biologische stikstofverwijderingsprocessen en beoordeelt deze systemen experimenteel (*via* laboratoriumschaalstudies) en theoretisch (*via* wiskundige modellen en simulaties).

In hoofdstuk 1 wordt een korte geschiedenis van biologische stikstofverwijdering uit afvalwater beschreven, met aandacht voor de belangrijkste biologische stikstofomzettingen en de interacties tussen stikstof- en koolstofverwijderingsprocessen. Een overzicht van op anammox gebaseerde processen wordt ook gegeven, met verschillende paden om nitriet te leveren voor de anammox-conversie. Bovendien worden enkele uitdagingen in innovatieve biologische verwijderingsprocessen uitgelegd, waar dit proefschrift een (gedeeltelijk) antwoord op wil bieden.

De koolstofvoetafdruk, d.w.z. broeikasgasemissie, is een belangrijk duurzaamheidsaspect in afvalwaterzuivering. Een belangrijke zorg voor biologische stikstofverwijdering is de uitstoot van stikstofoxide (N_2O). Met een 297 keer sterker broeikas effect dan CO_2 (IPCC, 2014), kunnen zelfs kleine hoeveelheden N_2O -uitstoot aanzienlijk bijdragen aan de koolstofvoetafdruk van RWZI's. Bovendien zijn zowel N_2O als zijn voorloper stikstofmonoxide (NO) stoffen die betrokken zijn bij de aantasting van de ozonlaag (Ravishankara et al., 2009). Hoofdstuk 2 is gewijd aan de impact van instromende organische stof op de reactorperformantie en de N_2O -emissies van een alleenstaande anammox-reactor met korrelslib, en bootst het scenario na waarin het tweetraps-PNA-proces wordt toegepast voor de verwijdering van stikstof via een zijstroom. Een continu gevoede bellenkolom met korrelslib werd 405 dagen bedreven als anammox-reactor. De resultaten tonen aan dat een lage instromende CZV-concentratie de stikstofverwijdering van de anammox-reactor enigszins zou kunnen verbeteren (instromende CZV/TN-verhoudingen van circa $0.1 \text{ g CZV.g N}^{-1}$), ten koste van een gelijktijdige significante toename van de N_2O -emissies. De gemiddelde N_2O -emissie steeg 2.5 keer ($p < 0.05$) met een toenemende instromende CZV-concentratie, goed voor maximaal 0.46% van de instromende stikstofbelasting. Bovendien werden de wezenlijke verschillen in anammox-stoichiometrie, gerapporteerd in de literatuur, benadrukt. Een algemene methode werd aldus toegepast om de anammox-stoichiometrie af te leiden uit experimentele gegevens voor een verbeterde massabalans en deze methode bleek ook toepasbaar voor andere experimentele studies. Bovendien werd ontdekt dat de experimenteel gemeten opbrengstcoëfficiënt van de anammox biomassa in de totale metabole reactie ten onrechte werd gebruikt voor de katabole opbrengst in veel modelleringsstudies. Er werden oplossingen voorgesteld voor dit probleem.

Denitrificatie en dissimilerende nitraatreductie tot ammonium (DNRA) zijn twee microbiële processen die concurreren om nitraat en organische koolstof (CZV). Hun concurrentie heeft grote implicaties voor het lot van stikstof en broeikasgasemissies (d.w.z. N_2O). Bovendien kan gedeeltelijke denitrificatie en/of gedeeltelijke DNRA (nitraat tot nitriet) worden gezien als een alternatief voor nitrificatie (ammonium tot nitriet) om nitriet te produceren voor de anammox-reactie. Hoofdstuk 3 verduidelijkt de concurrentie tussen denitrificatie en DNRA voor nitraat en organische koolstof in continue culturen met behulp van de resource-ratio-theorie. Deze theorie beschrijft de interacties tussen concurrerende soorten op basis van hun gebruik van gedeelde hulpbronnen en laat toe om een mechanistische voorspelling te doen over de uitkomsten van multispecies-concurrentie. Eerst werd de resource-ratio-theorie geldig bevonden op basis van experimentele gegevens uit de literatuur over de concurrentieresultaten van heterotrofe denitrificatie en DNRA. Op basis van deze theorie werd de impact benadrukt van substraatconcentraties, de CZV/N-verhouding, de verdunningssnelheid en de microbiële fysiologische kenmerken op de concurrentieresultaten. In het bijzonder werd de collectieve impact van deze factoren op de concurrentieresultaten onthuld. De resultaten laten zien dat de CZV/N-verhouding bepalend was, maar niet voldoende voor voorspelling, omdat de concurrentieresultaten aanzienlijk afhingen van de absolute concentraties van de substraten (nitraat en/of CZV). De grensverhoudingen CZV/N voor verschillende concurrentieresultaten bij hoge concentraties van substraten werden hoofdzakelijk bepaald door de stoichiometrie (m.a.w. de hoeveelheid verbruik van CZV per hoeveelheid nitraat) van de twee concurrerende processen, terwijl kinetische parameters (namelijk affiniteit voor de substraten (K_s) en maximale specifieke groeisnelheid (μ_{max})) en verdunningssnelheid eveneens van belang waren bij lage concentraties van substraten (bijv. $<100 \mu M$). Het effect van substraatconcentraties op de concurrentieresultaten heeft grote implicaties, omdat verschillende ecosystemen een verschillend nitraataanbod hebben en daarom mogelijk verschillend reageren op de CZV/N-ratios. De nitraatconcentratie in natuurlijke aquatische en terrestrische ecosystemen is meestal laag ($<100 \mu M$), waardoor de grenzen van verschillende concurrentie-uitkomsten drastisch veranderden. Concurrentieonderzoeken op laboschaal leveren echter vaak een hoge nitraatconcentratie, waardoor de grenzen vrij stabiel waren en voornamelijk werden bepaald door de stoichiometrieën van denitrificerende en DNRA-bacteriën. Merk op dat de implicaties van de resultaten niet

beperkt zijn tot het specifieke geval dat werd onderzocht, maar ook kan gelden voor andere gevallen waarin meerdere soorten concurreren om twee potentieel gelimiteerde, essentiële substraten. Over het algemeen geven de resultaten inzicht in het begrip en het beheer van het lot van nitraat in zowel natuurlijke als artificiële ecosystemen (bijv. RWZI's) en bieden ze testbare hypothesen en hulpmiddelen voor verder onderzoek.

Het veelbelovende HRAS-PNA-systeem werd geëvalueerd in hoofdstuk 4, door middel van modellering en simulaties onder zowel steady-state als dynamische omstandigheden. De impact van procesomstandigheden werd eerst apart onderzocht voor de verschillende eenheidsprocessen en daarna werd het gecombineerde HRAS-PNA-systeem geëvalueerd. Simulatieresultaten toonden aan dat de werking van een HRAS-fase vaak een afweging inhoudt tussen het maximaliseren van CZV in het slib voor energierugwinning en het minimaliseren van uitstromende CZV voor het daaropvolgende PNA-proces. Gematigde zuurstofconcentraties ($0.3-0.5 \text{ g O}_2\cdot\text{m}^{-3}$) en slibverblijftijden ($0.3-0.5 \text{ d}$) werden daarom aanbevolen. Voor korrelslib PNA-reactoren zou een hogere biomassaconcentratie een lagere zuurstofconcentratie voor maximale stikstofverwijdering mogelijk maken. Het anammox-proces bleef het dominante proces voor stikstofverwijdering gedurende de evaluatieperiode van één jaar met een variërende instromende CZV/N ($1.3-4.3$) verhouding en temperatuur ($10-20 \text{ }^\circ\text{C}$), hetgeen de veerkracht van het PNA-systeem onder reguliere omstandigheden aangeeft. Zowel CZV-verwijdering (in HRAS) als N-verwijdering (in PNA) verminderde echter bij lage temperaturen en dynamische omstandigheden. Globaal toonden steady-state en dynamische simulaties aan dat het geïntegreerde HRAS-PNA-systeem een effluentkwaliteit kon bereiken die voldoet aan EU-regelgeving met aanzienlijk lagere operationele kosten in vergelijking met het conventionele actiefslibstelsel.

Hoofdstuk 5 vat de belangrijkste conclusies van dit proefschrift samen en beschrijft mogelijkheden voor toekomstig onderzoek. Er kan worden geconcludeerd dat stoichiometrie de basis vormt voor massabalansen, modellering, procesontwerp en een belangrijke rol speelt in microbiële competitie voor gedeelde hulpbronnen (d.w.z. denitrificatie en DNRA voor nitraat en CZV). Voorzichtigheid is geboden bij het kiezen van anammox-stoichiometrie en verder onderzoek is vereist om de stoichiometrie van

DNRA te bepalen. De resource-ratio-theorie die in deze studie werd toegepast, kan breder worden toegepast voor gelijkaardige multispecies-concurrentieonderzoek. Wat het geïntegreerde HRAS-PNA-systeem betreft, zou toekomstig onderzoek gericht moeten zijn op het verkrijgen van meer inzicht in het bioflocculatieproces om op die manier de uitstromende CZV/N verhouding van de HRAS-fase te kunnen sturen. De verdere integratie van technische, microbiologische en modelleringsinzichten is nodig voor de implementatie van mainstream anammox. Alternatieve op anammox gebaseerde processen (bijv. gedeeltelijke DNRA-anammox) en door anammox ondersteunde systemen (d.w.z. waar anammox een significante maar niet noodzakelijk dominante bijdrage levert aan stikstofverwijdering van de hoofdstroom) moeten verder worden onderzocht.

Chapter 1

General introduction

In this introductory chapter, a brief history of biological nitrogen removal from wastewater is presented. Subsequently, a few challenges in innovative biological removal processes are detailed, highlighting the research gaps and objectives of this thesis. An outline of the chapters of this thesis is also provided.

1.1 A brief history of biological nitrogen removal from wastewater

The global water demand is predicted to increase significantly over the coming decades, which also implies increased freshwater withdrawals. An estimated 56% (ca. 2.2×10^{12} m³) of the global freshwater withdrawals are released into the environment as wastewater, over 80% of which is released without adequate treatment (WWAP, 2017). Pollution from untreated wastewater has adverse effects on human health and the environment and reduces freshwater availability. In 2015, 29% of the global population still lacked safely managed drinking water supplies. Among the United Nations Sustainable Development Goals (SDGs), goal 6 concerns “*Ensure availability and sustainable management of water and sanitation for all*”. In this context, more sustainable wastewater treatment is needed. The major focus of this thesis is on biological nitrogen removal from wastewater. A brief history of biological nitrogen removal from wastewater is given here, highlighting the main biological nitrogen transformations (Fig. 1.1) as well as the interactions between nitrogen and carbon removal processes.

The history of biological nitrogen removal is driven by a continuous increase in sustainability demand. The most important driving force is the need of wastewater treatment, which changes over time and is constrained by economic, social, environmental and technological factors. From a simplified view, the need of nitrogen management in wastewater treatment initially comprised ammonium removal only and later evolved to nitrogen removal and then more sustainable nitrogen removal. Accordingly, the development of biological nitrogen removal was divided into three generations in this thesis (Fig. 1.2), namely N1.0 (Section 1.1.1), N2.0 (Section 1.1.2) and N3.0 (Section 1.1.3). Constraints such as stringent regulations, cost, and space drive technological development.

1.1.1 N1.0: Nitrification-based ammonium removal

The most widely used process for wastewater treatment is the activated sludge (AS) process, which was first presented in 1914 by Arden & Lockett (1914). In addition to the sanitary purpose, part of the driving force for wastewater treatment at that time was making the effluent safe for agricultural use of its fertilizer value especially that of nitrogen, which was short in supply (Barnard and Stensel, 2014). Therefore, wastewater treatment plants (WWTPs) were designed for the removal of organic

carbon (expressed as chemical oxygen demand (COD) or biodegradable oxygen demand (BOD)), while nitrogen was kept for irrigation to increase crop yields. Nevertheless, full nitrification was suggested as an indicator of stable operation of the treatment process (Ardern and Lockett, 1914; Gujer, 2010). Later it was realized that ammonium can cause oxygen depletion in the receiving waters and its oxidation byproduct nitrite is highly toxic to aquatic life. Therefore, nitrification became mandatory in many facilities. This can be defined as the first-generation biological nitrogen treatment (N1.0, Fig. 1.2)

The nitrogen present in municipal wastewater is mainly in the form of ammonium and organic nitrogen (Henze et al., 2008) that can be ammonified by microorganisms to ammonium, which can then undergo the transformations in nitrogen cycle (Fig. 1.1). Nitrification is a two-step process, during which ammonium is first oxidized to nitrite and further oxidized to nitrate (Eq.1a and Eq.1b, Table 1.1). The two steps were long believed to be carried out by distinct groups of bacteria, namely ammonium-oxidizing bacteria (AOB) and nitrite-oxidizing bacteria (NOB) (Daims and Wagner, 2010). Certain archaea were then found also capable of ammonium oxidation to nitrite, namely ammonium-oxidizing archaea (AOA) (Könneke et al., 2005). Recently it was discovered that certain *Nitrospira* species can even carry out complete ammonia oxidation (i.e., both steps 1a and 1b, Comammox), confirming earlier theoretical predictions (Costa et al., 2006; Daims et al., 2015; Van Kessel et al., 2015).

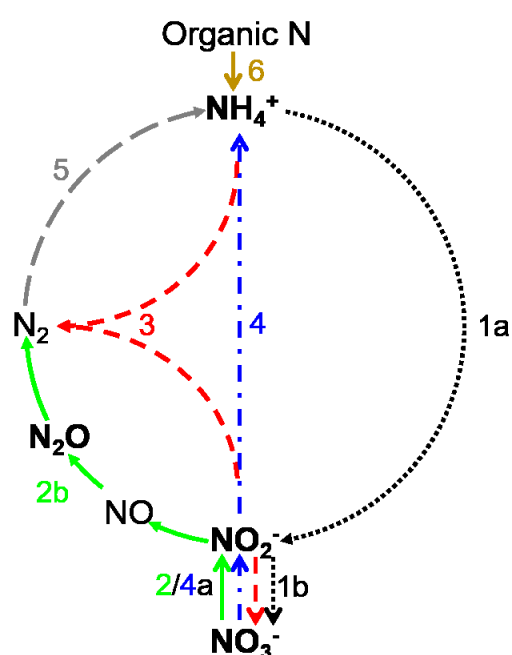


Figure 1.1. Simplified biological nitrogen cycle. Nitrification (1a nitritation + 1b nitratation), denitrification (2a denitratation + 2b denitritation), anaerobic ammonium oxidation (anammox, 3), dissimilatory nitrate reduction to ammonium (DNRA, 4), nitrogen fixation (5), and ammonification (6).

Nitrification is the single most important process in our development of today's theoretical understanding of biological wastewater treatment processes (Gujer, 2010). For several decades, empirical approaches (e.g., hydraulic residence time (HRT), food to microorganism ratio (F/M) and volumetric loading) were used for the design and sizing of bioreactors for wastewater treatment. The introduction of the chemostat in 1950 by Monod (1950) and Novick and Szilard (1950) set the basis for the understanding and mathematical modeling of continuous microbial culture systems. In 1960s, Downing et al. (1964) firstly developed a comprehensive theoretical concept for the design of nitrifying activated sludge plants based on kinetic concepts and reactor technology (Fig. 1.2). Since the mid-1980s, the Activated Sludge Models (ASM1, 2, 2D, and 3) have been widely accepted as reference tools for design and control strategies in activated sludge processes, facilitating the understanding and development of these processes (Henze et al., 2000).

1.1.2 N2.0: Heterotrophic denitrification-based nitrogen removal

Since the 1960s, eutrophication emerged as a new problem in surface water into which wastewater and agricultural run-off were discharged whereas in specific the phosphate and nitrogen from wastewater were most concerning (Henze et al., 2008). In addition, the proliferation of the Haber-Bosch process invented in 1913 also made the reservation of nitrogen in wastewater for agricultural use less relevant. Therefore, nitrogen removal to dinitrogen gas instead of ammonium removal (conversion to nitrate) only became a pressing need to maintain aquatic systems pristine. A combination of nitrification and denitrification (Eq. A, Table 1.1) was therefore used for this purpose, entering the era of the second-generation biological nitrogen removal (N2.0, Fig. 1.2).

Denitrification is a four-step process, during which nitrate is sequentially reduced to nitrite, nitric oxide (NO), nitrous oxide (N₂O), and eventually to N₂ (Fig. 1.1) (Zumft, 1997). In the conventional nitrification-denitrification process, ammonium is first oxidized to nitrate and subsequently reduced to dinitrogen gas (N₂). In WWTPs denitrification is usually carried out by heterotrophs, and thus organic carbon is required to provide an electron donor (Daims and Wagner, 2010). From an operational cost point of view, denitrification can recover about half the alkalinity consumed during nitrification (Eq. 1 and Eq. 2, Table 1.1) and reduce the oxygen demand for aerobic

COD removal (Henze et al., 2008). In case the wastewater does not contain sufficient organic carbon for denitrification (low COD/N ratios), external carbon (e.g., methanol and acetate) needs to be added to accomplish full denitrification. In order to eliminate or at least reduce this additional cost, processes have been designed to maximize the use of the organics present in influent wastewater. Examples are the Modified Ludzack- Ettinger (MLE) process and the four-stage Bardenpho process (Barnard, 1973). The scheme of a typical WWTP as such is presented in Fig. 1.3A. In these systems, nitrification and denitrification are achieved in separate reactors (zones). Recently, there have been significant efforts to stimulate simultaneous nitrification and denitrification (SND) in the same reactor. In this way, it is possible to reduce the required reactor volume and at the same time reduce operating costs by using the carbon generated from cell lysis to drive some of the denitrification (Henze et al., 2008; Münch et al., 1996).

Further cost savings could be realized by stimulating shortcut nitrification-denitrification, in which only the first step of nitrification is promoted and denitrification occurs on the produced nitrite (instead of nitrate). This process is also referred to as nitritation-denitritation. Nitrite is an intermediate of both nitrification and denitrification process (Fig. 1.1). By omitting the transformations between nitrite and nitrate, about 25% reduction in oxygen demand (and thus aeration energy) and 40% reduction in organic carbon can be achieved, compared to the nitrification-denitrification process (Table 1.1). Several processes have been put forward to realize nitrite production while suppressing nitrate formation, e.g., the SHARON process (Hellings et al., 1998). They have proven successful in the treatment of ammonium-rich wastewater at relatively high temperatures. However, the implementation of nitritation-denitritation for mainstream wastewater treatment is an ongoing challenge (Regmi et al., 2014), mainly due to the difficulties in mainstream nitritation at lower temperatures (detailed in Section 1.2.2).

Overall, it is clear that the driving force for the development of nitrogen removal processes has gradually shifted from purely pollution control (i.e., N removal) to also minimizing costs (e.g., aeration, external carbon addition, footprint).

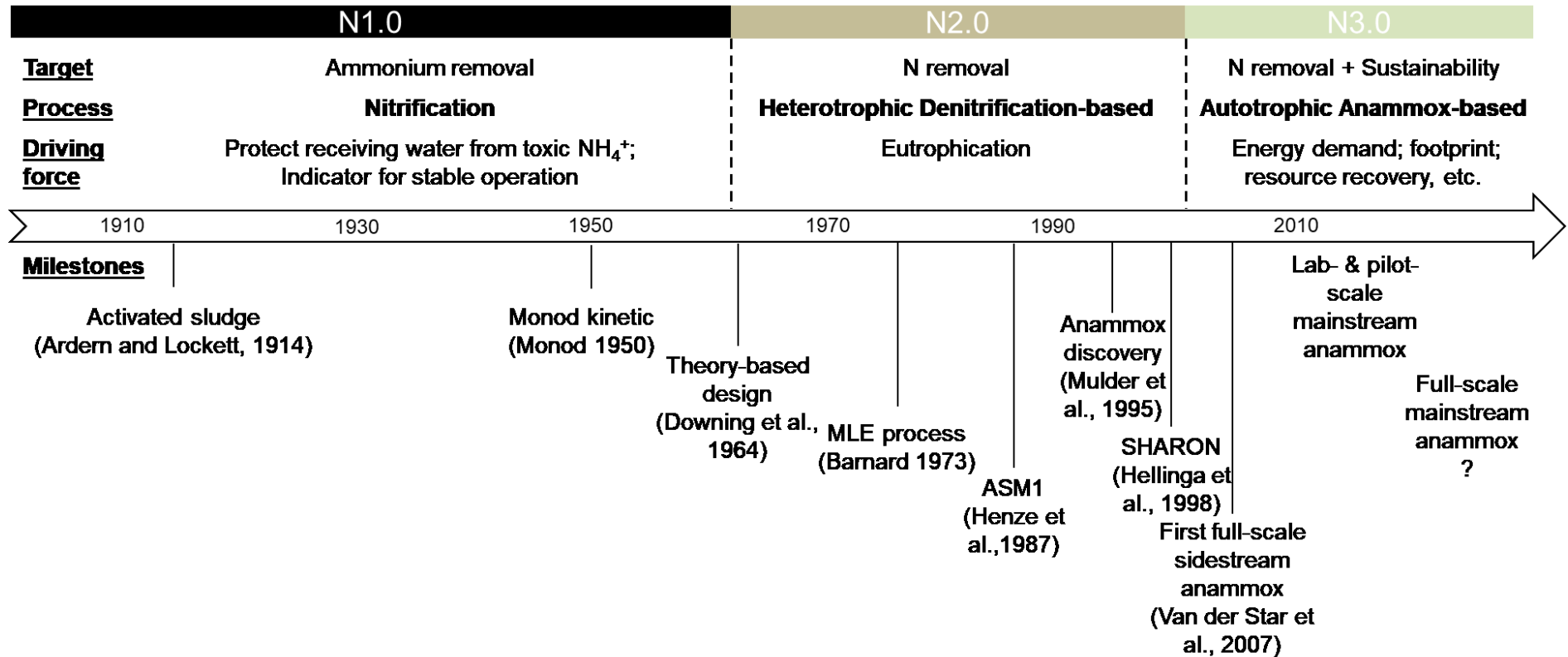


Figure 1.2. A brief history of biological nitrogen removal from wastewater. Abbreviations and references used here are explained in the main text.

Table 1.1. Stoichiometry of biological nitrogen conversion reactions (1 to 4) and resulting nitrogen removal processes (shaded in grey) in wastewater treatment. Only catabolic reactions are considered. The theoretical oxygen demand (O/N, g O₂ g N⁻¹) and organic carbon demand (COD/N, g COD g N⁻¹) per nitrogen converted are given as well.

Biological process	Equation number	Reaction	O/N (g O ₂ .g N ⁻¹)	COD/N (g COD.g N ⁻¹)
Nitrification	1a	$\text{NH}_4^+ + 3/2 \text{O}_2 \rightarrow \text{NO}_2^- + \text{H}_2\text{O} + 2 \text{H}^+$	3.43	0
Nitrification	1b	$\text{NO}_2^- + 1/2 \text{O}_2 \rightarrow \text{NO}_3^-$	1.14	0
Nitrification	1=1a+1b	$\text{NH}_4^+ + 2 \text{O}_2 \rightarrow \text{NO}_3^- + \text{H}_2\text{O} + 2 \text{H}^+$	4.57	0
Partial denitrification/ DNRA (PD)	2a/4a	$\text{NO}_3^- + 1/4 \text{CH}_3\text{COO}^- \rightarrow \text{NO}_2^- + 1/4 \text{CO}_2 + 1/4 \text{HCO}_3^- + 1/4 \text{H}_2\text{O}$	0	1.14
Denitrification	2b	$\text{NO}_2^- + 3/8 \text{CH}_3\text{COO}^- + \text{H}^+ \rightarrow 1/2 \text{N}_2 + 3/8 \text{CO}_2 + 3/8 \text{HCO}_3^- + 7/8 \text{H}_2\text{O}$	0	1.71
Denitrification	2=2a+2b	$\text{NO}_3^- + 5/8 \text{CH}_3\text{COO}^- + \text{H}^+ \rightarrow 1/2 \text{N}_2 + 5/8 \text{CO}_2 + 5/8 \text{HCO}_3^- + 9/8 \text{H}_2\text{O}$	0	2.86
Anammox	3	$1/2 \text{NH}_4^+ + 1/2 \text{NO}_2^- \rightarrow 1/2 \text{N}_2 + \text{H}_2\text{O}$	0	0
DNRA	4	$\text{NO}_3^- + \text{CH}_3\text{COO}^- + 2\text{H}^+ \rightarrow \text{NH}_4^+ + \text{CO}_2 + \text{HCO}_3^-$	0	4.57
Nitrification- Denitrification	A=1a+1b+2a+2b	$\text{NH}_4^+ + 2 \text{O}_2 + 5/8 \text{CH}_3\text{COO}^- \rightarrow 1/2 \text{N}_2 + 5/8 \text{CO}_2 + 5/8 \text{HCO}_3^- + 17/8 \text{H}_2\text{O} + \text{H}^+$	4.57	2.86
Nitrification- Denitrification	B=1a+2b	$\text{NH}_4^+ + 3/2 \text{O}_2 + 3/8 \text{CH}_3\text{COO}^- \rightarrow 1/2 \text{N}_2 + 3/8 \text{CO}_2 + 3/8 \text{HCO}_3^- + 15/8 \text{H}_2\text{O} + \text{H}^+$	3.43 (-25%)	1.71 (-40%)
PNA	C=1a+3	$\text{NH}_4^+ + 3/4 \text{O}_2 \rightarrow 1/2 \text{N}_2 + 3/2 \text{H}_2\text{O} + \text{H}^+$	1.71 (-62%)	0 (-100%)
PNPDA*	D=1a+1b+2a/4a+3	$\text{NH}_4^+ + \text{O}_2 + 1/8 \text{CH}_3\text{COO}^- \rightarrow 1/2 \text{N}_2 + 1/8 \text{CO}_2 + 1/8 \text{HCO}_3^- + 13/8 \text{H}_2\text{O} + \text{H}^+$	2.29 (-50%)	0.57(-80%)
PDA**	E=2a/4a+3	$1/2 \text{NH}_4^+ + 1/2 \text{NO}_3^- + 1/8 \text{CH}_3\text{COO}^- \rightarrow 1/2 \text{N}_2 + 1/8 \text{CO}_2 + 1/8 \text{HCO}_3^- + 9/8 \text{H}_2\text{O}$	0 (-100%)	0.57 (-80%)

Values between parentheses represent the reduction in relative to the conventional nitrification-denitrification process;

* Partial Nitrification Partial Denitrification/DNRA Anamnox when all NO₃⁻ comes from the nitrification of half the NH₄⁺ in the influent (i.e., partial nitrification);

** Partial Denitrification/DNRA Anamnox when NO₃⁻ equally presents as NH₄⁺ in the influent

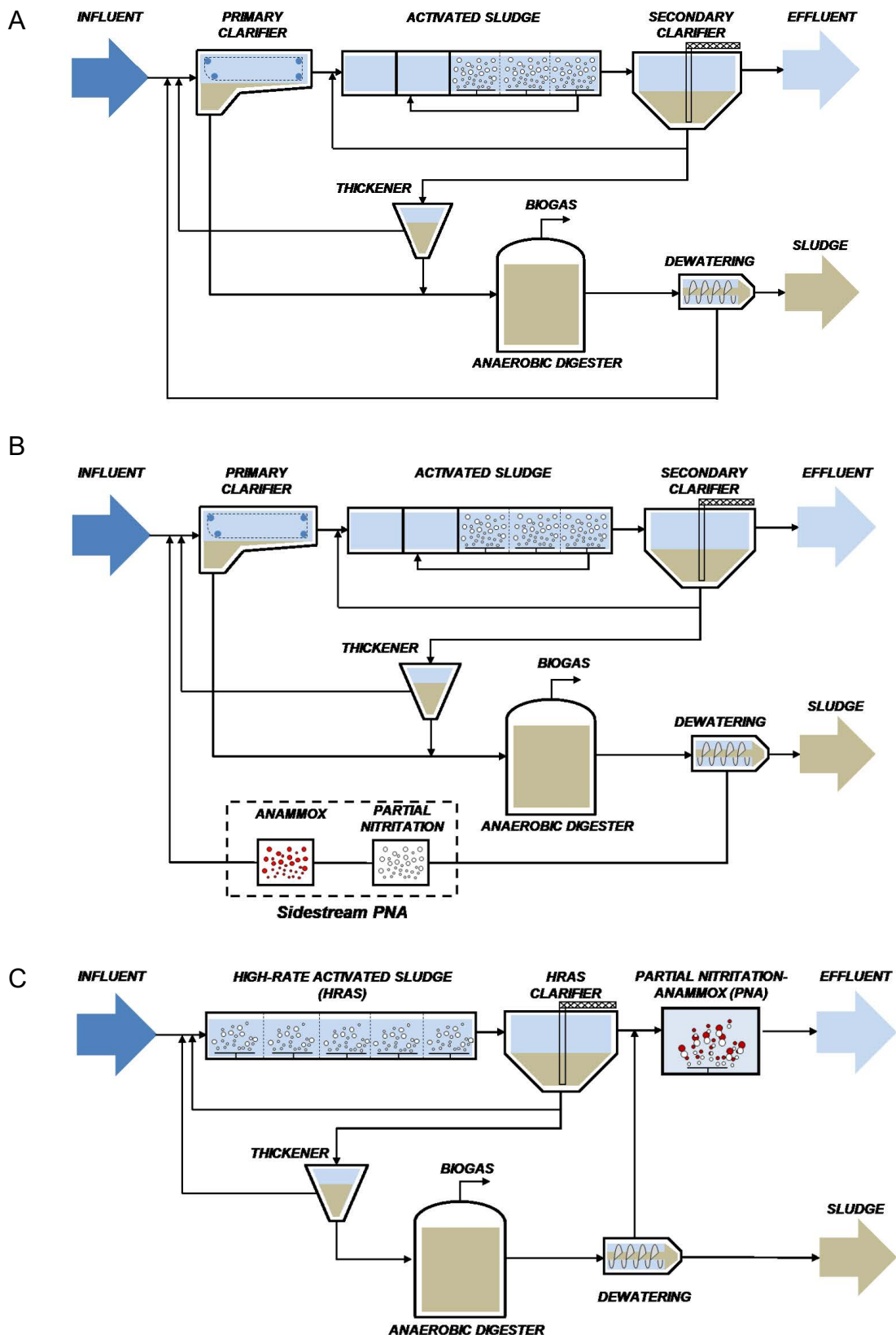


Figure 1.3 Typical wastewater treatment schemes: A) Conventional activated sludge (CAS) system; B) Conventional activated sludge coupled with sidestream PNA system, and C) High-rate activated sludge (HRAS) coupled with mainstream PNA system

1.1.3 N3.0: Autotrophic anammox-based nitrogen removal

The discovery of anaerobic ammonium oxidization (anammox) was an important step in the understanding of the global nitrogen cycle and has broadened the process optimization potential for nitrogen removal from wastewater. Anammox bacteria autotrophically convert ammonium and nitrite to N_2 in the absence of oxygen and COD (Eq. 3 and Fig. 1.1) (Strous et al., 2006, 1998). Nitrate is also produced during the anammox process (Strous et al., 1998). This process was first predicted by Broda (1977) based on thermodynamic analysis, but it was only evidenced until Mulder et al. (1995) discovered the disappearance of ammonium under anaerobic conditions. The anammox bacteria discovered so far are members of a deep-branching lineage in the bacterial phylum Planctomycetes (Kartal et al., 2012).

To apply anammox for nitrogen removal, a preceding step providing nitrite is required. The most widely used approach is the so-called partial nitrification (PN) process, during which approximately half of the ammonium in wastewater is oxidized to nitrite by AOB (Van Dongen et al., 2001). The other half of the ammonium can be subsequently oxidized with the converted nitrite by anammox bacteria. The combined partial nitrification and anammox (PNA, Eq.C, Table 1.1) process can be achieved either in two consecutive reactors (two-stage PNA, e.g., SHARON-Anammox (Van Dongen et al., 2001)) or in a single reactor (one-stage PNA). Different process options for the PNA process are found in the literature, bearing names such as SHARON-Anammox (Van Dongen et al., 2001), CANON (Sliekers et al., 2003), OLAND (Kuai and Verstraete, 1998) and DEMON (Wett, 2006). Compared to conventional heterotrophic denitrification-based nitrogen removal processes, the autotrophic PNA process decouples nitrogen and carbon removal, bringing the biological nitrogen treatment to the third generation (N3.0). Compared to conventional nitrification-denitrification over nitrate, the PNA process requires up to 62% less aeration energy, removes the need for external organic carbon addition (Eq. C, Table 1.1), emits less CO_2 , and produces 70-80% less sludge and associated costs (Siegrist et al., 2008).

The PNA process has been widely studied and applied in treating ammonium-rich wastewaters with low organic carbon to nitrogen ratios (COD/N) and mesophilic temperature, such as the sidestream generated from the reject water of anaerobically digested sludge, as demonstrated by the first full-scale anammox reactor (built in 2002)

(van der Star et al., 2007). By 2014, i.e., within less than 20 years of the discovery of anammox, PNA process has been applied in more than 100 full-scale applications (Lackner et al., 2014), making it among the most successful examples of how fundamental research into nitrogen-cycling microorganisms and their application have progressed concomitantly.

The implementation of anammox-based technologies in the mainstream of WWTPs (i.e., mainstream anammox or mainstream deammonification) is under investigation to transform wastewater treatment into energy-neutral or even into an energy-generating concept (Kartal et al., 2010; Verstraete and Vlaeminck, 2011). Soon after the discovery of anammox, Jetten and coauthors (1997) realized how anammox could enable significant improvement in the sustainability of wastewater treatment and proposed a new conceptual scheme therein. This conceptual scheme was a two-stage system, based on the A/B (Adsorption/Bio-oxidation) process already established in the 1970s (Boehnke, 1977). The first stage utilizes a high-rate activated sludge (HRAS) process (detailed in Section 1.1.4), in which COD is concentrated and redirected for subsequent energy recovery through anaerobic digestion. This stage is followed by a PNA stage for mainstream nitrogen removal, for which a granular sludge system was later put forward due to its high volumetric conversion rate and biomass retention (Fig. 1.3C) (Kartal et al., 2010). Since the early 2010s, significant progress has been achieved with respect to mainstream PNA, demonstrating its feasibility at lab- and pilot-scales (Cao et al., 2017a; De Clippeleir et al., 2013; Laurenzi et al., 2016; Lotti et al., 2015b; Ma et al., 2011; Winkler et al., 2012). The anammox-based processes are further detailed in Section 1.2.

1.1.4 Interactions between biological nitrogen and carbon removal

Nitrogen and carbon removal depend on one another. In the activated sludge process, organic carbon can be removed by heterotrophs with O₂ (aerobic conditions), or nitrate/nitrite (anoxic conditions) as an electron acceptor. The aerobic carbon removal pathway competes with AOB and NOB (and thus nitrification) for O₂, whereas the anoxic carbon removal pathway represents the denitrification process that drives conventional biological nitrogen removal.

The interactions between biological nitrogen and carbon removal can be demonstrated by the fate of the HRAS process. The HRAS process generally uses a higher food-to-

microorganism (F/M) ratio, a shorter sludge retention time (SRT < 2 d), a shorter HRT (~ 0.5 h) and a lower dissolved oxygen concentration (DO < 1 g O₂.m⁻³), compared to conventional activated sludge (CAS) processes (De Graaff et al., 2016; Jimenez et al., 2015). As a result, HRAS processes require less aeration energy and can be realized in more compact systems, also allowing a higher recovery of chemical energy contained in wastewater.

During the era of N1.0, nitrification was first used as an indicator of the stable operation of the COD removal process (Ardern and Lockett, 1914; Gujer, 2010). It was shown later that WWTPs could safely remove COD at a shorter retention time without nitrification, which then became the norm for the design of HRAS systems (Barnard and Stensel, 2014; Buswell and Long, 1923). Due to the short SRT in HRAS, full nitrification can only be realized in a second stage with longer SRT, i.e., the B-stage in the A/B process established in the 1970s (Boehnke, 1977). However, when nitrogen removal and thus heterotrophic denitrification became necessary (N2.0 era), the HRAS process became less relevant as its high COD removal efficiency would often leave largely insufficient COD for denitrification in the subsequent stage (Jetten et al., 1997). The mainstream autotrophic PNA process (N3.0 era) enables the decoupling of carbon and nitrogen removal, and thus allows a revival of the HRAS process.

1.2 A few challenges and research objectives

1.2.1 N₂O emission from biological nitrogen removal (Chapter 2)

One of the main driving forces in the current 'N3.0 era' is sustainability, in terms of resource recovery, carbon footprint, and space requirements, etc. When it comes to carbon footprint, the emission of nitrous dioxide (N₂O) is of unignorable concern for biological nitrogen removal. N₂O is a potent greenhouse gas, with 297 times stronger global warming potential (in 100 years) than CO₂ (IPCC, 2014). Even small amounts of N₂O emission can contribute significantly to the carbon footprint of WWTPs, which is of increasing concern in recent years (Massara et al., 2017). Climate change is real and is a global challenge that does not respect national borders. It is extremely likely that more than half of the observed increase in global average surface temperature from 1951 to 2010 was caused by the anthropogenic increase in GHG concentrations and other anthropogenic forcing together (IPCC, 2014). The wastewater sector needs to limit GHG emissions as well in order to combat climate change. Moreover, both N₂O

and its precursor nitric oxide (NO) are substances involved in ozone depletion, with N₂O named as the dominant ozone-depletion substance emitted in the 21st century (Ravishankara et al., 2009).

N₂O can be produced in several pathways during biological nitrogen removal: 1) as an intermediate of denitrification process (Fig. 1.1); 2) as a byproduct of incomplete oxidation of hydroxylamine (NH₂OH) to nitrite; and 3) as the final product of nitrifier denitrification by AOB (Kampschreur et al., 2009; Robertson and Kuenen, 1990). In addition, mixotrophic NOB are also known to incompletely denitrify until N₂O only (Freitag et al., 1987). Anammox bacteria are lacking the genes to produce N₂O (Kartal et al., 2012). Nevertheless, N₂O emission can be expected in stand-alone anammox reactors (as part of two-stage PNA systems, Fig. 1.3B) when heterotrophic denitrifiers are triggered by influent COD (Jia et al., 2018). Intensive studies have been carried out on N₂O emission from one-stage PNA reactors (Ali et al., 2016; Li et al., 2017) and from partial nitrification reactors (Mampaey et al., 2016). Studies on N₂O emission from stand-alone anammox reactors (as part of two-stage PNA or Partial Denitrification-Anammox (Section 1.2.2) systems) are rather limited, and the impact of influent COD on the N₂O emission from these reactors has not been investigated explicitly (Chapter 2).

Overall, to fully assess the potential of anammox-based processes, the emission of greenhouse gases needs to be carefully considered to ensure that the savings in CO₂ emissions due to the reduced (aeration) energy consumption and due to the autotrophic nature of the process are not overruled by increased N₂O production.

1.2.2 Providing nitrite for the anammox reaction (Chapter 2-4)

While ammonium is normally present in wastewater, the challenge for the implementation of anammox-based processes lies in nitrite supply. As shown in Fig.1.1, nitrite is involved in several biological nitrogen transformations, which offers both opportunities and challenges. Concerning the sources, nitrite can be biologically produced through ammonium oxidation and/or nitrate reduction (Fig. 1.4).

1.2.2.1 Aerobic ammonium oxidation to nitrite

Ammonium oxidation is carried out by AOB and/or AOA under aerobic conditions through the nitrification pathway (Eq. 1a, Table 1.1), which sets the basis for PNA

processes (Fig. 1.4A). Nitritation has by far been the most explored approach for nitrite supply (Zhang et al., 2019), due to its cost savings (Table 1.1) and successful application for ammonium-rich wastewater treatment at mesophilic temperature (Lackner et al., 2014). The main challenge here is the suppression of NOB and, thus, the prevention of nitrite oxidation to nitrate. The selection strategies of AOB over NOB are based on several principles: (1) AOB grow faster than NOB at mesophilic temperature, allowing for SRT based washout of NOB as done in the SHARON process (Hellings et al., 1998); (2) AOB generally have higher affinity for oxygen (i.e., lower K_{O_2}) than NOB, allowing for the washout of NOB at low DO concentrations (Pérez et al., 2014); (3) AOB is less sensitive to the inhibition of free ammonia (FA) and free nitrous acid (FNA) than NOB, aiding for NOB suppression in ammonium-rich wastewater treatment (Wang et al., 2017); (4) The lag phase in NOB activity at the beginning of aeration, allowing for on/off aeration strategy (i.e. transient anoxia) (Regmi et al., 2014); (5) Maintaining a certain level of residual ammonium concentration which favors AOB and anammox activity (Pérez et al., 2014); and (6) Bioaugmentation by transferring AOB and anammox bacteria from the sidestream PNA system (Wett et al., 2013).

Successful partial nitritation has been well established for sidestream treatment but remains challenging for mainstream sewage treatment. The low temperature and low ammonium concentration (20-75 mg $NH_4^+-N L^{-1}$) (Henze et al., 2008) of municipal wastewater are the main objections in this regard (Agrawal et al., 2018; Cao et al., 2017). To this end, AOA could potentially be a good candidate for nitritation and nitrite supply to anammox at low ammonium concentrations due to their high affinity for ammonia (Pan et al., 2016; Straka et al., 2019b). The discovery of comammox microorganisms, which were reported to have higher affinity for ammonia than AOB but lower affinity for nitrite than NOB (Dimitri Kits et al., 2017) and present as the dominant ammonia oxidizers in a mainstream low DO nitrifying reactor (Roots et al., 2019), further complicates nitritation at mainstream conditions (Winkler and Straka, 2019).

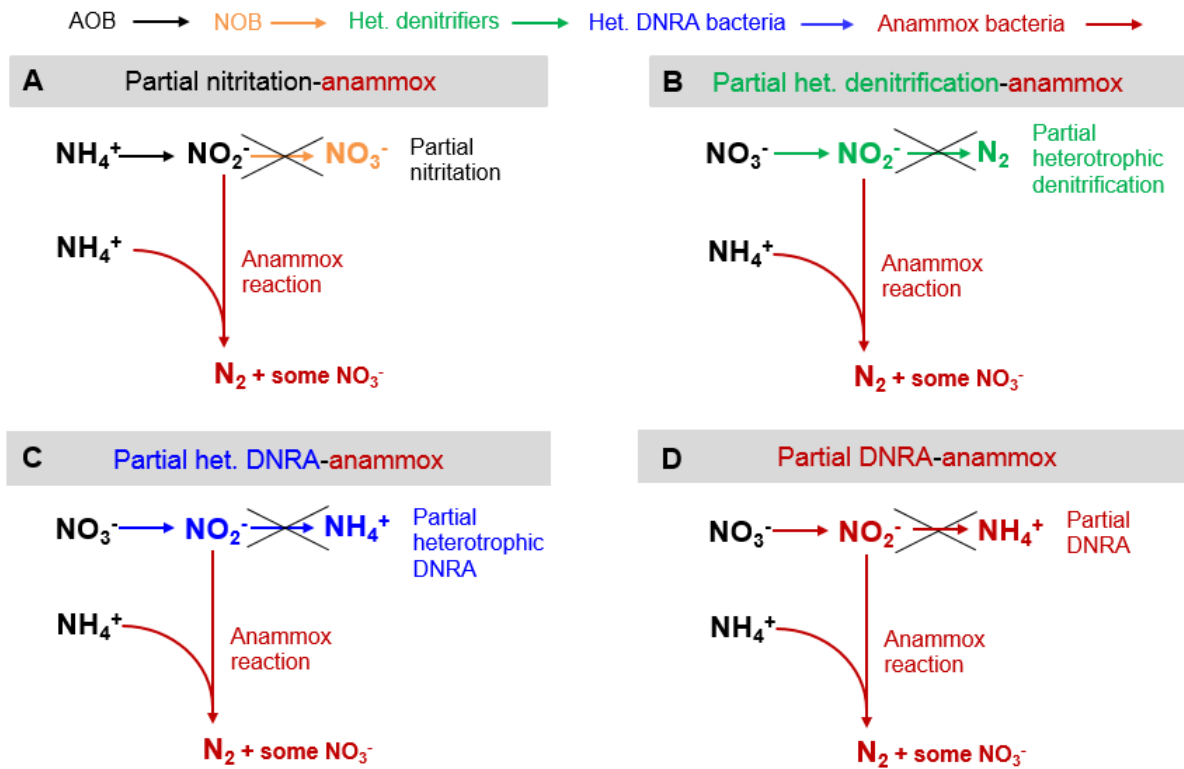


Figure 1.4 Overview of biological nitrite sources, sinks and process combinations for anammox-based nitrogen removal (adapted from Castro-Barros et al. (2017))

Successful partial nitritation has been well established for sidestream treatment but remains challenging for mainstream sewage treatment. The low temperature and low ammonium concentration (20-75 mg $\text{NH}_4^+\text{-N L}^{-1}$) (Henze et al., 2008) of municipal wastewater are the main objections in this regard (Agrawal et al., 2018; Cao et al., 2017). To this end, AOA could potentially be a good candidate for nitritation and nitrite supply to anammox at low ammonium concentrations due to their high affinity for ammonia (Pan et al., 2016; Straka et al., 2019b). The discovery of comammox microorganisms, which were reported to have higher affinity for ammonia than AOB but lower affinity for nitrite than NOB (Dimitri Kits et al., 2017) and present as the dominant ammonia oxidizers in a mainstream low DO nitrifying reactor (Roots et al., 2019), further complicates nitritation at mainstream conditions (Winkler and Straka, 2019).

1.2.2.2 Nitrate reduction to nitrite

Nitrate reduction to nitrite can be carried out under anoxic conditions, by heterotrophic denitrifiers through partial denitrification (Eq. 2a, Table 1.1; Fig. 1.4B, also referred to

as denitrification), with organic carbon as the electron donor. The coupling of partial denitrification and anammox (PDA) was already observed in the reactor where anammox was first discovered (Mulder et al., 1995). In addition, denitrification is known to help with the removal of the small amount of nitrate produced from anammox metabolism and thus improve the nitrogen removal efficiency of anammox-based reactors at low influent COD/N ratios (Mozumder et al., 2014; Ni et al., 2012). In natural, relatively cold ecosystems, anammox can obtain 67% or more of nitrite from nitrate reduction, and 33% or less from aerobic ammonia oxidation in the oxygen minimum zone (OMZ) of the ocean (Lam et al., 2009). Nonetheless, partial denitrification has only recently gained more interest as it represents an alternative and yet still promising way to the remaining challenging PN pathway for nitrite supply for utilizing anammox in the cold mainstream (Ma et al., 2017). Several lab-scale studies have demonstrated the feasibility of this new combined process for municipal wastewater treatment (Le et al., 2019; Ma et al., 2017), and for combined treatment of nitrate-rich streams with municipal wastewater (Du et al., 2019). Note, however, that the terminology 'partial denitrification-anammox (PDA)' used in literature may be misleading or at least incomplete. Indeed, a preceding partial nitrification step (i.e. conversion of half the ammonium to nitrate) may be needed for nitrate supply in case not yet available, as is the case for municipal wastewater. PNPDA (Partial Nitrification-Partial Denitrification-Anammox, Eq. D, Table 1.1) would, therefore, be a more accurate description in this case. It is clear that the benefits of the PDA process are maximized when the nitrate is provided from external streams (e.g., industrial wastewater) (Eq. E, Table 1.1).

Another, often ignored nitrate reduction pathway, is the dissimilatory nitrate reduction to ammonium (DNRA, Eq. 4). During the DNRA reaction, nitrate is first reduced to nitrite (partial DNRA, Eq. 4a), which can be further reduced to ammonium, depending on the availability of electron donors (e.g., COD) (Kraft et al., 2011). The catabolic reaction of partial DNRA is the same as partial denitrification (Eq. 2a/4a). Therefore, analogous to partial denitrification, partial DNRA can lead to a nitrite accumulation and could hence be coupled with anammox process as well (Eq. D & E and Fig. 1.4C). The full DNRA process can also provide the ammonium needed for anammox conversion, as observed in OMZ where DNRA provides substantial part of the NH_4^+ requirements for anammox (Lam et al., 2009). DNRA bacteria are often detected in anammox

reactors (Guo et al., 2016; Shu et al., 2015); however, their role in these systems is not yet clear.

Anammox bacteria can perform DNRA as well (also referred to as organotrophic anammox) (Güven et al., 2005; Kartal et al., 2007). This DNRA capacity of anammox bacteria increases their competitiveness in wastewater treatment as they can make use of some organic carbon present in the wastewater (Fig. 1.4D). Besides, in this way, residual nitrate present in the effluent of anammox bioreactors could also be removed (Winkler et al., 2012). Thermodynamic calculations indicate that low COD/N influent ratios favor the partial DNRA-anammox transformation (by anammox bacteria) over heterotrophic conversions since more free energy is gained (Castro-Barros et al., 2017). One feature of the DNRA by anammox bacteria is that organic carbon is oxidized to carbon dioxide rather than assimilating into biomass, resulting in no biomass production on carbon (Kartal et al., 2007; Tao et al., 2019; Winkler et al., 2012). A process scheme has been proposed to potentially utilize the dissimilatory nitrate reduction by anammox for MWW treatment (Castro-Barros et al., 2017).

Since the catabolic reactions are identical for heterotrophic partial denitrification, partial DNRA by heterotrophs and anammox bacteria (Eq. 2a/4a), the same abbreviation PD was used for these three reactions in this thesis. The main challenge in applying PDA (i.e., the three abovementioned nitrate reduction pathways for nitrite supply for anammox) is the management of heterotrophs. The strict control of heterotrophs is required for two reasons: (1) to avoid outcompetition of the slow-growing anammox bacteria; (2) to stop nitrate reduction at nitrite; and (3) to mitigate potential N₂O emission. Control strategies are being developed, such as relative low COD/N ratios, residual nitrate, and carbon source, to select partial denitrification over full denitrification (Cao et al., 2016; Du et al., 2019; Le et al., 2019). Analogous to the PNA process, the PDA process can be achieved either in two consecutive reactors (two-stage PDA, (Ma et al., 2017)) or in a single reactor (one-stage PDA, (Castro-Barros et al., 2017)).

Alternatively, there are also other nitrate reduction processes that can be possibly coupled with anammox process. such as the denitrifying anaerobic methane oxidation (DAMO) processes during which DAMO archaea reduce nitrate to nitrite using methane as electron donor (Ettwig et al., 2010; Xie et al., 2017), and autotrophic nitrate

reduction by microorganisms with inorganic electron donors (e.g., Fe^{2+} , S^{2-}) (Oshiki et al., 2013; Wu et al., 2016). This thesis does not focus on these options.

Overall, for the successful application of anammox-based processes, nitrite sources should be promoted and dictate how anammox-based processes can be implemented (Fig. 1.4), whereas the competition for nitrite between anammox and other nitrite sinks (i.e. NOB, heterotrophic denitrifiers and DNRA bacteria) should be minimized.

1.2.3 Factors governing the competition between denitrification and DNRA (Chapter 3)

Apart from serving as alternative sources of nitrite for anammox, the competition between denitrification and DNRA has broad implications. During denitrification, nitrate can be converted to nitrogen gas, thereby leading to nitrogen loss in natural and engineered ecosystems such as WWTPs. Nitrous oxide, a potent greenhouse gas, can be emitted during this process, posing an increasing concern (Canfield et al., 2010). In contrast, DNRA retains nitrogen locally by converting nitrate to bioavailable ammonium, which may be beneficial for natural ecosystems but unwanted for WWTPs (Van Den Berg et al., 2015). Growing evidence suggests that DNRA can be significant in both aquatic and terrestrial ecosystems, and it was shown to be present in activated sludge systems (Giblin et al., 2013; Rütting et al., 2011; Van Den Berg et al., 2015). Nevertheless, little is known about the importance of DNRA and its relative contribution in global N-cycling and biological nitrogen removal systems in WWTPs (Burgin and Hamilton, 2007; Kraft et al., 2011; Kuypers et al., 2018). Therefore, there is a pressing need to better comprehend the factors influencing the competition between denitrification and DNRA for nitrate (Chapter 3).

1.2.4 Feasibility of the integrated HRAS-PNA system (Chapter 4)

There is currently a changing paradigm in the water sector, focusing on resource recovery, as reflected by the change of renaming wastewater treatment plants to water resource recovery facilities (WRRFs). The conceptual two-stage HRAS-PNA system has been proposed for future energy-neutral or even energy-positive WRRFs (Jetten et al., 1997; Kartal et al., 2010; Verstraete and Vlaeminck, 2011). In this two-stage system (Fig. 1.3C), sufficient COD removal in the HRAS stage is crucial for avoiding the proliferation of heterotrophs and thus allow a successful PNA stage. However, a

higher COD removal in the HRAS stage does not necessarily mean a higher energy recovery (Jimenez et al., 2015; Nogaj et al., 2015). While the HRAS process has already been successfully applied at full-scale in the past to maximize energy recovery from the influent COD (Boehnke et al., 1997), the additional challenge for it herein is to simultaneously realize a sufficiently high COD removal efficiency in order to meet the influent requirements (i.e., low COD/N of HRAS effluent) of the downstream PNA stage.

The feasibility of the PNA process under mainstream conditions has been demonstrated in several laboratory and pilot-scale studies (De Clippeleir et al., 2013; Laurenzi et al., 2016; Lotti et al., 2014a). Nevertheless, these studies also point out that the long-term stability of PNA process (i.e., maintaining high process rate and low effluent nitrogen concentration) under varying temperature (especially low temperature) and loading rates (e.g., COD removal in the preceding HRAS stage) in full-scale WWTPs should be evaluated further (Cao et al., 2017; Hoekstra et al., 2019).

Overall, to comprehensively assess the combined HRAS-PNA system, a plant-wide perspective is needed (Chapter 4), as applied in the past for the evaluation of sidestream anammox processes (Volcke et al., 2006). Model-based investigations are useful for fast and rigorous assessment of the performance of WWTPs, in particular, to analyse the interrelations among unit processes. Up till now, the HRAS-PNA system and/or similar systems (e.g., bioflocculation and two-stage PNA) have only been evaluated *via* rough mass and energy balance calculations (Siegrist et al., 2008) and steady-state simulations (Bozileva et al., 2017; Fernández-Arévalo et al., 2017; Khiewwijit et al., 2015). A few studies applied life-cycle analysis for environmental assessment of systems with PNA in the mainline (Besson et al., 2017; Schaubroeck et al., 2015). Still, the feasibility and long-term stability of the HRAS-PNA system under dynamic conditions (e.g., temperature, hydraulic load, and substrate concentrations) remain to be evaluated.

1.3 Outline of the thesis

This thesis focuses on microbial interactions during biological nitrogen removal processes and assesses these systems both experimentally, through lab-scale studies and theoretically, with mathematical modelling and simulations.

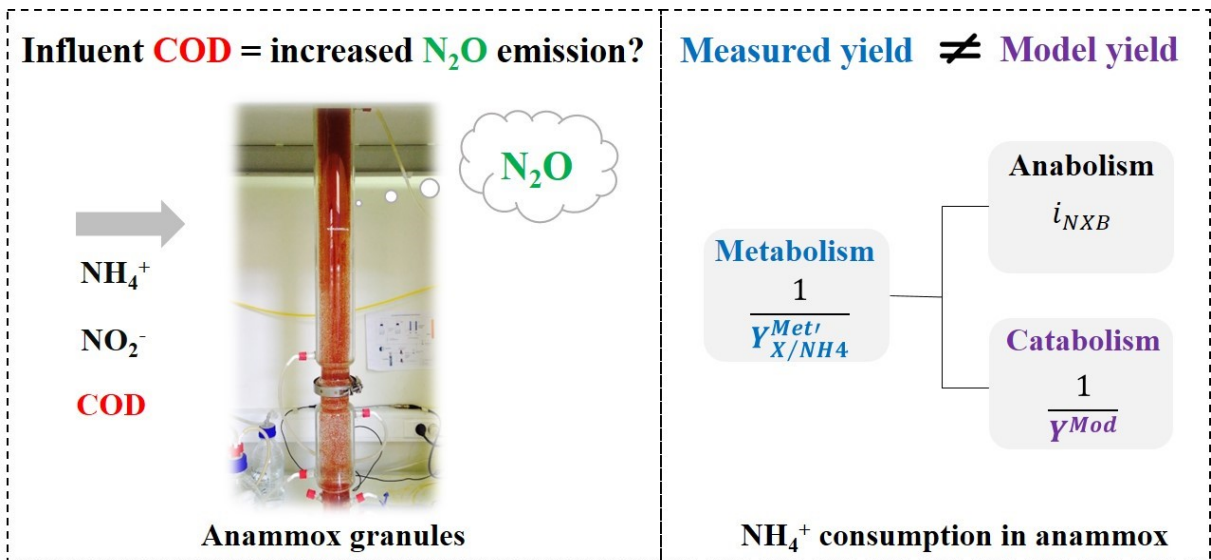
Chapter 1 introduces the nitrogen cycle and involved technological concepts. **Chapter 2** is dedicated to the impact of organic matter on the reactor performance and N_2O emission of a standalone granular sludge anammox reactor, mimicking the scenario where two-stage PNA is used for sidestream nitrogen removal (Fig. 1.3B). A lab-scale continuously fed bubble column granular sludge anammox reactor was operated over 400 days. A generalized method was demonstrated and applied to derive the anammox stoichiometry from experimental data for improved mass balance. In addition, a widely made mistake concerning the anammox yield coefficient in modelling of anammox process was identified, with solutions proposed.

Apart from anammox bacteria, heterotrophic denitrifiers and DNRA bacteria can carry out nitrate reduction as well, which can provide nitrite for anammox bacteria besides nitrification. **Chapter 3** elucidates the competition between denitrification and DNRA for nitrate and organic carbon using the resource-ratio theory. Firstly, the resource-ratio theory was proven applicable for predicting the competition outcome of heterotrophic denitrification and DNRA. Based on this theory, the importance of resource concentrations, COD/N ratio, dilution rate, and microbial physiological features to the competition outcome was highlighted. In particular, how these factors jointly define the boundaries for different competition outcomes was revealed. The results challenge prevailing perceptions and provide testable hypotheses and tools for further research.

Wastewater treatment plants of the future aim at energy autarky. This could potentially be realized through an HRAS process for COD redirection followed by a mainstream PNA process for nitrogen removal (Fig. 1.3C). This promising process option was evaluated in **Chapter 4** through modelling and simulations. The impact of operating conditions on the unit processes was investigated first, followed by a plant-wide assessment of the combined HRAS-PNA system, illustrating the feasibility of mainstream anammox. In addition, the combined HRAS-PNA system was compared with the conventional activated sludge (CAS) system, in terms of effluent quality and operational cost, under both steady-state and dynamic conditions.

Chapter 5 gives concluding remarks on how the findings of this thesis and their implications contribute to the understanding of biological nitrogen removal from wastewater and of the nitrogen cycle in general, concerning methodology, the fate of nitrate and process evaluation.

Impact of organic matter on the performance and N₂O emission of a granular sludge anammox reactor



2.0 Abstract

A continuously fed bubble column granular sludge anammox reactor was operated for 405 days to investigate the effect of organic matter on the reactor performance and N₂O emission. Results showed that influent COD improved the nitrogen removal of the anammox reactor at low influent COD/TN ratios (ca. 0.1 g COD.g N⁻¹); however, a concurrent increase in N₂O emission was observed. The average N₂O emission increased by 2.5 times ($p < 0.05$) with increasing influent COD concentration, accounting for up to 0.46% of the incoming nitrogen load. A generalized method was demonstrated and applied to derive the anammox stoichiometry from experimental data for improved mass balance. Mass balance revealed that approximately 18% of the nitrate produced from anammox conversion was reduced via heterotrophic denitrification to nitrite, and 29% of this produced nitrite was further released as N₂O. In addition, it was found that the experimentally measured anammox biomass yield in the overall metabolic reaction has been mistakenly used for the catabolic yield in many modelling studies. Solutions were proposed.

Chapter redrafted after:

Jia, M., Castro-Barros, C.M., Winkler, M.K.H. and Volcke, E.I.P. (2018) Effect of organic matter on the performance and N₂O emission of a granular sludge anammox reactor. *Environmental Science: Water Research & Technology* 4, 1035–1046.

2.1 Introduction

The discovery of anaerobic ammonium oxidization (anammox) has changed the understanding of the global nitrogen cycle and revolutionized nitrogen removal from wastewater. Anammox bacteria can autotrophically convert ammonium (NH₄⁺) and nitrite (NO₂⁻) to dinitrogen gas in the absence of oxygen (Strous et al., 1998). To provide the nitrite needed by the anammox reaction, approximately half of the ammonium in the wastewater is oxidized to nitrite by ammonium-oxidizing bacteria (AOB), i.e., the so-called partial nitrification (PN) process (Van Dongen et al., 2001). The other half of the ammonium can be subsequently oxidized with the converted nitrite by anammox bacteria. The combined partial nitrification and anammox (PN/A) steps can be achieved either in two consecutive reactors (two-stage PN/A) (Van Dongen et al., 2001) or in a single reactor (one-stage PN/A) (Sliemers et al., 2003). Compared to the conventional nitrification-denitrification process, the PN/A process requires up to 63% less aeration energy, produces 70-80% less sludge, removes the need for external organic carbon addition, and emits almost no CO₂ (Siegrist et al., 2008). It has thus been widely studied and applied in treating ammonium-rich wastewaters with low organic carbon to nitrogen ratios (COD/N) and elevated temperature, such as the side stream generated from the reject water of anaerobically digested sludge (Lackner et al., 2014). The implementation of anammox-based technologies in the mainstream of WWTPs (i.e., mainstream anammox) is under investigation to transform wastewater treatment into energy-neutral or even energy-generating (Jetten et al., 1997; Kartal et al., 2010; Verstraete and Vlaeminck, 2011). For this purpose, two-stage PN/A systems, where anammox process is achieved in a stand-alone reactor following a partial nitrification reactor, are considered as a suitable configuration (Pérez et al., 2015).

One of the major challenges of mainstream anammox is the presence of organic matter in most wastewater streams (Cao et al., 2017). The influent COD can stimulate the growth of fast-growing heterotrophic denitrifiers, which compete with the slow-growing anammox bacteria for nitrite, resulting in system failure, especially at high COD/N ratios (Cao et al., 2017). On the other hand, heterotrophic denitrifiers may increase nitrogen removal efficiency in anammox reactors under low COD/N ratios (Mozumder et al., 2014; Winkler et al., 2012). This is due to the further reduction of accumulated nitrate with organic carbon as electron donors by heterotrophs via denitrification (Ma et al., 2017) and/or by anammox bacteria via dissimilatory nitrate reduction to

ammonium (DNRA) (Winkler et al., 2012). However, the impact of COD in anammox systems has not been evaluated in many anammox studies (Schielke-Jenni et al., 2015) but might be important to thoroughly comprehend reactor performance. Simple mass balance calculations offer a good tool to correct for the contribution of heterotrophic denitrification and anammox in the nitrogen removal in anammox reactors, as demonstrated in this contribution.

The accuracy of mass balances depends on the accurate knowledge of the involved reactions and their stoichiometry. Different anammox stoichiometries were reported diverging from the stoichiometry determined by Strous et al. (1998) (Eq. 2.1, Table 2.2), which is commonly used for mass balance, modelling and design of anammox process. The stoichiometry of anammox process and the elemental composition of anammox bacteria were identified again by Lotti et al. (2014b) in a nearly pure (ca. 98%) anammox culture (Eq. 2.2, Table 2.2). Despite a comparable biomass yield over ammonium (0.066 vs. 0.071 mole C-x/mole NH₄-N) obtained in both studies, the results also highlighted substantial differences in terms of biomass composition as well as stoichiometric ratios of consumed NO₂-N to consumed NH₄-N ($\Delta\text{NO}_2^-/\Delta\text{NH}_4^+$) and produced NO₃-N to consumed NH₄-N ($\Delta\text{NO}_3^-/\Delta\text{NH}_4^+$). For example, the nitrate production per mole ammonium consumed ($\Delta\text{NO}_3^-/\Delta\text{NH}_4^+$) is 38% lower in Eq. 2.2 than in Eq.1 (0.161 vs. 0.26, Table 2.2). To understand these significant inconsistencies and to obtain a more reliable mass balance, a better understanding of anammox stoichiometry is needed.

The presence of influent COD may also stimulate the formation of nitrous oxide (N₂O) in anammox reactors. N₂O is a potent greenhouse gas, with 297 times stronger global warming potential than CO₂ (IPCC, 2014). Even small amounts of N₂O emission contribute significantly to the carbon footprint of WWTPs, which is of increasing concern in recent years (Kampschreur et al., 2009; Massara et al., 2017). Anammox bacteria are lacking the genes to produce N₂O (Strous et al., 2006) in which they differ from heterotrophic denitrifiers that are capable of emitting N₂O as an intermediate of the denitrification process. Nevertheless, N₂O emission can be expected in stand-alone anammox reactors (as part of two-stage PN/A systems) when heterotrophic denitrifiers are triggered by influent COD. Intensive studies have been carried out on N₂O emission from one-stage PN/A reactors (Ali et al., 2016; Li et al., 2017; Mampaey

et al., 2016) and from stand-alone partial nitritation reactors (Mampaey et al., 2016). Studies on N₂O emission from stand-alone anammox reactors (as part of two-stage PN/A systems) are rather limited, and the impact of influent COD on the N₂O emission from these reactors has not been investigated explicitly.

This contribution assesses the impact of influent organic matter on the overall performance and N₂O emission of a lab-scale granular sludge anammox reactor. The nitrogen removal and N₂O emission were measured without and with influent COD. A general method to calculate the anammox stoichiometry corresponding with case-specific experimental observations was applied and demonstrated. Mass balances were further set up to quantify the contribution of heterotrophic denitrification and the anammox process. Moreover, a commonly made mistake regarding the yield coefficient of anammox bacteria in modelling and simulations was addressed.

2.2 Materials and methods

2.2.1 Reactor setup and operation

A lab-scale continuously fed bubble column reactor with a working volume of 6.5L (Fig. 2.1) was operated for more than 400 days. The inoculum for the granular anammox sludge originated from the full-scale anammox reactor in the Dokhaven WWTP, Rotterdam, the Netherlands (van der Star et al., 2007). The initial biomass concentration in the reactor was 3.36 g VSS.L⁻¹. The pH was maintained at 7.2 ± 0.1 by dosing 1M hydrochloric acid and 1M sodium hydroxide. The temperature was controlled at 30 ± 1°C by using a heating water jacket connected to a circulating bath. The off-gas, mainly N₂ and CO₂, was recirculated to suspend the biomass. The reactor was kept anoxic by recirculating the off-gas at a constant flow rate of 1 L.min⁻¹. Besides, N₂ was added when the dissolved oxygen (DO) was higher than 0.05 mg O₂.L⁻¹.

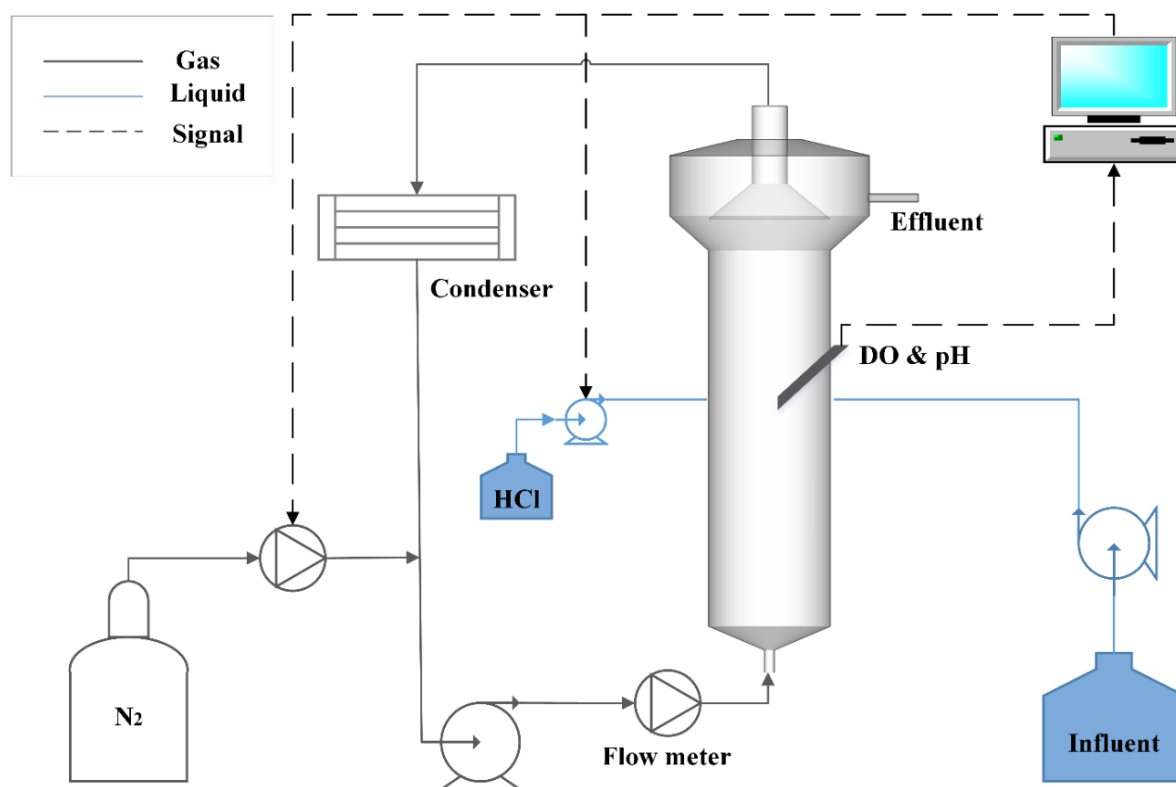


Figure 2.1. Schematic representation of the lab-scale setup

Both inorganic and organic synthetic wastewater media were prepared. The inorganic synthetic influent contained ammonium (in the form of $(\text{NH}_4)_2\text{SO}_4$), nitrite (in the form of NaNO_2), and mineral medium, while organic synthetic wastewater was prepared by adding sodium acetate (CH_3COONa) to the inorganic synthetic wastewater. The composition of the mineral medium was 0.41 mM $\text{MgSO}_4 \cdot 7\text{H}_2\text{O}$, 10 mM KHCO_3 , 4.19 mM K_2HPO_4 , 0.76 mM KH_2PO_4 , and 1.25 mL.L⁻¹ of trace element solution I and trace element solution II (Van De Graaf et al., 1996). The trace element solution I contained (g.L⁻¹): EDTA 5, FeSO_4 5; the trace element solution II contained (g.L⁻¹): EDTA 15, H_3BO_4 0.014, $\text{MnCl}_2 \cdot 4\text{H}_2\text{O}$ 0.99, $\text{CuSO}_4 \cdot 5\text{H}_2\text{O}$ 0.25, $\text{ZnSO}_4 \cdot 7\text{H}_2\text{O}$ 0.43, $\text{NiCl}_2 \cdot 6\text{H}_2\text{O}$ 0.19, $\text{NaSeO}_4 \cdot 10\text{H}_2\text{O}$ 0.21, $\text{NaMoO}_4 \cdot 2\text{H}_2\text{O}$ 0.22. Before being fed, the medium was adjusted to a pH of 7.0 ± 0.1 and flushed with N_2 gas for 20min to remove the dissolved oxygen in the medium.

The reactor was operated in four phases and was first fed with inorganic and then organic synthetic wastewater (Table 2.1). In phase I (day 1-130), the influent concentrations of NH_4^+ and NO_2^- were first increased progressively (50-550 mg NH_4^+ -N.L⁻¹ and 50-650 mg NO_2^- -N.L⁻¹) to adapt the anammox bacteria to higher nitrogen load (up to 1.2 kg N.m⁻³d⁻¹) and then gradually decreased. In phase II (day 131-336),

the reactor was fed with medium of constant NH₄⁺ and NO₂⁻ concentrations to establish a stable operation. In phase III (day 337-383), the influent concentrations of NH₄⁺ and NO₂⁻ were kept constant, while the influent COD concentration was increased progressively (8, 12 and 20 mg COD.L⁻¹) to adapt the anammox biomass to influent COD in the first 21 days (phase III_1) and then fixed at 40 mg COD.L⁻¹ (phase III_2) to study the effect of influent COD. Correspondingly, the ratio of COD from sodium acetate over the incoming total nitrogen (COD/TN) varied from zero to 0.1 (g COD.g N⁻¹). In phase IV (day 384-405), following blocking of the reactor effluent on day 384, the reactor was opened and cleaned for troubleshooting, resulting in unstable operation and some biomass loss. The HRT was increased from 1 to 2 days to lower the NLR and to enable the recovery of the anammox reactor. The reactor was stopped on day 405.

Table 2.1. Operational conditions of the granular sludge anammox reactor

Phase	Days	Influent (mg N or COD.L ⁻¹)					HRT (d)	NLR (kg N.m ⁻³ d ⁻¹)
		NH ₄ ⁺	NO ₂ ⁻	CH ₃ COONa	NO ₂ -N /NH ₄ -N	COD /TN		
I Start-up	1-130	50-550	50-650	0	1.-1.3	0	1	0.1-1.2
II Stable anammox	131-336	350	400	0	1.1	0	2	0.37
III COD addition	337-383	200	200	0-40	1	0-0.1	1	0.4
IV Recovery test	384-405	200	200	40	1	0.1	1-2	0.4-0.2

2.2.2 Analytical procedures

The biomass concentration was determined as total suspended solids (TSS) and volatile suspended solids (VSS) according to standard methods (APHA, 1998). Liquid samples were filtered through a 0.45µm disposable Millipore filter. Ammonium, nitrite, nitrate, and COD were determined with standard test kits (Macherey-Nagel, Germany). However, the COD measurement showed uncertainty, as the carbon mass balance did not always match up with the media composition, e.g., the effluent COD was higher than the influent COD in some paired samples. It was thought that the elevated effluent COD could be attributed to soluble microbial products (SMP) and decay released substrate from the metabolism of anammox bacteria, as described in Ni et al. (2012), where heterotrophs accounted for 23% of the total bacteria in an anammox biofilm

without addition of external organic carbon. The potential SMP production in phase III in our reactor was calculated to be approximately 6.2 mg COD.L⁻¹ (corresponds to 2.5 mg DOC.L⁻¹ if all SMP were assumed to be acetate), using the stoichiometric coefficients for SMP production from anammox biofilm reported by Ni et al. (2012). This SMP production is in the same range as average values in similar systems (6.6 mg DOC. L⁻¹ in Ni et al. (2012) and 10.5 mg DOC.L⁻¹ in Zhang et al. (2016). However, the calculated SMP concentration could not fully explain the higher COD in the effluent compared to the influent in some cases, hence delineating the importance of conducting the calculations as presented in this study. The concentration of N₂O and CO₂ in the off-gas of the reactor were monitored on-line with a gas phase analyser (X-STREAM, EMERSON, Germany). The one-way ANOVA method was used to determine whether the differences of the measured N₂O emission during different phases were statistically significant (SPSS 24 software, IBM).

2.2.3 Calculation of the anammox reaction stoichiometry

This study presents a generalized calculation scheme for the determination of the theoretical stoichiometry of anammox reaction with a general biomass composition (CH_xO_yN_z), following the generalized method of Kleerebezem and van Loosdrecht (2010). This stoichiometry derivation method is a refinement of the electron-based method developed by McCarty (1975) and Rittmann and McCarty (2001) and the method based on degree of reduction and elemental balances described by Heijnen (1999), as it 1) enables free definition of electron acceptors and donors in the anabolic reaction equation, 2) does not use predefined reference states (e.g., carbon dioxide for carbon) for any of the elements involved in the redox reactions, 3) is optimized for straightforward implementation in a calculation procedure (e.g., spreadsheet) (Kleerebezem and Van Loosdrecht, 2010). The complete metabolic reaction (*Met*) of anammox process combines the catabolic (*Cat*) and anabolic (*An*) reaction. Ammonium and nitrite are converted to nitrogen gas in the catabolic reaction, while the anabolic reaction comprises biomass growth, reducing inorganic carbon with nitrite/nitrate as the electron-donor couple and assuming ammonium as the N-source (Lotti et al., 2014b; Strous et al., 1998). In the presented calculation scheme, the stoichiometries of the catabolic and anabolic reactions were defined by closing the elemental and charge balances of the electron donor and electron acceptor half-

reactions. Catabolism and anabolism are linked through the measured yield: $Y_{X/S}^{Met}$ (mole C-x.(mole S)⁻¹, where X represents biomass, S substrate and Met metabolism) or, alternatively, the measured ratio of the consumption/production rate of two compounds ($Y_{NO_2^-/NH_4^+}^{Met} = \Delta NO_2^-/\Delta NH_4^+$) participating in the reaction system. The overall metabolic reaction equation of the anammox process was thus derived as a function of the biomass composition (CH_xO_yN_z) and the measured parameter (e.g., Y_{X/NH_4}^{Met} or $\Delta NO_2^-/\Delta NH_4^+$). This method was documented in a stepwise manner (Section A2.1, Appendix) and demonstrated in a spreadsheet (Spreadsheet A2.1, Appendix).

2.2.4 Mass balance for process rate estimation

Mass balances were applied to quantify the contribution of potential processes in the granular sludge anammox reactor. The process rates concerning growth and decay of anammox bacteria and denitrifiers were determined by balancing measured nitrogen conversions (NH₄⁻, NO₂⁻ and NO₃⁻) and assumed COD conversions, following the equation (Schielke-Jenni et al., 2015):

$$A \cdot \rho = r$$

A denotes the matrix of the stoichiometric coefficients (Table A2.1, Appendix), ρ is the vector of unknown process rates (g COD.m⁻³.d⁻¹, e.g., the ρ_j is the process rate for process j) and r groups the measured net conversion rates of compounds in the reactor (g N or COD.m⁻³.d⁻¹, e.g., r_{NH_4} is the net conversion rate of NH₄-N expressed as g NH₄-N.m⁻³ d⁻¹; $r_{NH_4}^j$ is the conversion rate of NH₄-N in process j ; $r_{NH_4}^j/r_{NH_4}$ is the contribution of process j in the net conversion of NH₄-N). The procedure for the derivation of this mass balance is documented in detail in the Appendix (Section A2.2 and Spreadsheet A2.2).

2.3 Results and discussion

2.3.1 Reactor performance without and with influent organic carbon

The overall reactor performance is displayed in Fig. 2.2. A high nitrogen removal efficiency (NRE) was achieved when only ammonium and nitrite were fed (50-550 mg NH₄⁺-N.L⁻¹ and 50-650 mg NO₂⁻-N.L⁻¹ in phase I; 350 mg NH₄⁺-N.L⁻¹ and 400 mg NO₂⁻-N.L⁻¹ in phase II), with average removal efficiencies of 91.4 ± 5.2%, 98.2 ± 2.8% and

86.1 ± 3.0% for NH₄-N, NO₂-N and total nitrogen (TN), respectively. The measured ratios of $\Delta\text{NO}_2^-/\Delta\text{NH}_4^+$ and $\Delta\text{NO}_3^-/\Delta\text{NH}_4^+$ were 1.24 ± 0.07 and 0.22 ± 0.05 , respectively. They were both lower than the corresponding stoichiometric ratios determined by Strous et al. (1998) (1.32 and 0.26, Eq. 1) and higher than those of Lotti et al. (2014b) (1.146 and 0.161, Eq. 2.2). The reactor operation aimed at anoxic conditions, given that anammox bacteria are sensitive to oxygen and can be completely inhibited at a low DO concentration of 0.2 mg.L⁻¹ (Joss et al., 2011). However, the DO was elevated for several cycles in phase I and II due to issues in reactor operation (e.g., day 131). A quick recovery was established within 24h by temporarily lowering the nitrogen load and adding N₂ gas (e.g., day 131), indicating that the granular sludge anammox system was robust and of high resiliency.

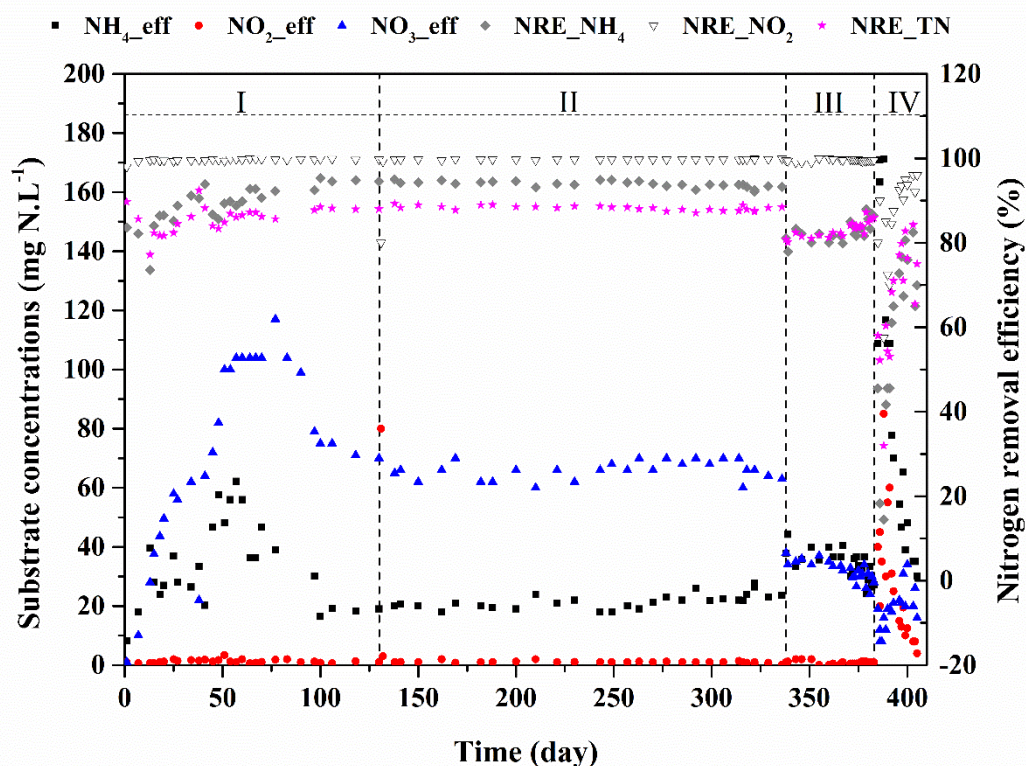


Figure 2.2. Effluent concentrations ('eff') and nitrogen removal efficiency (NRE) of the granular sludge anammox reactor

Phase III (200 mg NH₄⁺-N.L⁻¹ and 200 mg NO₂⁻-N.L⁻¹ in the influent) was divided into two stages. In stage 1 the COD concentration was 8-20 mg COD.L⁻¹ which was raised to 40 mg COD.L⁻¹ in stage 2. The average removal efficiencies of NH₄-N and TN were $80.9 \pm 6.2\%$ and $81.53 \pm 3.4\%$ in the adaptation stage (phase III₁), which slightly

increased (81.6 ± 4.1 % and 82.4 ± 2.4 %) during the stable operation stage (phase III_2), indicating that the increase of influent COD improved nitrogen removal performance but not significantly. It is worth noting that the NRE is subject to the influent composition and can be directly compared between different operation phases only when the influent ammonium to nitrite concentration ratio is the same. Due to the lower NO₂⁻-N to NH₄⁺-N influent concentration ratio in phase III than in phase I and II (Table 2.1), the NRE of phase III could not be compared to that of phase I and II. On the other hand, the measured ratios of $\Delta\text{NO}_2^-/\Delta\text{NH}_4^+$ and $\Delta\text{NO}_3^-/\Delta\text{NH}_4^+$ are directly related to the stoichiometry of the actual conversions in the reactor and thus could be used for direct comparison between different operation phases. The measured ratios of $\Delta\text{NO}_2^-/\Delta\text{NH}_4^+$ and $\Delta\text{NO}_3^-/\Delta\text{NH}_4^+$ were 1.23 ± 0.02 and 0.21 ± 0.02 in phase III_1, which decreased to 1.21 ± 0.06 and 0.20 ± 0.03 in phase III_2. The lower $\Delta\text{NO}_3^-/\Delta\text{NH}_4^+$ ratio in phase III compared to that of phase I & II (without COD addition), indicates that less NO₃⁻ was accumulated per NH₄⁺ consumed, i.e., NO₃⁻ produced in the anammox reaction was partly reduced due to the influent COD addition. The even lower $\Delta\text{NO}_3^-/\Delta\text{NH}_4^+$ in phase III_2 than in phase III_1 indicates that more NO₃⁻ was reduced with the increase of influent COD (see also Fig. A2.2), as confirmed in the decreased effluent NO₃⁻ concentration in phase III_2 (Fig. 2.2). Analogously, the lower $\Delta\text{NO}_2^-/\Delta\text{NH}_4^+$ ratio in phase III than in phase I & II indicates that more NH₄⁺ was consumed per influent NO₂⁻ due to the influent COD addition as NO₂⁻ was the limiting substrate in the influent and was nearly completely consumed throughout the first three phases (mostly < 1 mg NO₂⁻-N.L⁻¹ in the effluent, Fig. 2.2). The interpretation of these observations is further elaborated in Section 2.3.3.

The effluent of the reactor was blocked on day 384 and the reactor was thus opened and cleaned, leading to air exposure (thus possible oxygen inhibition on anammox activity) and to some biomass loss. Consequently, the nitrogen removal efficiency sharply dropped at the beginning of phase IV, resulting in a high concentration of ammonium and nitrite in the effluent (Fig. 2.2). Nevertheless, the reactor recovered gradually by lowering the nitrogen load rate from 0.4 to 0.2 kg N.m⁻³d⁻¹ (Table 2.1), as shown by the decreasing ammonium and nitrite concentration and increasing nitrate concentration and nitrogen removal efficiencies (Fig. 2.2).

2.3.2 Stoichiometry of the Anammox process

2.3.2.1 Application of general procedure – verification to literature reports

The anammox stoichiometry is crucial for the design, modelling and mass balancing of anammox-based processes. Regarding the anammox stoichiometry, substantially different results were reported in the literature (e.g., Eq. 2.1 vs. Eq. 2.2, Table 2.2). Following the generalized method of Kleerebezem and van Loosdrecht (2010) (detailed in Appendix, Section A2.1), the theoretical stoichiometry of the overall anammox metabolism (Eq. 2.5, Table 2.2) was derived from the underlying catabolic and anabolic reactions (Eq. 2.3 and Eq. 2.4, Table 2.2) as a function of biomass composition (CH_xO_yN_z) and the measured yield coefficient Y_{X/NH_4}^{Met} .

The theoretical anammox stoichiometry was calculated (as Eq. 2.5, Table 2.2) for the measured biomass composition and yield from the studies of Strous et al. (1998) and Lotti et al. (2014b) as Eq. 2.6 and Eq. 2.7 (Table 2.2), respectively. Comparison of the original anammox stoichiometry reported by Strous et al. (1998) with the theoretical one based on the experimental values from the same paper (Eq. 2.1 vs. Eq. 2.6, Table 2.2) shows a mismatch: the $\Delta NO_2^-/\Delta NH_4^+$ ratios diverge by 13.6% (1.140 vs. 1.32) and the $\Delta NO_3^-/\Delta NH_4^+$ ratios by 42.7% (0.160 vs. 0.26). In contrast, the stoichiometry put forward by Lotti et al. (2014b) perfectly matched the theoretical calculation in this study (Eq. 2.2 vs. Eq. 2.7, Table 2.2).

Table 2.2. Stoichiometry of the anammox reaction: general expression. Negative stoichiometric coefficients indicate consumption (for substrates); positive stoichiometric coefficients are for products.

Source	NH ₄ ⁺	NO ₂ ⁻	HCO ₃ ⁻	H ⁺	CH _x O _y N _z	NO ₃ ⁻	N ₂	H ₂ O	Equation number
Literature expressions									
Strous et al. (1998)	-1.000	-1.32	-0.066	-0.13	0.066	0.26	1.02	2.03	Eq. 2.1
Lotti et al. (2014)	-1.000	-1.146	-0.071	-0.057	0.071	0.161	0.986	2.002	Eq. 2.2
Generalized stoichiometry #									
Catabolism	-1.000	-1.000					1.000	2.000	Eq. 2.3
Anabolism	-z	$-\frac{4+x-2y-3z}{2}$	-1.000	-(1-z)	1.000	$\frac{4+x-2y-3z}{2}$		$\frac{2-x+3z}{2}$	Eq. 2.4
Metabolism	$-\frac{1}{Y_{X/NH_4}^{Met}}$	$-\left(\frac{4+x-2y-3z}{2} + \frac{1}{Y_{X/NH_4}^{Met}} - z\right)$	-1.000	-(1-z)	1.000	$\frac{4+x-2y-3z}{2}$	$\frac{1}{Y_{X/NH_4}^{Met}} - z$	$\frac{2-x-z}{2} + \frac{2}{Y_{X/NH_4}^{Met}}$	Eq. 2.5
Calculation based on generalized stoichiometry and measured values ##									
Strous et al. (1998)	-1.000	-1.140	-0.066	-0.056	0.066	0.150	0.990	1.995	Eq. 2.6
Lotti et al. (2014)	-1.000	-1.146	-0.071	-0.057	0.071	0.160	0.986	2.002	Eq. 2.7
This study	-1.000	-1.240	-0.117	-0.093	0.117	0.263	0.977	2.003	Eq. 2.8

#Defined per mole C-x formed for a general biomass composition (CH_xO_yN_z); ##Calculated according to the generalized method while keeping the measured biomass composition and yield as in the original articles, i.e., CH₂O_{0.5}N_{0.15} and 0.066 mole C-x.(mole NH₄-N)⁻¹ for Strous et al. (1998) CH_{1.74}O_{0.31}N_{0.20} and 0.071 mole C-x.(mole NH₄-N)⁻¹ for Lotti et al. (2014b)

The reported stoichiometric ratios of $\Delta\text{NO}_2^-/\Delta\text{NH}_4^+$ (1.32) and $\Delta\text{NO}_3^-/\Delta\text{NH}_4^+$ (0.26) from Strous et al. (1998) (Eq. 2.1, Table 2.2) were in many cases well in line with measurements from other studies (Table A2.3). For example, the corresponding values from the measurement in a full-scale anammox reactor were 1.31 ± 0.46 and 0.25 ± 0.09 , respectively (van der Star et al., 2007). These two ratios were thus often used as operation indicators and design parameters of the upstream partial nitritation process and the anammox process. Nevertheless, the accuracy of the anammox stoichiometry defined by Strous et al. (1998) may have been compromised due to: 1) the 50% uncertainty in the VSS measurement; 2) the incomplete (74%) enrichment degree of anammox bacteria in the SBR reactor; 3) the significant error in the electron balance of the measured conversion rates used for stoichiometric equation calculation (Lotti et al., 2014b; Strous et al., 1998). On the other hand, the long-term steady-state data set used in Lotti et al. (2014b) was statistically more stable than that of Strous et al. (1998) as apparent from the deviations of the measured data set and the balanced data set before and after applying data reconciliation (see Table A2.4) (Lotti et al., 2014b).

The overall metabolic anammox stoichiometry and the biomass yield coefficient in this study were also determined (Eq. 2.8, Table 2.2, detailed in Example 2 in Appendix) from the measured $\Delta\text{NO}_2^-/\Delta\text{NH}_4^+$ (1.24) during the reactor operation without COD addition (phase I&II) and assuming the same anammox biomass composition ($\text{CH}_{1.74}\text{O}_{0.31}\text{N}_{0.20}$) as in Lotti et al. (2014b). The calculated yield coefficient ($Y_{X/\text{NH}_4}^{\text{Met}}$) was $0.117 \text{ mole C-x.}(\text{mole NH}_4\text{-N})^{-1}$, which is in the range of previously reported values in literature (0.066-0.146 mole C-x.(mole NH₄-N)⁻¹, Table A2.3). This yield coefficient (corresponding to 0.301 g COD.g NH₄-N⁻¹) was further used in the mass balance calculations in Section 2.3.3.

Noteworthy is that the generalized method demonstrated in this study can be easily used to derive case-specific anammox stoichiometry for other studies with commonly measured parameters.

2.3.2.2 Anammox stoichiometry expressed in ASM format

Mathematical models are powerful tools for process design and optimization. Based on the concept of the Activated Sludge Models (ASMs) (Henze et al., 2000), the

anammox process stoichiometry has been typically expressed as in Eq. 2.9 (Table 2.3) (Hao et al., 2002a; Ni et al., 2012; Volcke et al., 2010). The state variables of the ASMs are expressed in g COD.m⁻³ and g N.m⁻³ and the stoichiometric coefficients are defined accordingly (Table 2.3). Unit conversion is thus required to compare these stoichiometric coefficients with those expressed in mole.mole⁻¹ (Table 2.2), as demonstrated with an example in the Appendix (A2.3, Eq. A2.22).

The widely applied ASM-based anammox reaction stoichiometry (Eq. 2.9, Table 2.3) can be divided into a catabolic and an anabolic reaction stoichiometry (Eq. 2.10 and Eq. 2.11, Table 2.3). It thus becomes clear that NH₄-N is consumed in both catabolic and anabolic reactions (Eq. 2.10 and Eq. 2.11, Table 2.3) in the anammox process, while the yield coefficient Y^{Mod} (g COD.g NH₄-N⁻¹) in the model only accounts for the NH₄-N consumed in the catabolic reaction. In practical experiments, the overall ratio of biomass formed to NH₄-N consumed is measured (defined as $Y_{X/NH_4}^{Met'}$, g COD.g NH₄-N⁻¹), accounting for NH₄-N consumed in both catabolic and anabolic reaction. Therefore, the experimentally measured yield ($Y_{X/NH_4}^{Met'}$) cannot be directly implemented as Y^{Mod} in Eq. 2.9 (Table 2.3). The yield for the overall metabolic reaction, experimentally determined by Strous et al. (1998) ($Y_{X/NH_4}^{Met'}=0.066$ mole C-biomass per mole NH₄-N or correspondingly 0.172 g COD.g NH₄-N⁻¹) was mistakenly used in many simulation studies (Hao et al., 2002a; Ni et al., 2012; Volcke et al., 2010) as if it were Y^{Mod} (Eq. 2.9, Table 2.3). This is conceptually wrong and may induce systematic errors in simulation studies.

Table 2.3. Anammox stoichiometry expressed in ASM format

Source		NH ₄ -N (g N.m ⁻³)	NO ₂ -N (g N.m ⁻³)	X _{AN} (g COD.m ⁻³)	NO ₃ -N (g N.m ⁻³)	N ₂ -N (g N.m ⁻³)	Equation number
Literature e.g., Volcke et al. (2010)	Met	$-\left(\frac{1}{Y^{Mod}} + i_{NXB}\right)$	$-\left(\frac{1}{Y^{Mod}} + \frac{1}{1.14}\right)$	1	$\frac{1}{1.14}$	$\frac{2}{Y^{Mod}}$	Eq. 2.9
	Cat	$-\frac{1}{Y^{Mod}}$	$-\frac{1}{Y^{Mod}}$			$\frac{2}{Y^{Mod}}$	Eq. 2.10
	An	$-i_{NXB}$	$-\frac{1}{1.14}$	1	$\frac{1}{1.14}$		Eq. 2.11
Alternative, this study	Met	$-\frac{1}{Y_{X/NH_4}^{Met'}}$	$-\left(\frac{1}{1.14} + \frac{1}{Y_{X/NH_4}^{Met'}} - i_{NXB}\right)$	1	$\frac{1}{1.14}$	$2^*\left(\frac{1}{Y_{X/NH_4}^{Met'}} - i_{NXB}\right)$	Eq. 2.12
	Cat	$-\left(\frac{1}{Y_{X/NH_4}^{Met'}} - i_{NXB}\right)$	$-\left(\frac{1}{Y_{X/NH_4}^{Met'}} - i_{NXB}\right)$			$2^*\left(\frac{1}{Y_{X/NH_4}^{Met'}} - i_{NXB}\right)$	Eq. 2.13
	An	$-i_{NXB}$	$-\frac{1}{1.14}$	1	$\frac{1}{1.14}$		Eq. 2.14

$Met = Cat + An$; Y^{Mod} represents the biomass production per amount of NH₄-N consumed in the catabolic reaction (g COD.g NH₄-N⁻¹), which is the yield coefficient used in many simulation studies; i_{NXB} represents the nitrogen content of anammox bacteria (g N.g COD⁻¹); $Y_{X/NH_4}^{Met'}$ represents the biomass production per g NH₄-N consumed in the overall metabolic reaction, i.e., the metabolic yield coefficient of anammox biomass over ammonium (g COD.g NH₄-N⁻¹).

Since the model yield Y^{Mod} in Eq. 2.9 (Table 2.3) cannot be determined in a straightforward way, we propose for use in an ASM modelling context an alternative anammox stoichiometric equation based on the biomass yield per amount of NH₄-N consumed in the overall metabolic reaction, $Y_{X/NH_4}^{Met'}$, as denoted in Eq. 2.12 (Table 2.3). The underlying catabolic and anabolic reaction stoichiometries are given by Eq. 2.13 and Eq. 2.14 (Table 2.3), respectively. Alternatively, Eq.9 (Table 2.3) can be kept. However, in this case, the Y^{Mod} in the widely used anammox model needs to be recalculated from the measured $Y_{X/NH_4}^{Met'}$ through Eq. 2.15.

$$Y^{Mod} = \frac{1}{\frac{1}{Y_{X/NH_4}^{Met'}} - i_{NXB}} \quad (2.15)$$

The same modelling issue also arises for other bioconversion reactions in which the substrate, relative to which the yield coefficient is defined, is consumed in both the catabolic and anabolic reaction. For instance, aerobic ammonium-oxidizing microorganisms (AOM, including ammonium-oxidizing bacteria/archaea and comammox bacteria) consume ammonium as an electron donor to produce nitrite/nitrate in the catabolic reaction and as N-source for biomass synthesis in the anabolic reaction. Also in these cases, Eq. 2.15 can be used for the correction of yield coefficient over ammonium while modelling of AOM in ASM format.

2.3.3 Process identification and quantification using mass balances

The anammox reactor was in anoxic operation and fed with ammonium, nitrite and organic carbon. Therefore five processes were considered to possibly take place: anammox conversion of NH₄⁺ and NO₂⁻ to nitrogen gas and NO₃⁻ (P1), decay of anammox bacteria (P2), heterotrophic denitrification of NO₂⁻ to N₂O or N₂ (P3, denitrification) and of NO₃⁻ to NO₂⁻ (P4, partial denitrification, i.e., denitrification) and decay of heterotrophic denitrifiers (P5) (Fig. 2.3a). In order to identify which of these five processes contributed to nitrogen and COD conversion and to quantify their respective activities, mass balances were set up to describe phase III_2 in which the COD concentration was the highest. In doing so, ingoing and outgoing component concentrations were linked to the conversion rates (see Section 2.2.4 and Spreadsheet A.2.2 in Appendix). In brief, four independent mass balances equations were set up from the measured ammonium, nitrite, nitrate, and assumed COD conversions. The

decay rate of anammox bacteria (ρ_2) was calculated from the decay coefficient (Hao and van Loosdrecht, 2004) and the measured biomass concentration in the reactor (Spreadsheet A.2.2 in Appendix), reducing the number of unknown process rates from 5 to 4. The remaining four unknown process rates could thus be solved from four independent mass balances.

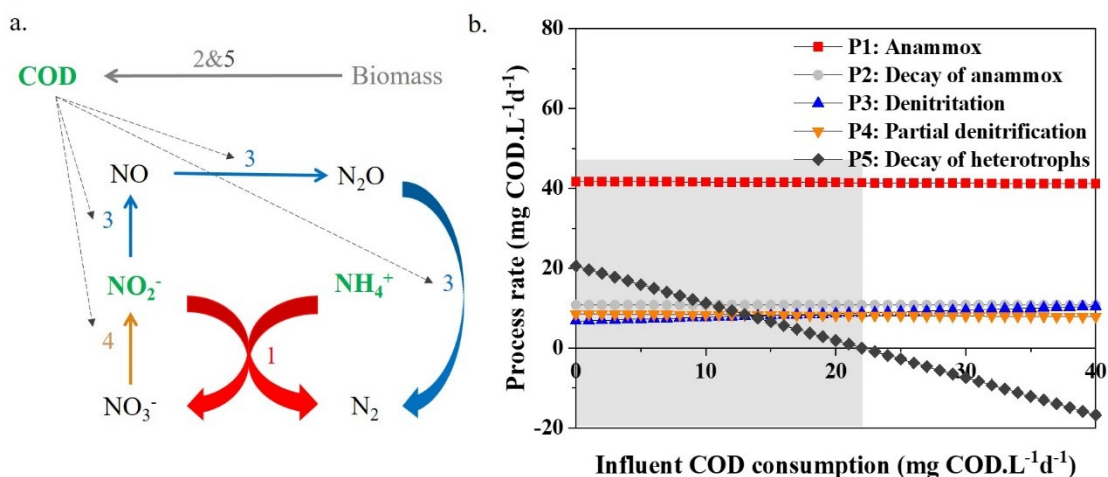


Figure 2.3. Possible processes in the anoxic granular sludge anammox reactor (a) and calculated process rates (ρ) in terms of assumed influent COD consumption (b).

Due to the large uncertainty in the COD measurement, mass balance calculations were performed within a range of 0 to 80 mg COD.L⁻¹.d⁻¹ to estimate the actual COD consumption and the resulting process rates (ρ) are presented in Fig. 2.3b. Positive process rates were obtained for a COD consumption rate up to 22 mg COD.L⁻¹.d⁻¹, corresponding to a converted amount of influent COD equal to 22 mg COD.L⁻¹ (given the HRT=1d.), which is lower than the applied influent concentrations (40 mg COD.L⁻¹). Overall, the calculated process rates (ρ) for the four processes were relatively constant, and the influent COD consumption only strongly affected the process rate of decay of heterotrophs (P5, Fig. 2.3b).

The contribution of the five processes in the conversion of each substrate was further illustrated in Fig. 2.4. As expected, the anammox process (P1) was the dominant process for ammonium conversion and all other ammonium conversion processes were negligible (Fig. 2.4a). The nitrate produced from the anammox process (P1) hardly varied with varying influent COD consumption (36.4-36.6 mg N.L⁻¹.d⁻¹). The

mass balance revealed that approximately 18% of the produced nitrate was reduced to nitrite by partial denitrification (P4) (Fig. 2.4b). The nitrite produced via partial denitrification (P4) could be further reduced by the anammox process (P1) and/or denitrification process (P3). The calculation shows that 53-72% of the produced nitrite was converted by denitrification (P3) to nitrogen gas and/or N₂O (P3 relative to P4, Fig. 2.4c). The remainder of the produced nitrite was converted by the anammox process (P1). Regarding the COD conversion, partial denitrification (P4) and denitrification (P3) almost equally contributed to COD consumption, whereas the predicted COD production from the decay of heterotrophs (P5) decreased with increasing assumed influent COD consumption (Fig. 2.4d) as together they were providing the COD for consumption.

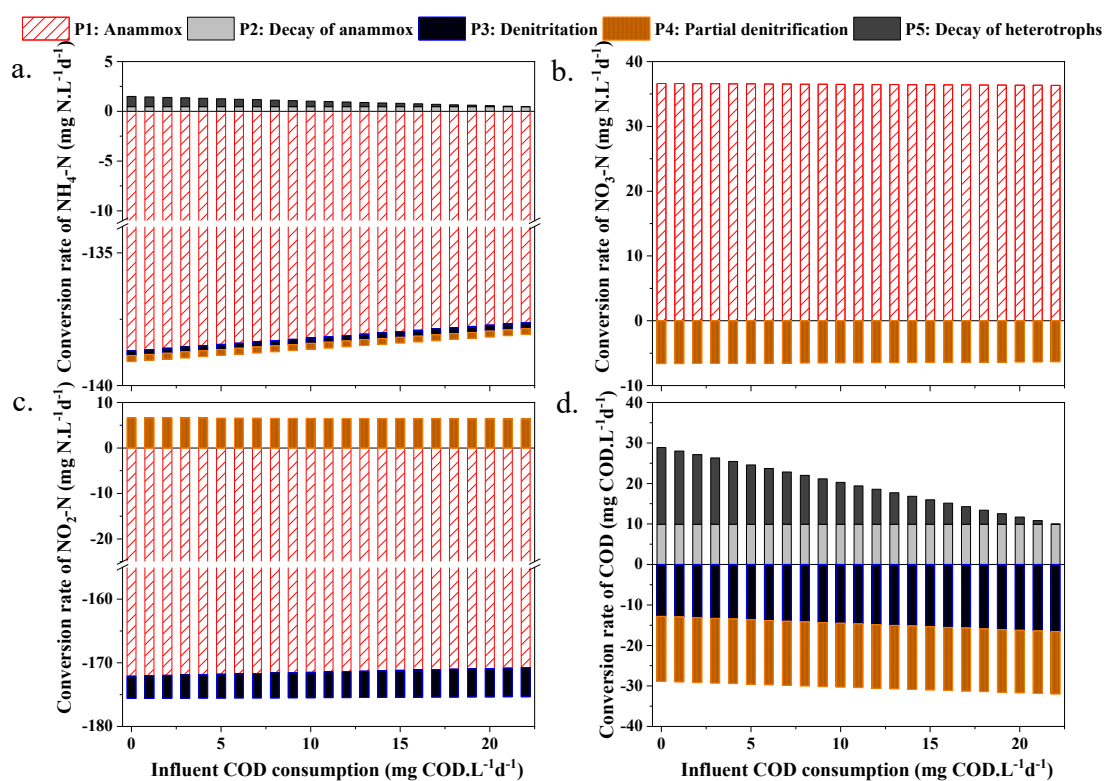


Figure 2.4. Contribution of individual processes in the conversion of NH₄-N (a), NO₃-N (b), NO₂-N (c) and COD (d), as a function of influent COD consumption rate (expressed as conversion rate r , positive values for production and negative values for consumption)

The results from this study were in line with previous experimental (Kumar and Lin, 2010; Ni et al., 2012) and modelling (Hao and van Loosdrecht, 2004; Mozumder et al., 2014) studies which showed that the availability of some influent COD can lower the

effluent nitrate concentration due to heterotrophic denitrification and thus increase the total nitrogen removal efficiency of anammox reactors. Another possible explanation for the nitrate reduction is the dissimilatory nitrate reduction to ammonium (DNRA) by anammox bacteria (Kartal et al., 2007). In the DNRA process, nitrate is first reduced to nitrite (partial DNRA) and further reduced to ammonium, using organic carbon as an electron donor. Partial DNRA by anammox bacteria was shown to be thermodynamically favourable over heterotrophic denitrification under low COD/N conditions, i.e., more Gibbs free energy production per unit of organic carbon in the partial DNRA-anammox process (Castro-Barros et al., 2017). In our system, the maximum nitrate production by normal anammox reaction in phase III was 40 mg NO₃-N.L⁻¹, yielding a COD/NO₃-N ratio of approximately 1 (g COD.g NO₃-N⁻¹), which might have promoted the partial DNRA (NO₃⁻ → NO₂⁻) by anammox bacteria (Winkler et al., 2012). However, adding the partial DNRA by anammox bacteria to the current mass balance equation system would result in an underdetermined equation system (i.e., the rank of the equation system is lower than the unknowns) and was therefore not determined in this study.

In many anammox studies, the presence of heterotrophs was ignored and the COD in the reactor was neither measured nor considered in mass balances (Schielke-Jenni et al., 2015). Nevertheless, heterotrophic denitrifiers have been widely found in anammox reactors and can account for up to 23% of the biomass in biofilm reactors even without organic matter in the influent (Kumar and Lin, 2010; Ni et al., 2012). Besides, most wastewater streams fed to anammox reactors contain certain amounts of organic matter (Cao et al., 2017). Even though in two-stage PN/A systems most of the easily biodegradable COD (e.g., acetate) is normally removed in the preceding partial nitrification step, residual particulate COD could be hydrolyzed to volatile fatty acids due to long retention time of the anammox granules (De Graaff et al., 2011). Besides, organic carbon entering the anammox reactor can also be expected in alternative process configurations, such as in the DEAMOX (DENitrifying AMmonium OXidation) process (Kalyuzhnyi et al., 2006) which consists of partial denitrification (nitrate to nitrite) by heterotrophic denitrifiers followed by an anammox process and which is applied for the treatment of nitrate-rich industrial wastewaters (Cao et al., 2016; Du et al., 2017) or as an alternative way of implementing anammox in the mainstream (Ma et al., 2017). In this process, the presence of the easily biodegradable COD (e.g.,

acetate) is a prerequisite for nitrite production in the partial denitrification step. The effluent of the partial denitrification reactor contains both nitrite and a small amount of residual COD, which will then be fed together with the ammonium-containing stream to the anammox reactor. Overall, it is clear that heterotrophs will be of importance to anammox-based systems. The method demonstrated in this study can be easily used to estimate the impact of heterotrophic denitrification in anammox reactors even without COD measurement.

2.3.4 Impact of influent organic matter on N₂O emission

The measured N₂O concentration and calculated N₂O emission factor (EF_{N₂O}, defined as the ratio of N₂O-N over incoming nitrogen load) in the different operating phases are displayed in Fig. 2.5. The average N₂O emission factor was 0.13% in phase II without organic substrate in the influent. It increased significantly ($p < 0.05$) to 0.17% in phase III_1 with influent COD concentration of 8 mg COD.L⁻¹ (corresponds to COD/TN~0.02). This trend further increased significantly ($p < 0.05$) to 0.46% in phase III_2 when the influent COD concentration was 40 mg COD.L⁻¹ (corresponds to COD/TN~0.1). This emission factor in phase III_2 (0.46%) was 2.7 times and 3.5 times as high as in phase III_1 (0.17%) and phase II (0.13%), respectively.

The N₂O emission level (0.13-0.46% of the incoming nitrogen load) in this study was comparable to the values reported in other studies concerning a granular sludge anammox reactor following a partial nitrification stage. For example, the N₂O emission from the granular sludge anammox reactor was 0.36% of the nitrogen load in a full-scale two-stage PN/A process treating reject water (Kampschreur et al., 2008) and 0.1% ± 0.07% of the nitrogen load in a lab-scale two-stage PN/A process receiving inorganic synthetic wastewater mimicking typical sidestream conditions (Okabe et al., 2011). The latter is close to that of phase II in this study (0.1% vs. 0.13%) where no organic matter was fed either.

Regarding the source of N₂O production, since anammox bacteria are lacking the genes to produce N₂O (Strous et al., 2006), the relatively high N₂O emission with influent COD can be attributed to heterotrophic denitrifiers. Previous studies with micro-sensors and isotopic analyses suggested that the N₂O production in anammox granular sludge originated from heterotrophic denitrifiers present in the inner part of

the granules (Ali et al., 2016; Okabe et al., 2011). Our results from the mass balance calculations showed that the denitrification process by heterotrophic bacteria increased with increasing COD concentration (Fig. 2.4d). The concurrent increase in N₂O emissions in phase III corroborates that the denitrification process contributed to N₂O production. The N₂O emission in phase II (without COD addition) was most likely generated by heterotrophs that grew on decay products.

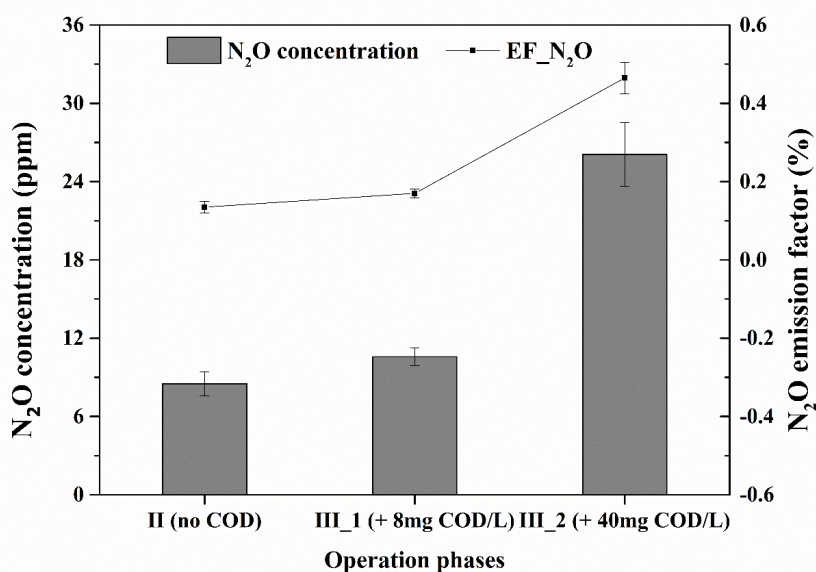


Figure 2.5. N₂O concentration in the off-gas and emission factor of the granular sludge anammox reactor. The error bar indicates standard deviations of the measurements.

Mass balancing over N₂O further revealed that the nitrogen released as N₂O was 1.9 mg N₂O-N.L⁻¹d⁻¹ in phase III_2 (COD/TN~0.1), accounting for approximately 29% of the nitrate being reduced by partial denitrification (P4 in Fig. 2.4b, i.e., 5% of the nitrate produced by the anammox reaction (P1 in Fig. 2.4b)). This was most likely the result of the carbon-limited condition in phase III (the theoretically maximum COD/NO₃-N ratio was approximately 1 in phase III, see paragraph 4 in Section 2.3.3), which is known to favor N₂O accumulation and emission during heterotrophic denitrification (Kampschreur et al., 2009). The gas recirculation for mixing and suspension of granules in this bubble column reactor may also facilitate the N₂O produced to be emitted into the gas phase. Besides, the CO₂ concentration in the off-gas was also measured and the CO₂ emission increased concurrently with the increasing influent COD (Fig. A2.3, Appendix). These results suggest that although small amounts of COD

can increase nitrogen removal efficiency, the greenhouse gas emissions (and thus the carbon footprint) will increase at the same time.

The N₂O emission from an anammox reactor with COD present in the influent could be potentially mitigated by several means: 1) by maintaining a low nitrite concentration in the reactor as nitrite is known to increase N₂O during denitrification (Kampschreur et al., 2009), e.g., by keeping nitrite as the limiting substrate in the influent (De Graaff et al., 2011); 2) by avoiding rapid changing process conditions (e.g., caused by varying influent nitrite concentrations) (Law et al., 2012); 3) through selective removal of flocs or smaller granules in the granular sludge anammox reactor as the fast growing heterotrophs are reported to preferably grow in these forms (Laureni et al., 2015; Winkler et al., 2011); 4) by lowering the gas flow rate and thus reduce stripping of produced N₂O – while keeping a minimum gas flow rate to ensure the mass transfer (mixing) in the reactor and the shear force acting on granules; 5) by increasing the availability of COD (higher COD/N ratio) as low COD/N conditions favor N₂O emission during heterotrophic denitrification (Kampschreur et al., 2009) – however, this may lead to the proliferation of heterotrophs and thus the washout of anammox bacteria. Further research is needed to evaluate the effect of COD on the nitrogen removal efficiency of and N₂O emissions from anammox reactor systems to ensure that the improvement of effluent quality is not offset by increased greenhouse gas emissions.

2.4 Conclusions

The effect of influent organic matter on the performance and N₂O emission of a lab-scale granular sludge anammox reactor was investigated in this study. The stoichiometry of anammox process and the contribution of processes potentially taking place in the reactor were analysed through elemental and mass balances, respectively.

- The overall anammox stoichiometry was calculated as a function of the biomass composition (CH_xO_yN_z) and the measured yield coefficient, according to a general procedure that can easily be applied for other experimental studies.
- The anammox biomass yield coefficient on the amount of ammonium consumed in the overall metabolic reaction has been mistakenly used in many simulation studies as if it were the yield coefficient relative to the ammonium consumed in the catabolic reaction. Approaches for correction were proposed.

- Small amounts of influent COD (COD/TN~0.1 g COD.g N⁻¹) resulted in a lower effluent nitrate concentration and thus slightly improved the nitrogen removal efficiency of the anammox reactor.
- The average N₂O emission in the granular sludge anammox reactor increased by 2.5 times with increasing influent COD concentration and accounted for up to 0.46% of the incoming nitrogen load (COD/TN~0.1 g COD.g N⁻¹).
- Mass balance analysis revealed that approximately 18% of the nitrate produced from the anammox conversion was reduced to nitrite by heterotrophic denitrification and the nitrogen emitted as N₂O could account for 29% of this produced nitrite (COD/TN~0.1 g COD.g N⁻¹).

Acknowledgements

Mingsheng Jia acknowledges the support from China Scholarship Council (CSC) and the special research fund (BOF) from Ghent University. Celia M. Castro-Barros has received funding from the People Program (Marie Curie Actions) of the European Union's Seventh Framework Programme FP7/2007-2013 (Project SANITAS) and the special research fund (BOF) (no. 01DI4415), Ghent University. Mari Winkler was funded by a Marie Curie Intra-European fellowship (PIEF-GA-2012-329328). The authors further thank the staff of the Dokhaven WWTP in Rotterdam (NL) for providing the biomass used in this study.

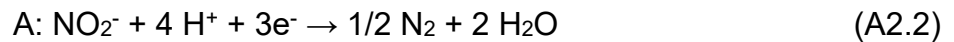
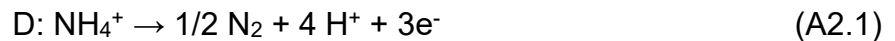
Appendix

A2.1 Calculation of the anammox reaction stoichiometry

This section presents a calculation scheme for the catabolic and anabolic reaction stoichiometry of the anammox conversion, for a general biomass composition (CH_xO_yN_z). The catabolic and anabolic reactions were subsequently linked through a general parameter to be determined in practice (yield or product ration), resulting in a general reaction stoichiometry for the overall metabolic anammox reaction. The generalized method of Kleerebezem and Van Loosdrecht (2010) was followed.

A2.1.1 Stoichiometry of the catabolism

To determine the stoichiometry of any other redox reaction, it is convenient to first define the electron donor and electron acceptor half-reaction. Regarding the catabolic reaction of the anammox process, the electron donor and acceptor reaction equations (D and A) are:

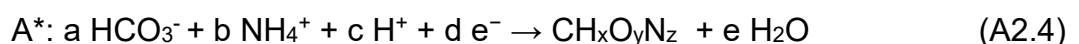


By balancing the electrons in Eq. A2.1 and Eq. A2.2, the overall stoichiometry of the catabolism (Cat) is obtained as:



A2.1.2 Stoichiometry of the anabolism

The anabolic reaction describes the production of biomass from a carbon and a nitrogen source. For the anammox process, the carbon source is bicarbonate (HCO₃⁻) and the nitrogen source is ammonium (NH₄⁺). Since the carbon source (HCO₃⁻) is more oxidized than biomass, the half-reaction for anammox biomass production with a general elemental composition (CH_xO_yN_z) is an electron acceptor reaction and can be written as:

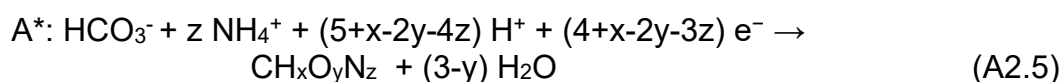


where CH_xO_yN_z represents a generalized elemental composition of anammox biomass. Note that the stoichiometry of the anabolic reaction equation is defined per C-mole of biomass (C-x) formed. The stoichiometric coefficients a, b, c, d and e are

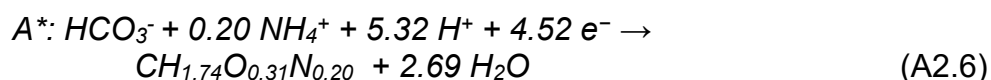
derived as a function of biomass composition (x, y and z), from the elemental and charge balances, as follows:

- (1) C-balance: $a = 1$
- (2) N-balance: $b = z$
- (3) O-balance: $3 \cdot a = y + e$
- (4) H-balance: $a + 4 \cdot b + c = x + 2 \cdot e$
- (5) Charge-balance: $(-1) \cdot a + 1 \cdot b + 1 \cdot c + (-1) \cdot d = 0$

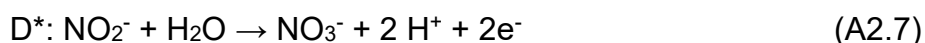
Solving these equations, the half reaction of anammox biomass production (Eq. A2.4) becomes:



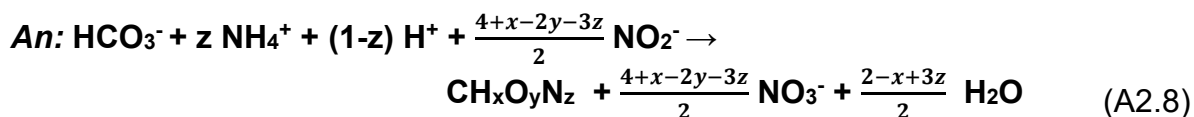
Example 1a: for an anammox biomass composition $\text{CH}_{1.74}\text{O}_{0.31}\text{N}_{0.20}$ (Lotti et al., 2014b), Eq. A2.5 becomes:



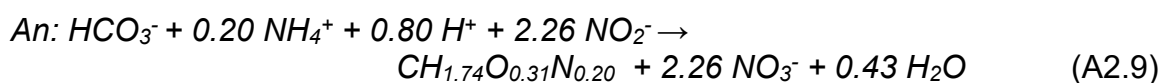
The electrons needed in the anabolism reaction (Eq. A2.5) are obtained from nitrite (NO_2^-) as the electron donor, according to the following half-reaction for electron donor (D^*):



The overall stoichiometry of the anabolism of anammox process is obtained by balancing the electrons in Eq. A2.5 and Eq. A2.7:



To continue with the Example 1a, for a biomass composition of $\text{CH}_{1.74}\text{O}_{0.31}\text{N}_{0.20}$, the overall anabolism is:



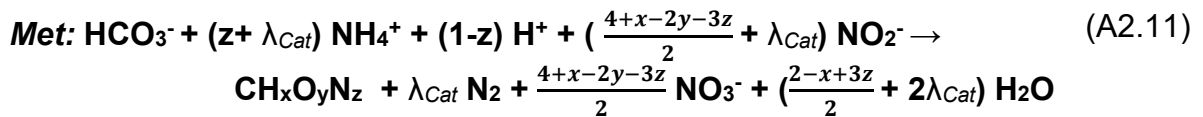
A2.1.3 Stoichiometry of the overall anammox metabolism

The stoichiometry of the metabolic reaction (Met) can be defined as a linear combination of the catabolic (Cat) and anabolic (An) reaction stoichiometries:

$$Met = \lambda_{Cat} \cdot Cat + \lambda_{An} \cdot An \quad (A2.10)$$

As for the anabolic reaction equation, the metabolic reaction stoichiometry will be defined per C-mole biomass formed, so $\lambda_{An} = 1$. Thermodynamically, the multiplication factor of the catabolism (λ_{Cat}) can be regarded as the number of times the catabolic reaction needs to run to generate sufficient Gibbs energy to produce one C-mol of biomass.

Following Eq. A2.10, the metabolic reaction (Met) is expressed as a function of biomass composition and the multiplication factor of the catabolism (λ_{Cat}):



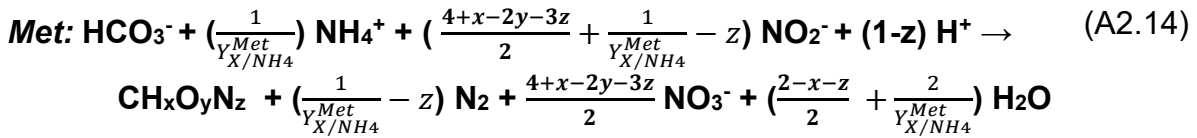
One stoichiometric coefficient that links the catabolism with the anabolism needs to be determined experimentally in order to derive λ_{Cat} and thus the overall metabolic reaction stoichiometry. Typically, this stoichiometric coefficient is the biomass yield coefficient $Y_{X/S}^{Met}$ (mole C-x/mole S), i.e., the biomass (X) production per unit of substrate (S) consumed in the overall metabolic reaction (Met). For instance, identification of the measured anammox biomass yield on ammonium, Y_{X/NH_4}^{Met} (mol C-x/mol NH₄⁺, absolute value), with Eq. A2.11 results in:

$$Y_{X/NH_4}^{Met} = \frac{1}{z + \lambda_{Cat}} \quad (A2.12)$$

From Eq. (A2.12), the multiplication factor of the catabolism (λ_{Cat}) follows as:

$$\lambda_{Cat} = \frac{1}{Y_{X/NH_4}^{Met}} - z \quad (A2.13)$$

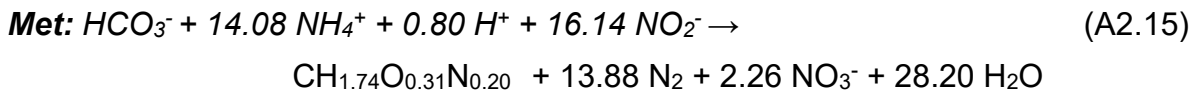
Substitution of Eq. A2.13 in Eq. A2.11 yields the stoichiometry of the overall metabolic reaction for the anammox conversion, as a function of the biomass composition and the biomass yield on ammonium:



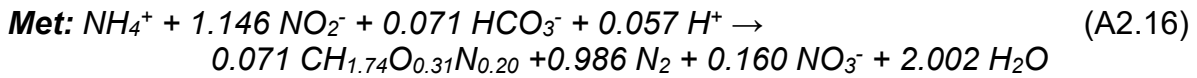
To continue with Example 1a, for a measured biomass composition of CH_{1.74}O_{0.31}N_{0.20} and a measured biomass yield Y_{X/NH_4}^{Met} of 0.071 mole C-x/ mole NH₄⁺ (Lotti et al., 2014b), the multiplication factor (λ_{Cat}) is calculated from Eq. A2.13 as:

$$\lambda_{Cat} = \frac{1}{Y_{X/NH_4}^{Met}} - z = \frac{1}{0.071} - 0.20 = 13.9$$

and the overall metabolic reaction Eq. A2.14, expressed per C-mole biomass formed, becomes:



The overall metabolic reaction can also be defined per mole NH₄⁺ consumed:



While Eq. A2.14 represents the overall metabolic anammox conversion stoichiometry as a function of the biomass yield on ammonium, this stoichiometry can alternatively be expressed based on the measurement of the rates of consumption or production of any two compounds participating in the metabolic system. The determination of the biomass yield on ammonium can be regarded as a specific case where the biomass (X) production rate and a substrate (S) consumption rate were determined. In the case of the anammox reaction, often the ratio of the consumption rates of nitrite and ammonium in the overall anammox process is determined (Y_{NO_2/NH_4}^{Met} , in mole NO₂/mole NH₄). By definition, the Y_{NO_2/NH_4}^{Met} can be expressed from Eq. A2.11 as:

$$Y_{NO_2/NH_4}^{Met} = \frac{\frac{4+x-2y-3z}{2} + \lambda_{Cat}}{z + \lambda_{Cat}} \quad (\text{A2.17})$$

The multiplication factor of the catabolism (λ_{Cat}) is derived from Eq. A2.16 as:

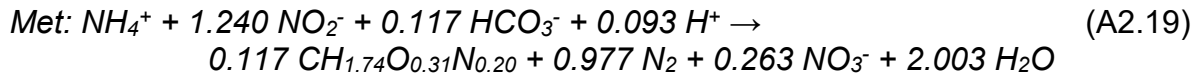
$$\lambda_{Cat} = \frac{Y_{NO_2/NH_4}^{Met} \cdot z - \frac{4 + x - 2y - 3z}{2}}{1 - Y_{NO_2/NH_4}^{Met}} \quad (A2.18)$$

Example 1b: The stoichiometry of Lotti et al. (2014b) can also be expressed based on the ratio of the measured consumption rates of nitrite and ammonium (Y_{NO_2/NH_4}^{Met}), namely 1.146 and the measured biomass composition of $CH_{1.74}O_{0.31}N_{0.20}$. The multiplication factor (λ_{Cat}) is then calculated from Eq. A2.17 as

$$\lambda_{Cat} = \frac{Y_{NO_2/NH_4}^{Met} \cdot z - \frac{4 + x - 2y - 3z}{2}}{1 - Y_{NO_2/NH_4}^{Met}} = \frac{1.146 * 0.20 - 2.26}{1 - 1.146} = 13.9$$

which is the same as the one calculated based on the measured biomass yield. The corresponding overall metabolic stoichiometry is thus identical to Eq. A2.16.

Example 2: In our study, with the ratio of the measured consumption rates of nitrite and ammonium (Y_{NO_2/NH_4}^{Met}) amounted to 1.240. Assuming an anammox biomass composition of $CH_{1.74}O_{0.31}N_{0.20}$ (Lotti et al., 2014b), the λ_{Cat} is then calculated from Eq. A2.18 as 8.4, yielding an overall metabolic reaction (per mole ammonium consumed) of:



A2.1.4 Demonstration of the calculation scheme in a spreadsheet

The procedure to calculate the overall metabolic anammox stoichiometry was implemented in a spreadsheet (Spreadsheet A2.1), following the general method of Kleerebezem & Van Loosdrecht (Kleerebezem and Van Loosdrecht, 2010). This procedure consists of the following steps (Fig. A2.1):

- (1) Definition of the elemental composition and charge of all compounds participating in the reactions. The anammox biomass composition ($CH_xO_yN_z$) may vary between different studies and needs to be set by the user;
- (2) The anammox catabolic reaction (Cat) is determined by Eq. A2.3, closing the elemental and charge balances for the electron donor (D) and electron

acceptor (A) half-reactions; No user intervention is required when dealing with the same catabolic reaction, in this case the anammox catabolic reaction.

(3) The anammox anabolic reaction (An) is determined by Eq. A2.8, closing the elemental and charge balances for the electron donor (D*) and electron acceptor (A*) half-reactions; This reaction stoichiometry depends on the user-defined biomass composition.

(4) Definition of the parameter that links the catabolism and anabolism, e.g., Y_{X/NH_4}^{Met} or Y_{NO_2/NH_4}^{Met} , according to case-specific measurement results;

(5) Calculation of the corresponding overall metabolic reaction stoichiometry.

The Spreadsheet A2.1 contains the implementation of this procedure for the aforementioned examples. The stoichiometry of the anammox metabolic reaction was defined both per C-mole biomass formed and per mole ammonium consumed. The mass and charge balances were checked for all the reactions. Case-specific anammox stoichiometry can be obtained by changing the corresponding yellow shaded values.

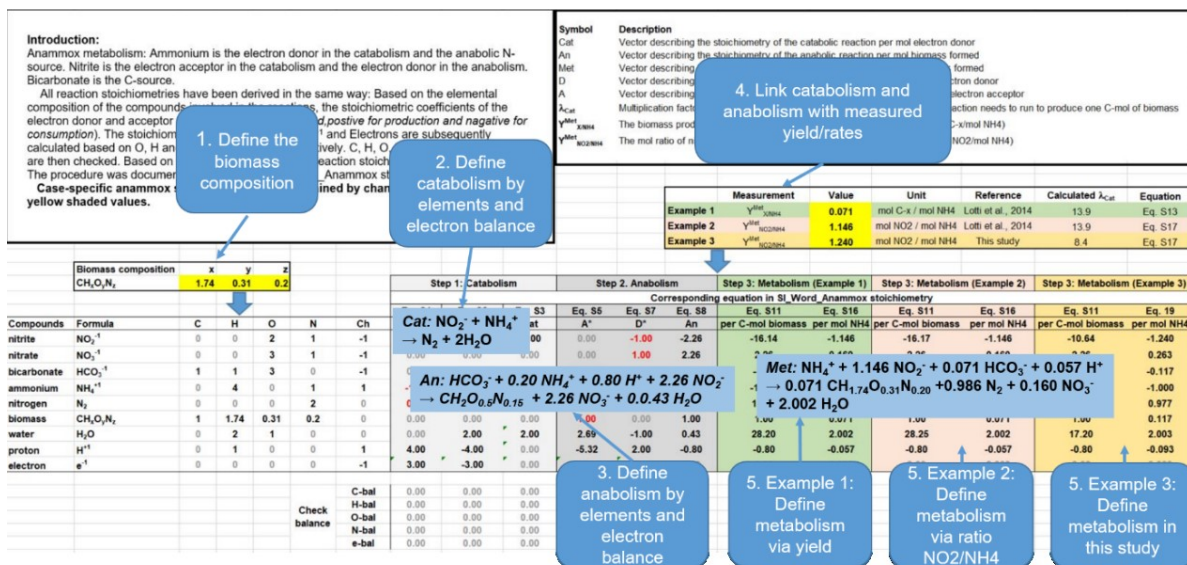


Figure A2.1. Anammox stoichiometry calculation procedure.

A2.2. Mass balance calculations principles

The mass balance calculation used in this study is further demonstrated in Spreadsheet A2.2 in the Appendix. For a reactor operated in steady state, the difference between the ingoing and outgoing concentration of a component is related to its conversion rate according to Eq. A2.20:

$$(C_{i,out} - C_{i,in}) * \frac{Q}{V} = r_i \quad (\text{A2.20})$$

$C_{i,in}$ and $C_{i,out}$ denote the measured concentrations of component i in influent and effluent (g N or COD.m⁻³), V is the reactor volume (assumed constant, in m³), Q is the influent flow rate (which equals the outgoing flow rate, in m³.d⁻¹), and r_i is the net conversion rate of component i in the reactor (g N or COD.m⁻³.d⁻¹).

The conversion rate of component i is related to the process rates ρ_j through the stoichiometric coefficients A_{ij} :

$$r_i = \sum_j A_{ij} * \rho_j \quad (\text{A2.21})$$

A_{ij} represents the stoichiometric coefficient of compound i in process j . The stoichiometric coefficients and the process rates considered in this study are summarized in Table A2.1.

Example: following Eq. A2.21, the net conversion rate for soluble organic substrate (Ss) in the reactor is obtained as :

$$r_{Ss} = 0 * \rho_1 + (1 - f_I) * \rho_2 + \left(-\frac{1}{Y_{H,NO_2}}\right) * \rho_3 + \left(-\frac{1}{Y_{H,NO_3}}\right) * \rho_4 + (1 - f_I) * \rho_5$$

The substrate conversion rate during heterotrophic bacteria growth on nitrite (process 3) is:

$$r_{Ss}^3 = \left(-\frac{1}{Y_{H,NO_2}}\right) * \rho_3$$

So the contribution of this process (in %) to the Ss consumption amounts to

$$C_{Ss}^3 = \frac{r_{Ss}^3}{r_{Ss}} * 100$$

Table A2.1. Stoichiometric matrix used for mass balance calculation

A_{ij}	i component →	S_s (gCOD.m ⁻³)	S_{NH} (gN.m ⁻³)	S_{NO_2} (gN.m ⁻³)	S_{NO_3} (gN.m ⁻³)	S_{N_2} (gN.m ⁻³)	X_{AN} (gCOD.m ⁻³)	X_H (gCOD.m ⁻³)	X_I (gCOD.m ⁻³)	Process rate
j process ↓										
1. Anammox conversion			$-\frac{1}{Y_{X/NH_4}^{Met'}}$	$-\left(\frac{1}{1.14} + \frac{1}{Y_{X/NH_4}^{Met'}}$ $- i_{NXB_AN}\right)$	1/1.14	$2^*\left(\frac{1}{Y_{X/NH_4}^{Met'}}$ $- i_{NXB_AN}\right)$	1			ρ_1
2. Decay of Anammox		1- f_i	$i_{NXB_AN} - f_i i_{NXI} - (1-f_i) i_{NSS}$				-1		f_i	ρ_2
3. Denitrification		$-\frac{1}{Y_{H,NO_2}}$	$-i_{NXB_H} + 1/Y_{H,NO_2} \cdot i_{NSS}$	$-\frac{1 - Y_{H,NO_2}}{1.71 Y_{H,NO_2}}$		$\frac{1 - Y_{H,NO_2}}{1.71 Y_{H,NO_2}}$		1		ρ_3
4. Partial Denitrification		$-\frac{1}{Y_{H,NO_3}}$	$-i_{NXB_H} + 1/Y_{H,NO_3} \cdot i_{NSS}$		$-\frac{1 - Y_{H,NO_3}}{1.14 Y_{H,NO_3}}$			1		ρ_4
5. Decay of heterotrophs		1- f_i	$-i_{NXB_H} - f_i i_{NXI} - (1-f_i) i_{NSS}$					-1	f_i	ρ_5
gCOD/unit comp		1	0	-3.43	-4.57	-1.715	1	1	1	
gN/unit comp		i_{NSS}	1	1	1	1	i_{NXB}	i_{NXB}	i_{NXI}	

Table A2.2. Stoichiometric parameters used for mass balance calculation

Parameter	Definition	Value	Unit	Source
Y_{X/NH_4}^{Metr}	Yield of anammox bacteria on ammonium	0.301	g COD.g N ⁻¹	This study
Y_{H, NO_2}	Yield of heterotrophs on nitrite	0.53	g COD.g COD ⁻¹	(Muller et al., 2003)
Y_{H, NO_3}	Yield of heterotrophs on nitrate	0.53	g COD.g COD ⁻¹	(Muller et al., 2003)
i_{NXB_AN}	N content of Anammox biomass	0.077	g N.g COD ⁻¹	(Strous et al., 1998)
i_{NXB_H}	N content of Heterotrophic biomass	0.083	g N.g COD ⁻¹	(Wiesmann, 1994)
i_{NXI}	N content of X _I	0.07	g N.g COD ⁻¹	(Wiesmann, 1994)
i_{NSS}	N content of S _s	0.03	g N.g COD ⁻¹	(Henze et al., 2000)
f_i	Fraction of X _I in decay	0.08	g COD.g COD ⁻¹	(Henze et al., 2000)

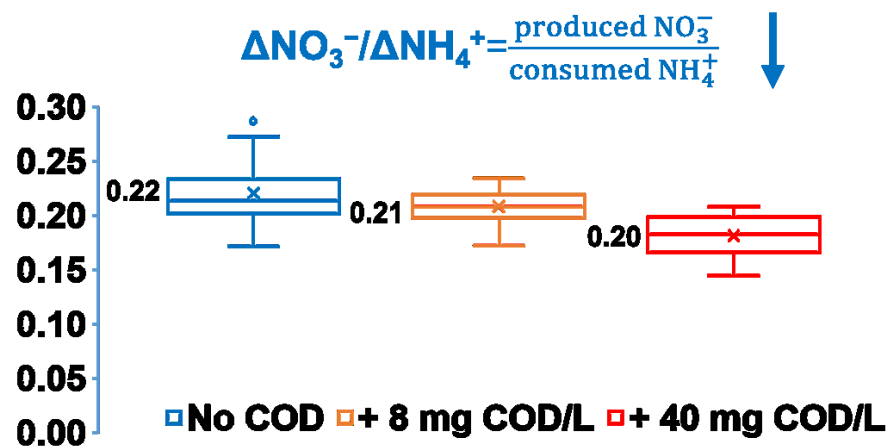


Figure A2.2. The ratio of nitrate produced to ammonium consumed with different influent COD concentration.

Table A2.3. Overview of observed ratios of consumed nitrite and produced nitrate over consumed ammonium ($\Delta\text{NO}_2^-/\Delta\text{NH}_4^+$ and $\Delta\text{NO}_3^-/\Delta\text{NH}_4^+$) in anammox reactors

Reactor	Scale	Biomass	Enrichment degree of anammox	$\Delta\text{NO}_2^-/\Delta\text{NH}_4^+$ (mole N/ mole N)	$\Delta\text{NO}_3^-/\Delta\text{NH}_4^+$ (mole N/ mole N)	Yield (mole C/mole NH ₄ -N)	Reference
SBR	lab-scale	Granules	74%	1.32	0.26	0.066	(Strous et al., 1998)
SBR	lab-scale	Granules	N.R.	1.28	0.26	N.R.	(Dapena-Mora et al., 2004)
SBR	lab-scale	Granules	85%	1.32 ± 0.05	0.23 ± 0.05	N.R.	(López et al., 2008)
Gas-lifted	lab-scale	Suspended biofilm	N.R.	1.11	0.2	N.R.	(Dapena-Mora et al., 2004)
Gas-lifted	full-scale	Granules	N.R.	1.31 ± 0.46	0.25 ± 0.09	N.R.	(van der Star et al., 2007)
MBR	lab-scale	Flocs	97.6%	1.1-1.3	0.1-0.25	N.R.	(Van Der Star et al., 2008)
MBR	lab-scale	Flocs	N.R.	1.278	0.353	0.105	(Puyol et al., 2013)
MBR	lab-scale	Suspended free cells	98.1%	1.21 ± 0.01	0.20 ± 0.01	0.071 ± 0.02	(Lotti et al., 2014b)
MBR	lab-scale	Suspended free cells	98.1%	1.146	0.161	0.071	(Lotti et al., 2014b)
UASB	lab-scale	Granules	N.R.	1.31 ± 0.03	0.23 ± 0.01	0.146	(Tang et al., 2011)
UASB	lab-scale	Granules	N.R.	1.32 ± 0.06	0.25 ± 0.02	0.139	(Tang et al., 2011)
EGSB	lab-scale	Granules	N.R.	1.31 ± 0.06	0.32 ± 0.01	N.R.	(Puyol et al., 2013)
Bubble Colum	lab-scale	Granules	N.R.	1.24 ± 0.07	0.22 ± 0.07	0.117*	This study

N.R.: not reported; *calculated from the generalized calculation scheme (Spreadsheet A2.1)

A2.3 Unit conversion of anammox biomass yield coefficient

The anammox biomass yield coefficient expressed in g COD biomass per g NH₄-N consumed, $Y_{X/NH_4}^{Met'}$ is related to the anammox biomass yield coefficient expressed in C-mole biomass per mole NH₄, Y_{X/NH_4}^{Met} , by Eq. A2.22. Noteworthy, the right biomass composition should be used in the unit conversion, as it correlates to the COD equivalent of biomass.

$$Y_{X/NH_4}^{Met'} = Y_{X/NH_4}^{Met} \cdot \frac{COD_X^e}{M_{NH_4-N}} = Y_{X/NH_4}^{Met} \cdot \frac{(4 + x - 2y - 3z) \cdot 8}{14} \quad (A2.22)$$

Where COD_X^e is the COD equivalent of one C-mole biomass (g COD/ mole CH_xO_yN_z), i.e., the COD equivalent of the electrons transferred to form one C-mole biomass (Eq. A2.8), namely $(4 + x - 2y - 3z) \cdot 8$ (g COD/ mole CH_xO_yN_z) (Kleerebezem and Van Loosdrecht 2010). $M_{NH_4-N} = 14$ is the molar weight of nitrogen (g N/ mole N).

Table A2.4. Comparison of measured data set for the derivation of anammox stoichiometry. SD=standard deviation; CV= coefficient of variation, i.e., the ratio of the standard deviation (SD) to the mean.

Compound		Strous et al. (1998)* (mmol.h ⁻¹)			Lotti et al. (2014b)** (mmol.L ⁻¹)			CV_1/CV_2
		Mean	SD	CV_1 (%)	Mean	SD	CV_2 (%)	
Influent	NH ₄ ⁺	23.1	0.7	3.0	60	0.6	1.0	3.0
	NO ₂ ⁻	22.4	0.7	3.1	60	0.6	1.0	3.1
Effluent	NH ₄ ⁺	4.6	0.6	13.0	10.56	0.12	1.1	11.5
	NO ₃ ⁻	4.7	0.3	6.4	10.34	0.12	1.2	5.5
	Biomass	0.1	0.05	50.0	21.1	5	23.7	2.1

*Data from Table 2 in Strous et al. (1998); **Data from Table 2A in Lotti et al. (2014b) – values before data reconciliation

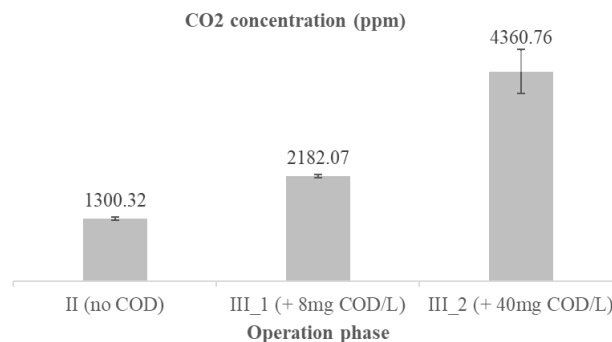


Figure A2.3. Measured CO₂ concentration in the off-gas of the reactor in this study

Spreadsheet A2.1. Spreadsheet for deriving anammox stoichiometry from experimental data

Introduction:
 Anammox metabolism: Ammonium is the electron donor in the catabolism and the anabolic N-source. Nitrite is the electron acceptor in the catabolism and the electron donor in the anabolism. Bicarbonate is the C-source.

All reaction stoichiometries have been derived in the same way: Based on the elemental composition of the compounds involved in the reactions, the stoichiometric coefficients of the electron donor and acceptor couples are identified (*in red, positive for production and negative for consumption*). The stoichiometric coefficients of H₂O, H⁺ and Electrons are subsequently calculated based on O, H and Charged balance, respectively. C, H, O, N, and Charge balance are then checked. Based on the half reactions all other reaction stoichiometries are calculated. The procedure was documented in stepwise in SI_Word_Anammox stoichiometry.docx.

Case-specific anammox stoichiometry can be obtained by changing the corresponding yellow shaded values.

Symbol	Description
Cat	Vector describing the stoichiometry of the catabolic reaction per mol electron donor
An	Vector describing the stoichiometry of the anabolic reaction per mol biomass formed
Met	Vector describing the stoichiometry of the metabolic reaction per mol biomass formed
D	Vector describing the stoichiometry of the electron donor reaction per mol electron donor
A	Vector describing the stoichiometry of the electron acceptor reaction per mol electron acceptor
λ_{Cat}	Multiplication factor of the catabolism, i.e. the number of times the catabolic reaction needs to run to produce one C-mol of biomass
Y_{X/NH_4}^{Met}	The biomass production per unit of ammonium in the metabolic reaction (mol C-x/mol NH ₄)
Y_{NO_2/NH_4}^{Met}	The mol ratio of nitrite and ammonium consumption in metabolic reaction (mol NO ₂ /mol NH ₄)

Measurement	Value	Unit	Reference	Calculated λ_{Cat}	Equation
Example 1a	0.071	mol C-x / mol NH ₄	Lotti et al., 2014	13.9	Eq. S13
Example 1b	1.146	mol NO ₂ / mol NH ₄	Lotti et al., 2014	13.9	Eq. S17
Example 2	1.240	mol NO ₂ / mol NH ₄	This study	8.4	Eq. S17

Biomass composition		x	y	z	Step 1: Catabolism						Step 2: Anabolism			Step 3: Metabolism (Example 1)		Step 3: Metabolism (Example 2)		Step 3: Metabolism (Example 3)	
CH ₂ O ₂ N _z		1.74	0.31	0.2	Eq. S1	Eq. S2	Eq. S3	Eq. S5	Eq. S7	Eq. S8	Eq. S11	Eq. S16	Eq. S11	Eq. S16	Eq. S11	Eq. S16			
Compounds	Formula	C	H	O	N	Ch	D	A	Cat	A*	D*	An	per C-mol biomass	per mol NH ₄	per C-mol biomass	per mol NH ₄	per C-mol biomass	per mol NH ₄	
nitrite	NO ₂ ⁻¹	0	0	2	1	-1	0.00	-1.00	-1.00	0.00	-1.00	-2.26	-16.14	-1.146	-16.17	-1.146	-10.64	-1.240	
nitrate	NO ₃ ⁻¹	0	0	3	1	-1	0.00	0.00	0.00	0.00	1.00	2.26	2.26	0.160	2.26	0.160	2.26	0.263	
bicarbonate	HCO ₃ ⁻¹	1	1	3	0	-1	0.00	0.00	0.00	-1.00	0.00	-1.00	-1.00	-0.071	-1.00	-0.071	-1.00	-0.117	
ammonium	NH ₄ ⁺¹	0	4	0	1	1	-1.00	0.00	-1.00	-0.20	0.00	-0.20	-14.08	-1.000	-14.11	-1.000	-8.58	-1.000	
nitrogen	N ₂	0	0	0	2	0	0.50	0.50	1.00	0.00	0.00	0.00	13.88	0.986	13.91	0.986	8.38	0.977	
biomass	CH ₂ O ₂ N _z	1	1.74	0.31	0.2	0	0.00	0.00	0.00	1.00	0.00	1.00	1.00	0.071	1.00	0.071	1.00	0.117	
water	H ₂ O	0	2	1	0	0	0.00	2.00	2.00	2.69	-1.00	0.43	28.20	2.002	28.25	2.002	17.20	2.003	
proton	H ⁺¹	0	1	0	0	1	4.00	-4.00	0.00	-5.32	2.00	-0.80	-0.80	-0.057	-0.80	-0.057	-0.80	-0.093	
electron	e ⁻¹	0	0	0	0	-1	3.00	-3.00	0.00	-4.52	2.00	0.00	0.00	0.000	0.00	0.000	0.00	0.000	
Check balance		C-bal	0.00	0.00	0.00	0.00	0.00	0.00	0.00	0.00	0.00	0.00	0.00	0.00	0.00	0.00	0.00	0.00	0.00
		H-bal	0.00	0.00	0.00	0.00	0.00	0.00	0.00	0.00	0.00	0.00	0.00	0.00	0.00	0.00	0.00	0.00	0.00
		O-bal	0.00	0.00	0.00	0.00	0.00	0.00	0.00	0.00	0.00	0.00	0.00	0.00	0.00	0.00	0.00	0.00	0.00
		N-bal	0.00	0.00	0.00	0.00	0.00	0.00	0.00	0.00	0.00	0.00	0.00	0.00	0.00	0.00	0.00	0.00	0.00
		e-bal	0.00	0.00	0.00	0.00	0.00	0.00	0.00	0.00	0.00	0.00	0.00	0.00	0.00	0.00	0.00	0.00	0.00

References:
 Lotti, T., et al. (2014). "Physiological and kinetic characterization of a suspended cell anammox culture." *Water Research* 60(0): 1-14.
 Kleerebezem, R. and M. C. Van Loosdrecht (2010). "A generalized method for thermodynamic state analysis of environmental systems." *Critical Reviews in Environmental Science and Technology* 40(1): 1-54.

Spreadsheet A2.2. Spreadsheet for mass balance analysis

Step 1: Stoichiometric matrix of possible processes

A _i component	S _C	S _{NH}	S _{NO2}	S _{NO3}	S _{N2}	S _{N2O}	S _N	S _{CH4}	S _{CO2}	Process rate
j process	[gCOD.m ⁻³]	[gN.m ⁻³]	[gN.m ⁻³]	[gN.m ⁻³]	[gN.m ⁻³]	[gCOD.m ⁻³]	[gCOD.m ⁻³]	[gCOD.m ⁻³]	[gCOD.m ⁻³]	[gCOD.m ⁻³ .d ⁻¹]
1. Anammox	1	-1	0	0	0	0	0	0	0	p1
2. Decay of anammox	1-f _i	-f _i	0	0	0	0	0	0	0	p2
3. Denitrification	1	0	-1	0	0	0	0	0	0	p3
4. Partial Denitrification	1	0	-1	0	0	0	0	0	0	p4
5. Decay of heterotrophs	1-f _i	-f _i	0	0	0	0	0	0	0	p5

Step 2: Mass balance set-up and calculation

Principals: Mass balances over measured NH₄-N, NO₂-N, NO₃-N and COD, following the equations below:

$A \cdot p = r$

where, A is the matrix of the stoichiometric coefficients (Table S1), p is the vector of unknown process rates (g COD m⁻³ d⁻¹), r is the vector of measured net conversion rates of substrate in the reactor (g N or COD m⁻³ d⁻¹), e.g. the p₁ is the process rate for process 1, expressed as g COD m⁻³ d⁻¹ and r is the measured net conversion rate of substrate in the reactor (g N or COD m⁻³ d⁻¹), e.g. r_{NO2} is the net conversion rate of NO₂-N expressed as g NH₄-N m⁻³ d⁻¹; r_{NO3} is the conversion rate of NH₄-N in process i; r_{NO2}/r_{NO3} is the contribution of process i in the net conversion of NH₄-N

The goal is to calculate the process rate (p_i) for each process in the table above. By setting up mass balances for NH₄-N, NO₂-N, NO₃-N and COD, we can get 4 equations with 5 unknown process rates (p_i) of which the process rate for Decay of anammox (p₂) can be first calculated, resulting in 4 equations with 4 unknown process rate (p_i) to solve.

Solution:

A		r		p		r	
0.0000	-1.8868	-1.8868	0.9200	p1	-21.936	Ss(COD)	
-3.3223	-0.0264	-0.0264	0.0498	p2	-138.073	NH4-N	
-4.1225	-0.5186	0.7779	0.0000	p3	-169.000	NO2-N	
0.8772	0.0000	-0.7779	0.0000	p4	30.000	NO3-N	

To solve: (A⁻¹)⁻¹ * r = p

0.0146	-0.2695	-0.0394	-0.0656	p1	-21.936
-0.0913	1.6864	-1.6820	-1.5178	p2	-138.073
0.0164	-0.3039	-0.0444	-1.3595	p3	-169.000
0.9335	2.8353	-3.5406	-5.9010	p4	30.000

To check: p = (A⁻¹)⁻¹ * r

41.57	10.80	7.88	8.31	9.37
-------	-------	------	------	------

Process rate of decay of Anammox (p2): p2 = 10.8

Reactor operation:

Measurement	ΔC	Unit	-ΔC*Q/V	Unit
Q (m ³ /d)	0.0065	1 Ss(COD)	12.0	[gCOD.m-3.d-1]
V (m ³)	0.0065	2 NH4-N	137.6	[gN.m-3.d-1]
HRT:V/Q (d)	1.00	3 NO2-N	169	[gN.m-3.d-1]
		4 NO3-N	30.00	[gN.m-3.d-1]

*Note: ΔC was taken from the average value of measurement from day 362-383. For COD, it should be in the range of 0-40 mgCOD/L

Equation systems:

A		r		p		r	
0.0000	0.9200	-1.8868	-1.8868	0.9200	p1	-21.936	Ss(COD)
-3.3223	0.0438	-0.0264	-0.0264	0.0498	p2	-137.60	NH4-N
-4.1225	0.0000	-0.5186	0.7779	0.0000	p3	-169.00	NO2-N
0.8772	0.0000	0.0000	-0.7779	0.0000	p4	30.00	NO3-N

Step 3: Brief summary of the results

Process rates:

unit	P1: Anammox	P2: Decay of anammox	P3: Denitrification	P4: Partial DEN	P5: Decay of H
Process rate [gCOD.m-3.d-1]	41.57	10.80	7.88	8.31	9.37

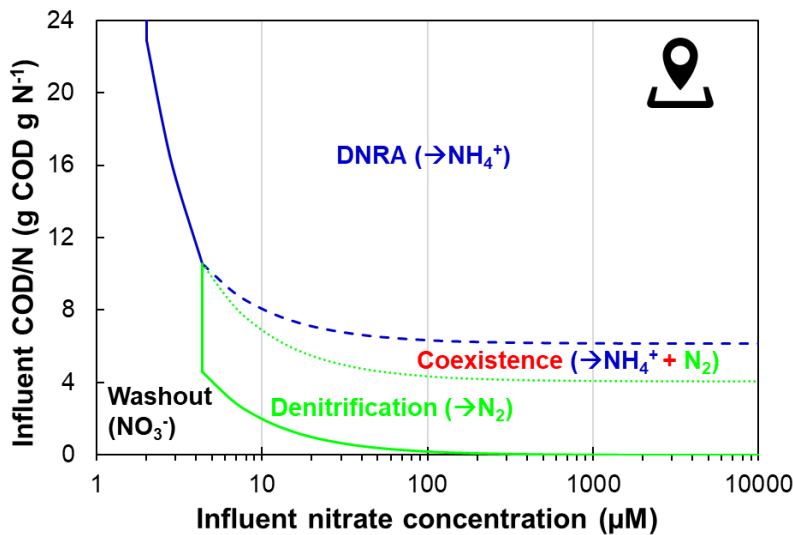
Conversion rates:

unit	P1: Anammox	P2: Decay of anammox	P3: Denitrification	P4: Partial DEN	P5: Decay of H	SUM (Σ ΔC*Q/V)
Ss [gCOD.m-3.d-1]	0.00	9.94	-14.88	-15.68	8.62	-12.00
NH4 [gN.m-3.d-1]	-138.11	0.47	-0.21	-0.22	0.47	-137.60
NO2 [gN.m-3.d-1]	-171.38	0.00	-4.09	6.47	0.00	-169.00
NO3 [gN.m-3.d-1]	36.47	0.00	0.00	-6.47	0.00	30.00

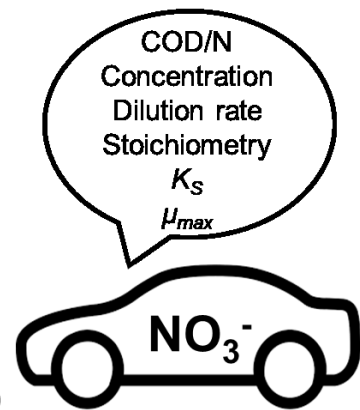
Conversion rate (g COD or N m⁻³ d⁻¹):

Stoichiometric diagram:

Elucidating the competition between heterotrophic denitrification and DNRA using the resource-ratio theory



Where is nitrate going?



3.0 Abstract

Denitrification and dissimilatory nitrate reduction to ammonium (DNRA) are two microbial processes competing for nitrate and organic carbon (COD). Their competition has great implications for nitrogen loss, conservation, and greenhouse gas emissions. Nevertheless, a comprehensive and mechanistic understanding of the governing factors for this competition is still lacking. We applied the resource-ratio theory and verified it with competition experiments of denitrification and DNRA in the literature. Based on this theory, we revealed how COD/N ratio, influent resource concentrations, dilution rate and stoichiometric and kinetic parameters individually and collectively define the boundaries for different competition outcomes in continuous cultures. The influent COD/N ratio alone was found not sufficient for prediction as the boundary COD/N ratio for different competition outcomes could change significantly with influent resource concentrations. The stoichiometry of the two processes was determinative for the boundaries, whereas the affinity for the resources (K_s), maximum specific growth rate (μ_{max}) of the two species and the dilution rate had significant impacts as well but mainly at low influent resource concentrations (e.g., <100 μM nitrate). The proposed approach allows for a more comprehensive understanding of the parameters controlling microbial selection beyond current approaches and explains apparently conflicting experimental results. The results also provide testable hypotheses and tools for understanding and managing the fate of nitrate in ecosystems and for other species that compete for the same resources.

Chapter redrafted after:

Jia, M., Winkler, M.K.H. and Volcke, E.I.P. Elucidating the competition between heterotrophic denitrification and DNRA using the resource-ratio theory. In preparation

3.1 Introduction

Denitrification (DEN) and dissimilatory nitrate reduction to ammonium (DNRA, also termed as dissimilatory/respiratory/nitrate ammonification) are two main microbial processes competing for nitrate as an electron acceptor (Kraft et al., 2011). During denitrification, nitrate is converted to nitrogen gas, thereby leading to nitrogen loss in natural and manmade ecosystems such as wastewater treatment plants (WWTPs). Nitrous oxide, a potent greenhouse gas, can be emitted during this process, posing an increasing concern (Canfield et al., 2010). In contrast, DNRA retains nitrogen locally by converting nitrate to bioavailable ammonium, which may be beneficial for natural ecosystems but unwanted for WWTPs (Van Den Berg et al., 2015). Besides, DNRA seems not to contribute to N₂O emissions (Kraft et al., 2011). Growing evidence suggests that DNRA can be significant in both aquatic and terrestrial ecosystems (Giblin et al., 2013; Rütting et al., 2011). Nevertheless, little is known about the importance of DNRA and its relative contribution to global N-cycling (Burgin and Hamilton, 2007; Kraft et al., 2011; Kuypers et al., 2018). Therefore, there is a pressing need to better comprehend the factors influencing the competition between denitrification and DNRA for nitrate.

Energetics and kinetics are the general physiological features of microorganisms that explain and regulate the outcome of competition (Tiedje, 1988). Theoretically, the catabolic reaction of the denitrification pathway yields more free energy per unit of organic carbon oxidized (e.g., 802 vs. 505 kJ per mole acetate) whereas for the DNRA pathway slightly more free energy is liberated per unit of nitrate reduced (505 vs. 501 kJ per mole nitrate with acetate as electron donor) (Strohm et al., 2007; Van Den Berg et al., 2015). Moreover, the biomass yield per mole nitrate is 0.2-2 times higher from the DNRA process than that of the DEN process (Strohm et al., 2007; Van Den Berg et al., 2015). Therefore, from a thermodynamic standpoint, it can be justified that DEN should occur under organic carbon-limiting conditions (i.e., low COD/N), while DNRA is promoted under nitrate-limiting conditions (i.e., high COD/N) (Kraft et al., 2014; Tiedje, 1988; Van Den Berg et al., 2015; Yoon et al., 2015a). In addition, Tiedje (1988) proposed a theory that high labile carbon availability would favor organisms that use electron acceptors most efficiently; DNRA transfers eight electrons per mole of nitrate reduced, whereas denitrification only transfers five. According to this theory, DNRA should be more efficient and abundant under nitrate-limiting conditions. Previous

studies also suggest that DNRA bacteria generally have a lower maximum specific growth rate but a higher affinity for nitrate compared to denitrifiers (Tiedje, 1988; van den Berg et al., 2016). The higher affinity for nitrate may also explain the observed dominance of DNRA over denitrification under nitrate-limiting conditions (van den Berg et al., 2016). In opposition to the theoretical explanations that suggest DNRA dominance under nitrate-limiting conditions, results have shown that high COD/N ratios do not necessarily lead to a shift from DEN to DNRA (Behrendt et al., 2014; Sotta et al., 2008).

Apart from energetics and kinetics, environmental conditions affect the biological nitrate partitioning as well. There are multiple studies suggesting that the competition depends on dilution or growth rate (Kraft et al., 2014; Rehr and Klemme, 1989) and initial resource concentration (Tiedje, 1988). In addition, other studies conducted with a pure culture that encompasses a dual pathway showed that COD/N ratio alone was insufficient to explain pathway selection as at low resource concentrations the culture disproportionately utilizes DNRA rather than denitrification (Vuono et al., 2019). These results delineate that a comprehensive understanding of the factors that drive the partitioning or coexistence of both pathways is lacking, and a mathematical approach to explain competition outcome may be helpful.

Over the years, theoretical frameworks have been developed to predict the outcome of interspecies microbial competition for the same resources. One example is the resource-ratio theory, which describes the interactions between resources and growth of two or more competing species and can predict the outcomes of microbial competition for resources, in advance of actual competition experiments (Hsu et al., 1981; Tilman, 1980; Williamson and MacArthur, 1974). This theory takes both physiological properties and environmental conditions into account. It has been successfully demonstrated in predicting the outcome of microbial competition for a single nutrient (Hansen and Hubbell, 1980) as well as in an ecological competition between algae for two resources (phosphate and silicate) (Tilman, 1976). The analytical solutions of generalized competition scenarios in continuous systems (e.g., chemostat) have been investigated at steady state, and results revealed survival of one or coexistence of both species at given circumstance (e.g., (Hsu et al., 1981; Volcke et al., 2006)).

This study investigates the potential of the resource-ratio theory in elucidating the competition between denitrification and DNRA in continuous cultures. More specifically, it is studied whether this mathematical approach can match and explain the underlying principle for the conflicting measurements conducted at different COD/N ratios. To this end, the resource-ratio theory was applied to predict the experimental competition outcome of heterotrophic denitrifiers and DNRA bacteria in continuous cultures (van den Berg et al., 2016; Van Den Berg et al., 2015). After verification, the theory was used to test different conditions to understand what may drive pathway partitioning or coexistence. The results highlight the impact of COD/N ratio, resource concentrations, dilution rate, and microbial physiological properties on the competition outcome. A generalized spreadsheet was created and supplied to ease the application of this mechanistic theory to similar competition scenarios.

3.2 Materials and methods

After introducing the basics of the resource-ratio theory (section 3.2.1), this theory was implemented to predict the competition outcome of heterotrophic denitrification and DNRA (section 3.2.2). Its applicability was subsequently evaluated with experimental data available from literature case studies (van den Berg et al., 2016; Van Den Berg et al., 2015) (section 3.2.3).

3.2.1 Resource-ratio theory

The resource-ratio theory describes the interaction between resources and growth of competing species and enables to predict the outcome of microbial competition for shared resources, instead of or prior to actual competition experiments (Hsu et al., 1981; Tilman, 1980). The growth of the microorganisms on the limiting resources was assumed to follow Monod kinetics (Eq. 3.1) (Monod, 1950).

$$\mu_i = \mu_{max,i} \frac{S}{K_{Si} + S} \quad (3.1)$$

Where μ_i is the specific growth rate of species i (h^{-1}); $\mu_{max,i}$ is the maximum specific growth rate of species i (h^{-1}); K_{Si} is the half-saturation constant (i.e., affinity constant) of species i for S (μM); S is the concentration of resource S (μM).

For every limiting resource in a continuous system, there is a subsistence resource concentration at which the growth rate balances the dilution rate (D), which is defined as the parameter J_s (Eq. 3.2). J_s also represents the concentration of resource S at steady state (Hsu et al., 1977). Below this concentration, the net growth rate would be negative, and thus, the species cannot sustain. If n species are competing for a single limiting resource (S), the species i with the lowest subsistence resource concentration J_{si} can utilize the limiting resource to the lowest level at a given dilution rate and influent resource concentration and thus is the only possible winner at steady-state. This has been previously proven mathematically (Hsu et al., 1977) and experimentally (Hansen and Hubbell, 1980).

$$J_{si} = K_{si} \cdot \frac{D}{r_i} = K_{si} \cdot \frac{D}{\mu_{max,i} - D} \quad (3.2)$$

Where J_{si} is the subsistence concentration of growth-limiting resource S for species i (μM); D is the dilution rate (h^{-1}); r_i is the intrinsic growth rate and equals to $(\mu_{max,i} - D)$ (h^{-1});

The competition of two species (N_1 and N_2) for two resources (S and R) in a continuous culture is illustrated in Fig. 3.1, following a graphical-mechanistic approach that was developed to study the competition and predation in macroecology (Tilman, 1980). In this two resources plane (Fig. 3.1), for every species i , the so-called 'Zero Net Growth Isoclines' (ZNGIs) are drawn, which are defined by the subsistence resource concentrations (i.e. J parameter) for the two complementary resources. A species i cannot survive outside the boundary ZNGIs, i.e., for $S < J_{Si}$ and/or $R < J_{Ri}$, even in the absence of a competing species. Stable coexistence only occurs when the ZNGIs of the two species coincide (as in Fig.3.1), i.e. when each species has lower subsistence concentration (J) for one of the two resources. If the ZNGIs of two competing species do not cross, it means one species must have lower J parameters for both of the two resources, and as a result it would always win the competition (Hsu et al., 1981; Tilman, 1980). Moreover, it is assumed that the growth is restricted by the most limiting resource (i.e., the one that results in lower growth rate in Eq.3.1), as described by Eq. 3.3 (Hsu et al., 1981). To maintain an equilibrium population, the resource consumption rate must balance the resource supply rate. The consumption vector (defined as C_i , Eq. 3.4 and in Fig. 3.1) and the ZNGIs define the regions in which

either one of the two dominates or two species coexist (Fig. 3.1). The model based on this theory was further detailed in the Appendix (section A3.1).

$$\mu_i(S, R) = \min \left(\mu_{max,i} \frac{S}{K_{Si} + S}, \quad \mu_{max,i} \frac{R}{K_{Ri} + R} \right) \quad (3.3)$$

$$C_i = \frac{Y_{Si}}{Y_{Ri}} \quad (3.4)$$

Where Y_{Si} , Y_{Ri} are the yield of species i per unit of resource S or R consumed (mole biomass per mole S or R); therefore, C_i represents the ratio of the consumption of resource R to resource S by species i (mole R per mole S).

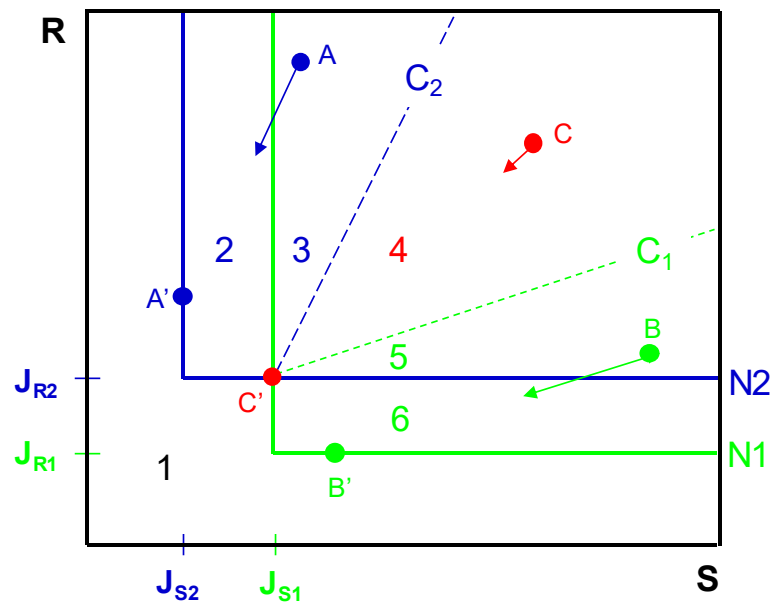


Figure 3.1. Graphical representation of resource competition of two species (N1 and N2) competing for two resources (S and R) at a specific dilution rate. The solid lines labeled N1 and N2 are the Zero Net Growth Isoclines (ZNGIs) for the two species. The dashed lines are the consumption vectors for the two species, with the slope of C_1 and C_2 , respectively. The competition outcomes can be predicted from the supply point (defined by the supplied concentration of resource S and R in this S - R plane, e.g., points A , B , and C). Region 1, no species can survive; Region 2, only species N2 can survive; Region 3, species N2 outcompetes species N1, dynamic behavior (trajectory) governed by slope C_2 ; Region 4, the two species stably coexist; Region 5, species N1 outcompetes species N2, dynamic behavior (trajectory) governed by slope C_1 ; Region 6, only species N1 can survive. The equilibrium points always fall on the ZNGIs. Points A' , B' , and C' represent the corresponding equilibrium points of supply points A , B , and C . Line A - A' has the same slope as C_2 , whereas line B - B' has the same slope of C_1 . All supply points in region 4 would reach the same equilibrium point C' .

Overall, with kinetic and stoichiometric parameters of the competing species (e.g. μ_{max} , K_s and Y) and environmental conditions (e.g., influent resource concentration and dilution rate), the resource-ratio theory enables to qualitatively and quantitatively predict the competition outcomes, the status of the competing species and resources (e.g., concentrations) at steady state (i.e., equilibrium points) and the dynamic (i.e. how the steady state is reached).

3.2.2 Application of the theory for denitrification and DNRA

In this study, heterotrophic denitrification and DNRA were assumed to be carried out by two distinct specialist species and directly compete for nitrate and organic carbon (COD, e.g., acetate). Their competition in continuous cultures (i.e., chemostat) can be regarded as a specific case of the general resource-ratio theory for two species competing for two resources (Fig. A3.1). The kinetic and stoichiometric parameters used in this study for the application of this theory are presented in Table 3.1 (and Table A3.2. in μM).

Table 3.1. Physiological parameters of heterotrophic denitrifiers and DNRA bacteria used for the implementation of resource-ratio theory (at 20 °C)

Parameter	Value*	Unit*	Source
μ_{max}^{DEN}	0.086	h^{-1}	(Henze et al., 1999)
Y_{COD}^{DEN}	0.256	g COD.g COD^{-1}	(van den Berg et al., 2016)
$Y_{NO_3}^{DEN}$	1.034	g COD.g N^{-1}	(van den Berg et al., 2016)
$K_{NO_3}^{DEN}$	0.140	g N.m^{-3}	(van den Berg et al., 2016)
K_{COD}^{DEN}	0.640	g COD.m^{-3}	(van den Berg et al., 2016)
μ_{max}^{DNRA}	0.052	h^{-1}	(van den Berg et al., 2016)
Y_{COD}^{DNRA}	0.256	g COD.g COD^{-1}	(van den Berg et al., 2016)
Y_{COD}^{DNRA}	1.574	g COD.g N^{-1}	(van den Berg et al., 2016)
$K_{NO_3}^{DNRA}$	0.028	g N.m^{-3}	(van den Berg et al., 2016)
K_{COD}^{DNRA}	0.640	g COD.m^{-3}	(van den Berg et al., 2016)

These values were used as the default (i) to verify the theory (section 3.3.1), (ii) to analyze the impact of influent resource concentration and dilution rate on the boundary COD/N ratios and thus the competition outcome (section 3.3.2 and 3.3.3), and (iii) to study the dynamic system behaviour (section 3.3.5). To date, kinetic and stoichiometric

parameters (e.g., Y , μ_{max} , and K_s) of heterotrophic DNRA microorganisms have only been limitedly reported. Therefore, a local sensitivity analysis was performed to investigate the potential impact of these parameters on the competition outcome (section 3.3.4).

3.2.3 Experimental cases for theory verification

To verify the resource-ratio theory, two experimental studies on the competition between heterotrophic denitrification and DNRA processes by van den Berg et al. (van den Berg et al., 2016; Van Den Berg et al., 2015) were used. In these studies, chemostat enrichment cultures were fed with different levels of acetate and nitrate (COD/N=1.8-8.5 g COD g N⁻¹), with an averaged dilution rate of 0.026 h⁻¹. The experimental conditions and observed competition outcomes are summarized in Table 3.2. The measured biomass and resources (i.e., acetate and nitrate) concentrations at steady state are available in Table A3.3.

Table 3.2. Experimental conditions and observed outcomes of competition between heterotrophic DEN and DNRA in chemostat enrichment cultures

	Influent				Measured competition outcome
	Acetate (μM)	Nitrate (μM)	Ac/N ratio (mol.mol ⁻¹)	COD/N g COD.g N ⁻¹	
Case 1 (van den Berg et al., 2016)	22050	11790	1.87	8.5	DNRA dominance
	17690	11790	1.50	6.9	DNRA dominance
	14500	11790	1.23	5.6	Coexistence
	13680	11790	1.16	5.3	Coexistence
	12730	11790	1.08	4.9	Coexistence
	10960	11790	0.93	4.2	Coexistence
	7780	11790	0.66	3.0	DEN dominance
Case 2 (Van Den Berg et al., 2015)	2616	6643	0.38	1.8	DEN dominance
	4356	5857	0.71	3.4	DEN dominance
	5125	5857	0.82	4.0	DEN dominance
	6278	5857	1.00	4.9	DEN dominance
	9866	5857	1.59	7.7	DNRA dominance

3.3 Results and discussion

3.3.1 Verification of the resource-ratio theory

This study used the results from two previously published chemostat enrichment cultures as case studies for theory verification (van den Berg et al., 2016; Van Den Berg et al., 2015). These cultures were fed with different levels of acetate and nitrate (COD/N=1.8-8.5 g COD g N⁻¹, Table 3.2). It was concluded that denitrifiers dominated under carbon-limiting (i.e., high COD/N) conditions, whereas DNRA bacteria dominated under nitrate-limiting (i.e., high COD/N) conditions (van den Berg et al., 2016; Van Den Berg et al., 2015). Moreover, the coexistence of denitrifiers and DNRA bacteria was found for a wide range of intermediate influent COD/N ratios (Table 3.2).

Fig. 3.2 compares the measured and predicted competition outcomes at 12 conditions tested in the case studies. The predictions agreed with the measurements under 11 conditions tested (Fig. 3.2). The only condition (influent 5857 μ M nitrate and 6278 μ M acetate) where denitrification dominance was observed whereas coexistence was predicted (Fig. 3.2), was close to the predicted boundary, and microbial community analysis clearly evidenced the strong presence of DNRA bacteria at that point (Van Den Berg et al., 2015), implying that steady state may not have been reached yet experimentally at this point. Quantitatively, the predicted steady-state biomass concentrations and abundance were in good agreement with the measurements under all 7 conditions tested in case study 1 (Fig. 3.3A and 3.3B, where influent resource concentrations were converted to COD/N ratio for simplicity). Overall, the predictions of this study were both qualitatively and quantitatively in close alignment with the measured data (Fig. 3.2 and Fig. 3.3). Therefore, the resource-ratio theory was considered valid for predicting the outcome of the competition between heterotrophic denitrifiers and DNRA bacteria in continuous systems.

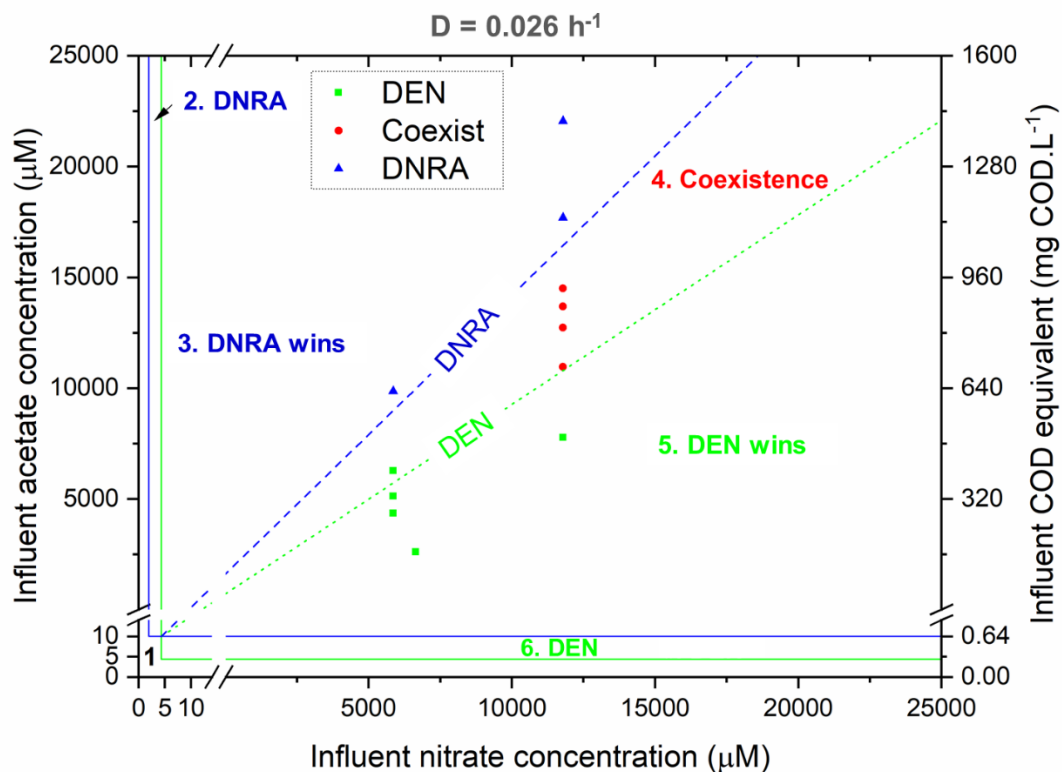


Figure 3.2. Predicted and observed outcomes of competition for nitrate and organic carbon by heterotrophic denitrifiers and DNRA bacteria in continuous cultures at a dilution rate of 0.026 h^{-1} . Experiments (van den Berg et al., 2016; van Den Berg et al., 2015) for which DEN was dominant are shown with green squares; those for which DNRA was dominant are shown with blue triangles, and those for which coexistence was observed are shown with red dots. The borders and the meaning of the operating zones distinguished by the resource-ratio theory are detailed in Figure 3.1. The consumption vectors (broken lines) have a slope of C_{DEN} ($4.04 \text{ g COD g N}^{-1}$) for denitrifiers and C_{DNRA} ($6.15 \text{ g COD g N}^{-1}$) for DNRA bacteria.

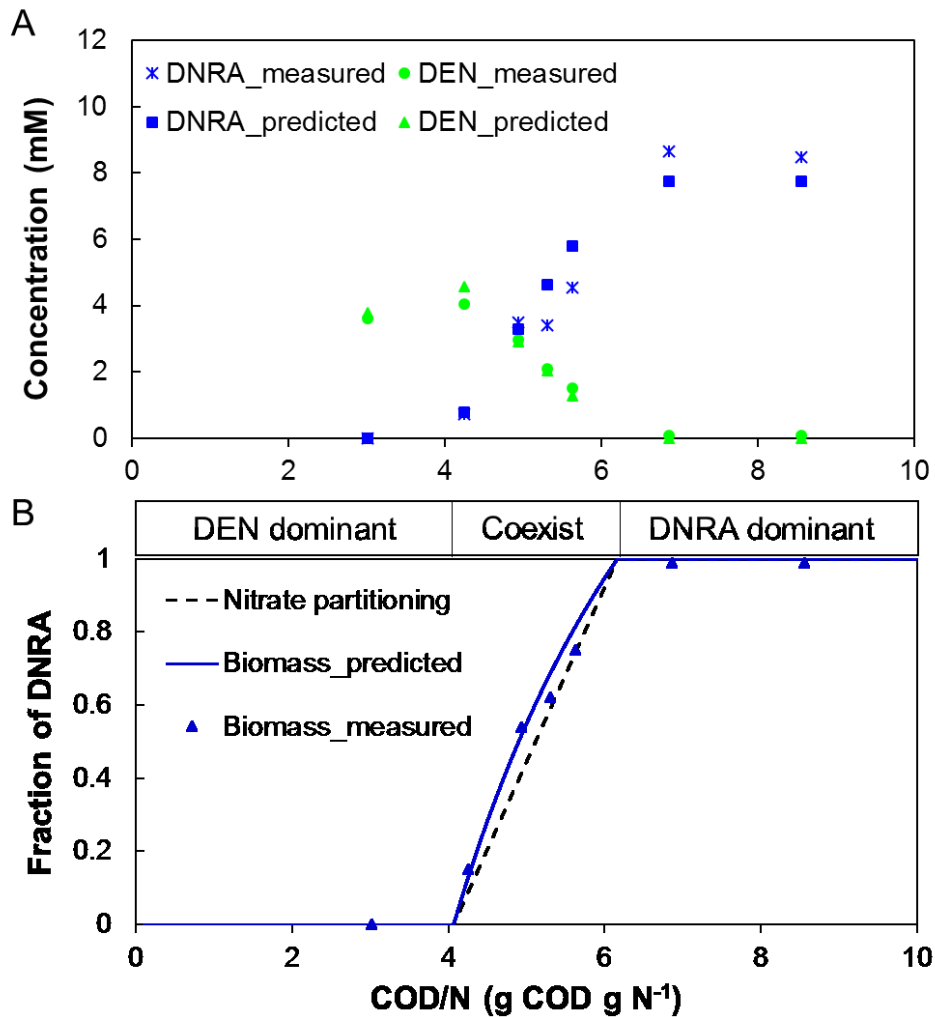


Figure 3.3. Prediction versus measurement at steady state (case study 1 (van den Berg et al., 2016)): (A) concentrations of heterotrophic denitrifiers and DNRA bacteria; (B) relative abundance of DNRA bacteria (to the total of denitrifiers and DNRA bacteria) and contribution of DNRA in nitrate partitioning at different influent COD/N ratios (at influent nitrate concentration of 1000 μM). The black triangles represent the measured DNRA biomass fraction (at influent nitrate concentration of 11790 μM (van den Berg et al., 2016))

3.3.2 Impact of resource concentration on competition outcomes

The boundaries of the different regions in Fig. 3.2 can be expressed by the COD/N ratio, which is often used in literature for competition and field studies (Kraft et al., 2014; Rütting et al., 2011; Van Den Berg et al., 2015; Yoon et al., 2015a). Fig. 3.4 illustrates the influent COD/N ratios of the boundaries at different influent nitrate concentrations. These boundaries COD/N ratios define the tipping point at which one process prevails over or coexists with the other. For instance, the upper boundary of the region for coexistence (i.e., region 4) represented the minimum influent COD/N

ratio for DNRA dominance, whereas its lower boundary represented the maximum influent COD/N ratio for DEN dominance (Fig. 3.4). Overall, the boundaries influent COD/N ratios changed significantly at low influent nitrate concentrations (e.g., < 100 μM) and gradually stabilized at high influent nitrate concentrations (e.g., > 1000 μM). With the increase of influent nitrate concentration, the region for coexistence (region 4) gradually widened and its upper and lower boundary influent COD/N ratios asymptotically approached to the stoichiometric values of C_{DNRA} (corresponds to COD/N of 6.15) and C_{DEN} (corresponds to COD/N of 4.04), respectively. The stabilized boundaries at high influent nitrate concentration (Fig. 3.4) were also confirmed in Fig. 3.3B. Despite the large difference in influent nitrate concentration (1000 μM used for prediction vs. 11790 μM in the experiments, Table 3.2), the predicted DNRA biomass fraction agreed with the measurements (Fig. 3.3B). The trend also held for different influent COD concentrations (Fig. A3.4)

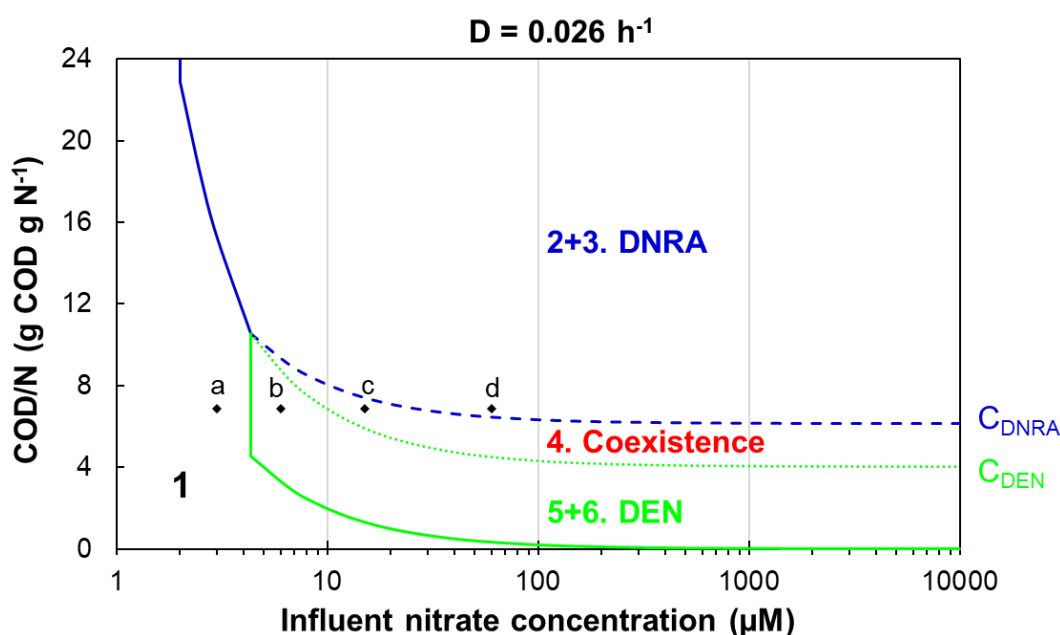


Figure 3.4. The boundary influent COD/N ratios at different influent nitrate concentrations. The regions correspond to the regions with the same numbers in Fig. 3.2. Points a, b, c, and d are supply points with the same COD/N ratio but different nitrate concentrations (detailed in Fig. A3.5).

Overall, the results clearly illustrate that, as a governing factor of the competition between the two nitrate partitioning pathways, the boundary influent COD/N ratios were not constant but could change significantly with influent resource concentrations. At high influent resource concentrations, process stoichiometry (reflected in C_i) of the

two competing processes was the determining factor of the boundary influent COD/N ratios, whereas kinetics (i.e., K_S and μ_{max} , reflected in J_S and thus the ZNGIs, Fig. 3.2 & Fig. 3.4) were important as well but only at low influent resource concentrations. This implies that influent COD/N ratio alone is not sufficient to predict the competition outcome of heterotrophic denitrification and DNRA. Different competition outcomes (resource limitation) could occur at the same influent COD/N ratio but varying influent resource concentrations (e.g., at the same influent COD/N ratio of 6.86, all four possible competition outcomes could occur for points a, b, c, and d in Fig. 3.4, detailed Fig. A3.5). In this theoretical study, the competition between DEN and DNRA is determined by both stoichiometries and growth kinetics. The stoichiometries were assumed to be constant. The change of the boundary COD/N ratio with influent nitrate level was a result of the change of growth rate of two species and thus the contribution of the two processes at different influent nitrate concentrations.

The result also raises the question of how to anticipate the threshold of resource limitation in continuous cultures. Resource limitation is normally anticipated based on the process stoichiometry; for instance, nitrate is expected to be the limiting resource when it is lower than the stoichiometry would require in relation to COD (Vuono et al., 2019). Our results show that this stoichiometry-based definition is inadequate. For example, nitrate limitation (and thus DNRA dominance) would occur when the influent COD/N ratio was above 6.16 (close to the DNRA stoichiometry) at influent nitrate concentration of 1000 μM , whereas it would only occur with the COD/N ratio above 8.05 at influent nitrate concentration of 10 μM (Fig. 3.4).

The impact of resource concentrations on competition outcomes has significant implications, as different ecosystems have various nitrate availability (i.e., influent nitrate concentration) (Table 3.3) and, therefore, possibly different boundary COD/N ratios for nitrate partitioning. High nitrate concentrations have been reported in some ecosystems, for example, in groundwater at a nuclear waste site (up to 233mM (Fortney et al., 2015)), in soil adjacent to bats guano caves (Pellegrini and Ferreira, 2013), and in coastal rockpools affected by gull guano where high level of ammonium that can further result in high nitrate level due to nitrification was observed (e.g., 1600 μM (Loder et al., 1996)). However, the nitrate concentrations in natural aquatic and terrestrial ecosystems are normally low (e.g., <100 μM , Table 3.3), at which the boundaries of different competition outcomes changed dramatically (Fig. 3.4). Lab-

scale competition studies often supply high concentrations of nitrate ($> 1000 \mu\text{M}$, e.g., in (Rehr and Klemme, 1989; Van Den Berg et al., 2015; Yoon et al., 2015a)) at which the boundaries were rather stable and mainly defined by the stoichiometries of denitrifiers and DNRA bacteria (Fig. 3.4). The thresholds obtained from these high-nitrate environments were closely resembled with our model. However, litter experimental data are available for environmentally relevant low influent nitrate conditions. It would be interesting to design experiments to check the theory under these conditions.

Table 3.3 Typical nitrate concentrations in several ecosystems

Ecosystems	NO_3^- (μM)	Source
Seawater	< 30	(Lam and Kuypers, 2011)
Groundwater	< 806	(Spalding and Exner, 1993)
Surface water	< 161	(EC, 2018)
Marine sediments	3.7-17.8	(Bonin, 1996)
Terrestrial ecosystems ^a	0.01-4.96 ^b	(Rütting et al., 2011)
WWTPs	$< 4200^c$	(Henze et al., 2008)

a: Forest, grassland, riparian;

b: in μM /g soil

c: assuming all the influent ammonium is converted to nitrate for a medium strength municipal wastewater

In the context of WWTPs, nitrate concentrations and COD/N ratios could change in a wide range along the treatment line. DNRA bacteria were shown to be enriched from activated sludge in chemostats with high COD/N ratio influent (Van Den Berg et al., 2015) and coexisted with denitrifiers in wastewater treatment wetlands (Jahangir et al., 2017; Rahman et al., 2019). Besides, the use of biofilm reactors is increasing, where substrate gradients can be formed within the biofilm and may thus create microenvironments with high COD/N for DNRA to proliferate. The role of DNRA in WWTPs needs to be further characterized.

Some of the seemingly conflicting results concerning the impact of COD/N ratio may partially attribute to the type of system used for investigation, i.e., continuous (i.e., chemostat) versus batch cultures. In continuous cultures, the competition outcome is determined by the subsistence concentration for the limiting resource (J_s , Eq. 3.2), as shown in this study. Stable resource limitation can be reached in continuous cultures but not in batch cultures (Kuenen and Johnson, 2009; van den Berg et al., 2016). In batch cultures, the competition outcome of different microorganisms is determined by

their maximum growth rate (Veldkamp and Kuenen, 1973). Using both systems with a dual-pathway pure culture, Yoon et al. (2014) suggested that the batch systems cannot resolve the impact of COD/N ratio on pathways selection between denitrification and DNRA. In a batch incubation system, the shift from DEN to DNRA with increasing initial COD/N ratios, as expected in continuous cultures, was not established (Behrendt et al., 2014). Fig. A3.6 demonstrates a straightforward comparison between these two systems. With the same initial conditions (COD/N ratio of 6.86, same of amount of DNRA and DEN bacteria), DNRA outcompeted DEN in a continuous culture at steady state with nitrate being the limiting substrate, whereas the opposite competition outcome was obtained in a batch culture (Fig. A3.6). Therefore, caution is required when comparing the results obtained from batch and continuous cultures.

3.3.3 Impact of dilution rate on competition outcomes

In chemostats, the dilution rate (D) dictates the rate of resource supply and biomass washout. A species cannot survive in chemostats above a certain dilution rate (lower than its μ_{max}). The impact of D on single species has been well documented, for instance, in Kuenen and Johnson (2009). The impact of D on the coexistence of two species was thus focused. According to the resource-ratio theory, stable coexistence is only possible when denitrifiers and DNRA bacteria each have lower subsistence concentration for one of the two resources (i.e., $J_{NO_3^{DEN}} > J_{NO_3^{DNRA}}$ and $J_{COD^{DEN}} < J_{COD^{DNRA}}$). A critical dilution rate ($D_C = 0.0435 \text{ h}^{-1}$) for coexistence was thus calculated as a function of the maximum growth rate and affinity constant for nitrate of the two species (detailed in A3.7). Below D_C , all four possible competition outcomes could occur, whereas above D_C , DNRA could not outcompete denitrification (Fig. 3.5A).

The boundaries of the region for coexistence (i.e., region 4 in Fig. 3.4) were used for illustrating the impact of investigated factors on competition outcomes since it is the conjunction region. Fig. 3.5B illustrates the impact of D on the boundaries of coexistence when D was lower than D_C . Firstly, with the increase of D , the J_s also increased (Eq. 3.2) and thus the minimum requirement for resources to sustain the biomass. Secondly, the impact of D was marginal at high influent nitrate concentrations (e.g., $>1000 \mu\text{M}$) but significant at low concentrations (Fig. 3.5B). At high influent concentrations, the upper and lower boundary COD/N ratios were asymptotically approaching the stoichiometric values of C_{DNRA} and C_{DEN} , respectively. At low influent

concentrations, the impact became increasingly profound as D was approaching the critical dilution rate ($D_c = 0.0435 \text{ h}^{-1}$, Fig. 3.5B). For instance, the boundary COD/N ratios (g COD g N^{-1}) for coexistence were 4.3-6.4 and 7.8-9.6 for a dilution rate of 0.026 and 0.043 h^{-1} (at influent nitrate concentration of 100 μM , Fig. 3.5B), respectively.

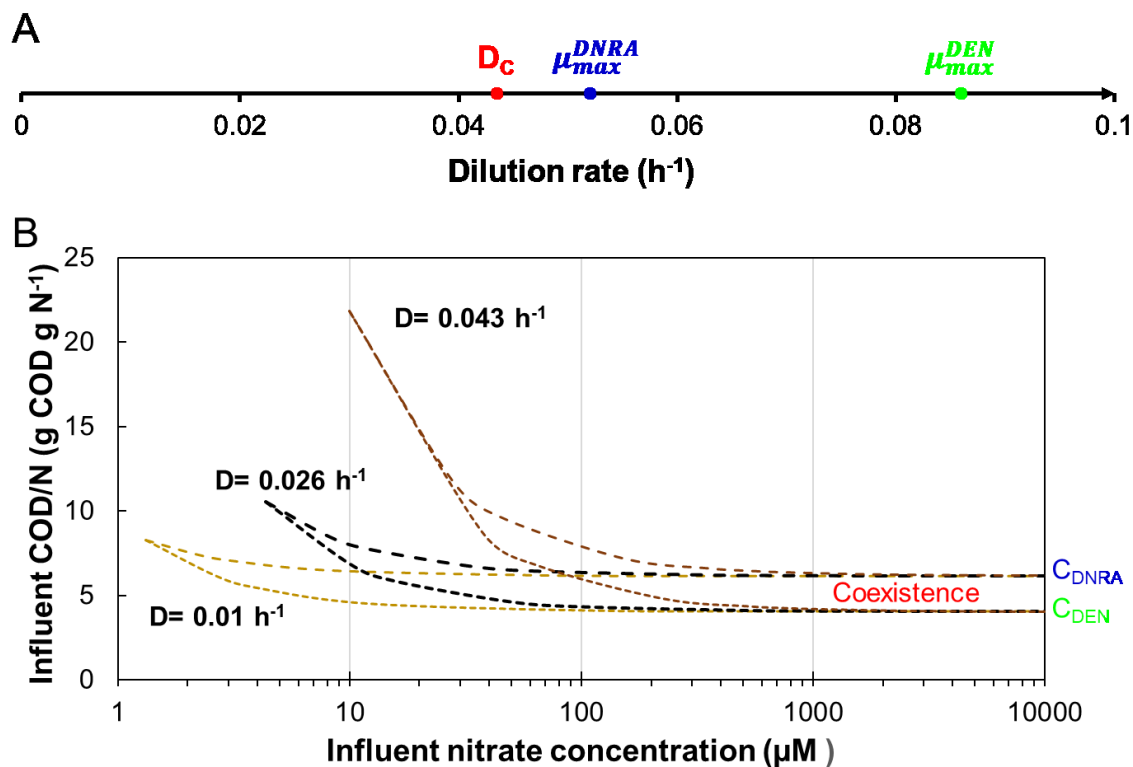


Figure 3.5. Impact of dilution rate on (A) possible competition outcomes; (B) the boundaries of coexistence.

Overall, the results highlight the importance of dilution rate on competition outcome, especially at low resource concentration and/or at high dilution rate. The critical dilution rate for coexistence (D_c) enabled to justify the measured competition outcomes by Rehr and Klemme (1989). In mixed pure cultures of DNRA bacteria (*Citrobacter freundii*) and denitrifiers (*Pseudomonas stutzeri*) competing for nitrate and lactate, stable coexistence was obtained at low dilution rate (0.05 h^{-1}) whereas DNRA bacterium started to be washed out at a dilution rate (0.1 h^{-1}) much lower than its μ_{max} (0.19 h^{-1}) (Rehr and Klemme, 1989). The results on the impact of dilution rate were in agreement with the observations in environmental enrichments by Kraft et al. (2014) where denitrifiers outcompeted DNRA bacteria at lower generation time (thus higher dilution rate) even under nitrate-limiting conditions. Regarding the COD/N range for

coexistence, van den Berg et al. (2016) suggested that it should be independent of the dilution rate. Apparently, this only holds at high resource concentrations (as used in their study) but not at low resource concentrations (e.g., < 1000 μM , Fig. 3.5B). In a similar competition scenario, Tilman (1977) studied the impact of the ratio of two nutrients on the competition outcomes of two algae species and found an apparent curvature of the boundary between stable coexistence and one species dominance at high flow rate (i.e., dilution rate), confirming the impact shown in Fig. 3.5B.

3.3.4 Impact of kinetic and stoichiometric parameters on competition outcome

A sensitivity analysis was conducted to investigate the impact of kinetic and stoichiometric parameters (i.e., K_s , μ_{max} , and Y) on the competition outcome (Fig. 3.6). The default values of these parameters (Table S2) were used for the reference case. These parameters are species-specific and may change between different denitrifiers and DNRA bacteria. The fate of nitrate is therefore subject to the local communities in an (micro-) ecosystem. The parameters for the same bacteria may also be affected by the environmental conditions (e.g., temperature and pH). For instance, the μ_{max} increases with temperature within a certain temperature range. Consequently, the difference between the μ_{max} of DNRA and DEN may also increase due to global warming and thus affect the fate of nitrate. The sensitivity analysis has the power to unravel the trend in response to the variation of the parameters and can thus give insight into their potential impact on the competition outcome.

3.3.4.1 Affinity constants for the resources

The ratio of the affinity constants of the two species for nitrate/COD was changed in two magnitudes (Fig. 3.6A). Stable coexistence (i.e., $0 < \text{fraction of DNRA} < 1$) was only possible when the ratio of the affinity constant for nitrate (i.e., $K_{\text{NO}_3^{\text{DNRA}}} / K_{\text{NO}_3^{\text{DEN}}}$) was lower than 0.43 (Fig. 3.6A, section A3.8), indicating that a sufficiently higher affinity of DNRA for nitrate relative to DEN is required. In contrast, the ratio of the affinity constant for COD (i.e., $K_{\text{COD}^{\text{DNRA}}} / K_{\text{COD}^{\text{DEN}}}$) had to be higher than 0.43 for coexistence (Fig. 3.6A, section A3.8). This threshold (i.e., 0.43) was determined by the μ_{max} of the two species and the D of the continuous culture (detailed in section A3.8). Regarding the absolute values of affinity constants, with the simultaneous increase of $K_{\text{NO}_3^{\text{DNRA}}}$ and $K_{\text{NO}_3^{\text{DNRA}}}$ (at fixed $K_{\text{NO}_3^{\text{DNRA}}} / K_{\text{NO}_3^{\text{DEN}}}$ ratio), the pattern changed from DNRA-favored (reference

case) to coexistence-favored and further to DEN-favored pattern (Fig. 3.6B). This implies that the lower the affinity for nitrate of the two competing species, the lower the threshold (minimum COD/N ratio) for DNRA dominance, especially at low nitrate concentration.

Affinity for the competing resources are often used to predict competition outcomes (Dimitri Kits et al., 2017; Straka et al., 2019b). The result demonstrated that the species with higher affinity (i.e., lower K_s) for the limiting resources did not necessarily outcompete other species in continuous cultures (e.g., when $K_{NO_3}^{DNRA}/K_{NO_3}^{DEN}=0.2$ and $K_{COD}^{DNRA}/K_{COD}^{DEN}=0.5$, DNRA bacteria would have a higher affinity for both nitrate and COD. Nevertheless, stable coexistence rather than the displacement of DEN was possible (Fig. 3.6A)). This illustrates that affinity alone was not sufficient to predict the competition outcome in continuous cultures. The μ_{max} and D need to be taken into account as well, as expressed by J_s parameter (Eq. 3.2) (Hansen and Hubbell, 1980; Hsu et al., 1981; Winkler et al., 2017).

3.3.4.2 Maximum specific growth rate

The difference between the μ_{max} of the two species (i.e., $\Delta\mu_{max}=\mu_{max}^{DEN}-\mu_{max}^{DNRA}$) was used for sensitivity analysis (Fig. 3.6C). The increase of $\Delta\mu_{max}$ led to no pattern change but a higher threshold for coexistence, whereas the decrease of $\Delta\mu_{max}$ resulted in a gradual shift towards the coexistence-favored pattern. This implies that the bigger the difference between the μ_{max} of the two competing species, the more likely the dominance of denitrification at low resource concentrations would be (i.e., the higher the maximum COD/N ratio for DEN dominance). The constraint for μ_{max} to allow stable coexistence was detailed in section A3.8.

3.3.4.3 Yield coefficient

Regarding the yield coefficient, the C criterion (i.e., the ratio of Y_{NO_3} to Y_{COD} , Eq. 3.4) of the two competing species was used for sensitivity analysis (Fig. 3.6D). Results show that it only affected the upper or lower limits. The higher the difference between C_{DNRA} and C_{DEN} (i.e., higher ΔC), the broader the region for coexistence (Fig. 3.6D). This was in line with the observations of the two case studies used for theory verification (Table S3). A lower ΔC was measured in case 2 (Van Den Berg et al., 2015) relative to case 1 (van den Berg et al., 2016) and thereby a narrowed region for

coexistence in case 2. Noteworthy, if C_{DNRA} were lower than C_{DEN} , stable coexistence would no longer be possible (Hsu et al., 1981; Tilman, 1980), which in turn supported the measured higher biomass yield over nitrate of DNRA bacteria than that of denitrifiers (Strohm et al., 2007; Van Den Berg et al., 2015).

3.3.4.4 Summary of sensitivity analysis

The sensitivity analysis illustrated that kinetic and stoichiometric parameters (i.e., K_s , μ_{max} , and Y) affected both the possibility and the boundaries of stable coexistence of denitrifiers and DNRA bacteria. When stable coexistence is possible, process stoichiometries (i.e., consumption of COD per nitrate) of the two competing processes were the determining factor of the boundary COD/N ratios at high influent resource concentrations, whereas kinetics (i.e., K_s and μ_{max}) had a significant impact on the boundaries (pattern) and thus the competition outcome mainly at low influent resources concentrations (e.g., $<100 \mu\text{M}$ nitrate). The stoichiometries (reflected on C_i) could shift the boundaries across all concentration spectrum and had greater impact at high influent resource concentrations than at low influent resource concentrations.

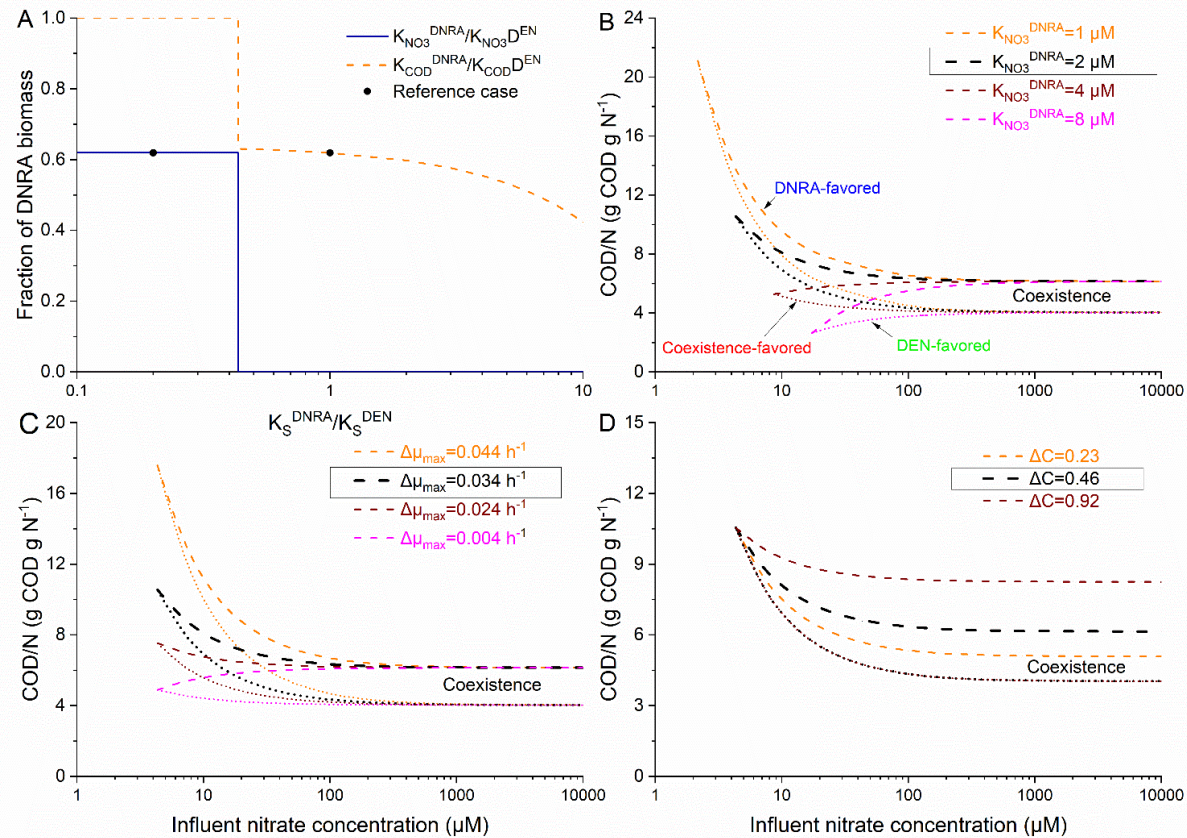


Figure 3.6. Impact of microbial kinetics and energetics on the boundaries for coexistence: (A) the ratio of the affinity constants of the two species for the same resource (conditions: influent COD/N=5.3 with 1000 μM nitrate and fixed affinity constants for denitrifiers); (B) affinity for nitrate, expressed as $K_{NO_3}^{DNRA}$, with fixed $K_{NO_3}^{DNRA}/K_{NO_3}^{DEN}$; (C) maximum growth rate, expressed as $\Delta\mu$ (i.e., $\mu_{max}^{DEN} - \mu_{max}^{DNRA}$) and (D) yield coefficient, expressed as ΔC (i.e., $C_{DNRA} - C_{DEN}$). The values in the box were default values at the reference case.

3. 3.5 Dynamic system behaviour

Fig. 3.7 demonstrates the trajectories to stable coexistence at a steady state, with the evolution of the two competing species and two resources in Fig. 3.7A and the calculated growth rates (μ , Eq.1&3) in Fig. 3.7B. In the dynamic system behaviour, four phases could be distinguished based on the limiting resource for the growth of DNRA (Fig. 3.7B).

In phase I, the growth of DNRA was limited by acetate ($\mu_{\text{DNRA}} = \mu_{\text{DNRA,C}}$, Fig. 3.7B). The concentration of nitrate and acetate in the chemostat decreased with the growth of denitrifiers and DNRA bacteria (Fig. 3.7A), which in turn resulted in their decreased growth rates (Fig. 3.7B). By the end of phase I, nitrate concentration reached $J_{\text{NO}_3^{\text{DNRA}}}$ ($< J_{\text{NO}_3^{\text{DEN}}}$), at which the growth rate of denitrifiers (μ_{DEN}) could not balance the loss rate ($\mu_{\text{DEN}} < D$, Fig. 3.7B) and the biomass concentration of denitrifiers thus decreased (Fig. 3.7A). In phase II, the growth of DNRA was limited by nitrate ($\mu_{\text{DNRA}} = \mu_{\text{DNRA,N}}$, Fig. 3.7B) and the low nitrate concentration favored DNRA bacteria, i.e., $\mu_{\text{DNRA}} > \mu_{\text{DEN}}$ (Fig. 3.7B). Meanwhile, acetate concentration decreased further and reached a point where the growth of DNRA bacteria shifted to become acetate-limited again ($\mu_{\text{DNRA}} = \mu_{\text{DNRA,C}}$, phase III, Fig. 3.7B). In phase III, μ_{DNRA} started decreasing with decreasing acetate concentration, resulting in a lower nitrate consumption by DNRA bacteria. Consequently, the nitrate concentration gradually recovered to reach $J_{\text{NO}_3^{\text{DEN}}}$. Simultaneously, the acetate concentration further decreased to reach $J_{\text{COD}^{\text{DNRA}}}$ ($> J_{\text{NO}_3^{\text{DEN}}}$) by the end of phase III. From this point, the growth rate of the two competing species became identical and equaled to the dilution rate of the chemostat and thereby reached the steady state (phase IV).

Noteworthy, both nitrate and acetate were limiting (i.e., dual limitation) in phase III&IV, with DNRA being acetate-limited ($J_{\text{COD}^{\text{DNRA}}} > J_{\text{COD}^{\text{DEN}}}$) and DEN nitrate-limited ($J_{\text{NO}_3^{\text{DEN}}} > J_{\text{NO}_3^{\text{DNRA}}}$). Therefore, coexistence occurred at a steady state because each species was limited by the resource for which its rival has the lower subsistence concentration (J_s) and thus competitive advantage, i.e., DNRA by acetate, whereas DEN by nitrate. This is in line with the proposed theoretical condition for coexistence (Bader, 1978; Hsu et al., 1981; Tilman, 1980) and observed competition behavior (i.e., dual-limitation of acetate and nitrate at stable coexistence (van den Berg et al., 2016)).

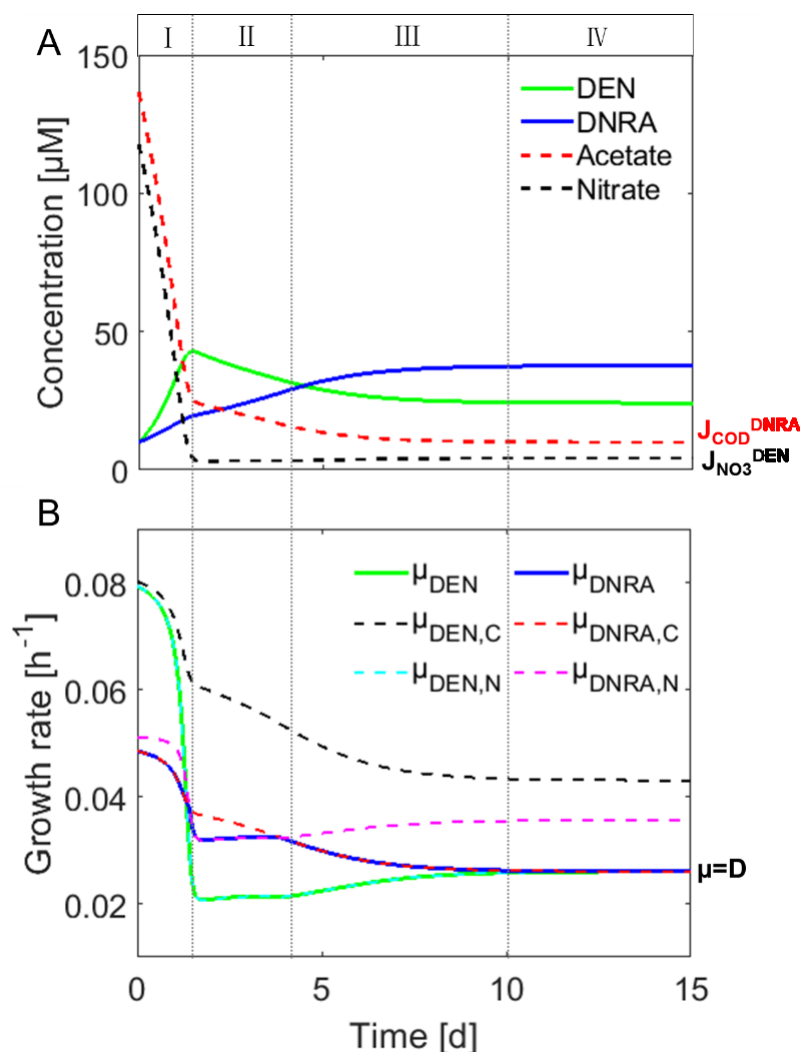


Figure 3.6. Trajectories of: (A) resources and species concentrations; (B) calculated growth rate in a chemostat fed with acetate and nitrate at a COD/N ratio of 5.3, under which stable coexistence of DEN and DNRA was observed (van den Berg et al., 2016) and predicted (this study). The denitrifiers and DNRA bacteria were initially equally presented in a chemostat.

3.3.6 Model limitations and their implications

In this study, denitrification and DNRA were assumed to directly compete for nitrate and be carried out by two distinct specialist species. This section discusses the role of nitrite, the potential difference between specialist and dual-pathway species and the complexity of electron donor (organics), and their implications in predicting the competition outcome.

Nitrite is the common intermediate and the branching point of the two pathways, and both nitrate and nitrite can be the terminal electron acceptors in DEN and DNRA (Kraft et al., 2011). However, there is still a lack of consensus about the role of nitrite in their

competition. Kraft et al. (2014) found a shift from DNRA to DEN when nitrate was replaced by nitrite in a continuously fed chemostat enrichment systems with marine sediments and postulated nitrite as a determining factor in the selection of the two pathways, suggesting that denitrifiers have a comparatively higher affinity for nitrite. Yoon et al. (2015) showed the ratio of nitrite to nitrate was a determining factor in pathway selection in a chemostat study with dual-pathway pure culture, with DNRA dominated at higher nitrite/nitrate ratios. In contrast, van den Berg et al. (2017b) demonstrated that nitrite does not generally control the competition between denitrification and DNRA in chemostat enrichment cultures. In general, if there is nitrite accumulation, there is no need to consider nitrite in the model. If the competition of denitrification and DNRA only lies in the nitrite reduction, then the resource-ratio theory could be easily implemented in the same way. However, the parameters related to nitrite (e.g., K_s and yield) are still largely missing and need further determination. In the case where nitrite accumulation is observed, the applicability of the resource-ratio theory would be limited as it would be thus unable to describe DEN and DNRA as one-step reactions.

Partial DNRA (nitrate to nitrite) can be an alternative pathway for nitrite supply to the anammox conversion. Previous studies show that it can be coupled with anammox process (i.e., Partial DNRA-Anammox, PDA, Chapter 1) in standalone anammox (Chapter 2 and (Castro-Barros et al., 2017)) or integrated partial nitrification-anammox systems (Winkler et al., 2012). By doing so, the nitrate produced from anammox reaction could be reduced and thereby improve the nitrogen removal of these systems. In fact, the combined partial DNRA-anammox reaction by anammox bacteria was found thermophilically favourable at low COD/N ratio conditions (Castro-Barros et al., 2017). Nonetheless, maintaining a low influent COD/N ratio is vital for this purpose as heterotrophic denitrification and/or DNRA (nitrate to ammonium) would otherwise be promoted at relatively high COD/N ratio conditions as shown in this chapter.

The possible difference between dual-pathway and specialist DNRA microorganisms deserves further clarification. In dual-pathway microorganisms, the first step (i.e., nitrate reduction to nitrite) might be catalyzed by the same enzyme, and the competition of the two pathways thus lies on nitrite. For example, the dual-pathway *Shewanella loihica* PV-4 utilizes NapA and *I. calvum* utilizes NarG for nitrate reduction (Vuono et al., 2019). This may explain the observed determining effect of nitrite on

pathway selection in *Shewanella loihica* PV-4 (Yoon et al., 2015b) but not in the enrichment cultures where different bacteria are responsible for denitrification and DNRA (van den Berg et al., 2017b). Moreover, the competition between two species could result in the displacement of the rival, whereas competition of two pathways within the same microorganism may depend on the maximum benefit (e.g., maximum energy production or electron transfer) of the microorganism under certain conditions.

The results in this study confirmed the governing effect of COD/N ratio (i.e., electron donor/acceptor) in the selection of denitrification and DNRA and revealed what determined the boundary values, using a non-fermentative acetate as an example for electron donor. However, the nature of the electron donors (i.e., organic carbon) can be complex and have been shown to affect the competition outcome (Kraft et al., 2014; Rehr and Klemme, 1989; van den Berg et al., 2017a). The presence of fermentative organic carbon (e.g., lactate) may stimulate fermentative bacteria which can directly compete for both nitrate and organic carbon through fermentative DNRA process (Cole, 1996) and/or alter the organic carbon available for DNRA process (van den Berg et al., 2017a). Previous study suggested that the nitrogen conversions in the oxygen minimum zones (OMZs) of the ocean were likely regulated by organic carbon (Lam and Kuypers, 2011). The composition and concentration of organic carbon can change both spatially and temporally, and different organic compounds may have different influences on various microbial processes (Kovárová-Kovar and Egli, 1998; Lam and Kuypers, 2011; Muscarella et al., 2019). More detailed organic geochemical analyses in different ecosystems and incorporation of fermentative bacteria in the DNRA modelling are thus called for.

3.3.7 Potential application of the resource-ratio theory in other studies

One commonly accepted theory for interspecies competition for the same substrate is the K/r strategist hypothesis (Andrews and Harris, 1986; Dorodnikov et al., 2009). With the default kinetics currently available, DNRA resembles a K-strategist (species with high substrate affinity and low μ_{max}) and DEN an r-strategist (species with low substrate affinity and high μ_{max}). According to this theory, DNRA would win the competition against DEN when both organisms are subjected to low-nitrate conditions (i.e., high COD/N), which agrees with the prediction of the resource-ratio theory that was used here (Fig. 3.4) and that are also confirmed experimentally (Rehr and Klemme, 1989;

Van Den Berg et al., 2015). Nevertheless, the K/r strategist hypothesis only considers one limiting substrate (nitrate or COD), whereas the resource-ratio theory simultaneously takes both limiting substrates (and dilution rate) into account and is thus more comprehensive.

In this study, the resource-ratio theory was applied to elucidate the competition between denitrification and DNRA for nitrate and organic carbon. Nevertheless, the conclusions and their implications can be extended to other similar competition scenarios, for instance, the competition between ammonia-oxidizing bacteria (AOB), archaea (AOA), and comammox microorganisms for ammonia and oxygen. As demonstrated in this study and previously (Bellucci et al., 2015; Miller et al., 2005; Smith et al., 1998), the resource ratio-theory offers mechanistic insights and quantitative prediction of competition outcomes between microorganisms for common resources. Despite its relatively easy implementation and great value, its application in the microbial competition is still rather limited. To ease the application, a decision tree (Fig. A3.2) and a spreadsheet model (Spreadsheet A.3.1, Appendix) were created and provided for the generalized scenario where two species exploitatively compete for two essential resources, as is the case for DEN and DNRA.

3.4 Conclusions

The resource-ratio theory was applied to elucidate the competition between heterotrophic denitrification and DNRA in continuous cultures and verified with experimental results. The results highlight the impact of resource concentrations, dilution rate and microbial kinetic and stoichiometric parameters on the boundary COD/N ratios and thus the competition outcome. The COD/N ratio dictated the competition between the two nitrate partitioning pathways; however, the boundary values changed significantly with influent resource concentrations. At high influent resource concentrations, the stoichiometries (i.e., consumption of COD per nitrate) of the two competing processes was the determining factor of the boundary COD/N ratios, whereas kinetics (i.e., K_S and μ_{max}) was important as well but only at low influent resource concentrations. The dilution rate became significant at low influent resource concentration and/or high values close to the critical ones. At stable coexistence, the growth of DNRA and DEN was limited by COD and nitrate, respectively. The results also provide testable hypotheses concerning the nitrate partitioning at environmentally

relevant low nitrate conditions for further research. The conclusions based on the verified resource-ratio theory potentially have broad implications for similar competition scenarios.

Acknowledgments

Mingsheng Jia acknowledges the support from China Scholarship Council (CSC) and the special research fund (BOF) from Ghent University.

Appendix

A3.1 The resource-ratio theory

A3.1.1 Model description through mass balances

The system under study consists of two species (N1 and N2) competing for two essential resources (S, R), which can be described by the set of mass balances (Hsu et al., 1981). When applied to the competition between heterotrophic denitrification (DEN: $\text{NO}_3^- \rightarrow \text{N}_2$) and DNRA ($\text{NO}_3^- \rightarrow \text{NH}_4^+$), the subscripts 1 and 2 respectively denote DEN and DNRA species, while S and R respectively denote the two shared resources, namely nitrate and COD (Fig. A3.1).

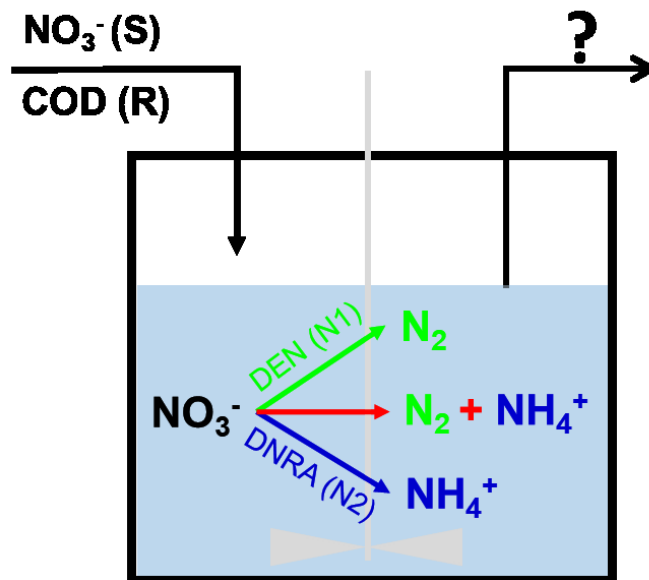


Figure A3.1. Graphic representation of the continuous system under investigation

$$\mu_i(S, R) = \min \left(\mu_{max,i} \frac{S}{K_{Si} + S}, \mu_{max,i} \frac{R}{K_{Ri} + R} \right) \quad (\text{A3.1})$$

$$\frac{dX_{N1}}{dt} = [\mu_1(S, R) - D]X_{N1} \quad (\text{A3.2})$$

$$\frac{dX_{N2}}{dt} = [\mu_2(S, R) - D]X_{N2} \quad (\text{A3.3})$$

$$\frac{dS}{dt} = (S_0 - S)D - \frac{1}{Y_{S1}}\mu_1(S, R)X_{N1} - \frac{1}{Y_{S2}}\mu_2(S, R)X_{N2} \quad (\text{A3.4})$$

$$\frac{dR}{dt} = (R_0 - R)D - \frac{1}{Y_{R1}}\mu_1(S, R)X_{N1} - \frac{1}{Y_{R2}}\mu_2(S, R)X_{N2} \quad (\text{A3.5})$$

where,

$\mu_i(S, R)$ is the actual growth rate of species with resources S and R;

$\mu_{max,i}$ is the maximum growth rate of species i (h^{-1});

K_{Si} is half-saturation constant of species i for S (μM);

K_{Ri} is half-saturation constant of species i for R (μM);

S_0 is the influent concentration of resource S (μM);

S is the concentration of resource S (μM);

R_0 is the influent concentration of resource R (μM);

R is the concentration of resource R (μM);

D is the dilution rate (h^{-1});

Y is the yield coefficient of the species over resource S or R (mold X per mole S or R);

X_{N1} is the biomass concentration of species N1;

X_{N2} is the biomass concentration of species N1;

A3.1.2 Procedures for the application of the resource-ratio theory

To ease the application of the resource-ratio theory, a decision tree was made in stepwise (Fig. A3.2), accompanied by a demonstration in Spreadsheet A3.1.

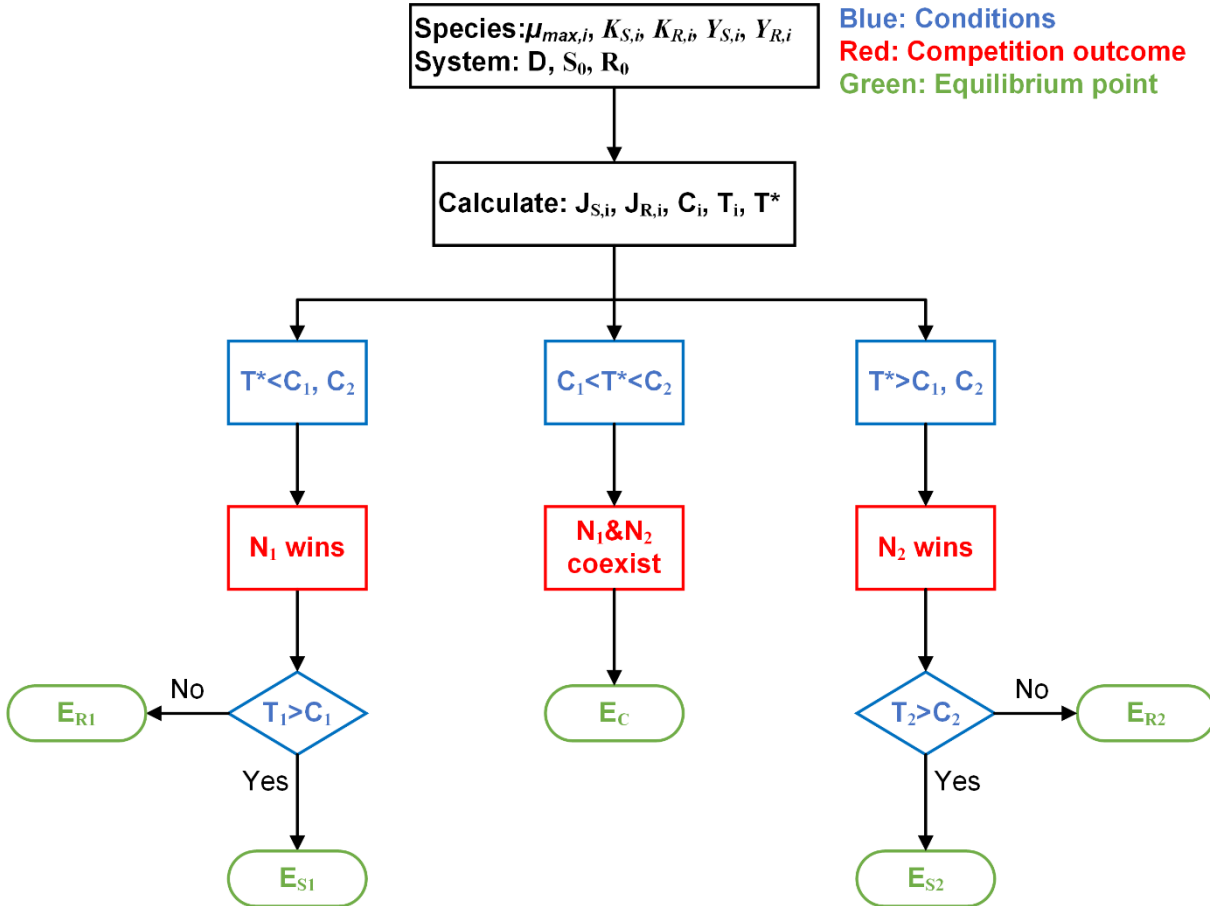


Figure A3.2. The decision tree for predicting the competition outcome of two species competing for two essential resources using the resource-based competition theory (Assumptions: $S_0 > J_{S1} > J_{S2} > 0$, $R_0 > J_{R2} > J_{R1} > 0$ and $C_1 < C_2$). E_{S1} represents the equilibrium point where species 1 wins the competition and is S-limited at steady state (Table A3.1)).

The J and C criteria are respectively defined in Eq. 2 and Eq. 4. Two new criteria are introduced in this figure:

$$T_i = \frac{R_0 - J_{Ri}}{S_0 - J_{Si}} \tag{A3.6}$$

$$T^* = \frac{R_0 - J_{R2}}{S_0 - J_{S1}} \tag{A3.7}$$

The biological meaning of the two criteria can be found in (Hsu et al., 1981). For example, by comparing T_1 with C_1 , we can determine whether species 1 is S-limited or R-limited and thus the equilibrium point. For example, if $T_1 > C_1$, then the growth rate of species 1 is S-limited because S is supplied at a steady-state rate slower than R with respect to the required consumption ratio for species 1. The analytical solutions of the concentrations of the two species and two resources for each equilibrium point are summarized in Table A3.1.

Table A3.1. The analytical solutions of status at the equilibrium points in Fig. A3.2, derived from (Hsu et al., 1981)

Equilibrium point	Nitrate (S^*)	COD (R^*)	DEN (N_1^*)	DNRA (N_2^*)	Competition outcome
E_{s1}	J_{s1}	$R_0 - \frac{N_1^*}{y_{R1}}$	$y_{s1}(S_0 - J_{s1})$	0	N_1 wins
E_{r1}	$S_0 - \frac{N_1^*}{y_{s1}}$	J_{R1}	$y_{R1}(R_0 - J_{R1})$	0	N_1 wins
E_{s2}	J_{s2}	$R_0 - \frac{N_2^*}{y_{R2}}$	0	$y_{s2}(S_0 - J_{s2})$	N_2 wins
E_{r2}	$S_0 - \frac{N_2^*}{y_{s2}}$	J_{R2}	0	$y_{R2}(R_0 - J_{R2})$	N_2 wins
E_C	J_{s1}	J_{R2}	$\frac{y_{s1}(S_0 - J_{s1})(C_2 - T^*)}{C_2 - C_1}$	$\frac{y_{s2}(S_0 - J_{s1})(T^* - C_1)}{C_2 - C_1}$	Coexistence
E_0	S_0	R_0	0	0	All washout

A3.1.3 Mathematical conditions for each region in Fig. 3.1

The conditions with respect to the influent concentration of resource S and R for the 6 regions in Fig. 3.1 are given here.

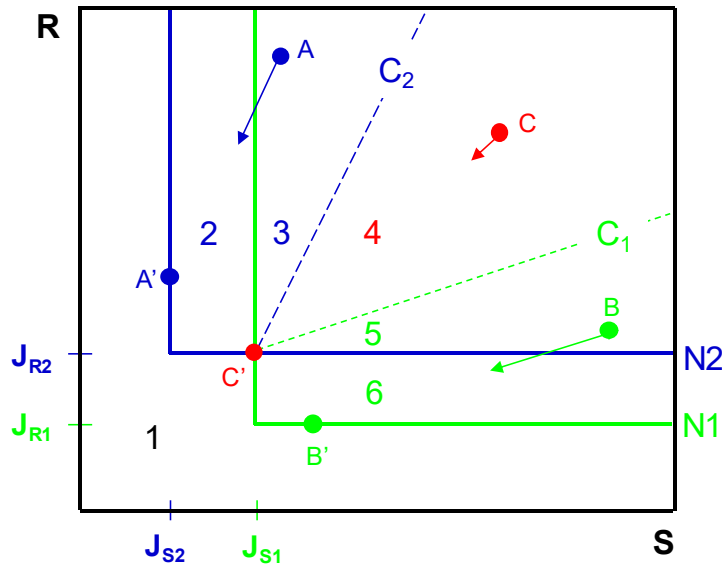
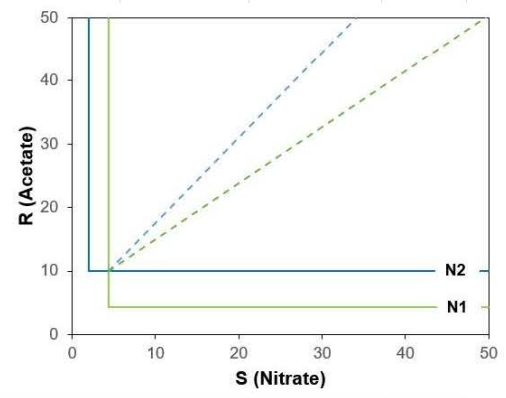


Figure A3.3. Graphical representation of resource competition of two species (N1 and N2) competing for two resources (S and R) at a specific dilution rate (the same as Fig. 3.1)

- Region 1, no species can survive, i.e., all washout;
Conditions: $S_0 < J_{S1}$ or $R_0 < J_{R1}$
- Region 2, only species N2 (i.e., DNRA) can survive;
Conditions: $J_{S2} < S_0 < J_{S1}$ and $R_0 > J_{R2} > J_{R1}$
- Region 3, species N2 outcompete N1, i.e., DNRA outcompete DEN;
Conditions: $S_0 > J_{S1} > J_{S2}$, $R_0 > J_{R2} > J_{R1}$ and $T^* > C_2 > C_1$
- Region 4, species N1 and N2 can coexist, i.e., DEN and DNRA can coexist;
Conditions: $S_0 > J_{S1} > J_{S2}$, $R_0 > J_{R2} > J_{R1}$ and $C_1 < T^* < C_2$
- Region 5, species N1 outcompete N2, i.e., DEN outcompete DNRA;
Conditions: $S_0 > J_{S1} > J_{S2}$, $R_0 > J_{R2} > J_{R1}$ and $T^* < C_1 < C_2$
- Region 6, only species N1 (i.e., DEN) can survive;
Conditions: $S_0 > J_{S1} > J_{S2}$, $J_{R1} < R_0 < J_{R2}$

Spreadsheet A3.1. Spreadsheet for outcome prediction of the competition between two species for two shared resources

Implementation of Resource-Ratio Theory							Assumptions						
Input	Physiological parameters	General	Definition	DEN (N1)	DNRA (N2)	Unit	Assumptions check assumptions						
		Ys1	Yield per mole nitrate (S)	0.431	0.656	C-mol X/mol NO3	OK	S0>Js1>Js2>0					
		Yr1	Yield per mole acetate (R)	0.488	0.488	C-mol X/mol Ac	OK	R0>Jr2>Jr1>0					
		$\mu_{max,i}$	maximum growth rate	0.086	0.052	h ⁻¹	OK	C1<C2					
		Ks1	K_NO3, affinity constant	10.0	2.0	μ M							
	Kr1	K_Ac, affinity constant	10.0	10.0	μ M								
	System parameter	D	Dilution rate		0.026	h ⁻¹							
Resource input	S0	Influent nitrate con.		11790.00	μ M								
	R0	Influent acetate con.		15000.00	μ M								
Calculation	Criteria	Js1	Substance con. for nitrate	4.333	2.000	μ M							
		Jr1	Substance con. for Ac	4.333	10.000	μ M							
		Ci	consumption of R per S	0.883	1.344								
		Ti	T parameter	1.272	1.272								
		T*	T* parameter		1.272								
Output	Competition outcome						Coexist						
	Equilibrium point:						Es1						
	If N1 wins, check this						Er2						
	If N2 wins, check this						Ec						
Status of equilibrium point (Table A3.3)													
Equilibrium point		Es1	Er1	Ec	Es2	Er2							
S	μ M	4.33	-5188.85	4.33	2.00	638.90							
R	μ M	4590.94	4.33	10.00	-846.16	10.00							
N1	μ M	5079.62	7317.89	797.40	0.00	0.00							
N2	μ M	0.00	0.00	6517.72	7732.93	7315.12							
Graphical display													
Isoclines	X	Y	Consumption vectors		X	Y							
	μ M	μ M			μ M	μ M							
ZNGI_1Y	4.333	4.333	(Js1, Jr1)	C1_line	4.333	10.000	(Js1, Jr2)						
	4.333	50.000			50.000	50.333							
ZNGI_1X	4.333	4.333		C2_line	4.333	10.000							
	50.000	4.333			34.089	50.000							
ZNGI_2Y	2.000	10.000	(Js2, Jr2)										
	2.000	50.000											
ZNGI_2X	2.000	10.000											
	50.000	10.000											
Case study: van den Berg et al., 2016 (Example)													
Ac/N	COD/N				Criteria	Predicted outcome	Experiment	Equilibrium point	Nitrate (S)	Acetate (R)	DEN (N1)	DNRA (N2)	
1.23	3.72	S0		11790.00	μ M	C1<T*<C2	Coexist	Coexist	Ec	4.333	10.000	1263.209	4321.136
	Dual-limit	R0		14501.70	μ M								
	case c	Ti	1.230	1.2294									
		T*		1.2296									
1.5	6.86	S0		11790.00	μ M	T*>C1, C2 & T2>C2	DNRA (N2) wins	DNRA (N2) wins	Es2	2.000	1838.836	0.000	7732.928
	N-limit	R0		17685.00	μ M								
		Ti	1.500	1.4994									
		T*		1.4997									



A3.2 Application of the theory for denitrification and DNRA

Table A3.2. Physiological parameters of heterotrophic denitrifiers and DNRA bacteria used for the implementation of resource-ratio theory (in μM)

Parameter	Value	Unit	Source
μ_{max}^{DEN}	0.086*	h^{-1}	(Henze et al., 1999)
Y_{COD}^{DEN}	0.488	$\text{mol C}_x \cdot \text{mol}^{-1} \text{Ac}^-$	(van den Berg et al., 2016)
$Y_{NO_3}^{DEN}$	0.431	$\text{mol C}_x \cdot \text{mol}^{-1} \text{NO}_3^-$	(van den Berg et al., 2016)
$K_{NO_3}^{DEN}$	10	μM	(van den Berg et al., 2016)
K_{COD}^{DEN}	10	μM	(van den Berg et al., 2016)
μ_{max}^{DNRA}	0.052*	h^{-1}	(van den Berg et al., 2016)
Y_{COD}^{DNRA}	0.488	$\text{mol C}_x \cdot \text{mol}^{-1} \text{Ac}^-$	(van den Berg et al., 2016)
Y_{COD}^{DNRA}	0.656	$\text{mol C}_x \cdot \text{mol}^{-1} \text{NO}_3^-$	(van den Berg et al., 2016)
$K_{NO_3}^{DNRA}$	2	μM	(van den Berg et al., 2016)
K_{COD}^{DNRA}	10	μM	(van den Berg et al., 2016)

*Temperature dependent parameters (at 20 °C)

A3.3 Experimental cases for theory verification

To verify the resource-ratio theory, two experimental case studies on the competition between heterotrophic denitrification and DNRA by van den Berg et al. (2016, 2015) were used. The experimental conditions and observed competition outcomes are further summarized in Table A3.3.

Table A3.3. Measured concentrations of biomass and resources at steady state

	COD/N (g COD.g N ⁻¹)	Measured competition outcome	Biomass concentration (μM)		
			DEN*	DNRA*	Total
Case 1 (van den Berg et al., 2016)	8.5	DNRA dominance	86	8465	8551
	6.9	DNRA dominance	87	8655	8742
	5.6	Coexistence	1510	4529	6039
	5.3	Coexistence	2082	3396	5478
	4.9	Coexistence	2965	3480	6445
	4.2	Coexistence	4042	713	4755
	3.0	DEN dominance	3601	0	3601

N.A., not available; * Calculated from the total biomass concentration and the relative abundance obtained from cell counts of the FISH analyses (van den Berg et al., 2016).

A3.4 Impact of resource concentration on competition outcome

Fig. A3.4 shows the impact of influent COD (acetate) concentrations on the boundaries of different competition outcomes.

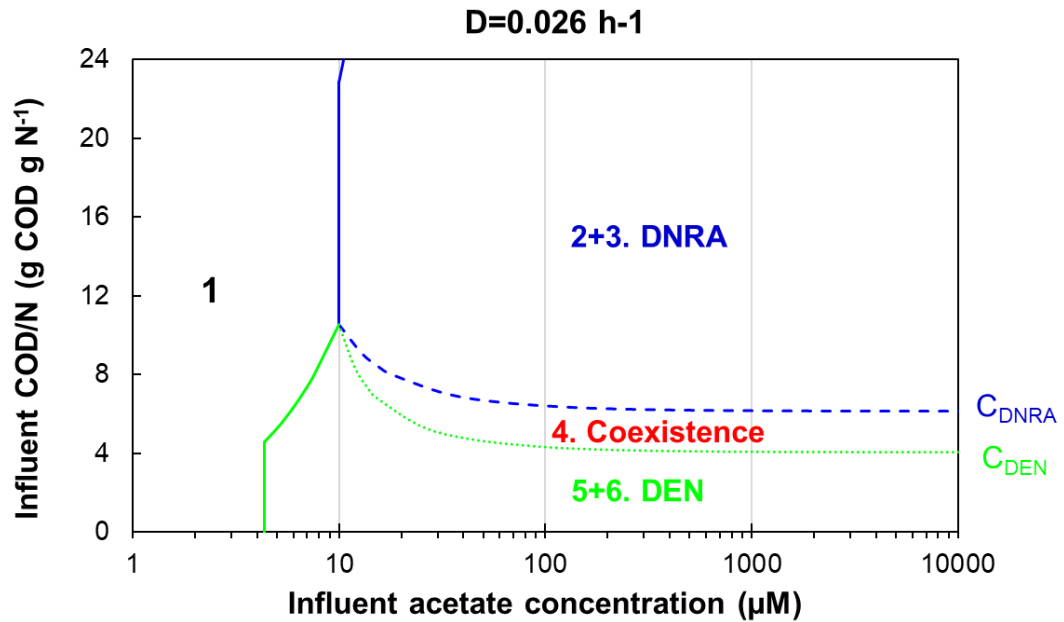


Figure A3.4. The boundary influent COD/N ratios at different influent acetate (COD) concentrations. The regions correspond to the regions with the same numbers in Fig. 3.2 and Fig. 3.4.

For a continuous culture with the same initial concentrations of DEN and DNRA bacteria, different competition outcomes can occur when it was fed with the same influent COD/N ratio but different influent resource concentrations, as demonstrated in Fig. A3.5. This illustrates the impact of resource concentration on competition outcomes.

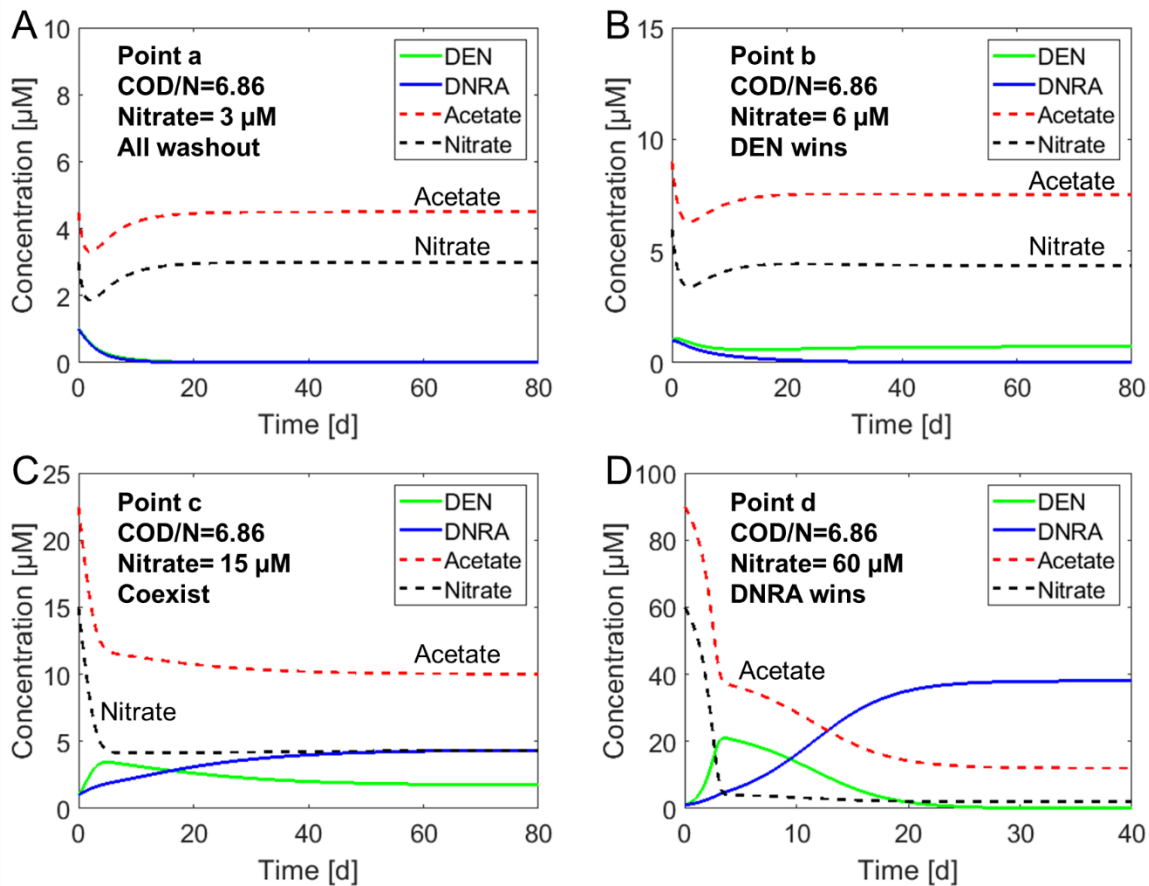


Figure A3.5. With the same influent COD/N ratio (6.86, i.e., Ac/N=1.5) at the same dilution rate (0.026 h^{-1}) but different influent resources concentrations, all four possible competition outcomes could occur (corresponding to the points a, b, c, and d in Fig. 3.4)

A3.5 Comparison between continuous and batch cultures

A chemostat and a batch system were compared to illustrate the different competition mechanisms in these two systems. The chemostat was fed with an influent COD/N ratio of 6.86 (g COD.g N⁻¹, 9000 μM acetate and 6000 μM nitrate, Fig. A3.6A), whereas the same COD/N ratio was applied as the initial conditions of the batch system (0.5d a cycle with a fixed fraction of biomass removed each cycle, Fig. A3.6B). The initial biomass concentration for DNRA and DEN was set the same (1000 μM, Fig. A3.6A and A3.6B). DNRA outcompeted DEN in the chemostat at a steady state with the nitrate being the limiting substrate (low concentration but not zero, Fig. A3.6A). This outcompetition was due to the lower J_s of DNRA for nitrate (i.e., $J_{NO_3}^{DNRA} < J_{NO_3}^{DEN}$), which translates to a higher growth rate of DNRA (μ_{DNRA}) at nitrate-limiting conditions (Fig. A3.6C). On the contrary, DEN outcompeted DNRA in the batch culture after 20 cycles (Fig. A3.6B) due to the higher growth rate of DEN compared to DNRA at high resource concentration (Fig. A3.6D).

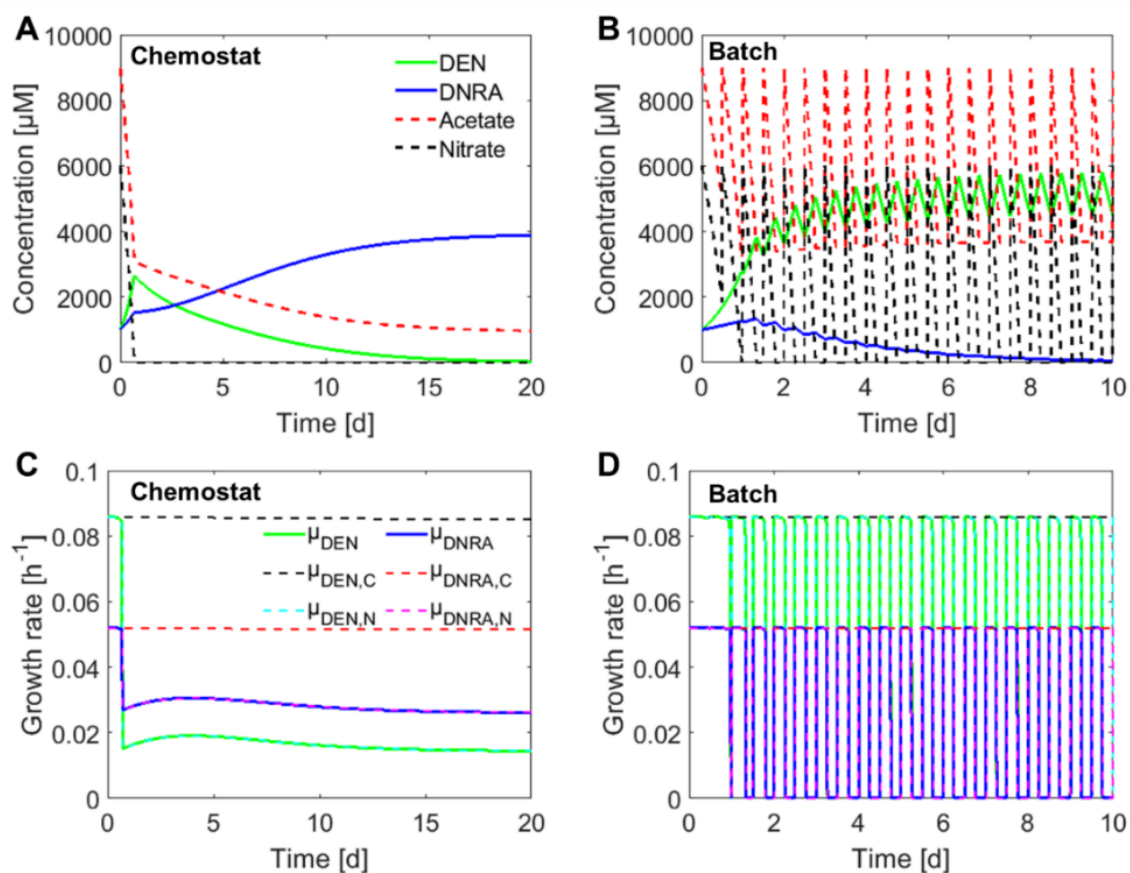


Figure A3.6. The comparison between a chemostat and a batch system in terms of the trajectories of resources and biomass (A vs. B) and the calculated growth rates (C vs. D).

A3.6 Conditions for stable coexistence

A3.6.1 Conditions for stable coexistence

According to the resource-ratio theory, for two species to stably coexist on two resources, each species need to have a lower subsistence concentration for one of the two resources (Hsu et al., 1981; León and Tumpson, 1975; Tilman, 1980). This condition sets the constraints for the parameters to allow stable coexistence (Eq. A3.8 and A3.9). When applied to the competition between heterotrophic denitrification (DEN) and DNRA, the subscripts 1 and 2 respectively denote DEN and DNRA, and S and R respectively denote nitrate and COD.

From $J_{NO_3}^{DEN} > J_{NO_3}^{DNRA}$

$$K_{S1} \cdot \frac{D}{\mu_1^{max} - D} > K_{S2} \cdot \frac{D}{\mu_2^{max} - D} \quad (A3.8)$$

From $J_{NO_3}^{DEN} < J_{COD}^{DNRA}$

$$K_{R1} \cdot \frac{D}{\mu_1^{max} - D} < K_{R2} \cdot \frac{D}{\mu_2^{max} - D} \quad (A3.9)$$

A3.6.2 What defines the COD/N ratio and patterns of the boundaries for coexistence?

The boundary (expressed as COD/N ratio) for coexistence is constrained by the two stoichiometric consumption vectors, with the slope of C_{DEN} and C_{DNRA} , respectively. DEN and DNRA can only co-exist at region 4 (Fig. 3.2 and Fig. A3.7).

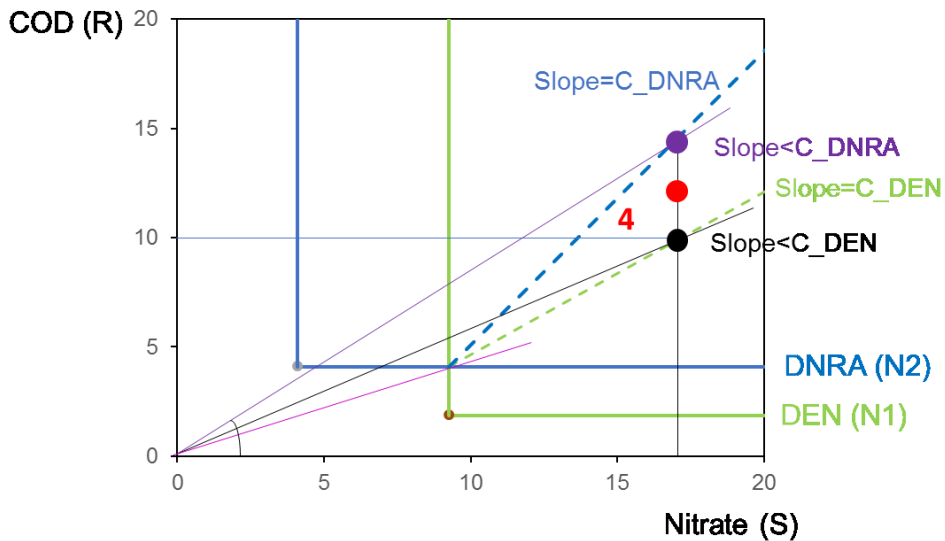


Figure A3.7. Graphical representation of boundaries of coexistence of two species (N1 and N2, in this case, DEN and DNRA, respectively) competing for two resources (S and R).

The two consumption vectors (C_{DEN} and C_{DNRA}) define the boundaries for coexistence.

- For supply point (S_0, R_0) on the consumption vector of DNRA (upper limit):

$$\frac{(R_0 - J_{R2})}{(S_0 - J_{S1})} = C_{DNRA}$$

When $R_0 \gg J_{R2}$ and $S_0 \gg J_{S1}$,

$$\frac{COD}{N} = \frac{R_0}{S_0} \approx \frac{(R_0 - J_{R2})}{(S_0 - J_{S1})} = C_{DNRA}$$

- For supply point (S_0, R_0) on the consumption vector of DEN (lower limit):

$$\frac{(R_0 - J_{R2})}{(S_0 - J_{S1})} = C_{DEN}$$

When $R_0 \gg J_{R2}$ and $S_0 \gg J_{S1}$,

$$\frac{COD}{N} = \frac{R_0}{S_0} \approx \frac{(R_0 - J_{R2})}{(S_0 - J_{S1})} = C_{DEN}$$

Therefore, the COD/N ratio in region 4 is bounded by C_{DNRA} and C_{DEN} . The boundary COD/N ratios of coexistence were always asymptotically approaching the stoichiometric ratios C_{DNRA} and C_{DEN} with increasing nitrate concentrations (e.g., Fig. 3.4). The differences lay in how the boundary COD/N ratios approach these two ratios. Theoretically, there are three possible patterns depending on the $J_{COD}^{DNRA}/J_{NO_3}^{DEN}$ in relative to C_{DNRA} and C_{DEN} (Fig. 3.6):

- (1) If $J_{COD}^{DNRA}/J_{NO_3}^{DEN} > C_{DNRA}$, then the upper limit $> C_{DNRA}$ and lower limit $> C_{DEN}$ (reference case), termed as DNRA-favored pattern, under which the region for DNRA dominance widened with increasing resource concentration, i.e., boundary COD/N for DNRA dominance decreases;
- (2) If $C_{DEN} < J_{COD}^{DNRA}/J_{NO_3}^{DEN} < C_{DNRA}$, then $C_{DEN} < \text{boundary COD/N} < C_{DNRA}$, termed as coexistence-favored pattern, under which only the region for coexistence widened with increasing resource concentration;
- (3) If $J_{COD}^{DNRA}/J_{NO_3}^{DEN} < C_{DEN}$, then upper limit $< C_{DNRA}$ and lower limit $< C_{DEN}$ (Fig. A3.4), DEN-favored pattern, under which the region for DEN dominance widened with increasing resource concentrations.

A3.7. Impact of dilution rate on coexistence

The conditions for coexistence (Eq. A3.8 and Eq. A3.9, in section A3.6) set two constraints for all the parameters. To determine the range of one (pair) parameter, one can substitute the other parameters with their default values (Table A3.2). The range of dilution rate to allow for coexistence can be thus calculated.

$$\left(\frac{K_{R1}}{K_{R2}} - 1\right)D > \frac{K_{R1}}{K_{R2}}\mu_2^{max} - \mu_1^{max} \quad (\text{A3.10})$$

$$\left(\frac{K_{S1}}{K_{S2}} - 1\right)D < \frac{K_{S1}}{K_{S2}}\mu_2^{max} - \mu_1^{max} \quad (\text{A3.11})$$

If $\frac{K_{R1}}{K_{R2}} < \frac{\mu_1^{max}}{\mu_2^{max}}$, as in the reference case, then

$$0 < D < \frac{\frac{K_{S1}}{K_{S2}}\mu_2^{max} - \mu_1^{max}}{\frac{K_{S1}}{K_{S2}} - 1} = 0.0435 = D_c$$

Below D_c , stable coexistence is possible with sufficient influent resources, whereas above D_c , DNRA would have higher J for both nitrate and COD and thus unable to compete with DEN, i.e., no stable coexistence.

If $\frac{\mu_1^{max}}{\mu_2^{max}} < \frac{K_{R1}}{K_{R2}} < \frac{\mu_1^{max-D}}{\mu_2^{max-D}}$, then

$$\frac{\frac{K_{R1}}{K_{R2}}\mu_2^{max} - \mu_1^{max}}{\frac{K_{R1}}{K_{R2}} - 1} < D < \frac{\frac{K_{S1}}{K_{S2}}\mu_2^{max} - \mu_1^{max}}{\frac{K_{S1}}{K_{S2}} - 1}$$

Below the lower limit, DNRA would have lower J for both nitrate and COD and thus be favored. Between the two limits, stable coexistence is possible, whereas above the higher limit, DEN would lower J for both nitrate and COD, and thus be favored.

A3.8. Sensitivity analysis

The conditions for coexistence (Eq. A3.8 and Eq. A3.9, in section A3.6) set two constraints for all the parameters. To determine the range of one (pair) parameter, one may substitute the other parameters with their default values (Table A3.2 and 0.026 h⁻¹ for dilution rate).

A3.8.1 Sensitivity analysis for affinity constant (Ks)

From Eq. A3.8 and Eq. A3.9,

$$\frac{K_{S2}}{K_{S1}} < \frac{\mu_2^{max} - D}{\mu_1^{max} - D} \quad (\text{A3.12})$$

$$\frac{K_{R2}}{K_{R1}} > \frac{\mu_2^{max} - D}{\mu_1^{max} - D} \quad (\text{A3.13})$$

For affinity for nitrate:

$$\frac{K_{S2}}{K_{S1}} < \frac{\mu_2^{max} - D}{\mu_1^{max} - D} = \frac{0.052 - 0.026}{0.086 - 0.026} = 0.433$$

Analogously, for affinity for COD:

$$\frac{K_{R2}}{K_{R1}} > \frac{\mu_2^{max} - D}{\mu_1^{max} - D} = 0.433$$

A3.8.2 Sensitivity analysis for maximum specific growth rate (μ_{max})

From Eq. A3.12 and Eq. A3.13,

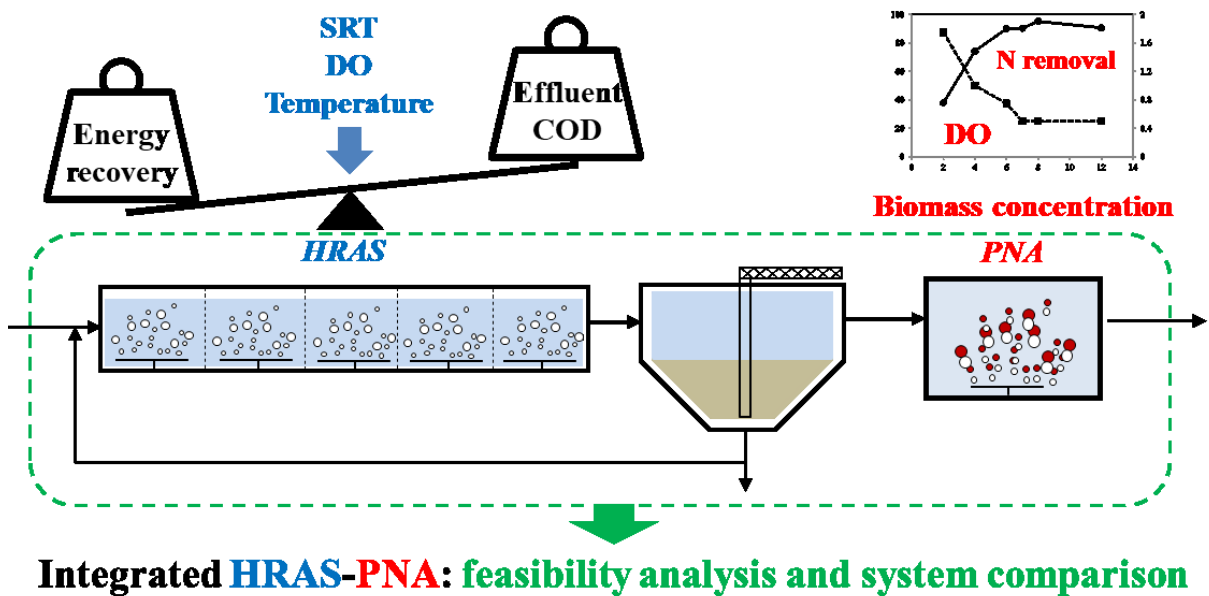
$$\mu_1^{max} > \frac{K_{R1}}{K_{R2}} (\mu_2^{max} - D) + D = 0.052$$

$$\mu_1^{max} < \frac{K_{S1}}{K_{S2}} (\mu_2^{max} - D) + D = 0.156$$

$$\mu_2^{max} > \frac{\mu_1^{max} + \left(\frac{K_{S1}}{K_{S2}} - 1\right) D}{\frac{K_{S1}}{K_{S2}}} = 0.038$$

$$\mu_2^{max} < \frac{\mu_1^{max} + \left(\frac{K_{R1}}{K_{R2}} - 1\right) D}{\frac{K_{R1}}{K_{R2}}} = 0.08$$

Model-based evaluation of an integrated high-rate activated sludge and mainstream anammox system



4.0 Abstract

Wastewater treatment plants of the future aim at energy autarky. This could potentially be realized through a high-rate activated sludge (HRAS) process for organics (expressed as Chemical Oxygen Demand, COD) redirection followed by a mainstream partial nitrification-anammox (PNA) process for nitrogen removal. This combination of processes was evaluated in this study through modelling and simulation. The impact of operating conditions on the unit processes was investigated first. The operation of a HRAS stage often implied a trade-off between maximizing the COD capture for energy recovery and minimizing residual COD in the effluent fed to the subsequent autotrophic PNA process. Moderate DO concentrations (0.3-0.5 g O₂.m⁻³) and SRT (0.3-0.5 d) were suggested to balance these needs, whereas maximizing settling efficiency in the subsequent settler was always desirable. Regarding the mainstream PNA process, the optimal DO setpoint corresponding with maximum nitrogen removal decreased with increasing biomass concentrations. Anammox remained the dominating nitrogen removal process during long-term dynamic simulations with fluctuating HRAS stage effluent (1.3-4.3 g COD.g N⁻¹, 10-20°C), indicating the resilience and long-term stability of the PNA process at mainstream conditions. Overall, plant-wide evaluations revealed that the combined HRAS-PNA system could achieve a comparable effluent quality as the conventional activated sludge (CAS) system, complying with EU regulations, while allowing around 50% more influent COD to be redirected to the sludge line for energy recovery and over 60% savings in aeration energy. This illustrates the potential of being energy-neutral of the integrated HRAS-PNA system. However, the effluent quality of the HRAS-PNA system was found less satisfactory under dynamic conditions than under steady-state conditions.

Chapter redrafted after:

Jia, M., Solon, K., Vandeplassche, D., Venugopal, H. and Volcke, E.I.P. (2019) Model-based evaluation of an integrated high-rate activated sludge and mainstream anammox system. *Chemical Engineering Journal, in press*

4.1 Introduction

Conventional municipal wastewater treatment plants (WWTPs) are typically designed to obtain a high removal efficiency of organic matter (expressed as chemical oxygen demand - COD) and nitrogen. This does not only require a large amount of aeration energy but also leads to the loss of the energy present in COD as metabolic heat (Jetten et al., 1997; McCarty et al., 2011). New configurations have been proposed to shift from the current energy-inefficient WWTPs towards energy-neutral ones (Jetten et al., 1997; Kartal et al., 2010; Verstraete and Vlaeminck, 2011), based on the AB process already established in the 1970s (Boehnke, 1977). The first stage of such energy-neutral (or even energy-positive) WWTPs utilizes a high-rate activated sludge (HRAS) process, in which COD is concentrated and then redirected for subsequent energy recovery or high-value end-products production through anaerobic digestion (Kleerebezem et al., 2015). This stage is followed by a partial nitrification-anammox (PNA) process for nitrogen removal (Fig. 4.1).

The HRAS process generally uses a higher food-to-microorganism (F/M) ratio, a shorter sludge retention time (SRT < 2d), a shorter hydraulic retention time (HRT ~ 0.5 h) and a lower dissolved oxygen concentration ($DO < 1 \text{ g O}_2\cdot\text{m}^{-3}$), compared to conventional activated sludge (CAS) process (Jimenez et al., 2015). These differences indicate a less energy-intensive (lower aeration energy) and a more compact HRAS system. They also affect the COD removal behaviour. For instance, due to the low SRT in an HRAS process, fast-growing heterotrophic bacteria are selected, which are only able to use the most readily biodegradable organics. As a result, part of the soluble COD, which is treated as easily biodegradable in long-SRT (> 3d) CAS system should be considered as inert in the short-SRT HRAS system (Haider et al., 2003). Therefore, the impact of operating conditions on the COD conversions in the HRAS process needs to be further explored.

The PNA process consists of two steps. During the partial nitrification step, about half of the ammonium in the wastewater is oxidized to nitrite by ammonium-oxidizing bacteria (AOB), while further oxidation to nitrate by nitrite-oxidizing bacteria (NOB) is prevented. In the subsequent anammox conversion step, the remaining ammonium and the produced nitrite are combined to form dinitrogen gas (N_2), in the absence of oxygen and using CO_2 as a carbon source (Strous et al., 2006). Compared to the conventional

nitrogen removal processes based on nitrification-denitrification over nitrate, the PNA process: (1) consumes up to 63% less aeration energy; (2) does not require external COD for denitrification, which omits the need for chemical addition and at the same time maximizes the possible use of the COD present in municipal wastewater for energy production through anaerobic digestion; (3) produces less sludge and thus, reduces costly sludge disposal and (4) emits less CO₂ due to the autotrophic nature of the process and lower energy requirements (Jetten et al., 1997; Siegrist et al., 2008). The two steps of the PNA process can be realized in either two separate reactors or in a single reactor. By 2014, there were already more than 100 full-scale PNA reactors in operation. They were successfully applied to treat various types of warm wastewater with high ammonium concentrations, such as reject water originating from anaerobic digestion (i.e., sidestream treatment) (Lackner et al., 2014). More than 80% of them were single reactor systems, as will be considered in this study. Moreover, granular sludge systems were put forward because of its high volumetric conversion rate and biomass retention (Kartal et al., 2010).

The current challenge is in applying the innovative PNA process for the treatment of municipal wastewater in the mainline of the WWTP (i.e., mainstream anammox) (Kartal et al., 2010). The major issues in this respect are the low temperature and low ammonium concentration of municipal wastewater, combined with the presence of COD, which may stimulate the growth of heterotrophs, outcompeting the slowly growing anammox bacteria (Agrawal et al., 2018; Cao et al., 2017). The feasibility of PNA under mainstream conditions has been demonstrated in several laboratory and pilot-scale studies (De Clippeleir et al., 2013; Laurenzi et al., 2016; Lotti et al., 2014a). Nevertheless, these studies also point out that the long-term stability of PNA process (i.e., maintaining high process rate and low effluent nitrogen concentration) under varying temperature (especially low temperature) and loading rates (e.g., COD and ammonium) in full-scale WWTPs should be further evaluated (Cao et al., 2017; Hoekstra et al., 2019).

Sufficient COD removal in the HRAS stage is crucial for avoiding the proliferation of heterotrophs and, thus, for a successful PNA stage. However, a higher COD removal in the HRAS stage does not necessarily mean a higher energy recovery (Jimenez et al., 2015; Nogaj et al., 2015). While the HRAS process has already been successfully applied at full-scale in the past to maximize energy recovery from the influent COD, as

the first step in a conventional AB process (Boehnke et al., 1997), the additional challenge for it nowadays is to simultaneously achieve a sufficiently high COD removal efficiency in order to meet the influent requirements (i.e., low COD/N) of the downstream PNA stage. Therefore, to comprehensively assess the combined HRAS-PNA system, a plant-wide perspective is needed, as applied in the past for the evaluation of sidestream anammox processes (Volcke et al., 2006).

Model-based investigations are useful for fast and rigorous assessment of the performance of WWTPs, in particular, to analyse the interrelations among unit processes. As such, they can also be utilized for feasibility studies of leading-edge technologies and their integration with other wastewater treatment unit processes. Up until now, the HRAS-PNA system and/or similar systems (e.g., bioflocculation and two-stage PNA) have only been evaluated *via* rough mass and energy balance calculations (Siegrist et al., 2008) and steady state simulations (Bozileva et al., 2017; Fernández-Arévalo et al., 2017; Khiewwijit et al., 2015). A few studies applied life-cycle analysis for environmental assessment of systems with PNA in the mainline (Besson et al., 2017; Schaubroeck et al., 2015). However, the feasibility and long-term stability of the HRAS-PNA system under dynamic conditions (e.g., temperature, hydraulic load and substrate concentrations) remain to be evaluated.

In this contribution, the feasibility and long-term stability of the HRAS process for COD removal and capture, combined with a granular sludge PNA reactor for nitrogen removal, was evaluated through dynamic modelling and simulation. The effect of operating conditions (e.g., SRT, DO, and biomass concentration) on the individual HRAS and PNA processes was investigated first, followed by steady-state and dynamic evaluations of the combined HRAS-PNA system in a plant-wide context. Finally, the latter system was compared against a conventional activated sludge (CAS) system in terms of effluent quality and operational costs.

4.2 Materials and methods

4.2.1 The integrated HRAS-PNA system

The integrated HRAS-PNA system (Fig. 4.1) was put forward as proposed by Kartal et al. (Kartal et al., 2010). In this system, the HRAS stage is mainly responsible for organic carbon removal and redirection, whereas the PNA stage is mainly responsible for

nitrogen removal. For the latter purpose, a compact granular sludge reactor was considered (Kartal et al., 2010). The sludge line (i.e., thickener, anaerobic digester, dewatering unit, and storage tank) was also included for a comprehensive plant-wide evaluation and was modelled as in the Benchmark Simulation Model no. 2 (BSM2) (Gernaey et al., 2014). The BSM2 offers a benchmark for the evaluation of process performance and control strategies in a typical WWTP based on conventional activated sludge process (Gernaey et al., 2014).

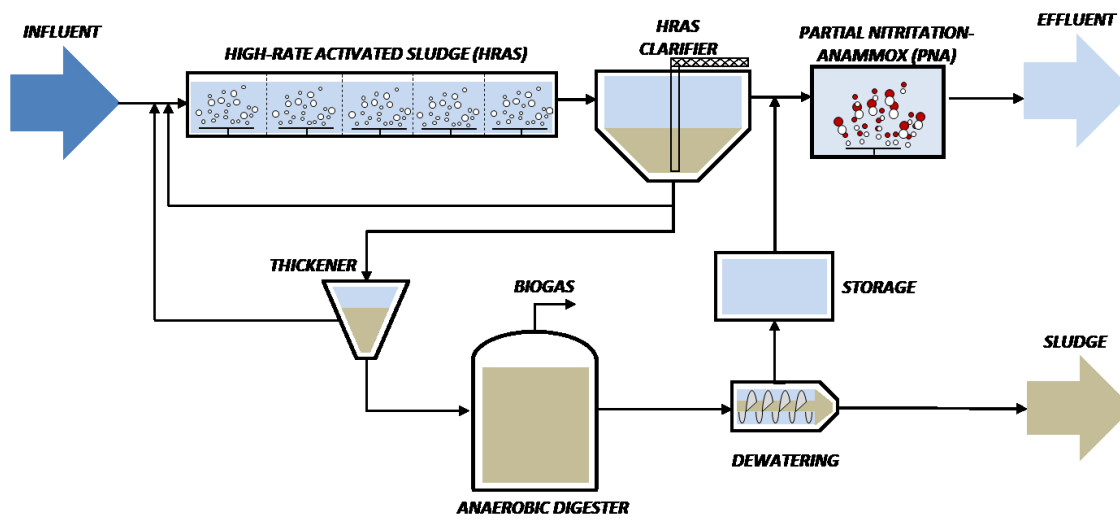


Figure 4.1. Schematic plant layout of the integrated HRAS-PNA system

4.2.2 High-rate activated sludge (HRAS) stage model

The possible biological COD conversions in an HRAS process are illustrated in Fig. 4.2. The short SRT in an HRAS system compared to a CAS system results in different COD removal behavior, which requires system-specific modelling assumptions. The widely-used Activated Sludge Model no. 1 (ASM1) which focuses on long-SRT (> 3d) activated sludge systems (i.e., CAS system), is not directly applicable without considering new physical-chemical processes or at least an adequate settler model for the modelling of a short-SRT HRAS system, as clearly stated by the authors themselves (Henze et al., 2000) and demonstrated by Nogaj et al. (2015).

The HRAS stage was modelled through an adapted ASM1, according to the approach by Smitshuijzen et al. (2016). In this approach, the efficiency of adsorption/bioflocculation (r_9 in Fig. 4.2) in the HRAS unit and the efficiency of liquid/solid separation in the subsequent clarifier are lumped into a single parameter, f_{settler} , which represents the fraction of particulates removed and is estimated from plant data

(detailed in A1.2). All particulates are assumed to adsorb and settle equally well. The stoichiometric matrix and process rate expressions of the HRAS unit model are the same as the ASM1 implemented in the Benchmark Simulation Model no. 2 (BSM2) (Gernaey et al., 2014) and are detailed in Table A4.1 and A4.2, respectively. The associated parameter values of the HRAS unit model are detailed in Table A4.3.

The HRAS stage is composed of the HRAS unit and the subsequent clarifier (Fig. 4.1). The HRAS unit was modelled as five completely mixed aerated reactors in series to simulate a pseudo-plug flow configuration as typically done in practice (De Graaff et al., 2016). The total volume of the HRAS reactors was calculated to be 2500 m³, based on the mass concentration of mixed liquor suspended solids (MLSS) that was expected in the reactors. As the key operating parameters in the HRAS process, the SRT was controlled by manipulating the waste sludge flow rate (detailed in A1.2), while the DO was controlled at a setpoint of 0.5 g O₂.m⁻³ at the 4th bioreactor by applying a closed control loop (Smitshuijzen et al., 2016). The same oxygen transfer coefficient ($K_L a$) in the 4th reactor was then applied to all other bioreactors in the model. The model was implemented in Matlab & Simulink® (version R2016b).

4.2.3 Partial nitrification-anammox (PNA) model

The granular sludge PNA reactor was modelled as 1-D biofilm based on Mozumder et al. (2014), including four bacterial groups: ammonium-oxidizing bacteria (X_{AOB}), nitrite-oxidizing bacteria (X_{NOB}), anammox bacteria (X_{AN}) and heterotrophic bacteria (X_H). The effect of temperature was taken into account (Table A4.7) according to the approach in Hao et al. (2002b). The stoichiometric matrix, process rates, and associated parameter values of the PNA model are detailed in Table A4.5-A4.7.

The granular sludge PNA reactor has a fixed total volume (granules + bulk liquid) of 2500 m³. This was determined based on the biomass concentration (4 kg VSS.m⁻³) and specific nitrogen loading rate (0.125 kg N.kg VSS⁻¹.d⁻¹) derived from a pilot-scale granular sludge PNA reactor treating real HRAS stage effluent (Lotti et al., 2015b) and the influent of the PNA stage (i.e., effluent of the preceding HRAS stage) (detailed in A2.2). The granules were assumed to be of equal size with a radius of 0.75 mm. The bulk DO concentration was controlled by a constant set-point, and the biomass concentration was manipulated by changing the number of granules in the reactor. The PNA model was implemented in AQUASIM v2.1 (Reichert, 1994).

4.2.4 Plant-wide comparison with conventional activated sludge (CAS) system

The behavior of the HRAS-PNA system was compared with the one of a conventional activated sludge (CAS) system. The latter was simulated using the closed-loop configuration of BSM2 (Fig. A4.4, (Gernaey et al., 2014)). The BSM2 CAS system also includes a primary clarifier, a thickener, an anaerobic digester, a dewatering unit and a storage tank for the reject water, allowing for plant-wide evaluation in terms of effluent quality, operational cost and energy recovery potential (Gernaey et al., 2014). The constant and dynamic influent datasets from BSM2 were used for steady-state and dynamic simulations, respectively, for both systems.

4.2.5 Evaluation criteria for plant-wide comparison

The influence of operating conditions on the HRAS and the PNA stages was evaluated by analysis of the COD distribution and nitrogen removal efficiency, respectively. As for the comparison between the HRAS-PNA and CAS systems, this study used the default evaluation criteria of BSM2, which provide a simple and objective means for comparison and have been developed specifically for comparing dynamic responses (Gernaey et al., 2014). The evaluation criteria consist of the effluent quality index (EQI, in kg pollution units.d⁻¹) and operational cost index (OCI) (detailed in A3.2). The EQI is a weighted average of relevant effluent concentrations (e.g., total nitrogen (TN), COD and TSS). The OCI is calculated as a weighted sum of different costs, including aeration energy, pumping energy, mixing energy, sludge production for disposal, external carbon addition, methane production, and the heating energy. The aeration energy in the HRAS stage was calculated in the same way as for the CAS system in BSM2, whereas the aeration energy in the PNA reactor was calculated based on the oxygen consumption and a typical engineering approach related to the SOTE (standard oxygen transfer efficiency, kg O₂.kWh⁻¹) (detailed in A3.3). The evaluation period considered was the last 364 days of the dynamic simulations.

4.2.6 Simulation strategies

The influence of operating conditions on the individual HRAS and PNA stages was investigated first, followed by a plant-wide evaluation of the combined HRAS-PNA system. Finally, the latter system was compared to a CAS system in terms of effluent

quality and operational costs. An overview of the simulation strategies is summarized in Table 4.1.

Table 4.1. Overview of simulation strategies

Scenario	COD _{in} g COD.m ⁻³	TN _{in} g N.m ⁻³	SRT in HRAS day	DO g O ₂ .m ⁻³	T °C	f _{settler} -	Biomass concentration kg VSS.m ⁻³
HRAS stage⁽¹⁾							
Reference case	593	55	0.3	0.5	15	0.984	-
Factors influencing COD redirection	593	55	0.1-2	0.1-2	10-30	0.85-1	-
PNA stage⁽²⁾							
Reference case	50	46	-	1	15	-	4
Effect of biomass concentration and DO	50	46	-	0.5-2	15	-	2-12
Plant-wide: HRAS-PNA vs. CAS⁽⁴⁾							
Steady state ⁽¹⁾	593	55	0.4	0.5 ⁽⁵⁾	15	0.984	8
Dynamic ⁽³⁾	variable	variable	0.4	0.5 ⁽⁵⁾	variable	0.984	8

⁽¹⁾BSM2 constant influent; ⁽²⁾Effluent of the HRAS stage at reference scenario; ⁽³⁾BSM2 dynamic influent; ⁽⁴⁾The CAS system was controlled as in the closed-loop BSM2 (Gernaey et al., 2014); ⁽⁵⁾The same DO was applied for the HRAS and PNA reactors

The influent dataset of BSM2, which consists of both constant influent and full dynamic influent data (609 days), was used as input for the simulations. The constant influent file contains the average values of one full year dynamic data that represents the influent of the municipal wastewater treatment plant in BSM2. The average influent COD and TN concentrations are 593 mg COD.L⁻¹ and 55 mg N.L⁻¹, respectively, with an average flow rate of 20 648 m³.d⁻¹ (Table 4.1, detailed in Table A4.4).

For the HRAS stage, the effect of the operating conditions (DO, SRT and temperature) and combined adsorption/bioflocculation and settling efficiency (f_{settler}) on the performance was evaluated through steady-state simulations. For the PNA stage, the individual and combined influence of biomass concentration and bulk DO concentration on nitrogen removal was evaluated through steady-state simulations (Table 4.1). The effluent of the HRAS stage at reference scenario was used as the influent of the PNA stage for these simulations. For steady-state simulations, the HRAS stage model (in Matlab & Simulink) was run with the constant influent data (Table A4.4) for 500 days, while the PNA stage model (in AQUASIM) was run with the effluent from the HRAS stage under reference case for 4000 days to ensure steady state was

reached. The behaviour of the HRAS-PNA system under dynamic conditions was evaluated using the full 609-days dynamic influent data. The last 364 days (i.e., day 245-609) of the dynamic simulation were used for performance evaluation.

4.3 Results and discussion

4.3.1 HRAS stage for COD redirection

The HRAS models available in the literature are reviewed first, detailing and motivating the model structure adopted in this study. Subsequently, this HRAS model was applied to study factors influencing COD redirection.

4.3.1.1 Modelling the HRAS stage

The biological conversions of COD and nitrogen in wastewater treatment systems are presented in Fig. 4.2. The shorter SRT and HRT in an HRAS system compared to a CAS system results in different COD removal behaviour in the two systems, which requires system-specific modelling assumptions.

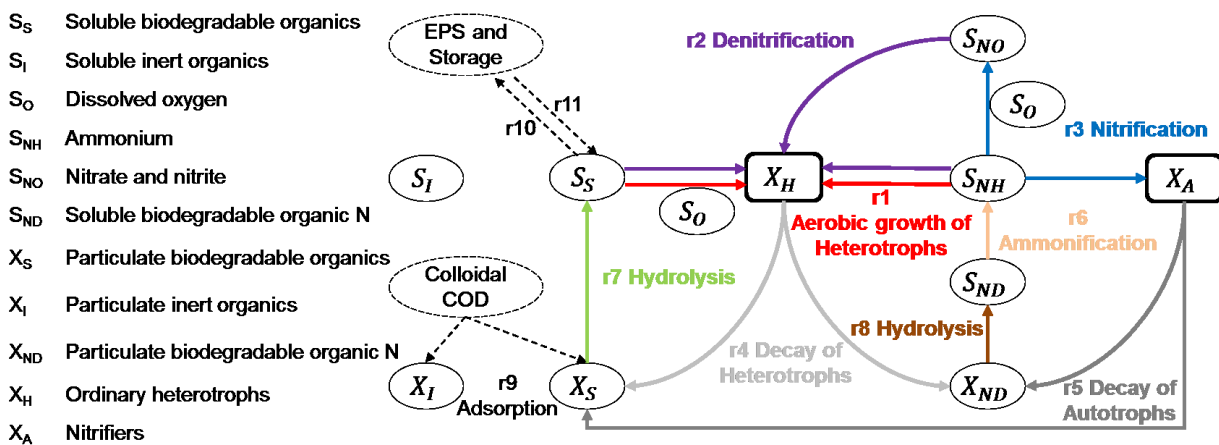


Figure 4.2. The biological COD and nitrogen conversions in a high-rate activated sludge (HRAS) system. The state variables and processes with solid lines (r1-r8) are included in the model used in this study (i.e., ASM1 (Henze et al., 2000) and Smitshuijzen et al. (2016) – see Table A4.1 and Table A4.4). The state variables and processes with dashed lines (r9-r11) are additionally included in the model of Nogaj et al. (2015).

The readily biodegradable COD (S_S) is modelled as a single substrate with a single kinetic for CAS systems (i.e., ASM1) (Henze et al., 2000). However, the low SRT in the HRAS process favours fast-growing bacteria, which are only able to use the most

readily biodegradable organic, i.e., part of the S_s in ASM1 (Haider et al., 2003; Nogaj et al., 2015). Therefore, the effluent of an HRAS process often has a higher soluble biodegradable COD fraction compared to a CAS process (Haider et al., 2003). To describe this, three different approaches (S1-S3) have been proposed in the literature: (S1) split the S_s into fast and slow fractions (i.e., dual soluble substrate) and model them separately (Haider et al., 2003; Nogaj et al., 2015); (S2) distribute a part of X_s to S_s (Smitshuijzen et al., 2016) and (S3) increase the half-saturation constant K_s for S_s (Haider et al., 2003).

The difference in modelling the removal of suspended COD (particulate COD (X_s) and colloidal COD) lies in whether one needs to model the adsorption/bioflocculation process explicitly. Suspended COD needs to be adsorbed by active biomass before being hydrolyzed and oxidized. The adsorption of suspended COD is a fast process and is considered instantaneous in ASM1 (Henze et al., 2000). However, due to the short HRT (i.e., contact/reaction time) in the HRAS process, only a part of the suspended COD can be enmeshed by biomass (Jimenez et al., 2005). To model the adsorption/ bioflocculation process, two different approaches (X1-X2) have been proposed: (X1) integrate the production of extracellular polymeric substances (EPS), storage compounds (r_{10} , Fig. 4.2) and adsorption of colloidal COD (r_9 , Fig. 4.2) into the ASM1 (Jimenez et al., 2005; Nogaj et al., 2015) and (X2) lump adsorption/bioflocculation and settling efficiency into a single parameter (f_{settler} , detailed in A1.2) that can be identified with routinely measured data in WWTPs (Smitshuijzen et al., 2016).

Regarding the nitrogen conversions in the HRAS model, for reasons of simplicity, nitrification in the HRAS model was described as a single-step process, following the ASM1. This implies the assumption that the conversion by AOB is rate-limiting, which is reasonable at the prevailing low temperature (15°C). In any case, the low SRT (<1 day) that is typically applied for HRAS (De Graaff et al., 2016; Jimenez et al., 2015) is not sufficient to sustain AOB nor NOB (the minimum SRT (Henze et al., 2008) to sustain AOB would be $1/(\mu_{\text{max, AOB}} - b_{\text{AOB}}) = 1.8$ days at 15°C, Table A4.7). In addition, the high COD/N ratio in the HRAS reactors also makes nitrification less likely to take place (Smitshuijzen et al., 2016). The simulation results confirmed that no nitrification took place in the HRAS stage.

Currently, there are only a few dedicated models available for the HRAS system. Nogaj et al. (2015) presented a mechanistic model (Approach S1&X1), in which new state variables (e.g., colloidal COD) and processes (e.g., r9-r11, Fig. 4.2) were added to ASM1. Despite its potential advantage of revealing more insights into the underlying processes, the introduction of new state variables and kinetic parameters requires an additional set of measurements (e.g., influent colloidal COD) that are usually not available for parameter estimation and model calibration. In contrast, Smitshuijzen et al. (2016) presented a simpler model adaptation of ASM1 (Approach S2&X2) by implementing the combined adsorption/bioflocculation and settling efficiency (f_{settler}) and applying influent COD fractionation. Even though the general applicability of the lumped f_{settler} parameter may require further validation when applied to other WWTPs, its simplicity allows for easier integration of the HRAS process model in plant-wide models. For this reason, the modelling approach of Smitshuijzen et al. (2016) was implemented in this study.

4.3.1.2 Factors influencing COD redirection

The influent COD entering the HRAS system can go into three possible routes: (1) loss due to mineralization (i.e., oxidation of COD to CO_2 by biomass, r1-2, Fig. 4.2); (2) ends up in the HRAS effluent and fed to the PNA stage; (3) captured in the sludge and fed to the anaerobic digester for energy recovery. The COD distribution between these routes is crucial in determining the energy recovery potential and performance of the downstream autotrophic N removal process. A high COD capture in sludge is preferred for energy recovery, while a low effluent COD (i.e., low COD/N ratio) is required for subsequent mainstream PNA. The COD distribution was influenced by DO, SRT and temperature (T) as key operational parameters as well as by the combined adsorption and settling efficiency (characterized by the parameter f_{settler}), as summarized in Fig. 4.3. For the reference case, 22% of the influent COD was mineralized, 14% was in the effluent and 64% was captured in sludge, with an effluent COD/N ratio of 2.4 (g COD.g N^{-1}) (Fig. 4.3).

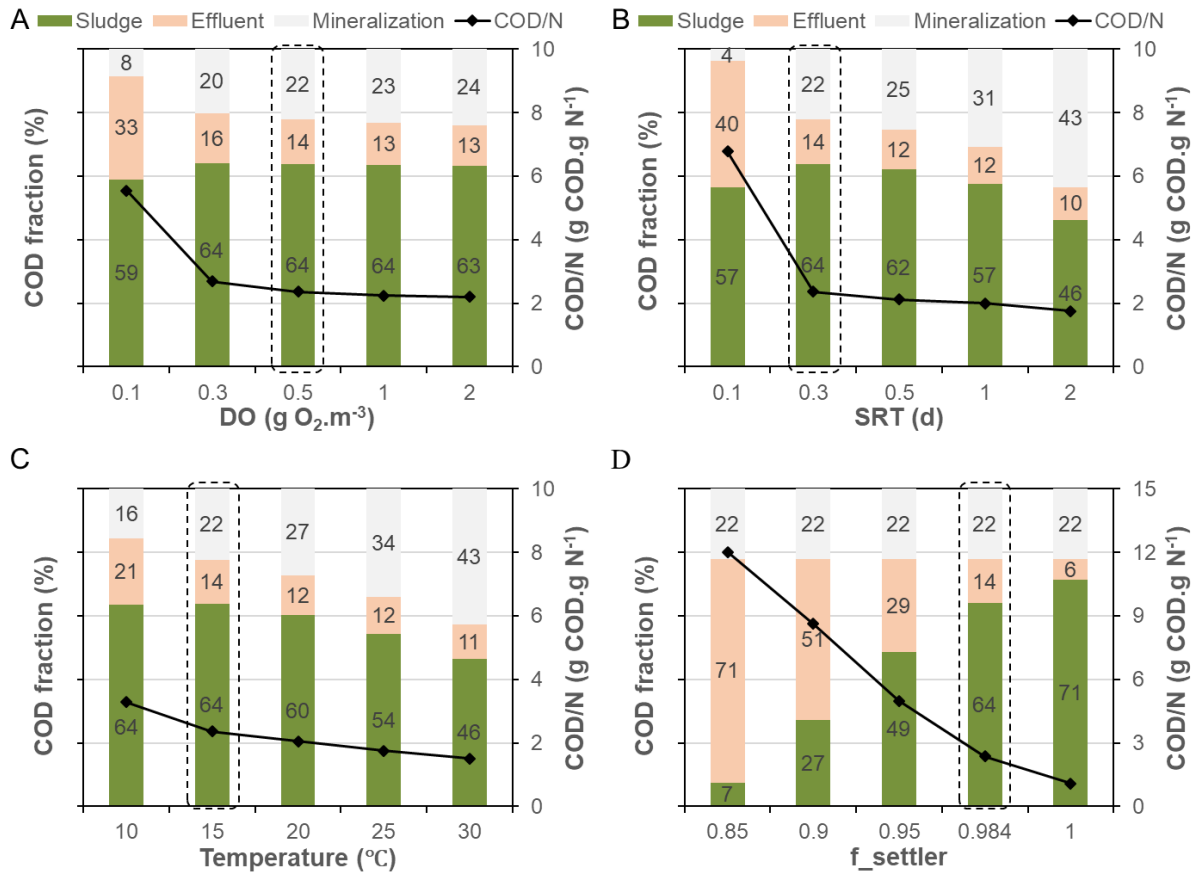


Figure 4.3. Model predicted COD distribution (as a fraction of influent COD) and effluent COD/N ratio with different (A) DO, (B) SRT, (C) temperature and (D) f_{settler} in the HRAS stage. Influent COD=593 g COD.m⁻³, of which $X_s=218$ g COD.m⁻³ and $S_s=204$ g COD.m⁻³. The reference case (SRT=0.3 d; DO=0.5 g O₂.m⁻³; T=15 °C; $f_{\text{settler}}=0.984$) is marked with a dashed box.

For DO concentrations lower than 0.5 g O₂.m⁻³, the effluent COD concentration decreased sharply with increasing DO concentration while the COD mineralization and COD capture in the sludge increased accordingly (Fig. 4.3A). The lower effluent COD concentration was mainly attributed to the improved soluble biodegradable COD removal at higher DO concentration (r_1 in Fig. 4.2). However, further increase of the DO concentration (>0.5 g O₂.m⁻³) only had a marginal effect on influent COD distributions (Fig. 4.3A), indicating that DO was no longer the limiting factor for COD removal in an HRAS process operated at the prevailing SRT (0.3 d) and temperature (15 °C). Noteworthy, the impact of DO on the COD distribution could be more pronounced if a higher SRT (or temperature) than the reference case was applied (e.g., 0.5d vs. 0.3d). This trend is in line with the findings of the pilot-scale study from Nogaj et al. (2015) and the full-scale investigations from de Graaff et al. (2016). The results imply that moderate DO setpoint (0.3-0.5 g O₂.m⁻³) should be applied in the HRAS

stage for sufficient COD removal and COD redirection for energy recovery while avoiding unnecessary aeration cost.

With increasing SRT, the effluent COD concentration decreased while the mineralization of influent COD increased (Fig. 4.3B). Concerning the COD capture in the sludge, it first increased (SRT of 0.1-0.3 d) and then decreased gradually (SRT of 0.3-2d). The SRT determines the period during which particulates/biomass are retained within the system and was regulated by changing the waste sludge flow (Q_w) in this model. At a low SRT (0.1 d), the biomass concentration was too low, and the removal of S_s was therefore limited, resulting in a high effluent COD (40%, Fig. 4.3B). With increasing SRT, the S_s removal increased and so did the mineralization of influent COD. So less COD ended up in the sludge (Fig. 4.3B). A similar trend was observed by Jimenez et al. (2015) in a pilot-scale HRAS system, for which COD directed to sludge peaked at a SRT of 0.3 d in the tested range of 0.1-2 d. The results imply that a high SRT is desired to minimize effluent COD while a moderate SRT (e.g., 0.3 d) is required to maximize the COD redirection for energy recovery. A SRT of 0.3-0.5 d seems advisable to balance these two needs.

With increasing wastewater temperature, the effluent COD concentration and COD capture in the sludge decreased while the COD mineralization increased (Fig. 4.3C). Higher temperatures improved biomass activities and overall process rates. This led to increased COD removal (low effluent COD) and mineralization through heterotrophic growth (r_{1-2} in Fig. 4.2). The hydrolysis of X_s and biomass decay (r_7 and r_{4-5} in Fig. 4.2) would be enhanced as well. Consequently, the COD capture in the sludge decreased. These results imply that higher temperatures may be favourable for COD removal in the HRAS stage but not necessarily beneficial for energy recovery. Decreasing the SRT might help reduce the mineralization of influent COD and thereby counterbalance the effect of increased temperature. In regions that experience large (seasonal) temperature variations, this could have a significant effect on the system performance throughout the year. Low temperature (e.g., in winter) may result in insufficient COD removal in the HRAS stage and thus affects the autotrophic nitrogen removal in the subsequent PNA stage, as observed at the WWTP Dokhaven during winter (Hoekstra et al., 2019). However, temperature depends on environmental conditions and cannot be easily or economically manipulated in full-scale WWTPs, which limits its potential use as a control strategy.

One of the most important parameters of the HRAS model adapted in the present study is the combined adsorption/bioflocculation and settling efficiency (f_{settler}). By definition (detailed in A1.2), the removal of particulate COD increases with increasing f_{settler} . The effluent COD decreased accordingly, while the mineralization of influent COD remained unaffected (Fig. 4.3D). The higher the f_{settler} , the better the energy recovery is. Therefore, more effort is required on improving the adsorption/bioflocculation in the HRAS unit (e.g., by adding chemicals or pretreatment with chemically enhanced primary treatment) and the settling efficiency in the subsequent settler (e.g., by applying coagulation or use of dissolved air flotation).

Overall, the operation of an HRAS stage aims at maximizing COD capture in the sludge for energy recovery and minimizing effluent COD for the subsequent nitrogen removal in PNA. A trade-off was observed for the selection of SRT and temperature while improving the efficiency of adsorption/bioflocculation and settling was always desirable. Moderate DO concentrations (0.3-0.5 g O₂.m⁻³) and SRT (0.3-0.5 d) were suggested for operating the HRAS stage.





4.3.2 The partial nitritation anammox (PNA) stage for nitrogen removal

4.3.2.1 Factors influencing nitrogen removal

Aiming at a high and stable N removal, the influence of several influent characteristics and operating conditions on the N removal of granular sludge one-stage PNA reactors has been reported in the literature (Table 4.2). For instance, an increasing influent ammonium concentration (i.e., load) results in a gradual decrease in N removal at a fixed DO concentration (Wan et al., 2019), while an increasing temperature improves N removal (Lotti et al., 2014a; Wan et al., 2019). The N removal first increases with increasing influent COD (or COD/N) and then declines as it further increases (Liu et al., 2017; Mozumder et al., 2014), which is also observed for bulk DO concentrations (Nielsen et al., 2005; Volcke et al., 2010). Aeration pattern influences the N removal as well, with continuous aeration leading to higher N removal than that of intermittent aeration (Corbalá-Robles et al., 2016). A minimum residual ammonium concentration in the PNA reactors is found necessary for NOB repression and therefore affects the N removal (Pérez et al., 2014). Granule size and its distribution have also been shown to affect the N conversions as well as operational windows of other parameters (e.g.,

DO) for optimal N removal (Vlaeminck et al., 2010; Volcke et al., 2012). The balance of microbial communities and their activities is crucial for a stable and efficient PNA process. The AOB, NOB and heterotrophic bacteria preferentially grow in small granules and flocs, which leads to another control strategy in granular sludge PNA reactors, being selective removal of small granules and flocs (Han et al., 2016b; Hubaux et al., 2015). Besides these influencing factors already reported in the literature, the biomass concentration is also likely to interact with other operating parameters and determine the reactor performance. However, its potential impact has not yet been studied for granular sludge PNA reactors.

Table 4.2. Overview of factors influencing the N removal from granular sludge one-stage PNA reactors reported in the literature. The second to the last column schematically shows a mini-graph (where applicable) representing how N removal reacts to changes of the influencing factors

Factors	Conditions			Approach	Graphic representation	Reference
	T (°C)	NH ₄ -N _{in} (g N.m ⁻³)	COD _{in} (g COD.m ⁻³)			
Influent NH₄-N concentration /load	30	100-800	0	Simulation		(Wan et al., 2019)
Influent COD concentration /load or COD/N	30	300	0-1000	Simulation		(Mozumder et al., 2014)
	18±3	190	25-100	Experiment		(Winkler et al., 2012)
	-	50	5-150	Simulation		(Liu et al., 2017)
T	10-20	60/160	0	Experiment		(Lotti et al., 2014a)
	20-35	300	0/300	Simulation		(Wan et al., 2019)
DO	30	131,6	0	Experiment		(Nielsen et al., 2005)
	30	300	0	Simulation		(Volcke et al., 2010)
Aeration pattern	20/30	1850	600	Simulation		(Corbalá-Robles et al., 2016)
Residual NH₄	10	70	0	Simulation		(Pérez et al., 2014)
	20/30	1850	600	Simulation		(Corbalá-Robles et al., 2016)
Granule size and its distribution	30	300	0	Simulation		(Volcke et al., 2010)
	30-35	250-350	200	Experiment		(Vlaeminck et al., 2010)
	30	300	0	Simulation		(Volcke et al., 2012)
Co-existing flocs	19-21	24	24-72	Experiment		(Han et al., 2016b)
	30	300	10-400	Simulation		(Hubaux et al., 2015)

4.3.2.2 Effect of biomass concentration

The impact of biomass concentration on the steady-state performance of the mainstream granular sludge PNA reactors was first investigated at a fixed DO concentration (Fig. 4.4). The interaction between the biomass and DO concentration was subsequently assessed (Fig. 4.5).

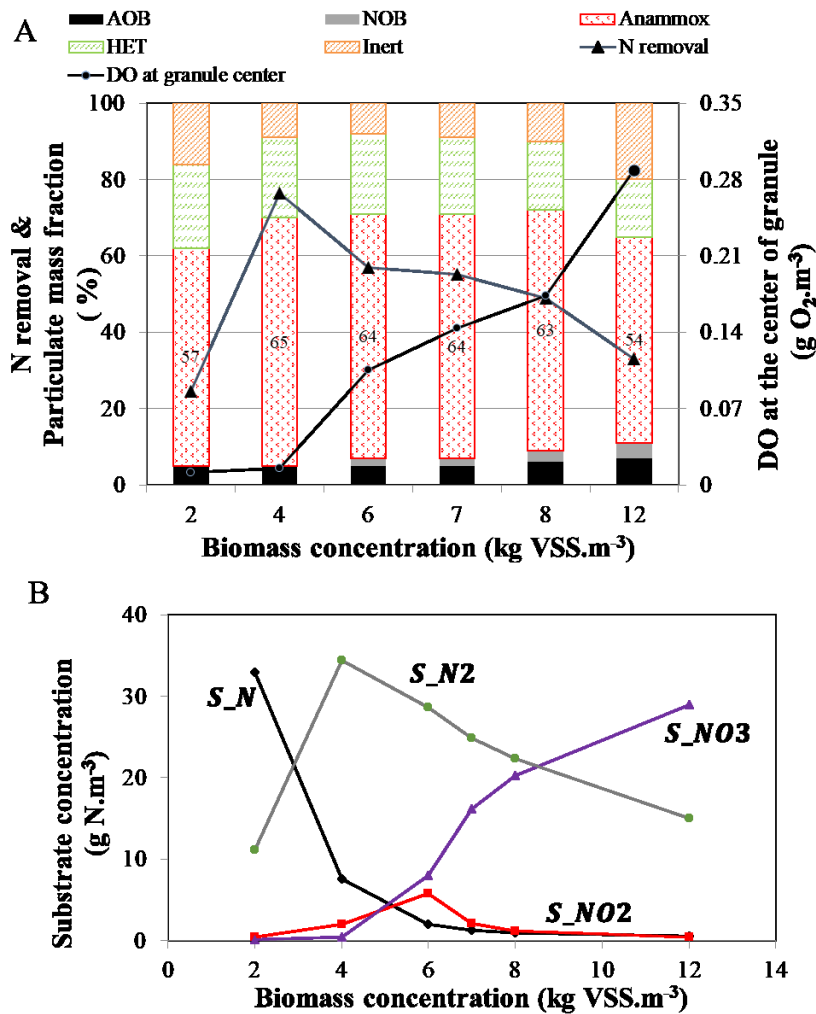


Figure 4.4. Influence of biomass concentration on the steady-state performance of the mainstream PNA process at a fixed DO concentration (1 g O₂.m⁻³): (A) particulate mass fractions, nitrogen removal efficiency and DO concentration at the center of the granules; (B) bulk concentrations of ammonium (S_{NH}), nitrite (S_{NO2}), nitrate (S_{NO3}) and nitrogen gas (S_{N2}).

With increasing biomass concentration, the N removal efficiency first increased and then decreased (Fig. 4.4A), as also reflected in the N₂ production (Fig. 4.4B). At low biomass concentrations (< 4 kg VSS.m⁻³), ammonium conversion was still largely incomplete (33 g NH₄⁺-N.m⁻³ remaining, 26.7% conversion). At intermediate biomass

concentrations (4-8 kg VSS.m⁻³), the anammox fraction in the granules increased (Fig. 4.4A) and N₂ became the primary nitrogen compound (Fig. 4.4B). As the biomass concentration further increased, the DO concentration at the center of the granules increased (Fig. 4.4A), which reflects the elevated oxygen penetration in the granules. Consequently, the NOB activity increased while the anammox activity got inhibited, as confirmed by the change in the corresponding biomass fractions (Fig. 4.4A) and the shift of the dominant nitrogen compound from N₂ to nitrate (Fig. 4.4B). Noteworthy, nitrite accumulation was observed at intermediate biomass concentrations (Fig. 4.4A), implying an overcapacity of nitrite producer (AOB) over nitrite consumers (NOB, anammox and heterotrophic bacteria) at these conditions.

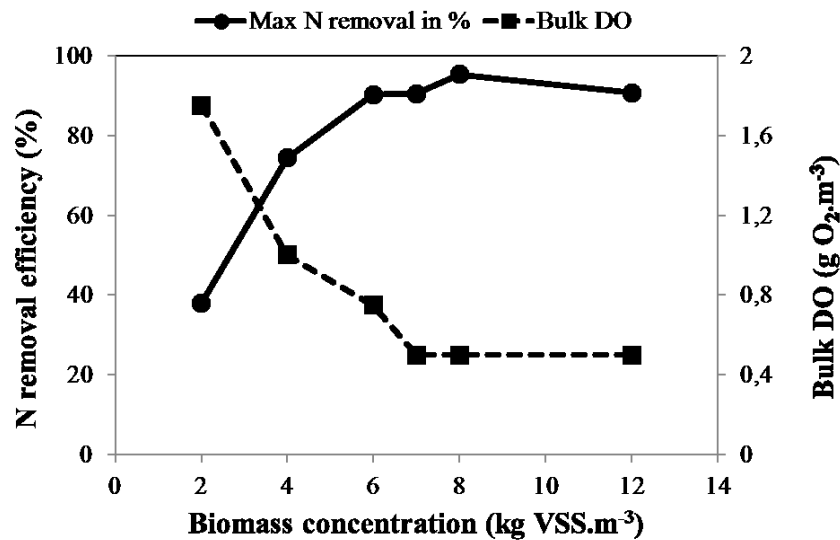


Figure 4.5. The optimal bulk DO concentrations at which maximum nitrogen removal was obtained in granular sludge PNA reactors with different biomass concentrations.

The increased DO penetration depth with increasing biomass concentrations (Fig. 4.4B) could be explained by the lower substrate (e.g., NH₄⁺) surface loads, as increasing biomass concentrations imply a higher biofilm surface. Previous studies have shown that ammonium surface load can inversely affect the oxygen penetration in granular sludge PNA reactors at sidestream conditions (Volcke et al., 2010). The influence of bulk DO concentration on the mainstream PNA reactor was evaluated as well and the results (Fig. A4.3) were consistent with previous studies (Table 4.2). The interaction of COD in the HRAS effluent with the PNA performance is discussed in Section 4.3.3.3.

The combined influence of biomass concentration and DO was studied by identifying the optimal bulk DO concentrations, corresponding with maximum N removal at different biomass concentrations (Fig. 4.5). Overall, the optimal bulk DO concentration for maximum N removal decreased with increasing biomass concentration. N removal efficiencies higher than 90% could be achieved with biomass concentrations above 6 kg VSS.m⁻³ and DO concentrations lower than 0.75 g O₂.m⁻³. The higher N removal efficiency as compared to if there would only be anammox process for N₂ production (89%, according to the anammox stoichiometry (Strous et al., 1998)) was a result of the positive interaction between anammox bacteria and heterotrophic denitrifiers under the tested scenarios (COD/N ~1, Table 4.1). This was confirmed by labeling and tracking the N₂ production in the model which is consistent with previous observations (Jenni et al., 2014; Liu et al., 2017; Mozumder et al., 2014).

Biomass concentrations of 25-35 kg VSS.m⁻³ have been applied in full-scale granular sludge PNA reactors for reject water treatment (Lackner et al., 2014). Therefore, the biomass concentrations used for scenario analysis (2-12 kg VSS.m⁻³) should be practically feasible to maintain. The results from this study indicate that a lower DO setpoint could be applied for mainstream granular sludge PNA reactors with higher biomass concentrations.

4.3.3 Plant-wide comparison of the HRAS-HRAS and CAS system

4.3.3.1 Steady-state COD and N mass balances

The steady-state simulation results for the combined HRAS-PNA system and the CAS system were summarized in terms of plant-wide mass balances for COD and total nitrogen (TN) (Fig. 4.6&4.7). With a comparable effluent COD (which reflects COD removal) in both systems (Fig. 4.6A), the HRAS-PNA system resulted in a lower COD mineralization and significantly more influent COD redirected to the anaerobic digester for energy recovery, compared to the CAS system (50.8% vs. 34.9%, Fig. 4.6A). As illustrated in Section 4.3.1.2, this was mainly due to the low SRT and DO applied to the HRAS stage. Moreover, less excess sludge was produced in the HRAS-PNA system, even though more sludge was directed to the anaerobic digester, indicating that the sludge from an HRAS process was more biodegradable than that of CAS system.

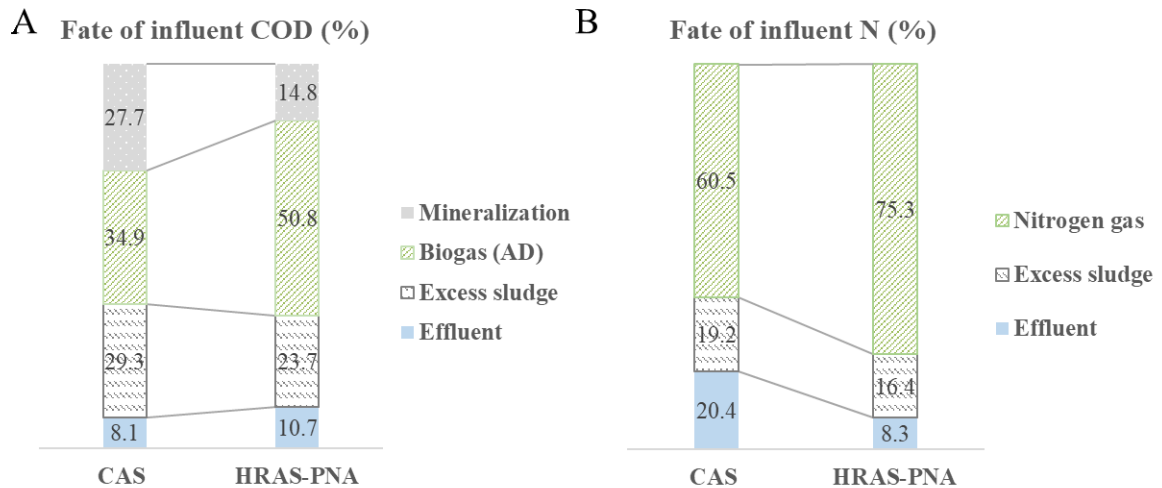


Figure 4.6. Plant-wide steady-state simulation results – comparison between HRAS-PNA system and CAS system in terms of: (A) fate of influent COD and (B) fate of influent TN. (conditions: HRAS: SRT=0.4 d, DO=0.5 g O₂.m⁻³; PNA: Biomass concentration=8 kg VSS.m⁻³, DO=0.5 g O₂.m⁻³; CAS: closed-loop BSM2)

As for nitrogen, the HRAS-PNA system had a higher TN removal (92%) than that of the CAS system (80%) at the tested conditions (Fig. 4.6B). No noticeable nitrogen removal was found in the HRAS reactors according to the mass balance (Fig. 4.7), indicating that there was no significant nitrification and, consequently, no nitrite/nitrate for heterotrophic denitrification at the tested HRAS stage conditions (i.e., SRT=0.4 d and DO=0.5 g O₂.m⁻³). Despite the low volumetric fraction (0.5%) of the reject water from the sludge line (sidestream), it accounted for a significant part (ca. 35%) of the nitrogen load to the PNA stage (Fig. 4.7).

The steady-state effluent COD (63.6 g COD.m⁻³), TN (4.6 g N.m⁻³) and TSS (27.6 g TSS.m⁻³) concentrations of the HRAS-PNA system were well below the limits for urban wastewater treatment (EU council directive 91/271/EEC, Fig. 4.9A), demonstrating the feasibility of this system, which was further assessed with dynamic simulations.

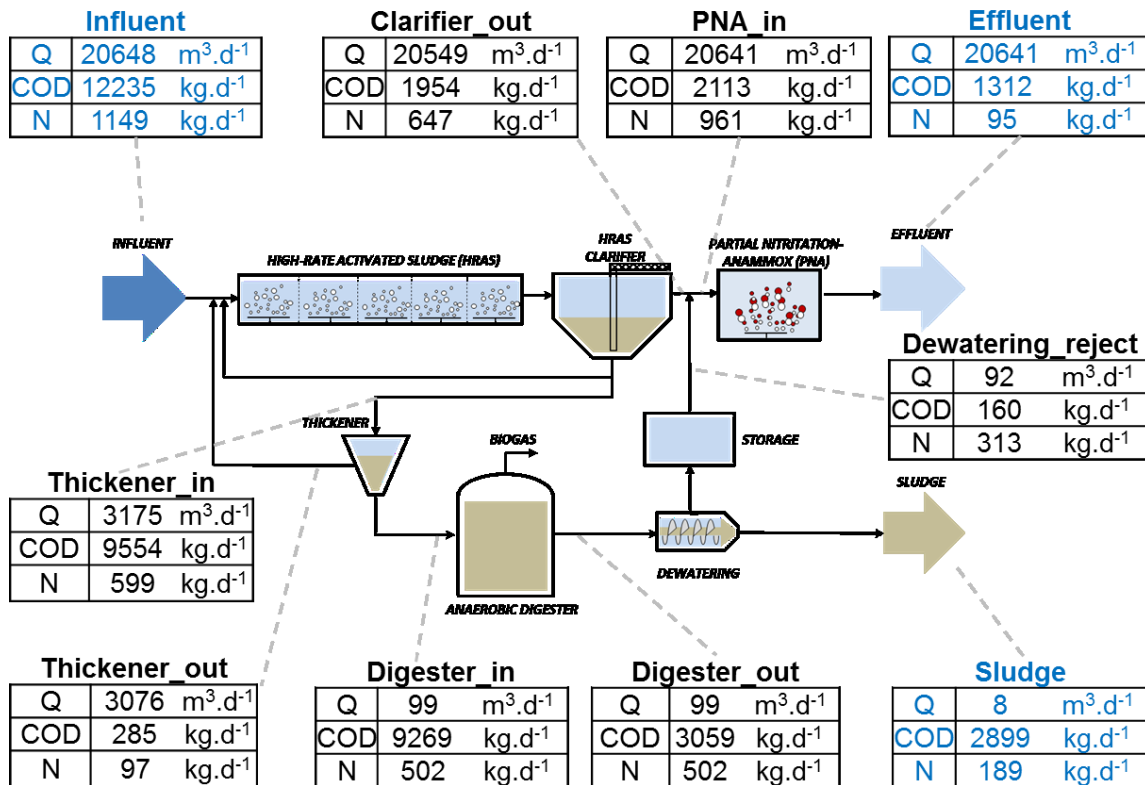


Figure 4.7. Process flowsheet including flow and mass (COD, TN) balances for the HRAS-PNA system at steady-state. (Conditions: HRAS: SRT=0.4 d, DO=0.5 g O₂.m⁻³; PNA: Biomass concentration=8 kg VSS.m⁻³, DO=0.5 g O₂.m⁻³)

4.3.3.2 Dynamic performance – overall effluent quality and operational costs

The dynamic simulation results of the HRAS-PNA system and CAS system are summarized in Fig. 4.8 with respect to the effluent quality and operational cost index (OCI). The yearly average effluent concentrations of COD, TN, and TSS of the HRAS-PNA system were all below the EU limits (Fig. 4.8A), agreeing with the results obtained from the steady-state simulations. It should be noted that the effluent TSS (averaged at 30.5 g TSS.m⁻³) was achieved without a secondary settler (after the granular sludge PNA reactor)). As a safety factor, one could add a secondary settler that is normally present in a CAS system or incorporate a settler within the PNA reactor (Lackner et al., 2014). The simulated effluent concentrations of the full-scale HRAS-PNA system were close to experimentally measured results from lab- or pilot-scale mainstream anammox reactors. For example, average effluent TN concentration below 10 g N.m⁻³ was also achieved in two long-term lab-scale mainstream anammox reactors treating pre-treated sewage (Laureni et al., 2016). The average effluent TSS in a pilot-scale granular sludge PNA reactor treating real HRAS stage effluent was 30 g.m⁻³ (Lotti et

al., 2015b). However, the effluent quality under dynamic simulations was less satisfactory than that under steady-state simulation (Fig. 4.8A), implying the need for performing dynamic simulation for feasibility analysis of a novel system layout.

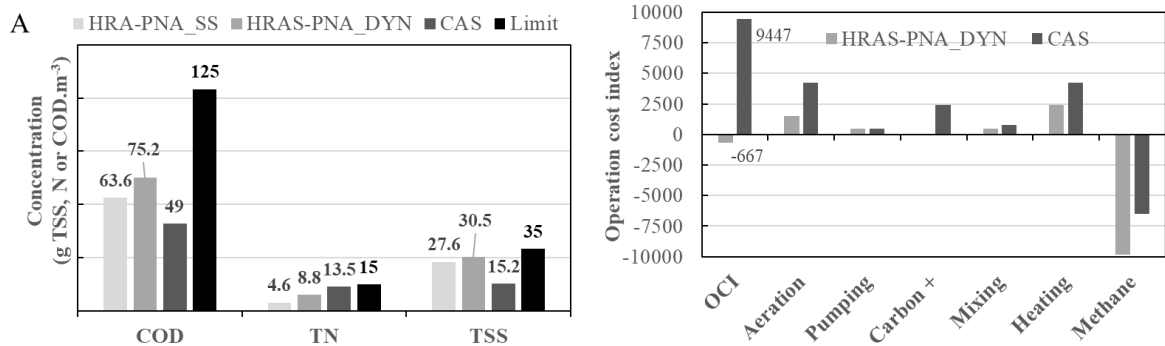


Figure 4.8. Comparison of dynamic simulation performance of the HRAS-PNA and CAS systems in terms of effluent quality and operational cost index (A3.2 and Table A4.11). HRAS-PNA_SS and HRAS-PNA_DYN represent the results of steady-state and dynamic simulations, respectively. The limits are set according to the EU council directive 91/271/EEC.

In terms of operational costs, the HRAS-PNA system has a 107% lower OCI than the CAS system (-667 vs. 9447, Fig. 4.8B). The significant reduction was mainly due to a 52% higher methane production (thus energy production), no carbon source dosage, and 64% lower aeration energy consumption in the former system (Fig. 4.8B and detailed in Table A4.11). The higher methane production was a result of the higher COD captured in the HRAS stage (Fig. 4.6A), while the savings on carbon source dosage was due to the autotrophic nitrogen removal in the PNA stage. As for the lower aeration energy, it was a combined effect of the lower DO concentration in the HRAS stage (i.e., less mineralization, Fig. 4.6A) and lower oxygen consumption in the partial nitrification pathway in the PNA stage compared to the full nitrification pathway in the CAS system. With respect to energy, the energy consumption in the HRAS-PNA system for aeration, pumping, mixing and heating (anaerobic digester) could be compensated by the energy production from methane, with a net production of 4918 kWh.d⁻¹, in contrast to a net consumption of 3179 kWh.d⁻¹ in the CAS system (Table A4.12). Even though the OCI does not consider all WWTP energy consumptions exhaustively (e.g., building energy requirements), this result illustrates the great potential of the HRAS-PNA to be energy-neutral or even energy-positive. Besides, due to the short HRT in the HRAS reactors and the high biomass concentration of the

granular sludge PNA reactor, the HRAS-PNA system has a much lower footprint than the CAS system (e.g., 5000 m³ vs. 12000 m³ for bioreactors in this study).

Overall, the HRAS-PNA system could achieve an effluent quality that complies with EU regulation with a significantly lower operational cost and footprint, compared to the CAS system.

4.3.3.3 Dynamic performance- feasibility of PNA process under dynamic mainstream conditions

To investigate in detail the feasibility of the PNA process under dynamic mainstream conditions, the profiles of the influent temperature, COD/N ratio and effluent TN concentration during the dynamic evaluation period (364 days) were zoomed in and plotted in Fig. 4.9. It seems clear that low temperature had a negative impact on the N removal (shown as effluent TN) of the HRAS-PNA system (Fig. 4.9A). However, when it comes to the impact of the influent COD/N ratios, it is not straightforward to interpret from the dynamic profiles (Fig. 4.9A&B). Therefore, correlation analysis was performed to further gain insight into the relationship between fluctuations of influent characteristics on the COD removal in the HRAS stage and N removal in the subsequent PNA stage (Table 4.3).

The COD removal (%) in the HRAS stage during the dynamic simulations was found positively correlated with influent temperature (9.5-20.5 °C, $R=0.16$), as observed before in steady-state simulations of the individual HRAS stage (Fig. 4.3C). Consequently, the COD/N ratios of the HRAS stage effluent (i.e., PNA stage influent) was negatively correlated with the influent temperature ($R=-0.47$). The N removal in the PNA stage was positively correlated with temperature ($R=0.47$) but was negatively correlated with the COD removal ($R=-0.28$) and effluent COD/N ratios ($R=-0.35$) of the preceding HRAS stage. Concerning the impact of the influent characteristics of the integrated HRAS-PNA system, the influent COD/N ratios were found rather unimportant for the COD removal in the HRAS stage ($R=0.04$) and therefore unimportant for the N removal in the PNA stage and the overall performance.

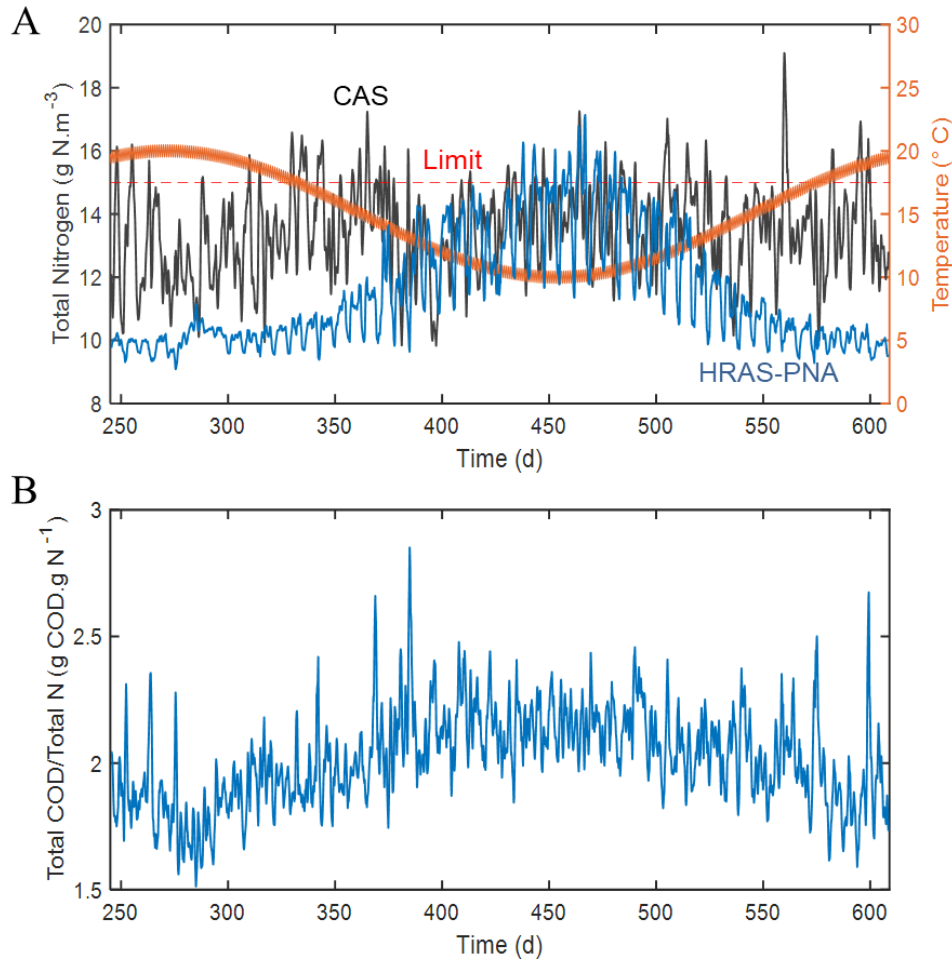


Figure 4.9. Dynamic profiles during the evaluation period (364 days) of: (A) influent temperature, effluent TN concentration of the HRAS-PNA system (blue line) and the CAS system (black line); and (B) influent (i.e., effluent of the HRAS stage) COD/N ratios of the PNA stage.

The results indicate that temperature could directly affect the PNA process and indirectly affect the PNA stage by influencing COD removal in the preceding HRAS stage. This implies that a high effluent TN and thus poor reactor performance could be expected for PNA reactors at low temperatures (e.g., winter), as reported in a pilot-scale reactor by Hoekstra et al. (2019). Furthermore, the results also indicate that high influent COD/N ratios (1.3-4.3 g COD.g N⁻¹) could be problematic for the PNA stage, which is in line with observations in previous experimental studies (Han et al., 2016a; Winkler et al., 2012). Organic matter can stimulate the growth of heterotrophic bacteria that compete with AOB for oxygen and with anammox bacteria for nitrite and thus affects the N removal. On the other hand, low influent COD/N ratios (e.g., <0.5 g bCOD.g⁻¹ N) could also help improve the nitrogen removal in anammox reactors (Jia et al., 2018; Liu et al., 2017; Winkler et al., 2012). Moreover, stronger correlations were

found between the bCOD/N ratios and all N-related parameters than that of COD/N ratio (Table 4.3), illustrating that the bCOD/N ratio could be a better indicator for predicting N removal in PNA reactors and for clarity when comparing results from different studies on the impact of organic matter.

Table 4.3. Pearson correlation analysis between influent characteristics, COD removal, nitrogen removal and effluent concentrations of the HRAS-PNA system during the 364 days dynamic evaluation period

	Influent				HRAS effluent				
	T	OLR _{in}	NLR _{in}	COD/N _{in}	C removal	OLR	NLR	COD/N	bCOD/N
HRAS C removal	0.16	0.73	0.67	-0.04	1.00	0.51	0.64	-0.29	0.01
eff									
COD	-0.10	0.25	-0.02	0.59	0.25	0.24	0.28	-0.14	0.17
COD/N	-0.47	0.08	0.12	-0.06	-0.29	0.30	-0.07	1.00	0.79
bCOD/N	-0.47	0.48	0.42	0.04		0.64	0.35	0.79	1.00
PNA N removal	0.47	-0.62	-0.59	0.16	-0.28	-0.72	-0.59	-0.35	-0.62
eff									
Con_AN	0.28	-0.21	-0.18	0.05	0.10	-0.32	-0.12	-0.44	-0.59
TN_{eff}	-0.57	0.40	0.22	0.23	0.23	0.53	0.49	0.12	0.39
COD_{eff}	-0.22	0.19	-0.07	0.53	0.22	0.22	0.28	-0.13	0.02
TSS_{eff}	-0.29	0.09	-0.17	0.55	0.10	0.16	0.22	-0.10	0.05

Note: All correlations are significant at the 0.01 level (2-tailed). N=34944. Green and red for positive and negative correlation coefficients (R), respectively. OLR represents organic loading rate (kg COD.d⁻¹); NLR represents nitrogen loading rate (kg N.d⁻¹); bCOD is the sum of S_s and X_s; Con_AN denotes the contribution of anammox bacteria in N removal (%).

Anammox process was found to be the primary process responsible for nitrogen removal in the PNA stage throughout the whole evaluation period, accounting for 75-95% of the nitrogen removal (Fig. A4.5). This implies that despite a negative impact of the influent COD/N ratios (1.3-4.3 g COD.g N⁻¹, corresponding to 0.5-2.4 g bCOD.g⁻¹ N) on the nitrogen removal of the PNA process, the heterotrophic bacteria cannot outcompete anammox bacteria, indicating the resilience of the PNA system under fluctuating mainstream conditions.

The effluent quality of this combined HRAS-PNA system was shown to adequately comply with the current EU regulations for yearly average (Fig. 4.9A), despite the variations of influent characteristics. However, the effluent TN concentration could violate the regulations on a daily basis during the low-temperature period (Fig. 4.9A). Moreover, the N removal in the HRAS-PNA system appears more sensitive to temperature compared to the CAS system (Fig. 4.9A). This raises questions on the long-term reliability of the combined system for municipal wastewater treatment;

therefore, active real-time control would be needed to achieve a more stable and reliable system performance.

Temperature and influent COD/N ratios of the PNA stage (i.e., effluent COD/N ratios of the preceding HRAS stage) were determined crucial for good system performance. Temperature is not an easily/economically manipulated variable but rather a disturbance variable in large scale applications; therefore, the COD/N ratios of the HRAS effluent (i.e., COD removal in the HRAS stage) should be the focus for potential control strategies. This can be tackled in two ways: 1) proactive management of COD removal in the HRAS stage; 2) reactive/counteractive control in the PNA stage while receiving influent with high COD/N ratios. In this regard, many control strategies have been proposed or tested for the PNA process for both sidestream (high-strength) and mainstream (low-strength) applications (Corbalá-Robles et al., 2016; Wu, 2017). However, control strategies for HRAS system are still largely lacking (Miller et al., 2017). As SRT and DO were shown to be important operational parameters, a real-time control strategy which can adjust the SRT (e.g., via MLSS control and waste sludge flow) and/or DO (e.g., aeration intensity) in accordance with the HRAS effluent COD/N ratio would be most desirable.

4.3.4 Model limitations and their implications

The model simulation results of this study do not only give insights into integrated process performance but also reveal some model implications. The results showed that the integrated HRAS-PNA system was capable of municipal wastewater treatment and producing effluent that adequately complies with the current EU regulations, with a much lower operational cost compared to the CAS system. The advantages of the HRAS-PNA system were found less pronounced under dynamic conditions than under steady-state conditions (e.g., effluent quality, Fig. 4.8A). The COD removal in the HRAS stage and N removal in the PNA stage were both reduced during the low-temperature period (Fig. 4.3C and Fig. 4.9A). Moreover, the dynamic simulations also highlighted that the N removal in the HRAS-PNA system was more sensitive to temperature compared to the CAS system (Fig. 4.9A). Therefore, it is important to use dynamic influent when evaluating the feasibility and performance of certain processes via modelling, as they can reproduce the behaviour of real influent and their effects on the effluent and sludge characteristics (Bisinella de Faria et al., 2015).

Concerning the HRAS stage model, the combined adsorption/bioflocculation and settling efficiency, f_{settler} , is a simple parameter to model the redirection of influent COD to the sludge line. However, it should be noted that in reality, the removal of particulate COD through adsorption/bioflocculation is affected by the SRT and DO (Jimenez et al., 2015; Nogaj et al., 2015). By lumping the efficiency of these two processes into a single parameter (f_{settler}), the general trend of the modelling results agrees with findings of experimental studies whereas the effect of SRT and DO on the adsorption/bioflocculation process cannot be fully reflected *via* this model. Given the importance of SRT and DO, a real-time control strategy that can adjust the SRT and/or DO in accordance with the effluent COD/N ratio would be most desirable. However, more research is needed to understand the fundamental mechanisms of the bioflocculation processes and thus the influence of operating conditions. Moreover, influent COD fractionation would also affect the COD distribution in the HRAS stage (Fig. A4.2 and (Smitshuijzen et al., 2016)) and the model outcome. Dedicated influent characterisation is needed in this respect for the modelling of the HRAS process (Solon et al., 2019).

It should be noted that the optimization of the two systems (e.g., maximal COD or N removal) was not the purpose of this study. Therefore, the operational conditions used in the simulations for comparison were not the optimal but the commonly applied conditions in practice for each system. Even though the results should not be interpreted in a fully quantitative way, they nevertheless provide a valuable indication of the potential and shortcomings of the conceptual HRAS-PNA system, from an integrated system perspective.

4.4 Conclusions

The performance of a promising combined HRAS-PNA system was evaluated through modelling and simulations, both on a unit process level and from a plant-wide perspective. Simulation results showed that the operation of a HRAS stage (i.e., manipulating the SRT and temperature) often implies a trade-off between maximizing the COD capture in the sludge for energy recovery and minimizing the effluent COD for the subsequent PNA process. For this purpose, moderate DO concentrations (0.3-0.5 g O₂.m⁻³) and SRT values (0.3-0.5 d) were recommended. For granular sludge PNA reactors, a higher biomass concentration required a lower DO set point for

maximum nitrogen removal. The anammox process remained the dominant process for nitrogen removal throughout the one-year evaluation period with varying influent COD/N (1.3-4.3) and temperature (10-20 °C), indicating the resilience and long-term stability of the PNA system at mainstream conditions. However, both COD removal (in HRAS) and N removal (in PNA) were compromised at low-temperature conditions. Overall, steady-state and dynamic simulations showed that the integrated HRAS-PNA system could achieve an effluent quality that complies with EU regulations with a significantly lower operational cost, compared to the CAS system.

Acknowledgements

Mingsheng Jia acknowledges the support from China Scholarship Council (CSC) and the special research fund (BOF) from Ghent University. The work of Kimberly Solon has received funding from the European Union's Horizon 2020 research and innovation programme under the Marie Skłodowska-Curie Grant Agreement No. 846316 (WISEFLOW).

Appendix

A4.1: High-rate activated sludge (HRAS) stage model

A4.1.1 Bioconversions in HRAS stage

Table A4.1. Stoichiometric matrix of the HRAS stage model (ASM1 (Henze et al., 2000))

A_{ij}	i component →	S_S [g COD.m ⁻³]	S_O [g O ₂ .m ⁻³]	S_{NH} [g N.m ⁻³]	S_{NO} [g N.m ⁻³]	X_S [g COD.m ⁻³]	X_H [g COD.m ⁻³]	X_A [g COD.m ⁻³]	X_P [g COD.m ⁻³]	S_{ND} [g N.m ⁻³]	X_{ND} [g N.m ⁻³]
j process ↓											
r1. Aerobic growth of heterotrophs		$-\frac{1}{Y_H}$	$-\frac{1 - Y_H}{Y_H}$	$-i_{XB}$			1				
r2. Anoxic growth of heterotrophs		$-\frac{1}{Y_{H,NO}}$		$-i_{XB}$	$-\frac{1 - Y_{H,NO}}{2.86Y_{H,NO}}$		1				
r3. Aerobic growth of autotrophs			$-\frac{4.57 Y_A}{Y_A}$	$-i_{XB} - \frac{1}{Y_A}$	$\frac{1}{Y_A}$			1			
r4. Decay of heterotrophs						$1 - f_P$	- 1		f_P		$i_{XB} - f_P * i_{XP}$
r5. Decay of autotrophs						$1 - f_P$		- 1	f_P		$i_{XB} - f_P * i_{XP}$
r6. Ammonification of soluble organic nitrogen				1						- 1	
r7. Hydrolysis of biodegradable particulate organics		1				-1					
r8. Hydrolysis of particulate organic nitrogen										1	-1

Table A4.2. Process rate expression of the HRAS stage model

Process	Process rate
r1. Aerobic growth of heterotrophs	$\mu_{max}^H \cdot \frac{S_O}{K_{O_2}^H + S_O} \cdot \frac{S_S}{K_S^H + S_S} \cdot \frac{S_{NH}}{K_{NH}^H + S_{NH}} \cdot X_H$
r2. Anoxic growth of heterotrophs	$\mu_{max}^H \cdot \eta_H \cdot \frac{S_{NO}}{K_{NO}^H + S_{NO}} \cdot \frac{S_S}{K_S^H + S_S} \cdot \frac{S_{NH}}{K_{NH}^H + S_{NH}} \cdot X_H$
r3. Aerobic growth of autotrophs	$\mu_{max}^A \cdot \frac{S_O}{K_{O_2}^A + S_O} \cdot \frac{S_{NH}}{K_{NH}^A + S_{NH}} \cdot X_A$
r4. Decay of heterotrophs	$b_H \cdot X_H$
r5. Decay of autotrophs	$b_A \cdot X_A$
r6. Ammonification of soluble organic Nitrogen	$k_a \cdot S_{ND} \cdot X_H$
r7. Hydrolysis of entrapped organics	$k_h \cdot \frac{X_S/X_H}{K_X + X_S/X_H} \cdot \left(\frac{S_O}{K_{O_2}^H + S_O} + \eta_h \cdot \frac{K_{O_2}^H}{K_{O_2}^H + S_O} \right) \cdot \frac{S_{NO}}{K_{NO}^H + S_{NO}} \cdot X_H$
r8. Hydrolysis of entrapped organic nitrogen	$k_h \cdot \frac{X_{ND}}{X_S} \cdot \frac{X_S/X_H}{K_X + X_S/X_H} \cdot \left(\frac{S_O}{K_{O_2}^H + S_O} + \eta_h \cdot \frac{K_{O_2}^H}{K_{O_2}^H + S_O} \right) \cdot \frac{S_{NO}}{K_{NO}^H + S_{NO}} \cdot X_H$

Table A4.3. Stoichiometric and kinetic parameters of the HRAS model

Parameter	Description	Value	Unit	Reference
Stoichiometric parameters				
Y_A	Yield coefficient for autotrophs	0.24	g COD.g N ⁻¹	(Henze et al., 2000)
Y_H	Aerobic yield coefficient for X_H	0.50	g COD.g COD ⁻¹	(Kobayashi et al., 1998)
$Y_{H,NO}$	Anoxic yield coefficient for X_H	0.53	g COD.g COD ⁻¹	(Muller et al., 2003)
i_{NXB}	Nitrogen content of biomass	0.07	g N.g COD ⁻¹	(Mozumder et al., 2014)
i_{NXI}	Nitrogen content of X_I	0.07	g N.g COD ⁻¹	(Mozumder et al., 2014)
i_{NSS}	Nitrogen content of S_S	0.03	g N.g COD ⁻¹	(Henze et al., 2000)
f_I	Fraction of X_I in biomass decay	0.08	g COD.g COD ⁻¹	(Henze et al., 2000)
f_P	Fraction of X_P in biomass decay	0.08	g COD.g COD ⁻¹	(Henze et al., 2000)
Kinetic parameters (at 15°C)				
μ_{max}^A	Maximum growth rate of autotrophs	0.5	d ⁻¹	(Henze et al., 2000)
μ_{max}^H	Maximum growth rate of X_H	4.24	d ⁻¹	(Henze et al., 2000)
b_A	Decay rate coefficient of autotrophs	0.05	d ⁻¹	(Henze et al., 2000)
b_H	Decay rate coefficient of X_H	0.35	d ⁻¹	(Henze et al., 2000)
$K_{O_2}^A$	S_{O_2} affinity constant for autotrophs	0.3	g O ₂ .m ⁻³	(Wiesmann, 1994)
$K_{O_2}^H$	S_{O_2} affinity constant for X_H	0.2	g O ₂ .m ⁻³	(Henze et al., 2000)
K_{NH}^A	S_{NH} affinity constant for X_A	1.1	g N.m ⁻³	(Wiesmann, 1994)
K_{NH}^H	S_{NH} affinity constant for X_H	0.02	g N.m ⁻³	(Mozumder et al., 2014)
K_{NO}^H	S_{NO} affinity constant for X_H	0.3	g N.m ⁻³	(Hellinga et al., 1999)
K_S^H	S_S affinity constant for X_H	4	g COD.m ⁻³	(Henze et al., 2000)
K_X	Half-saturation coefficient for hydrolysis	0.03	g X_S .(g X_{BH}) ⁻¹	(Henze et al., 2000)
k_a	Ammonification rate	0.05	m ³ .(g COD.d) ⁻¹	(Henze et al., 2000)
k_h	Maximum specific hydrolysis rate	3.0	g X_S .(g X_H COD.d) ⁻¹	(Henze et al., 2000)
η_H	Anoxic reduction factor for X_H	0.8	-	(Henze et al., 2000)
η_h	Anoxic hydrolysis correction factor	0.8	-	(Henze et al., 2000)

A4.1.2 Implementation of sludge retention time (SRT) and definition of f_{settler}

The flow scheme of the HRAS stage, which consists of a HRAS reactor and a settler, is depicted in Fig. A4.1.

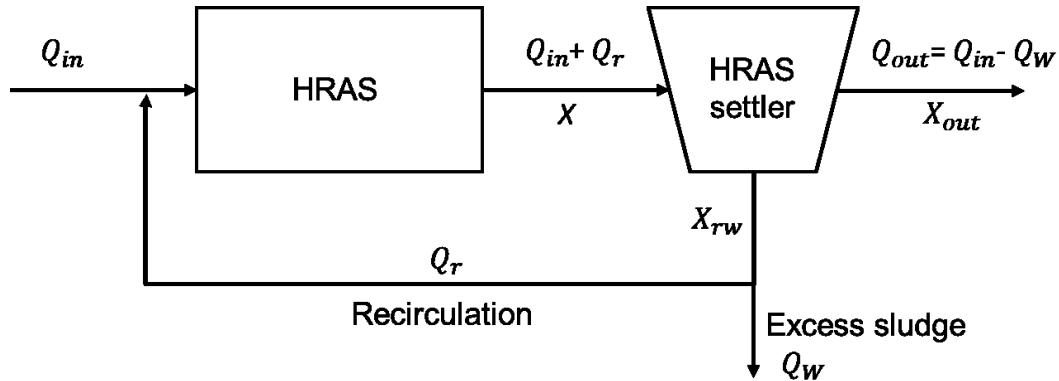


Figure A4.1. The HRAS stage flow scheme with variables for flow rates (Q) and biomass concentrations (X) for each flow, according to Smitshuijzen et al. (2016)

The SRT in the HRAS system is defined as the quantity of solids maintained in the reactor divided by the quantity of solids coming out of the reactor (Eq. A4.1).

$$\text{SRT} = \frac{X * V}{Q_w * X_{rw} + (Q_{in} - Q_w) * X_{out}} \quad (\text{A4.1})$$

where:

- V : the volume of the HRAS reactor (m^3), measured or designed
- Q_{in} : the influent flow rate ($\text{m}^3 \cdot \text{d}^{-1}$), measured
- Q_w : the flow of the excess sludge ($\text{m}^3 \cdot \text{d}^{-1}$)
- X : the biomass concentration in the HRAS reactor ($\text{g COD} \cdot \text{m}^{-3}$), measured or estimated
- X_{rw} : the biomass concentration in return sludge in the HRAS stage ($\text{g COD} \cdot \text{m}^{-3}$)
- X_{out} : the biomass concentration in the HRAS stage effluent ($\text{g COD} \cdot \text{m}^{-3}$), measured

In practice, the SRT is set by adjusting the waste sludge flow rate (Q_w), which is obtained by rearranging Eq. A4.1.

The parameter f_{settler} was defined as the separation efficiency of the settler, i.e., the fraction of the incoming particulate mass that is retained in the settler underflow. (Eq. A4.2).

$$f_{\text{settler}} = \frac{(Q_r + Q_w) * X_{rw}}{(Q_{in} + Q_r) * X} \quad (\text{A4.2})$$

$$1 - f_{\text{settler}} = \frac{X_{out} * Q_{out}}{(Q_{in} + Q_r) * X} \quad (\text{A4.3})$$

From Eq. A4.2 and A4.3, given a constant settling efficiency, the biomass concentration X_{rw} and X_{out} can be calculated by Eq. A4.4 and A4.5, respectively.

$$X_{rw} = \frac{(Q_{in} + Q_r) * X * f_{\text{settler}}}{Q_r + Q_w} \quad (\text{A4.4})$$

$$X_{out} = \frac{(Q_{in} + Q_r) * X * (1 - f_{\text{settler}})}{Q_{in} - Q_w} \quad (\text{A4.5})$$

The actual hydraulic retention time (HRT), taking into account dilution because of the recirculation flow (Q_r), is defined in Eq. A4.6.

$$\text{HRT} = \frac{V}{Q_r + Q_{in}} \quad (\text{A4.6})$$

The recirculation flow rate (Q_r) can be derived From Eq. A4.6 as Eq. A4.7 or measured in practice.

$$Q_r = \frac{V}{\text{HRT} (d)} - Q_{in} \quad (\text{A4.7})$$

By substituting X_{rw} (Eq. A4.4) and X_{out} (Eq. A4.5) in Eq. A4.1, the Q_w is obtained as a function of the SRT, the fraction of solids removed (f_{settler}), the volume of the HRAS reactors (V), the influent flow of the HRAS stage (Q_{in}) and the recirculation flow (Q_r) (Eq. A4.8).

$$Q_w = \frac{Q_r}{\frac{f_{\text{settler}}}{f_{\text{settler}} - 1 + \frac{V}{\text{SRT} * (Q_{in} + Q_r)}} - 1} \quad (\text{A4.8})$$

A4.1.3 Characteristics of influent used for simulations

The influent dataset of BSM2 (Gernaey et al., 2014), which consists of both constant influent and full dynamic influent data (609 days), was used as input for simulations. The constant influent file contains the average values of one full year dynamic data that represents the influent of the municipal wastewater treatment plant in BSM2 and is presented in Table A4.4.

Table A4.4. Influent characteristics for steady state simulations.

Variables	Description	Unit	Plant influent* BSM2	PNA stage influent**
S_I	Inert soluble COD	g COD.m ⁻³	27.2262	29.0892
S_S	Biodegradable soluble COD	g COD.m ⁻³	58.1762	11.2415
X_S	Slowly biodegradable particulate COD	g COD.m ⁻³	363.9435	28.6234
X_I	Inert particulate COD	g COD.m ⁻³	92.499	9.8234
X_P	Inert particulate COD from biomass decay	g COD.m ⁻³	0	0.18565
X_{BH}	Heterotrophic biomass	g COD.m ⁻³	50.6833	6.7003
S_{NH}	Ammonium	g N.m ⁻³	23.8595	40.7155
S_{ND}	Biodegradable soluble organic nitrogen	g N.m ⁻³	5.6516	2.9671
X_{ND}	Biodegradable particulate organic nitrogen	g N.m ⁻³	16.1298	1.2777
S_{NO}	Nitrite + nitrate	g N.m ⁻³	0	0
S_O	Dissolved oxygen	g O ₂ .m ⁻³	0	0.5
Q	Flow rate	m ³ .d ⁻¹	20648.361	20640.271
T	Temperature	°C	14.8581	14. 8581

*used for steady-state simulations of the HRAS stage (Section 4.3.1) and plant-wide HRAS-PNA system (Section 4.3.3.1);

**the effluent of the HRAS stage at reference scenario (Table 4.1), used for steady-state simulation of the PNA stage (Section 4.4.3.2)

A4.1.4 Influence of influent COD fractionation on COD redirection

The figure below illustrates the influence of influent COD fractionation between S_s and X_s on COD distribution in the HRAS stage. With more X_s distributed to S_s in the original BSM2 constant influent, the COD capture in sludge for energy recovery decreased while the COD mineralization increased.

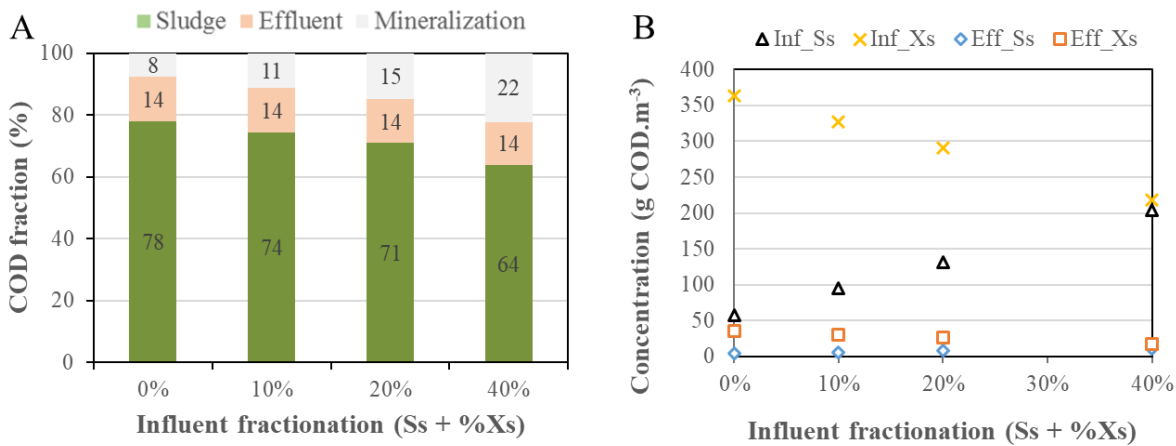


Figure A4.2. Influence of influent COD fractionation between S_s and X_s on: (A) COD mass balance of HRAS stage and (B) influent and effluent S_s and X_s concentrations (conditions: reference case of the HRAS model, Table 4.1)

A4.2: Partial nitrification-anammox (PNA) stage model

A one-dimensional biofilm model, only considering radial gradients in spherical biomass particles, was set up to describe the autotrophic and heterotrophic interaction in a granular sludge reactor. Spherical biomass particles (granules) were grown to a predefined steady-state granule radius, r_p of 0.75 mm. Besides, the biofilm porosity was assumed constant ($\epsilon_w = 0.75$). The density of granules was set to 60000 g VSS.m⁻³, corresponding to 80000 g COD.m⁻³ (for a typical conversion factor of 0.75 g VSS.COD⁻¹). The density of the heterotrophs was taken as 20000 g VSS.m⁻³, which is equivalent to 26666 g COD.m⁻³ (Mozumder et al., 2014).

A4.2.1 Bioconversions in PNA stage

Table A4.5. Stoichiometric matrix of the PNA stage model (according to Mozumder et al.(2014))

A _{ij}	i component →											
		S _S [g COD.m ⁻³]	S _{NH} [g N.m ⁻³]	S _{NO2} [g N.m ⁻³]	S _{NO3} [g N.m ⁻³]	S _{O2} [g O ₂ .m ⁻³]	S _{N2} [g N.m ⁻³]	X _{AOB} [g COD.m ⁻³]	X _{NOB} [g COD.m ⁻³]	X _{AN} [g COD. m ⁻³]	X _H [g COD.m ⁻³]	X _I [g COD. m ⁻³]
j process ↓												
AOB												
1. Growth			$-1/Y_{AOB} - i_{NXB}$	$1/Y_{AOB}$		$1 - 3.43/Y_{AOB}$		1				
2. Decay	$1-f_i$		$i_{NXB} - f_i \cdot i_{NXI} - (1-f_i) \cdot i_{NSS}$					-1				f_i
NOB												
3. Growth			$-i_{NXB}$	$-1/Y_{NOB}$	$1/Y_{NOB}$	$1 - 1.14/Y_{NOB}$			1			
4. Decay	$1-f_i$		$i_{NXB} - f_i \cdot i_{NXI} - (1-f_i) \cdot i_{NSS}$						-1			f_i
Anammox												
5. Growth			$-1/Y_{AN} - i_{NXB}$	$-(1/Y_{AN}) - (1/1.14)$	$1/1.14$		$2/Y_{AN}$			1		
6. Decay	$1-f_i$		$i_{NXB} - f_i \cdot i_{NXI} - (1-f_i) \cdot i_{NSS}$							-1		f_i
Heterotroph												
7. Aerobic growth	$-1/Y_H$		$-i_{NXB} + 1/Y_H \cdot i_{NSS}$			$1 - 1/Y_H$					1	
8. Anoxic growth on nitrite	$-\frac{1}{Y_{H,NO_2}}$		$-i_{NXB} + 1/Y_{H,NO_2} \cdot i_{NSS}$		$-\frac{1 - Y_{H,NO_2}}{1.71Y_{H,NO_2}}$		$\frac{1 - Y_{H,NO_2}}{1.71Y_{H,NO_2}}$				1	
9. Anoxic growth on nitrate	$-\frac{1}{Y_{H,NO_3}}$		$-i_{NXB} + 1/Y_{H,NO_3} \cdot i_{NSS}$		$\frac{1 - Y_{H,NO_3}}{1.14Y_{H,NO_3}}$		$-\frac{1 - Y_{H,NO_3}}{1.14Y_{H,NO_3}}$				1	
10. Decay	$1-f_i$		$i_{NXB} - f_i \cdot i_{NXI} - (1-f_i) \cdot i_{NSS}$								-1	f_i
Composition matrix												
gCOD/unit comp		1	0	-3.43	-4.57	-1	-1.71	1	1	1	1	1
gN/unit comp		i_{NSS}	1	1	1	0	1	i_{NXB}	i_{NXB}	i_{NXB}	i_{NXB}	i_{NXI}

Table A4.6. Kinetic rate expressions of the PNA stage model

Process	Process rate
1. growth of AOB	$\mu_{max}^{AOB} \cdot \frac{S_{O_2}}{K_{O_2}^{AOB} + S_{O_2}} \cdot \frac{S_{NH}}{K_{NH}^{AOB} + S_{NH}} \cdot X_{AOB}$
2. decay of AOB	$b_{AOB} X_{AOB}$
3. growth of NOB	$\mu_{max}^{NOB} \cdot \frac{S_{O_2}}{K_{O_2}^{NOB} + S_{O_2}} \cdot \frac{S_{NO_2}}{K_{NO_2}^{NOB} + S_{NO_2}} \cdot \frac{S_{NH}}{K_{NH}^{NOBH} + S_{NH}} X_{NOB}$
4. decay of NOB	$b_{NOB} X_{NOB}$
5. growth of anammox	$\mu_{max}^{AN} \cdot \frac{K_{O_2}^{AN}}{K_{O_2}^{AN} + S_{O_2}} \cdot \frac{S_{NH}}{K_{NH}^{AN} + S_{NH}} \cdot \frac{S_{NO_2}}{K_{NO_2}^{AN} + S_{NO_2}} \cdot X_{AN}$
6. decay of anammox	$b_{AN} X_{AN}$
7. aerobic growth of heterotrophs	$\mu_{max}^H \cdot \frac{S_S}{K_S^H + S_S} \cdot \frac{S_{O_2}}{K_{O_2}^H + S_{O_2}} \cdot \frac{S_{NH}}{K_{NH}^{NOBH} + S_{NH}} X_H$
8. anoxic growth of heterotrophs on NO_2^-	$\mu_{max}^H \cdot \eta_{NO_2} \frac{K_{O_2}^H}{K_{O_2}^H + S_{O_2}} \cdot \frac{S_{NO_2}}{K_{NO_2}^H + S_{NO_2}} \cdot \frac{S_{NO_2}}{S_{NO_2} + S_{NO_3}} \cdot \frac{S_S}{K_S^H + S_S} \cdot \frac{S_{NH}}{K_{NH}^{NOBH} + S_{NH}} X_H$
9. anoxic growth of heterotrophs on NO_3^-	$\mu_{max}^H \cdot \eta_{NO_3} \frac{K_{O_2}^H}{K_{O_2}^H + S_{O_2}} \cdot \frac{S_{NO_3}}{K_{NO_3}^H + S_{NO_3}} \cdot \frac{S_{NO_3}}{S_{NO_2} + S_{NO_3}} \cdot \frac{S_S}{K_S^H + S_S} \cdot \frac{S_{NH}}{K_{NH}^{NOBH} + S_{NH}} X_H$
10. decay of heterotrophs	$b_H X_H$

Table A4.7. Stoichiometric and kinetics parameters of the PNA stage model

Parameter	Definition	Value	Unit	Source
Stoichiometric parameters				
Y_{AOB}	Yield coefficient for AOB	0.20	g COD.g N ⁻¹	(Wiesmann, 1994) ⁽¹⁾
Y_{NOB}	Yield coefficient for NOB	0.057	g COD.g N ⁻¹	(Wiesmann, 1994) ⁽¹⁾
Y_{AN}	Yield coefficient for Anammox	0.17	g COD.g N ⁻¹	(Strous et al., 1998) ⁽²⁾
Y_{H, O_2}	Aerobic yield coefficient for X_H	0.67	g COD.g COD ⁻¹	(Henze et al., 2000)
Y_{H, NO_2}	Anoxic yield coefficient for X_H	0.53	g COD.g COD ⁻¹	(Muller et al., 2003)
Y_{H, NO_3}	Anoxic yield coefficient for X_H	0.53	g COD.g COD ⁻¹	(Muller et al., 2003)
i_{NXB}	Nitrogen content of biomass	0.07	g N.g COD ⁻¹	(Mozumder et al., 2014)
i_{NXI}	Nitrogen content of X_I	0.07	g N.g COD ⁻¹	(Mozumder et al., 2014)
i_{NSS}	Nitrogen content of S_s	0.03	g N.g COD ⁻¹	(Henze et al., 2000)
f_I	Fraction of X_I in biomass decay	0.08	g COD.g COD ⁻¹	(Henze et al., 2000)
Kinetic parameters (at 15°C)				
μ_{max}^{AOB}	Maximum growth rate of AOB	0.58	d ⁻¹	(Hao et al., 2002b) ⁽³⁾
μ_{max}^{NOB}	Maximum growth rate of NOB	0.5	d ⁻¹	(Hao et al., 2002b) ⁽³⁾
μ_{max}^{AN}	Maximum growth rate of Anammox	0.017	d ⁻¹	(Hao et al., 2002b) ⁽³⁾
μ_{max}^H	Maximum growth rate of X_H	4.24	d ⁻¹	(Henze et al., 2000) ⁽⁴⁾
b_{AOB}	Decay rate coefficient of AOB	0.031	d ⁻¹	(Hao et al., 2002b) ⁽³⁾
b_{NOB}	Decay rate coefficient of NOB	0.024	d ⁻¹	(Hao et al., 2002b) ⁽³⁾
b_{AN}	Decay rate coefficient of Anammox	0.0006	d ⁻¹	(Hao et al., 2002b) ⁽³⁾
b_H	Decay rate coefficient of X_H	0.35	d ⁻¹	(Henze et al., 2000) ⁽⁴⁾
$K_{O_2}^{AOB}$	S_{O_2} affinity constant for AOB	0.3	g O ₂ .m ⁻³	(Wiesmann, 1994)
$K_{O_2}^{NOB}$	S_{O_2} affinity constant for NOB	1.1	g O ₂ .m ⁻³	(Wiesmann, 1994)
$K_{O_2}^{AN}$	S_{O_2} inhibiting coefficient for Anammox	0.05	g O ₂ .m ⁻³	(Mozumder et al., 2014)
$K_{O_2}^H$	S_{O_2} affinity constant for X_H	0.2	g O ₂ .m ⁻³	(Henze et al., 2000)
K_{NH}^{AOB}	S_{NH} affinity constant for AOB	1.1	g N.m ⁻³	(Wiesmann, 1994)
K_{NH}^{NOBH}	S_{NH} affinity constant for NOB and H	0.02	g N.m ⁻³	(Mozumder et al., 2014)
K_{NH}^{AN}	S_{NH4} affinity constant for Anammox	0.03	g N.m ⁻³	(Mozumder et al., 2014)
$K_{NO_2}^{NOB}$	S_{NO_2} affinity constant for NOB	0.51	g N.m ⁻³	(Wiesmann, 1994)
$K_{NO_2}^{AN}$	S_{NO_2} affinity constant for Anammox	0.005	g N.m ⁻³	(Mozumder et al., 2014)
$K_{NO_2}^H$	S_{NO_2} affinity constant for X_H	0.3	g N.m ⁻³	(Hellinga et al., 1999)
$K_{NO_3}^H$	S_{NO_3} affinity constant for X_H	0.3	g N.m ⁻³	(Hellinga et al., 1999)
K_S^H	S_s affinity constant for X_H	20	g COD.m ⁻³	(Henze et al., 2000)
$\eta_{NO_2}=\eta_{NO_3}$	Anoxic reduction factor for X_H	0.8	-	(Henze et al., 2000)
Mass transfer				
D_{NH_4}	Diffusivity of NH ₄ in water	1.5x10 ⁻⁴	m ² .d ⁻¹	(Williamson and McCarty, 1976)

D_{NO_2}	Diffusivity of NO_2 in water	1.4×10^{-4}	$m^2 \cdot d^{-1}$	(Williamson and McCarty, 1976)
D_{NO_3}	Diffusivity of NO_3 in water	1.4×10^{-4}	$m^2 \cdot d^{-1}$	(Williamson and McCarty, 1976)
D_{O_2}	Diffusivity of O_2 in water	2.2×10^{-4}	$m^2 \cdot d^{-1}$	(Picioreanu et al., 1997)
D_{N_2}	Diffusivity of N_2 in water	2.2×10^{-4}	$m^2 \cdot d^{-1}$	(Williamson and McCarty, 1976)
D_S	Diffusivity of COD in water	1×10^{-4}	$m^2 \cdot d^{-1}$	(Hao and van Loosdrecht, 2004)

- (1) After unit conversion, using a typical biomass composition of $CH_{1.8}O_{0.5}N_{0.2}$, corresponding with $1.3659 \text{ g COD} \cdot \text{g}^{-1}$
- (2) After unit conversion, using an anammox biomass composition of $CH_2O_{0.5}N_{0.15}$ (Strous et al., 1998) corresponding with $36.4 \text{ g COD} \cdot \text{mole}^{-1}$ or $1.51 \text{ g COD} \cdot \text{g}^{-1}$
- (3) Conversion of values given by Hao et al. (2002) at 20°C to 15°C using the relationship proposed by these authors (written for X_{AOB} , analogous for X_{NOB} and X_{AN})

$$\mu_{max}^{AOB1}(T) = \mu_{max}^{AOB1}(T_{ref}) \cdot \exp\left(\frac{E_a^{AOB} \cdot (T - T_{ref})}{R \cdot T \cdot T_{ref}}\right)$$

with $E_a^{AOB} = 68 \text{ kJ} \cdot \text{mole}^{-1}$; $E_a^{NOB} = 44 \text{ kJ} \cdot \text{mole}^{-1}$; $E_a^{AN} = 70 \text{ kJ} \cdot \text{mole}^{-1}$ [10]; $R = 8.31 \text{ J} \cdot \text{mole}^{-1} \cdot \text{K}^{-1}$.

- (4) Conversion of ASM1-values given by Henze et al. (2000) at 10°C and 20°C to 15°C using temperature relationship proposed by these authors (ASM3).

$$r_T = r_{293} \cdot \exp[\theta_T(T - 293)]$$

$$\theta_T = \frac{\ln(r_{T1}/r_{T2})}{T1 - T2}$$

Where r_T is the reaction rate at temperature T , r_{293} is the rate at the standard temperature (293 K), T is the temperature (K), and θ is the temperature coefficient (1/K).

A4.2.2 Calculation of the PNA reactor volume

The volume of the PNA reactor in this study was calculated as:

$$V = \frac{NLR}{SNLR \cdot X} \cdot S \quad (\text{A4.9})$$

where V is the volume of the reactor (m^3), NLR is the nitrogen loading rate (g N.d^{-1}), $SNLR$ is the specific nitrogen loading rate ($\text{g N.g VSS}^{-1}.\text{d}^{-1}$), X is the biomass concentration (g VSS.m^{-3}), and S is a safety factor ($S=1.25$).

The nitrogen loading rate (NLR) is defined as:

$$NLR = Q_{inf} \times C_{inf} \quad (\text{A4.10})$$

where Q_{inf} is the flow rate ($\text{m}^3.\text{d}^{-1}$) and C_{inf} is the concentration of total nitrogen (g N.m^{-3}) in the influent of the PNA reactor.

The specific nitrogen loading rate ($SNLR$) is defined as the NLR per amount of biomass and was calculated from the values reported by Lotti et al. (2015b) for a pilot-scale granular sludge mainstream PNA reactor (Table A4.8)

Table A4.8. Calculation of the PNA reactor volume

Variable	Unit	Value	Source
Q_{inf}	$\text{m}^3.\text{d}^{-1}$	20640	This study (Table A4.4)
C_{inf}	g N.m^{-3}	45	This study (Table A4.4)
NLR	g N.d^{-1}	928800	$Q_{inf} \times C_{inf}$
X	kg VSS.m^{-3}	4	(Lotti et al., 2015b)
$SNLR$	$\text{g N.g VSS}^{-1}.\text{d}^{-1}$	0.125*	(Lotti et al., 2015b)
V	m^3	2500#	This study

*Calculated from the $NLR_p = 2 \text{ kg N.d}^{-1}$, $V_p = 4 \text{ m}^3$ and $X_p = 4 \text{ kg VSS.m}^{-3}$ for the pilot scale reactor in Lotti et al. (2015b); # after rounding.

A4.2.3 Influence of bulk dissolved oxygen (DO) concentration on N removal

The influence of bulk DO concentration on the mainstream PNA reactor was evaluated with scenario analysis and summarized in Fig. A4.3. The results showed that the nitrogen removal efficiency first increased ($< 1 \text{ g O}_2\cdot\text{m}^{-3}$) and then decreased (below 40% at $2 \text{ g O}_2\cdot\text{m}^{-3}$, Fig. A4.3) as the bulk DO concentration increased. This is consistent with earlier modelling and simulation studies which focused on sidestream PNA with planar biofilm or granules (e.g., (Hao et al., 2002b; Mozumder et al., 2014)).

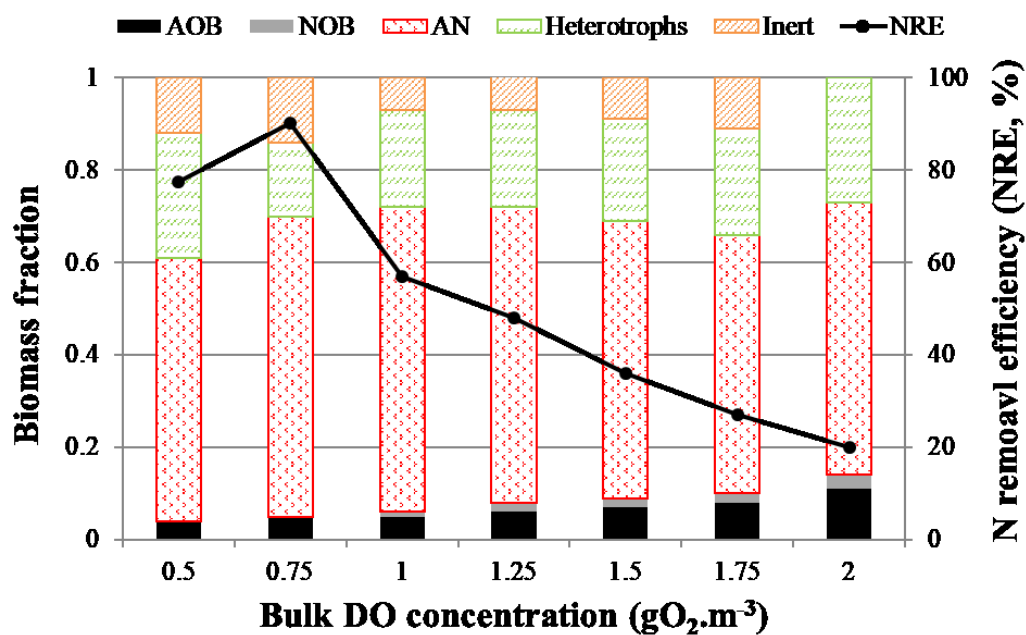


Figure A4.3. Influence of bulk DO concentration on the steady-state performance of the PNA process with a fixed biomass concentration ($4 \text{ kg VSS}\cdot\text{m}^{-3}$)

A4.3: Plant-wide comparison of the HRAS-PNA and CAS system

A4.3.1 Plant layout of the conventional activated sludge (CAS) system

The plant layout of the conventional activated sludge (CAS) system in the BSM2 was used for the comparison with the HRAS-PNA system in terms of effluent quality and operational cost.

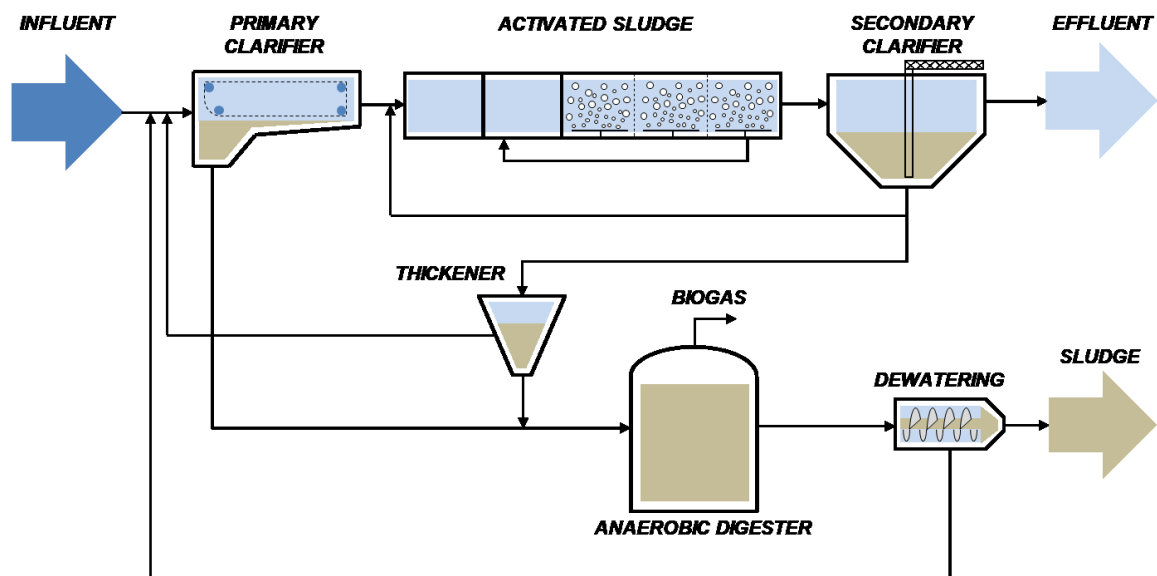


Figure A4.4. Plant layout of the CAS system used in this study (BSM2)

A4.3.2 Evaluation criteria for plant-wide comparison

The evaluation criteria used for comparison of the HRAS-PNA and CAS system under dynamic conditions are the effluent quality index (EQI) and the operational cost index (OCI) as defined in the Benchmark Simulation Model No. 2 (BSM2) (Gernaey et al., 2014), and detailed below.

- Effluent Quality Index (EQI)

The EQI ($\text{kg pollution units} \cdot \text{d}^{-1}$) reflects the amount of pollution discharged into surface waters. The EQI is calculated as a weighted sum of the effluent concentrations of total suspended solids (TSS), COD, Kjeldahl N (NKj), nitrate and nitrite nitrogen (NO) and BOD₅, averaged over the period (Eq. A4.11).

$$\text{EQI} = \frac{1}{t_{\text{obs}} \cdot 1000} \int_{t_{\text{start}}}^{t_{\text{end}}} \left(\beta_{\text{TSS}} \cdot \text{TSS}_e(t) + \beta_{\text{COD}} \cdot \text{COD}_e(t) + \beta_{\text{NKj}} \cdot S_{\text{NKj}_e}(t) + \beta_{\text{NO}} \cdot S_{\text{NO}_e}(t) + \beta_{\text{BOD}_5} \cdot \text{BOD}_{5_e}(t) \right) \cdot Q_e(t) \cdot dt \quad (\text{A4.11})$$

The subscript e denotes the effluent. Table A4.9 lists the values for the weighting factors β_i , which convert concentrations of individual components into general pollution units.

Table A4.9. Values of the EQI weighing factors (β_i)

Weighing factors	β_{TSS}	β_{COD}	β_{NKj}	β_{NO}	β_{BOD_5}
Value ($\text{g pollution unit} \cdot \text{g}^{-1}$)	2	1	30	10	2

- Operational Cost Index (OCI)

The OCI is an overall operating cost measure, which is calculated as a weighted sum of aeration energy (AE , kWh.d⁻¹), pumping energy (PE , kWh.d⁻¹), mixing energy (ME , kWh.d⁻¹), sludge production for disposal (SP , kg SS.d⁻¹), external carbon addition (EC , kg COD.d⁻¹), methane production (MP , kg CH₄.d⁻¹) and the required heating energy for the anaerobic digester heating energy (HE , kWh.d⁻¹, if the heat generated by the gas motor ($7MP$) is higher than HE then no external energy is required).

$$OCI = AE + PE + f_{SP} \cdot SP + f_{EC} \cdot EC + ME - f_{MP} \cdot MP + \max(0, HE - 7MP) \quad (A4.12)$$

The calculation of the individual cost factors is detailed in (Gernaey et al., 2014). Weighing factors, f_i (Table A4.10, BSM2) are introduced to express all cost factors in kWh.d⁻¹.

Table A4.10. Values of the OCI weighing factors (f_i)

Weighting factors	f_{SP}	f_{EC}	f_{MP}
Value	3	3	6

A4.3.3 Aeration energy calculation in the PNA stage

The aeration energy (AE) is part of the operational costs considered in the evaluation criteria of BSM2. The AE in the PNA stage was calculated following the method in Rittmann & McCarty (2001) and Gernaey et al. (2014). The calculation procedure is summarized in steps (1) to (6).

(1) Oxygen demand (OD) in the PNA reactor

The oxygen was consumed by AOB, NOB and heterotrophs (H) in the PNA reactor. To model the granular sludge reactor, the granules were divided into 50 layers. By summing up the oxygen demand by the three groups of bacteria in each layer, the oxygen demand of a granule was calculated. Subsequently, the overall oxygen demand (OD, kg O₂.d⁻¹) was calculated as:

$$OD = n * \sum_{i=1}^{i=50} V_i \cdot (ODR_{AOB,i} + ODR_{NOB,i} + ODR_{H,i}) \quad (A4.13)$$

Where,

OD = overall oxygen demand of the granular sludge reactor (kg O₂.d⁻¹)

n = the number of granules in the reactor

V_i = the volume the layer i in the granules (m³)

ODR_{AOB,i} = oxygen demand rate of AOB in layer i (kg O₂.m⁻³.d⁻¹)

ODR_{NOB,i} = oxygen demand rate of NOB in layer i (kg O₂.m⁻³.d⁻¹)

ODR_{H,i} = oxygen demand rate of heterotrophs in layer i (kg O₂.m⁻³.d⁻¹)

(2) Oxygen transfer rate (OTR)

$$OTR = K_L a \cdot (S_{O,T}^{sat} - S_O) / 1000 \quad (A4.14)$$

Where,

OTR = oxygen transfer rate per unit volume of reactor for clean water (kg O₂.m⁻³.d⁻¹)

K_La = volumetric mass transfer rate coefficient (d⁻¹)

S_{O,T}^{sat} = liquid phase oxygen concentration in equilibrium (mg L⁻¹)

S_O = liquid phase bulk oxygen concentration (mg L⁻¹)

(3) Correction factors (clean water to wastewater, temperature)

$$\alpha = \frac{K_L a (wastewater)}{K_L a (clean water)} \quad (A4.15)$$

α : varies from 0.3 to 1.1 for mechanical aeration

$$\beta = \frac{S_{O,T}^{sat} (\text{wastewater})}{S_{O,T}^{sat} (\text{clean water})} \quad (\text{A4.16})$$

β : a value of 0.95 is often assumed for municipal WW

$$K_L a (T) = K_L a (15) \cdot 1.024^{T-15} \quad (\text{A4.17})$$

$$OTR_c (T) = \alpha K_L a (T) \cdot (\beta \cdot S_{O,T}^{sat} - S_o) \quad (\text{A4.18})$$

$OTR_c (T)$ = the OTR after correction for wastewater and temperature (kg O₂.m⁻³.d⁻¹, with T in °C)

(4) Standard oxygen transfer efficiencies (SOTE)

$$\text{SOTE} = 1.8 \text{ kg O}_2 \cdot \text{kWh}^{-1} \text{ (@ } 15^\circ\text{C, BSM2)}$$

(5) Field oxygen transfer efficiencies (FOTE)

$$FOTE (T) = \text{SOTE} \cdot \frac{OTR_c (T)}{OTR (15)} = \text{SOTE} \cdot 1.024^{T-15} \cdot \alpha \cdot \frac{\beta \cdot S_{O,15}^{sat} - S_o}{S_{O,15}^{sat} - 0} \quad (\text{A4.19})$$

Where $FOTE (T)$ = the field oxygen transfer efficiencies for wastewater at T (kg O₂.kWh⁻¹)

$\alpha = 0.7$, $\beta = 0.95$, and $S_o = 0.5 \text{ mg L}^{-1}$; e.g., at T = 14.9 °C:

$$FOTE (14.9) = 1.12 \text{ kg O}_2 \text{ per kWh}$$

(6) Aeration energy (AE, kWh.d⁻¹) in the PNA reactor

$$AE = \frac{\text{OD}}{FOTE (T)} \quad (\text{A4.20})$$

A4.3.4 Calculated EQI, OCI and energy balance

The evaluation criteria used for comparison of the HRAS-PNA and CAS system under dynamic conditions are the effluent quality index (EQI) and the operational cost index (OCI) (A3.2). Table A4.11 summaries the calculated EQI and operational cost index for both HRAS-PNA system and CAS system.

Table A4.11. Comparison of dynamic simulation performance of CAS and HRAS-PNA systems in terms of effluent quality and operation cost

Variable	Unit	CAS	HRAS-PNA	Meets regulation?
Effluent quality related variables				
TSS concentration (limit = 30 g SS.m ⁻³)	g SS.m ⁻³	15.2	30.5	N
Kjeldahl N concentration	g N.m ⁻³	2.5	7.9	-
Total N concentration (limit = 18 g N.m ⁻³)	g N.m ⁻³	13.5	8.8	Y
Total COD concentration (limit = 100 g COD.m ⁻³)	g COD.m ⁻³	49.0	75.2	Y
BOD ₅ concentration (limit = 10 g.m ⁻³)	g COD.m ⁻³	2.7	6.5	Y
Effluent quality index (EQI)	kg poll units.d ⁻¹	5574	8177	-
Operation cost related variables				
				Change
Aeration energy	kWh.d ⁻¹	4223	1502	-64%
Pumping energy	kWh.d ⁻¹	445	482	+8%
Carbon source dosage	kg COD.d ⁻¹	800	0	-100%
Mixing energy	kWh.d ⁻¹	768	489	-36%
Heating energy	kWh.d ⁻¹	4225	2435	-42%
Methane gas production (1 kg = 13.8928 kWh)	kg CH ₄ .d ⁻¹	1085	1645	+52%
Total Operational Cost Index (OCI)	-	9447	-667	-107%

Table A4.12. Energy balance of the CAS and HRAS-PNA systems during the evaluation period (dynamic simulation)

Variable	Unit	CAS	HRAS-PNA	Change
Energy related variables				
Aeration energy	kWh.d ⁻¹	4223	1502	-64%
Pumping energy	kWh.d ⁻¹	445	482	+8%
Mixing energy	kWh.d ⁻¹	768	489	-36%
Heating energy	kWh.d ⁻¹	4225	2435	-42%
Methane gas production to energy*	kWh.d ⁻¹	-6482	-9826	+52%
Net energy consumption	kWh.d ⁻¹	3179	-4918	

calculated as methane gas production (kg CH₄.d⁻¹, Table A4.11) 13.8928 (kWh. kg⁻¹)*0.43 (BSM2)

A4.3.5 Additional result from the dynamic simulations

Fig. A4.5 shows the contribution of anammox process (Con_AN) in the N removal of the PNA reactor during the dynamic evaluation period. It was found that the anammox process was the primary process responsible for N removal, contributing to 75-95% of the total N removal.

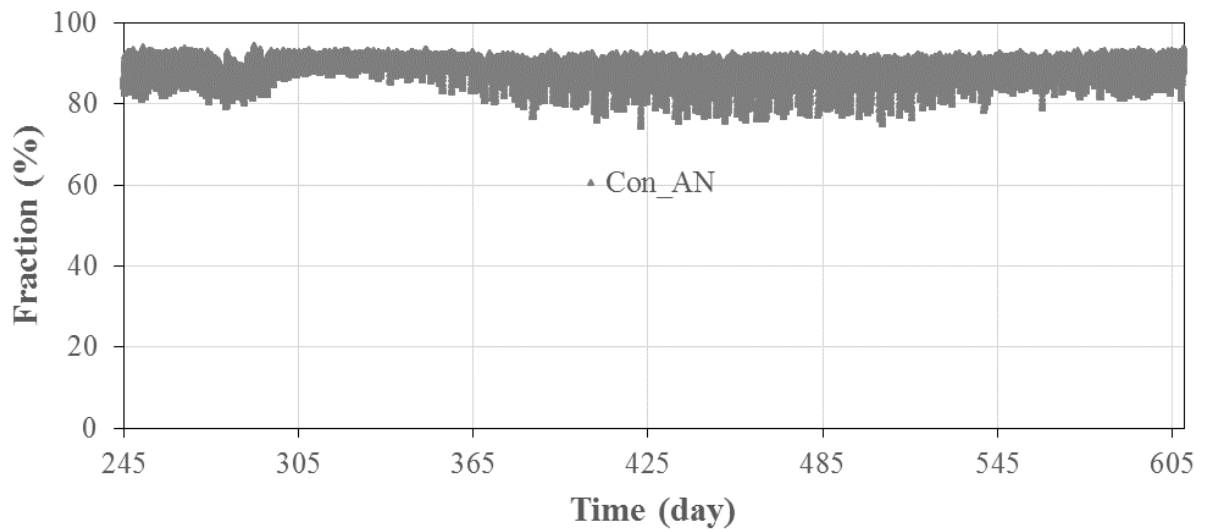


Figure A4.5. Contribution of anammox (Con_AN) in the nitrogen removal in the PNA reactor during the evaluation period (364 days) (dynamic simulation)

Chapter 5

General conclusions and perspectives

The focus of this thesis is on microbial interactions in biological nitrogen transformations, featuring the fate of nitrate and the evaluation of anammox-based processes from both individual and plant-wide systematic perspectives. The applied methodology concerns lab-scale experiments and mathematical modelling and simulations. This chapter gives concluding remarks on how the findings of this thesis and their implications contribute to the understanding of biological nitrogen removal from wastewater and of the nitrogen cycle in general, concerning methodology (Section 5.1), the fate of nitrate (Section 5.2) and process evaluation (Section 5.3).

5.1 Methodology

5.1.1 Stoichiometry matters

Stoichiometry gives quantitative insights into processes. This thesis illustrates the importance of stoichiometry in mass balance and modelling of anammox process (Chapter 2) and microbial competition for shared resources (Chapter 3).

5.1.1.1 Mass balance and modelling of anammox process

The accuracy of mass balances depends on the accurate knowledge of the involved reactions and their stoichiometry. In Chapter 2, the substantial differences in anammox stoichiometry reported in the literature were highlighted. For example, the nitrate production per mole ammonium consumed ($\Delta\text{NO}_3^-/\Delta\text{NH}_4^+$) is 38% lower in the stoichiometry determined by Lotti et al. (2014b) than in the most widely used one from Strous et al. (1998) (0.161 vs. 0.26, Table 2.2). This implies that significantly different interpretations may occur with respect to the contribution of individual processes in nitrogen conversions in anammox-based processes (e.g., anammox and denitrification in N removal), depending on the anammox stoichiometry used. Subsequently, a general anammox stoichiometry was presented as a function of biomass composition ($\text{CH}_x\text{O}_y\text{N}_z$) and the measured yield coefficient (e.g., $\Delta\text{NO}_2^-/\Delta\text{NH}_4^+$), following the generalized method of Kleerebezem and van Loosdrecht (2010). The approach was demonstrated with a spreadsheet that can easily be applied for other experimental studies (Spreadsheet A2.1, Chapter 2).

The anammox stoichiometry corresponding with our experimental measurements of $\Delta\text{NO}_2^-/\Delta\text{NH}_4^+$ in a granular sludge reactor was calculated with the general approach in Chapter 2. It should be noted; however, that other populations than anammox bacteria are likely to be present in granular sludge and biofilm reactors, which may affect ammonium and nitrite consumption and nitrate production and thus disturb the determination of the anammox stoichiometry based on the measured $\Delta\text{NO}_2^-/\Delta\text{NH}_4^+$. Only in case there are no significant side reactions affecting the concentration of the compounds used for yield calculation, in this case ammonium and nitrite, the yield coefficient obtained from this approach represents the intrinsic yield.

Further investigation of anammox stoichiometry in the literature found that the experimentally measured anammox biomass yield for the overall metabolic reaction

has been mistakenly used as the catabolic yield in many modelling studies (Chapter 2), for example in Chapter 4 of this thesis. This is conceptually wrong and may induce systematic errors in modelling and simulation studies. For instance, with the stoichiometry used in the past, slightly more ammonium is needed to form one unit of anammox biomass (e.g., +1.1% with $Y=0.17 \text{ g COD.g N}^{-1}$ and $i_{\text{NXB}}=0.07 \text{ g N.g COD}^{-1}$, (Strous et al., 1998)). Therefore, in terms of stoichiometry, anammox was weakened/underrepresented in previous simulation efforts. Even though the induced systematic errors are relatively small, it is important to rigorously distinguish between metabolic and catabolic yields. The same modelling issue could arise for other bioconversion reactions in which the substrate, relative to which the yield coefficient is defined, is consumed in both the catabolic and anabolic reaction. For example, aerobic ammonium-oxidizing microorganisms (AOMs, including AOB, AOA and comammox bacteria) consume ammonium as an electron donor to produce nitrite/nitrate in the catabolic reaction and as N-source for biomass synthesis in the anabolic reaction. Therefore, the overall impact of the erroneous use of yield coefficient in a model with both anammox and AOMs is less straightforward and may require more direct modelling studies. Solutions were proposed to address this modelling issue.

In the dynamic simulations of the PNA process in Chapter 4, the yield coefficient of anammox bacteria was assumed constant under different temperatures. Previous study indicates that the dominant anammox species may switch at different temperatures (De Cocker et al., 2018). Consequently, the yield and probably the whole set of kinetic parameters of anammox bacteria may need to be made temperature-dependent to account for this.

5.1.1.2 Microbial competition for shared resources

Chapter 3 takes a mathematical approach by applying the resource-ratio theory to unravel the competition between heterotrophic denitrification and dissimilatory nitrate reduction to ammonium (DNRA) for nitrate and organic carbon in continuous cultures. The results revealed that the boundary influent COD/N ratios for different competition outcomes at high influent resource concentrations were mostly determined by the stoichiometry (i.e., consumption of COD per nitrate, $Y_{\text{X/NO}_3}/Y_{\text{X/COD}}$) of the two competing processes, whereas kinetics (i.e., K_S and μ_{max}) became important as well at low resource concentrations.

The implications of these results are not limited to denitrification and DNRA but can potentially be used for any case where multispecies compete for two limiting essential resources. For further elucidation of the competition between denitrification and DNRA, the stoichiometry of the often-overlooked DNRA process still needs to be further determined, especially if nitrite instead of nitrate serves as the terminal electron acceptor.

5.1.2 Resource-ratio theory for interspecies competition studies

The resource-ratio theory was established in the early 1980s for ecology studies (Miller et al., 2005; Tilman, 1980). It describes species interactions based on the use of shared resources and enables to predict the outcomes of interspecies competition in advance of actual competition experiments (Hsu et al., 1981; Tilman, 1980). Mathematical models based on this theory were applied to reveal the competition between denitrification and DNRA for nitrate and organic carbon in continuous cultures and were proven valid with experimental data from the literature (van den Berg et al., 2016; Van Den Berg et al., 2015) (Chapter 3).

The same approach can be extended to other similar competition scenarios, for instance, the competition between ammonia-oxidizing bacteria (AOB), archaea (AOA) and comammox microorganisms for ammonia and oxygen. As demonstrated in this study and before (Bellucci et al., 2015; Miller et al., 2005; Smith et al., 1998), the resource-ratio theory offers mechanistic insights and quantitative prediction of competition outcomes between microorganisms for shared resources. Despite its relatively easy implementation and great value, its application in the microbial competition is still limited. Apparently, there is still a gap between the research fields of microbiologists and modellers in this respect. To facilitate the application, a decision tree and a spreadsheet model were provided for the generalized scenario where two species exploitatively compete for two essential resources (Chapter 3), as is the case for denitrification and DNRA.

5.2 Fate of nitrate during biological nitrogen conversions

Nitrate can be reduced through denitrification and DNRA processes (Kraft et al., 2011). During denitrification, nitrate is sequentially converted to nitrite, NO, N₂O, and nitrogen gas and thereby leading to nitrogen removal in natural and engineered systems such

as WWTPs. N_2O , a potent greenhouse and ozone-depleting gas, can be emitted during this process, posing an increasing concern (Canfield et al., 2010). In contrast, DNRA retains nitrogen locally by converting nitrate to nitrite and further to bioavailable ammonium, which may be beneficial for natural ecosystems but unwanted for WWTPs (Van Den Berg et al., 2015). Besides, partial denitrification/DNRA (i.e., nitrate reduction to nitrite) can supply nitrite for anammox, enabling the synergy with anammox. In this thesis, the fate of nitrate was dealt with in Chapter 2 and Chapter 3.

Chapter 2 focused on nitrate produced during the anammox conversion in standalone anammox reactors fed with ammonium and nitrite (with and without acetate). The produced nitrate limits the nitrogen removal of anammox process and needs to be further polished if stringent nitrogen effluent thresholds (e.g., low effluent TN) hold. The hypothesis was that a small amount of COD in the anammox reactors could trigger nitrate reduction through denitrification and/or DNRA and thus (partly) remove the excess nitrate. This was indeed observed in the experiments (Chapter 2). At influent COD/TN ratios of 0.1 (g COD.g N^{-1}), approximately 18% of the nitrate produced from anammox conversion was reduced, and the resulting N_2O could account for 29% of the reduced nitrate (further elaborated in Section 5.2.2), indicating that nitrate was most likely reduced through denitrification.

Chapter 3 elucidated the fate of nitrate in the competition between heterotrophic denitrification and DNRA in continuous cultures. The resource-ratio theory was applied for this purpose, following its validation with experimental data in the literature. The results highlight the impact of influent COD/N ratio (g COD.g $NO_3^- \cdot N^{-1}$), resource concentrations, dilution rate (D) and microbial physiological features (i.e., stoichiometry, μ_{max} and K_S) on the competition outcome, revealing how they jointly determine competition outcomes. The DNRA process was favored at high COD/N ratio conditions while denitrification was favored at low COD/N ratio conditions, which is in agreement with the previous studies. However, the results also challenge currently prevailing perceptions in several aspects: (1) The influent COD/N ratio alone is not sufficient to explain the competition outcome of denitrification and DNRA, as the boundary values (e.g., the threshold of high COD/N ratio) change with influent resource concentrations. Different competition outcomes (also resource limitation) can occur at the same influent COD/N ratio if the influent nitrate concentration varies. (2) The impact of influent resource concentrations on boundaries and thus the competition outcomes

has great implications, as different ecosystems have various nitrate availability (Table 3.3) and therefore possibly different boundary COD/N ratios triggering their perspective pathway selection. (3) Affinity for the competing resources are often used to predict competition outcomes (Dimitri Kits et al., 2017; Straka et al., 2019b). The result demonstrated that the species with higher affinity (i.e., lower K_s) for both of the two shared resources (i.e., nitrate and COD) did not necessarily outcompete other species at low concentrations in continuous cultures, illustrating that affinity alone was not sufficient to predict the competition outcome in continuous cultures. The μ_{max} and D need to be considered as well, as expressed by the J parameter (Eq. 3.2) (Hansen and Hubbell, 1980; Hsu et al., 1981; Winkler et al., 2017). (4) In addition, the results show that the dilution rate that allows for the coexistence or outcompetition of the two competing species was not determined by the μ_{max} alone but also influenced by the K_s for one of the shared resources (i.e., nitrate). The results also provide testable hypotheses with respect to the nitrate partitioning for further research, such as the shift of the boundary influent COD/N ratios for different competition outcomes at environmentally relevant low nitrate concentrations.

In the context of wastewater treatment plants, the typical influent COD/N ratio is 8-12 (g COD.g $\text{NH}_4\text{-N}^{-1}$). Results of Chapter 3 show that DNRA could take place simultaneously with denitrification at COD/N ratios of 4.04-6.15 (g COD.g $\text{NO}_3\text{-N}^{-1}$) and completely outcompete denitrification at COD/N ratios above 6.15 (g COD.g $\text{NO}_3\text{-N}^{-1}$) at high nitrate concentrations (e.g., $> 100 \mu\text{M}$ or 1.4 mg N.L^{-1}). The nitrate concentration and COD/ $\text{NO}_3\text{-N}$ ratios can change in a wide range along the treatment line and in different streams in WWTPs. In general, partial DNRA (nitrate to nitrite) is beneficial for nitrogen removal, whereas full DNRA (nitrate to ammonium) is often unwanted. Full DNRA may occur where nitrate from the internal recirculation stream is mixed with COD-rich influent, in the bottom of secondary settler, and also some nitrate may enter the anaerobic digester. In PNA systems, the influent COD/N ratio is typically low, but full DNRA may still be possible depending on the aeration regime. If the reactor is continuously aerated, the influent COD will be aerobically oxidized and will most likely not be available for nitrate reduction. If intermittent aeration is applied, the influent COD and the small amount of nitrate produced from anammox reaction (around 10% of influent ammonium) may trigger full DNRA during the anoxic period.

Acetate was used in the competition study in Chapter 3. In reality, the nature of the organic carbon can be complex and may affect the competition outcome (Kraft et al., 2014; Rehr and Klemme, 1989; van den Berg et al., 2017a). The presence of fermentative organic carbon (e.g., lactate) may stimulate fermentative bacteria which can directly compete for both nitrate and organic carbon through fermentative DNRA process (Cole, 1996) and/or alter the organic carbon available for DNRA process (van den Berg et al., 2017a). Besides, microorganisms may have metabolic preferences towards a certain type of organic carbon (Rehr and Klemme, 1989). The composition of COD in wastewater is rather complex, including, for example, inert and slowly biodegradable fractions. The boundary COD/N ratios obtained with well-defined organic carbon may not be directly applicable in WWTPs.

DNRA bacteria can be enriched from activated sludge by simply applying high COD/N ratio feed in a chemostat (Van Den Berg et al., 2015) and coexist with denitrifiers in wastewater treatment wetlands (Jahangir et al., 2017; Rahman et al., 2019). Besides, the application of biofilm reactors (e.g., MBBR, IFAS, and Granules) is increasing, where substrate gradients can be formed within the biofilm and may thus offer the possibility to have high COD/N microenvironment for DNRA to proliferate (Van Den Berg et al., 2015). The role of the unwanted full DNRA process (nitrate reduction to ammonium and thus retains nitrogen in wastewater) in WWTPs still needs to be better characterized in the future.

5.3 Process evaluation

5.3.1 N₂O emission from anammox reactors

With 297 times stronger global warming potential than CO₂, even small amounts of N₂O emission have a substantial impact on the carbon footprint of WWTPs. The impact of influent COD (acetate) on the N₂O emission from a continuously fed bubble column granular sludge anammox reactor (Chapter 2). Results show that influent COD slightly decreased the effluent nitrate concentration of the anammox reactor at low influent COD/TN ratios (ca. 0.1 g COD.g N⁻¹), at the cost of a significant concurrent increase in N₂O emission. The average N₂O emission increased by 2.5 times ($p < 0.05$) with increasing influent COD concentration, accounting for up to 0.46% of the incoming nitrogen load, and 29% of the nitrate reduced due to acetate addition.

This study resembles the anammox reactors in two-stage PNA and/or PDA configurations. In two-stage PNA, easily biodegradable COD (e.g., acetate) is most likely removed in the partial nitrification step. Nonetheless, residual particulate biodegradable COD entering the anammox reactor can be hydrolyzed to volatile fatty acids due to long retention time in anammox reactors. In two-stage PDA system, COD (e.g., acetate) is a prerequisite for nitrite production in the partial denitrification step. The effluent of the PD step contains both nitrite and likely small amounts of residual COD, which are fed together with the ammonium-containing stream to the anammox reactor. In both cases, most likely only a small amount of VFAs can be present in anammox reactors, as is the case in the studies presented in Chapter 2.

The results in Chapter 2 suggest that further research is needed to evaluate the effect of COD on the N₂O emissions from anammox reactors in two-stage configurations, especially in the increasingly popular PDA process. Any possible improvement in feasibility for implementation or effluent quality should not be offset by increased greenhouse gas emissions. Furthermore, various strategies for N₂O mitigation in biological nitrogen removal systems have been proposed and (partly) tested in lab-scale or modelling studies. They are yet to be demonstrated in large scale applications.

5.3.2 Feasibility of mainstream anammox

5.3.2.1 Integrated HRAS-PNA system

The performance of a promising combined HRAS-PNA system was evaluated through modelling and simulations, both from the unit process level and from a plant-wide perspective (Chapter 4). Steady-state and dynamic simulations were run with the influent dataset (from BSM2) that includes typical phenomena that are observed in full-scale WWTP influent data (Gernaey et al., 2014). Overall, the results show that the integrated HRAS-PNA system (without optimization) could achieve comparable effluent quality complying with EU regulations with a significantly lower operational cost. However, both COD (in HRAS) and N removal (in PNA) were compromised at low temperatures. Influent COD/N ratios of the PNA stage (i.e., effluent COD/N ratios of the preceding HRAS stage) were shown crucial for system performance as well. Temperature is not an easily/economically manipulated variable but rather a disturbance variable in large scale applications; therefore, the COD/N ratios of HRAS effluent should be the focus for potential control strategies. This can be tackled in two

ways: 1) proactive management of COD removal in the HRAS stage; 2) reactive control in the PNA stage. N₂O emission was not included in this modelling evolution, as the quantitative dynamic prediction of N₂O emissions with models remains a challenge (Mampaey et al., 2019). Nonetheless, modelling and simulation are powerful tools to identify N₂O formation pathways for the development of mitigation strategies in specific biological nitrogen removal systems (Mampaey et al., 2019).

Concerning the HRAS stage, an increase of SRT and DO was shown to have a positive impact on COD removal (Chapter 4). Therefore, a longer SRT and/or a higher DO could be implemented in case of low temperature, at the cost of most likely a lower net energy recovery. A real-time control strategy that can adjust the SRT (e.g., via MLSS control and waste sludge flow) and/or DO (e.g., aeration intensity) in accordance with the effluent COD/N ratio would be most desirable. MLSS-based SRT control in a pilot-scale HRAS reactor failed to significantly reduce the effluent COD/N variation but managed to reduce the COD removal variation by 90% (Miller et al., 2017). Control strategies for HRAS processes are still at its infancy due to a lack of mechanistic understanding of the bioflocculation process, which is the key to COD capture. Therefore, more research is needed in this regard.

The negative impact of low temperature was also identified in several lab- and pilot-scale mainstream anammox reactors treating aerobically pretreated municipal wastewater (Laureni et al., 2016) or real HRAS stage effluent (Hoekstra et al., 2019). Nevertheless, anammox remained dominant for nitrogen removal in the PNA stage throughout the simulated evaluation period (influent COD/N=1.3-4.3 g COD.g N⁻¹, corresponding to 0.5-2.4 g bCOD.g N⁻¹, 10-20 °C) accounting for 75-95% of the nitrogen removal. In principle, the intensification of anammox activity at low temperature is needed to deal with the negative influences, which can be done through the increase of anammox bacteria population and/or activity (Cao et al., 2017; Straka et al., 2019a). Examples are bioaugmentation from sidestream PNA (Wett et al., 2013), larger size of granules (or thicker biofilm) (Vlaeminck et al., 2012; Volcke et al., 2012; Winkler et al., 2012), using faster-growing flocculent/free anammox bacteria as seeds for immobilization (Lotti et al., 2015c), building an overcapacity of anammox during summer to retain treatment capacity in winter (Lotti et al., 2015b), robust on-line control (Cao et al., 2017), and reducing diffusion limits and inhibition of anammox bacteria activity at low temperature (Laureni et al., 2019).

5.3.2.2 Moving forward

In Chapter 1, an overview of biological nitrite sources, sinks, and process combinations for anammox-based nitrogen removal was presented (Fig. 1.4 and Table 1.1). To date, studies in various scales have proven the feasibility of mainstream anammox and highlighted the remaining challenges (see reviews, Agrawal et al., 2018; Cao et al., 2017). Here, full-scale references were analysed with a few reflections.

There are currently three full-scale references where anammox contributes significantly to the nitrogen removal in the mainstream of WWTPs: 1) the Strass WWTP in Austria (Wett et al., 2015, 2013); 2) the Changi Water Reclamation Plant (WRP) in Singapore (Cao et al., 2013; Cao et al., 2016) ; and 3) a WWTP in Xi'an, China (Li et al., 2019). Interestingly, these three references perfectly demonstrated the various ways for the implementation of mainstream anammox.

The Strass WWTP uses an A/B process for mainstream treatment and DEMON (i.e., PNA) process for sidestream treatment. Mainstream PNA was achieved by applying three strategies: 1) Enrichment of anammox biomass by the installation of cyclones in the wastage of the mainstream system; 2) Bioaugmentation of AOB and anammox bacteria from the sidestream PNA reactor; and 3) Intermittent aeration regime in the mainstream aeration tanks to suppress NOB by transient anoxia (Wett et al., 2015, 2013). However, the quantitative contribution of anammox in nitrogen removal is yet to be confirmed.

With a wastewater temperature of 28-32 °C year-around in a warm climate, the Changi WRP applies step-feed activated sludge process that was not intentionally designed for mainstream PNA. Anammox-based nitrogen removal was estimated to remove 38% of the total nitrogen in the primary effluent (Cao et al., 2013; Cao et al., 2016). Short aerobic SRT (~ 2.5 days) under the high operating temperature could be the main factor in achieving stable partial nitritation (Cao et al., 2013). The enrichment of anammox bacteria may attribute to the fast growth of flocculent/free suspended cell anammox bacteria at site temperature, which allows for retention at relatively low SRTs (e.g., 3 days) (Lotti et al., 2015a).

Classical anaerobic-anoxic-oxic (AAO) process was used in the WWTP in Xi'an, upgraded by adding moving carriers into the anoxic zone to form a build-in **anoxic-**

MBBR (Li et al., 2019). Anammox bacteria were found enriched *in situ* in the anoxic biofilm during the two years operation and estimated to contribute to 15.9% of the nitrogen removal. ^{15}N -stable isotope tracing tests showed anammox could be combined with nitrate reduction by the anoxic-carrier biofilms (i.e., PDA) (Li et al., 2019).

It should be noted that anammox was not yet reported as the primary contributor in nitrogen removal (i.e., accounting for >50% of nitrogen removal) in the three full-scale cases; therefore, the author would call these cases as anammox-assisted mainstream nitrogen removal systems. These anammox-assisted mainstream systems could already bring substantial benefits (e.g., higher nitrogen removal, lower aeration cost) and can be retrofitted from existing systems (e.g., the adding carrier to the anoxic zone as in the Xi'an case). Therefore, to harness the benefits of anammox process in the mainstream (in addition to the sidestream anammox if present), operators of WWTPs may not need to wait for breakthroughs in implementing anammox-dominant mainstream anammox systems and may start applying strategies that favor anammox-based processes (be it PNA or PDA) in the mainline based on site-specific conditions.

Fundamental physiological and biochemical research into nitrogen-cycling microorganisms and their application have always progressed hand in hand— newly discovered microorganisms (e.g., anammox) led to more efficient and sustainable treatment systems and vice versa (Kuypers et al., 2018). As a powerful tool, mathematical modelling facilitates the understanding and the application of established and cutting-edge processes. The integration of engineering, microbiological and modelling insights will continue to stimulate more sustainable nitrogen removal and wastewater treatment.

Bibliography

- Agrawal, S., Seuntjens, D., Cocker, P. De, Lackner, S., Vlaeminck, S.E., 2018. Success of mainstream partial nitritation/anammox demands integration of engineering, microbiome and modeling insights. *Curr. Opin. Biotechnol.* 50, 214–221.
- Ali, M., Rathnayake, R.M.L.D., Zhang, L., Ishii, S., Kindaichi, T., Satoh, H., Toyoda, S., Yoshida, N., Okabe, S., 2016. Source identification of nitrous oxide emission pathways from a single-stage nitritation-anammox granular reactor. *Water Res.* 102, 147–157.
- Andrews, J.H., Harris, R.F., 1986. *r- and K-Selection and Microbial Ecology*. Springer, Boston, MA, pp. 99–147.
- APHA, 1998. *Standard Methods for Examination of Water and Wastewater*, 20th ed, American Public Health Association, Washington, DC.
- Arden, E., Lockett, W.T., 1914. Experiments on the oxidation of sewage without the aid of filters. *J. Soc. Chem. Ind.* 33, 523–539.
- Bader, F.G., 1978. Analysis of double-substrate limited growth. *Biotechnol. Bioeng.* 20, 183–202.
- Barnard, J., 1973. Biological Denitrification. *Water Pollut. Control* 72, 705–720.
- Barnard, J.L., Stensel, H.D., 2014. The activated sludge process in service of humanity, in: *DSD International Conference*. Hong Kong.
- Behrendt, A., Tarre, S., Beliaevski, M., Green, M., Klatt, J., de Beer, D., Stief, P., 2014. Effect of high electron donor supply on dissimilatory nitrate reduction pathways in a bioreactor for nitrate removal. *Bioresour. Technol.* 171, 291–297.
- Bellucci, M., Ofițeru, I.D., Beneduce, L., Graham, D.W., Head, I.M., Curtis, T.P., 2015. A preliminary and qualitative study of resource ratio theory to nitrifying lab-scale bioreactors. *Microb. Biotechnol.* 8, 590–603.
- Besson, M., Tiruta-Barna, L., Spérandio, M., 2017. Environmental Assessment of Anammox Process in Mainstream with WWTP Modeling Coupled to Life Cycle Assessment, in: Mannina, G. (Ed.), *Frontiers in Wastewater Treatment and Modelling: FICWTM 2017*. Springer International Publishing, pp. 392–397.
- Bisinella de Faria, A.B., Spérandio, M., Ahmadi, A., Tiruta-Barna, L., 2015. Evaluation of new alternatives in wastewater treatment plants based on dynamic modelling and life cycle assessment (DM-LCA). *Water Res.* 84, 99–111.
- Boehnke, B., Diering, B., Zuckut, S.W., 1997. Cost-effective wastewater treatment process for removal of organics and nutrients. *Water Eng. Manag.* 144, 18–21.
- Boehnke, D.B., 1977. Installation for the treatment of waste water by the activated sludge process.
- Bonin, P., 1996. Anaerobic nitrate reduction to ammonium in two strains isolated from coastal marine sediment: A dissimilatory pathway. *FEMS Microbiol. Ecol.* 19, 27–38.
- Bozileva, E., Khiewwijit, R., Temmink, H., Rijnaarts, H.H., Keesman, K.J., 2017. Exploring the Feasibility of a Novel Municipal Wastewater Treatment System via Dynamic Plant-Wide Simulation, in: Mannina, G. (Ed.), *Frontiers in Wastewater Treatment and Modelling: FICWTM 2017*. Springer International Publishing, pp. 575–582.
- Broda, E., 1977. Two kinds of lithotrophs missing in nature. *Z. Allg. Mikrobiol.* 17, 491–493.
- Burgin, A.J., Hamilton, S.K., 2007. Have we overemphasized the role of denitrification

- in aquatic ecosystems? A review of nitrate removal pathways. *Front. Ecol. Environ.* 5, 89-96.
- Buswell, A.M., Long, H.L., 1923. *Microbiology and Theory of Activated Sludge*. J. Am. Water Works Assoc. 10, 309–321.
- Canfield, D.E., Glazer, A.N., Falkowski, P.G., 2010. The evolution and future of earth's nitrogen cycle. *Science*. 330(6001), 192-196.
- Cao, S., Li, B., Du, R., Ren, N., Peng, Y., 2016. Nitrite production in a partial denitrifying upflow sludge bed (USB) reactor equipped with gas automatic circulation (GAC). *Water Res.* 90, 309–316.
- Cao, Y., Hong, K.B., Van Loosdrecht, M.C.M., Daigger, G.T., Yi, P.H., Wah, Y.L., Chye, C.S., Ghani, Y.A., 2016. Mainstream partial nitrification and anammox in a 200,000 m³/day activated sludge process in Singapore: Scale-down by using laboratory fed-batch reactor. *Water Sci. Technol.* 74, 48–56.
- Cao, Y., Kwok, B., Yong, W., Chua, S., Wah, Y., Ghani, Y.A., 2013. Mainstream Partial Nitrification–ANAMMOX Nitrogen Removal in the Largest Full- Scale Activated Sludge Process in Singapore: process analysis, In: *Proceedings of WEF/IWA Nutrient Removal and Recovery 2013: Trends in Resource Recovery and Use*. Vancouver.
- Cao, Y., van Loosdrecht, M.C.M., Daigger, G.T., 2017. Mainstream partial nitrification–anammox in municipal wastewater treatment: status, bottlenecks, and further studies. *Appl. Microbiol. Biotechnol.* 101, 1365–1383.
- Castro-Barros, C.M., Jia, M., van Loosdrecht, M.C.M., Volcke, E.I.P., Winkler, M.K.H., 2017. Evaluating the potential for dissimilatory nitrate reduction by anammox bacteria for municipal wastewater treatment. *Bioresour. Technol.* 233, 363–372.
- Cole, J., 1996. Nitrate reduction to ammonia by enteric bacteria: Redundancy, or a strategy for survival during oxygen starvation? *FEMS Microbiol. Lett.* 136, 1-11.
- Corbalá-Robles, L., Picioreanu, C., Van Loosdrecht, M.C.M., Pérez, J., 2016. Analysing the effects of the aeration pattern and residual ammonium concentration in a partial nitrification-anammox process. *Environ. Technol.* 37, 694–702.
- Costa, E., Pérez, J., Kreft, J.U., 2006. Why is metabolic labour divided in nitrification? *Trends Microbiol.* 14, 213–219.
- Daims, H., Lebedeva, E. V., Pjevac, P., Han, P., Herbold, C., Albertsen, M., Jehmlich, N., Palatinszky, M., Vierheilig, J., Bulaev, A., Kirkegaard, R.H., Von Bergen, M., Rattej, T., Bendinger, B., Nielsen, P.H., Wagner, M., 2015. Complete nitrification by *Nitrospira* bacteria. *Nature* 528, 504–509.
- Daims, H., Wagner, M., 2010. *The Microbiology of Nitrogen Removal*. *Microbiol. Act. sludge* 259–280.
- Dapena-Mora, A., Campos, J.L., Mosquera-Corral, A., Jetten, M.S.M., Méndez, R., 2004. Stability of the ANAMMOX process in a gas-lift reactor and a SBR. *J. Biotechnol.* 110, 159–170.
- De Clippeleir, H., Vlaeminck, S.E., De Wilde, F., Daeninck, K., Mosquera, M., Boeckx, P., Verstraete, W., Boon, N., 2013. One-stage partial nitrification/anammox at 15 C on pretreated sewage: Feasibility demonstration at lab-scale. *Appl. Microbiol. Biotechnol.* 97, 10199–10210.
- De Cocker, P., Bessiere, Y., Hernandez-Raquet, G., Dubos, S., Mozo, I., Gaval, G., Caligaris, M., Barillon, B., Vlaeminck, S.E., Sperandio, M., 2018. Enrichment and adaptation yield high anammox conversion rates under low temperatures. *Bioresour. Technol.* 250, 505–512.
- De Graaff, M.S., Temmink, H., Zeeman, G., van Loosdrecht, M.C.M., Buisman, C.J.N.,

2011. Autotrophic nitrogen removal from black water: Calcium addition as a requirement for settleability. *Water Res.* 45, 63–74.
- De Graaff, M.S., Van Den Brand, T.P.H., Roest, K., Zandvoort, M.H., Duin, O., Van Loosdrecht, M.C.M., 2016. Full-Scale Highly-Loaded Wastewater Treatment Processes (A-Stage) to Increase Energy Production from Wastewater: Performance and Design Guidelines. *Environ. Eng. Sci.* 33, 571–577.
- Dimitri Kits, K., Sedlacek, C.J., Lebedeva, E. V., Han, P., Bulaev, A., Pjevac, P., Daebeler, A., Romano, S., Albertsen, M., Stein, L.Y., Daims, H., Wagner, M., 2017. Kinetic analysis of a complete nitrifier reveals an oligotrophic lifestyle. *Nature* 549, 269–272.
- Dorodnikov, M., Blagodatskaya, E., Blagodatsky, S., Fangmeier, A., Kuzyakov, Y., 2009. Stimulation of r- vs. K-selected microorganisms by elevated atmospheric CO₂ depends on soil aggregate size: Research article. *FEMS Microbiol. Ecol.* 69, 43–52.
- Downing, A.L., Painter, H.A., Knowles, G., 1964. Nitrification in the activated sludge process. *J. Proc. Inst. Sew. Purif.* 63, 130–158.
- Du, R., Cao, S., Li, B., Niu, M., Wang, S., Peng, Y., 2017. Performance and microbial community analysis of a novel DEAMOX based on partial-denitrification and anammox treating ammonia and nitrate wastewaters. *Water Res.* 108, 46–56.
- Du, R., Cao, S., Peng, Y., Zhang, H., Wang, S., 2019. Combined Partial Denitrification (PD)-Anammox: A method for high nitrate wastewater treatment. *Environ. Int.* 126, 707–716.
- EC, 2018. Report on the implementation of Council Directive 91/676/EEC concerning the protection of waters against pollution caused by nitrates from agricultural sources based on Member State reports for the period 2012-2015.
- Ettwig, K.F., Butler, M.K., Le Paslier, D., Pelletier, E., Mangenot, S., Kuypers, M.M.M., Schreiber, F., Dutilh, B.E., Zedelius, J., De Beer, D., Gloerich, J., Wessels, H.J.C.T., Van Alen, T., Luesken, F., Wu, M.L., Van De Pas-Schoonen, K.T., Op Den Camp, H.J.M., Janssen-Megens, E.M., Francoijs, K.J., Stunnenberg, H., Weissenbach, J., Jetten, M.S.M., Strous, M., 2010. Nitrite-driven anaerobic methane oxidation by oxygenic bacteria. *Nature* 464, 543–548.
- Fernández-Arévalo, T., Lizarralde, I., Fdz-Polanco, F., Pérez-Elvira, S.I., Garrido, J.M., Puig, S., Poch, M., Grau, P., Ayesa, E., 2017. Quantitative assessment of energy and resource recovery in wastewater treatment plants based on plant-wide simulations. *Water Res.* 118, 272–288.
- Fortney, J.L., Mehlhorn, T.L., Lowe, K.A., Earles, J.E., Phillips, J., Techtmann, S.M., Joyner, D.C., Elias, D.A., Bailey, K.L., Hurt, R.A., Preheim, S.P., Sanders, M.C., Yang, J., Mueller, M.A., Brooks, S., Watson, D.B., Zhang, P., He, Z., Dubinsky, E.A., Adams, P.D., Arkin, A.P., Fields, M.W., Zhou, J., Alm, E.J., Hazen, T.C., 2015. Natural Bacterial Communities Serve as Quantitative Geochemical Biosensors. *MBio* 6, 1–13.
- Freitag, A., Rudert, M., Bock, E., 1987. Growth of *Nitrobacter* by dissimilatory nitrate reduction. *FEMS Microbiol. Lett.* 48, 105–109.
- Gerardi, M.H., 2005. Nitrification in the Activated Sludge Process. *Water Encycl.* 130–258.
- Gernaey, K. V., Jeppsson, U., Vanrolleghem, P.A., Copp, J.B., 2014. Benchmarking of Control Strategies for Wastewater Treatment Plants, *Water Intelligence Online*. IWA Publishing, London, UK.
- Giblin, A.E., Tobias, C.R., Song, B., Weston, N., Banta, G.T., Rivera-Monroy, V.H., 2013. The importance of dissimilatory nitrate reduction to ammonium (DNRA) in

- the nitrogen cycle of coastal ecosystems. *Oceanography* 26, 124–131.
- Gujer, W., 2010. Nitrification and me - A subjective review. *Water Res.* 44, 1-19.
- Guo, J., Peng, Y., Fan, L., Zhang, L., Ni, B.J., Kartal, B., Feng, X., Jetten, M.S.M., Yuan, Z., 2016. Metagenomic analysis of anammox communities in three different microbial aggregates. *Environ. Microbiol.* 18, 2979–2993.
- Güven, D., Dapena, A., Kartal, B., Schmid, M.C., Maas, B., Van De Pas-Schoonen, K., Sozen, S., Mendez, R., Op Den Camp, H.J.M., Jetten, M.S.M., Strous, M., Schmidt, I., 2005. Propionate oxidation by and methanol inhibition of anaerobic ammonium-oxidizing bacteria. *Appl. Environ. Microbiol.* 71, 1066–1071.
- Haider, S., Svardal, K., Vanrolleghem, P.A., Kroiss, H., 2003. The effect of low sludge age on wastewater fractionation (SS, SI). *Water Sci. Technol.* 47, 203–209.
- Han, M., De Clippeleir, H., Al-Omari, A., Wett, B., Vlaeminck, S.E., Bott, C., Murthy, S., 2016a. Impact of carbon to nitrogen ratio and aeration regime on mainstream deammonification. *Water Sci. Technol.* 74, 375–384.
- Han, M., Vlaeminck, S.E., Al-Omari, A., Wett, B., Bott, C., Murthy, S., De Clippeleir, H., 2016b. Uncoupling the solids retention times of flocs and granules in mainstream deammonification: A screen as effective out-selection tool for nitrite oxidizing bacteria. *Bioresour. Technol.* 221, 195–204.
- Hansen, S.R., Hubbell, S.P., 1980. Single-nutrient microbial competition: Qualitative agreement between experimental and theoretically forecast outcomes. *Science* (80-). 207, 1491–1493.
- Hao, X. Di, van Loosdrecht, M.C.M., 2004. Model-based evaluation of COD influence on a partial nitrification-Anammox biofilm (CANON) process. *Water Sci. Technol.* 49, 83–90.
- Hao, X., Heijnen, J.J., Van Loosdrecht, M.C.M., 2002a. Sensitivity analysis of a biofilm model describing a one-stage completely autotrophic nitrogen removal (CANON) process. *Biotechnol. Bioeng.* 77, 266–277.
- Hao, X., Heijnen, J.J., Van Loosdrecht, M.C.M., 2002b. Model-based evaluation of temperature and inflow variations on a partial nitrification-ANAMMOX biofilm process. *Water Res.* 36, 4839–4849.
- Heijnen, J.J., 1999. Bioenergetics of microbial growth. *Encycl. Bioprocess Technol. Ferment. Biocatal. Biosep.* 267–291.
- Hellinga, C., Schellen, A.A.J.C., Mulder, J.W., Van Loosdrecht, M.C.M., Heijnen, J.J., 1998. The SHARON process: An innovative method for nitrogen removal from ammonium-rich waste water. *Water Sci. Technol.* 37, 135-142.
- Hellinga, C., van Loosdrecht, M.C.M., Heijnen, J.J., 1999. Model Based Design of a Novel Process for Nitrogen Removal from Concentrated Flows. *Math. Comput. Model. Dyn. Syst.* 5, 351–371.
- Henze, M., Gujer, W., Mino, T., 1999. Activated sludge model asm2d. *Water Sci. Technol.* 39, 165–182.
- Henze, M., Gujer, W., Mino, T., Van Loosedrecht, M., 2000. Activated sludge models ASM1, ASM2, ASM2d and ASM3. IWA Pub. London, UK.
- Henze, M., van Loosdrecht, M.C.M., Ekama, G.A., Brdjanovic, D., 2015. *Biological Wastewater Treatment: Principles, Modelling and Design*, Water Intelligence Online. IWA Pub. London, UK.
- Hoekstra, M., Geilvoet, S.P., Hendrickx, T.L.G., van Erp Taalman Kip, C.S., Kleerebezem, R., van Loosdrecht, M.C.M., 2019. Towards mainstream anammox: lessons learned from pilot-scale research at WWTP Dokhaven. *Environ. Technol.* 40, 1721–1733.
- Hsu, S.-B., Cheng, K.-S., Hubbell, S.P., 1981. Exploitative Competition of

- Microorganisms for Two Complementary Nutrients in Continuous Cultures. *SIAM J. Appl. Math.* 41, 422–444.
- Hsu, S.B., Hubbell, S., Waltman, P., 1977. A Mathematical Theory for Single-Nutrient Competition in Continuous Cultures of Micro-Organisms. *SIAM J. Appl. Math.* 32, 366–383.
- Hubaux, N., Wells, G., Morgenroth, E., 2015. Impact of coexistence of flocs and biofilm on performance of combined nitrification-anammox granular sludge reactors. *Water Res.* 68, 127–139.
- IPCC, 2014: Climate Change 2014: Synthesis Report. Contribution of Working Groups I, II and III to the Fifth Assessment Report of the Intergovernmental Panel on Climate Change [Core Writing Team, R.K. Pachauri and L.A. Meyer (eds.)]. IPCC, Geneva, Switzerland, 151 pp.
- Jahangir, M.M.R., Fenton, O., Müller, C., Harrington, R., Johnston, P., Richards, K.G., 2017. In situ denitrification and DNRA rates in groundwater beneath an integrated constructed wetland. *Water Res.* 111, 254–264.
- Jenni, S., Vlaeminck, S.E., Morgenroth, E., Udert, K.M., 2014. Successful application of nitrification/anammox to wastewater with elevated organic carbon to ammonia ratios. *Water Res.* 49, 316–326.
- Jetten, M.S.M., Horn, S.J., Van Loosdrecht, M.C.M., 1997. Towards a more sustainable municipal wastewater treatment system. *Water Sci. Technol.* 35, 171–180.
- Jia, M., Castro-Barros, C.M., Winkler, M.K.H., Volcke, E.I.P., 2018. Effect of organic matter on the performance and N₂O emission of a granular sludge anammox reactor. *Environ. Sci. Water Res. Technol.* 4, 1035–1046.
- Jimenez, J., Miller, M., Bott, C., Murthy, S., De Clippeleir, H., Wett, B., 2015. High-rate activated sludge system for carbon management - Evaluation of crucial process mechanisms and design parameters. *Water Res.* 87, 476–482.
- Jimenez, J.A., La Motta, E.J., Parker, D.S., 2005. Kinetics of Removal of Particulate Chemical Oxygen Demand in the Activated-Sludge Process. *Water Environ. Res.* 77, 437–446.
- Joss, A., Derlon, N., Cyprien, C., Burger, S., Szivak, I., Traber, J., Siegrist, H., Morgenroth, E., 2011. Combined nitrification-anammox: Advances in understanding process stability. *Environ. Sci. Technol.* 45, 9735–9742.
- Kalyuzhnyi, S., Gladchenko, M., Mulder, A., Versprille, B., 2006. DEAMOX-New biological nitrogen removal process based on anaerobic ammonia oxidation coupled to sulphide-driven conversion of nitrate into nitrite. *Water Res.* 40, 3637–3645.
- Kampschreur, M.J., Temmink, H., Kleerebezem, R., Jetten, M.S.M., van Loosdrecht, M.C.M., 2009. Nitrous oxide emission during wastewater treatment, *Water Res.* 43, 4093–4103.
- Kampschreur, M.J., van der Star, W.R.L., Wielders, H.A., Mulder, J.W., Jetten, M.S.M., van Loosdrecht, M.C.M., 2008. Dynamics of nitric oxide and nitrous oxide emission during full-scale reject water treatment. *Water Res.* 42, 812–826.
- Kartal, B., Kuenen, J.G., Van Loosdrecht, M.C.M., 2010. Sewage treatment with anammox. *Science.* 328, 702–703.
- Kartal, B., Kuypers, M.M.M., Lavik, G., Schalk, J., Op Den Camp, H.J.M., Jetten, M.S.M., Strous, M., 2007. Anammox bacteria disguised as denitrifiers: Nitrate reduction to dinitrogen gas via nitrite and ammonium. *Environ. Microbiol.* 9, 635–642.
- Kartal, B., van Niftrik, L., Keltjens, J.T., Op den Camp, H.J.M., Jetten, M.S.M., 2012.

- Anammox-Growth Physiology, Cell Biology, and Metabolism. *Adv. Microb. Physiol.* 60, 211–262.
- Khiewwijit, R., Temmink, H., Rijnaarts, H., Keesman, K.J., 2015. Energy and nutrient recovery for municipal wastewater treatment: How to design a feasible plant layout? *Environ. Model. Softw.* 68, 156–165.
- Kleerebezem, R., Joosse, B., Rozendal, R., Van Loosdrecht, M.C.M., 2015. Anaerobic digestion without biogas? *Rev. Environ. Sci. Biotechnol.* 14, 787–801.
- Kleerebezem, R., Van Loosdrecht, M.C.M., 2010. A generalized method for thermodynamic state analysis of environmental systems. *Crit. Rev. Environ. Sci. Technol.* 40, 1–54.
- Kobayashi, S., Inaba, K., Kimura, I., Kimura, M., 1998. Inhibitory effects of tetrandrine on angiogenesis in adjuvant-induced chronic inflammation and tube formation of vascular endothelial cells. *Biol. Pharm. Bull.* 21, 346–349.
- Könneke, M., Bernhard, A.E., De La Torre, J.R., Walker, C.B., Waterbury, J.B., Stahl, D.A., 2005. Isolation of an autotrophic ammonia-oxidizing marine archaeon. *Nature* 437, 543–546.
- Kovárová-Kovar, K., Egli, T., 1998. Growth kinetics of suspended microbial cells: from single-substrate-controlled growth to mixed-substrate kinetics. *Microbiol. Mol. Biol. Rev.* 62, 646–66.
- Kraft, B., Strous, M., Tegetmeyer, H.E., 2011. Microbial nitrate respiration - Genes, enzymes and environmental distribution. *J. Biotechnol.* 155, 104–117.
- Kraft, B., Tegetmeyer, H.E., Sharma, R., Klotz, M.G., Ferdelman, T.G., Hettich, R.L., Geelhoed, J.S., Strous, M., 2014. The environmental controls that govern the end product of bacterial nitrate respiration. *Science* 345, 676–679.
- Kuai, L., Verstraete, W., 1998. Ammonium removal by the oxygen-limited autotrophic nitrification- denitrification system. *Appl. Environ. Microbiol.* 64, 4500–4506.
- Kuenen, J.G., Johnson, O.J., 2009. Continuous Cultures (Chemostats), *Encyclopedia of Microbiology*. Elsevier Inc.
- Kumar, M., Lin, J.G., 2010. Co-existence of anammox and denitrification for simultaneous nitrogen and carbon removal-Strategies and issues. *J. Hazard. Mater.* 178, 1-9.
- Kuypers, M.M.M., Marchant, H.K., Kartal, B., 2018. The microbial nitrogen-cycling network, *Nature Reviews Microbiology.* 16, 263-276.
- Lackner, S., Gilbert, E.M., Vlaeminck, S.E., Joss, A., Horn, H., van Loosdrecht, M.C.M., 2014. Full-scale partial nitritation/anammox experiences - An application survey. *Water Res.* 55, 292–303.
- Lam, P., Kuypers, M.M.M., 2011. Microbial Nitrogen Cycling Processes in Oxygen Minimum Zones. *Ann. Rev. Mar. Sci.* 3, 317–345.
- Lam, P., Lavik, G., Jensen, M.M., Van Vossenberg, J. De, Schmid, M., Woebken, D., Gutiérrez, D., Amann, R., Jetten, M.S.M., Kuypers, M.M.M., 2009. Revising the nitrogen cycle in the Peruvian oxygen minimum zone. *Proc. Natl. Acad. Sci. U. S. A.* 106, 4752–4757.
- Laureni, M., Falås, P., Robin, O., Wick, A., Weissbrodt, D.G., Nielsen, J.L., Ternes, T.A., Morgenroth, E., Joss, A., 2016. Mainstream partial nitritation and anammox: Long-term process stability and effluent quality at low temperatures. *Water Res.* 101, 628–639.
- Laureni, M., Weissbrodt, D.G., Szivák, I., Robin, O., Nielsen, J.L., Morgenroth, E., Joss, A., 2015. Activity and growth of anammox biomass on aerobically pre-treated municipal wastewater. *Water Res.* 80, 325–336.
- Laureni, M., Weissbrodt, D.G., Villez, K., Robin, O., de Jonge, N., Rosenthal, A., Wells,

- G., Nielsen, J.L., Morgenroth, E., Joss, A., 2019. Biomass segregation between biofilm and flocs improves the control of nitrite-oxidizing bacteria in mainstream partial nitritation and anammox processes. *Water Res.* 154, 104–116.
- Law, Y., Ye, L., Pan, Y., Yuan, Z., 2012. Nitrous oxide emissions from wastewater treatment processes. *Philos. Trans. R. Soc. B Biol. Sci.* 367, 1265–1277.
- Le, T., Peng, B., Su, C., Massoudieh, A., Torrents, A., Al-Omari, A., Murthy, S., Wett, B., Chandran, K., deBarbadillo, C., Bott, C., De Clippeleir, H., 2019. Nitrate residual as a key parameter to efficiently control partial denitrification coupling with anammox. *Water Environ. Res.* 1140.
- León, J.A., Tumpson, D.B., 1975. Competition between two species for two complementary or substitutable resources. *J. Theor. Biol.* 50, 185–201.
- Li, J., Peng, Y., Zhang, L., Liu, J., Wang, X., Gao, R., Pang, L., Zhou, Y., 2019. Quantify the contribution of anammox for enhanced nitrogen removal through metagenomic analysis and mass balance in an anoxic moving bed biofilm reactor. *Water Res.* 160, 178–187.
- Li, K., Fang, F., Wang, H., Wang, C., Chen, Y., Guo, J., Wang, X., Jiang, F., 2017. Pathways of N removal and N₂O emission from a one-stage autotrophic N removal process under anaerobic conditions. *Sci. Rep.* 7, 42072.
- Liu, T., Ma, B., Chen, X., Ni, B.-J., Peng, Y., Guo, J., 2017. Evaluation of mainstream nitrogen removal by simultaneous partial nitrification, anammox and denitrification (SNAD) process in a granule-based reactor. *Chem. Eng. J.* 327, 973–981.
- Loder, T.C., Ganning, B., Love, J.A., 1996. Ammonia nitrogen dynamics in coastal rockpools affected by gull guano. *J. Exp. Mar. Bio. Ecol.* 196, 113–129.
- López, H., Puig, S., Ganigué, R., Rusalleda, M., Balaguer, M.D., Colprim, J., 2008. Start-up and enrichment of a granular anammox SBR to treat high nitrogen load wastewaters. *J. Chem. Technol. Biotechnol.* 83, 233–241.
- Lotti, T., Kleerebezem, R., Abelleira-Pereira, J.M., Abbas, B., van Loosdrecht, M.C.M., 2015a. Faster through training: The anammox case. *Water Res.* 81, 261–268.
- Lotti, T., Kleerebezem, R., Hu, Z., Kartal, B., De Kreuk, M.K., Van Erp Taalman Kip, C., Kruit, J., Hendrickx, T.L.G., Van Loosdrecht, M.C.M., 2015b. Pilot-scale evaluation of anammox-based mainstream nitrogen removal from municipal wastewater. *Environ. Technol.* 36, 1167–1177.
- Lotti, T., Kleerebezem, R., Hu, Z., Kartal, B., Jetten, M.S.M., van Loosdrecht, M.C.M., 2014a. Simultaneous partial nitritation and anammox at low temperature with granular sludge. *Water Res.* 66, 111–121.
- Lotti, T., Kleerebezem, R., Lubello, C., van Loosdrecht, M.C.M., 2014b. Physiological and kinetic characterization of a suspended cell anammox culture. *Water Res.* 60, 1–14.
- Lotti, T., Kleerebezem, R., van Loosdrecht, M.C.M., 2015c. Effect of temperature change on anammox activity. *Biotechnol. Bioeng.* 112, 98–103.
- Ma, B., Qian, W., Yuan, C., Yuan, Z., Peng, Y., 2017. Achieving Mainstream Nitrogen Removal through Coupling Anammox with Denitrification. *Environ. Sci. Technol.* 51, 8405–8413.
- Ma, B., Zhang, S., Zhang, L., Yi, P., Wang, J., Wang, S., Peng, Y., 2011. The feasibility of using a two-stage autotrophic nitrogen removal process to treat sewage. *Bioresour. Technol.* 102, 8331–8334.
- Mampaey, K.E., De Kreuk, M.K., van Dongen, U.G.J.M., van Loosdrecht, M.C.M., Volcke, E.I.P., 2016. Identifying N₂O formation and emissions from a full-scale partial nitritation reactor. *Water Res.* 88, 575–585.
- Mampaey, K.E., Spérandio, M., van Loosdrecht, M.C.M., Volcke, E.I.P., 2019.

- Dynamic simulation of N₂O emissions from a full-scale partial nitrification reactor. *Biochem. Eng. J.* 107356.
- Massara, T.M., Malamis, S., Guisasola, A., Baeza, J.A., Noutsopoulos, C., Katsou, E., 2017. A review on nitrous oxide (N₂O) emissions during biological nutrient removal from municipal wastewater and sludge reject water. *Sci. Total Environ.* 596–597, 106–123.
- McCarty, P.L., 1975. Stoichiometry of Biological Reactions. *Prog Water Technol* 7, 157–172.
- McCarty, P.L., Bae, J., Kim, J., 2011. Domestic wastewater treatment as a net energy producer-can this be achieved? *Environ. Sci. Technol.* 45, 7100–7106.
- Meerburg, F.A., Boon, N., Van Winckel, T., Vercamer, J.A.R., Nopens, I., Vlaeminck, S.E., 2015. Toward energy-neutral wastewater treatment: A high-rate contact stabilization process to maximally recover sewage organics. *Bioresour. Technol.* 179, 373–381.
- Miller, M.W., Elliott, M., DeArmond, J., Kinyua, M., Wett, B., Murthy, S., Bott, C.B., 2017. Controlling the COD removal of an A-stage pilot study with instrumentation and automatic process control. *Water Sci. Technol.* 75, 2669–2679.
- Miller, T.E., Burns, J.H., Munguia, P., Walters, E.L., Kneitel, J.M., Richards, P.M., Mouquet, N., Buckley, H.L., 2005. A critical review of twenty years' use of the resource-ratio theory. *Am. Nat.* 165, 439–448.
- Monod, J., 1950. La technique de culture continue: theorie et applications. *Ann Inst Pasteur* 390–410.
- Mozumder, M.S.I., Picioreanu, C., Van Loosdrecht, M.C.M., Volcke, E.I.P., 2014. Effect of heterotrophic growth on autotrophic nitrogen removal in a granular sludge reactor. *Environ. Technol. (United Kingdom)* 35, 1027–1037.
- Mulder, A., van de Graaf, A.A., Robertson, L.A., Kuenen, J.G., 1995. Anaerobic ammonium oxidation discovered in a denitrifying fluidized bed reactor. *FEMS Microbiol. Ecol.* 16, 177–183.
- Muller, A., Wentzel, M.C., Loewenthal, R.E., Ekama, G.A., 2003. Heterotroph anoxic yield in anoxic aerobic activated sludge systems treating municipal wastewater. *Water Res.* 37, 2435–2441.
- Münch, E. V., Lant, P., Keller, J., 1996. Simultaneous nitrification and denitrification in bench-scale sequencing batch reactors. *Water Res.* 30, 277–284.
- Muscarella, M.E., Boot, C.M., Broeckling, C.D., Lennon, J.T., 2019. Resource heterogeneity structures aquatic bacterial communities. *ISME J.*
- Ni, B.J., Rusalleda, M., Smets, B.F., 2012. Evaluation on the microbial interactions of anaerobic ammonium oxidizers and heterotrophs in Anammox biofilm. *Water Res.* 46, 4645–4652.
- Nielsen, M., Bollmann, A., Sliemers, O., Jetten, M., Schmid, M., Strous, M., Schmidt, I., Larsen, L.H., Nielsen, L.P., Revsbech, N.P., 2005. Kinetics, diffusional limitation and microscale distribution of chemistry and organisms in a CANON reactor. *FEMS Microbiol. Ecol.* 51, 247–256.
- Nogaj, T., Randall, A., Jimenez, J., Takacs, I., Bott, C., Miller, M., Murthy, S., Wett, B., 2015. Modeling of organic substrate transformation in the high-rate activated sludge process. *Water Sci. Technol.* 71, 971–979.
- Novick, A., Szilard, L., 1950. Description of the chemostat. *Science* 112, 715–6.
- Okabe, S., Oshiki, M., Takahashi, Y., Satoh, H., 2011. N₂O emission from a partial nitrification-anammox process and identification of a key biological process of N₂O emission from anammox granules. *Water Res.* 45, 6461–6470.
- Oshiki, M., Ishii, S., Yoshida, K., Fujii, N., Ishiguro, M., Satoh, H., Okabe, S., 2013.

- Nitrate-dependent ferrous iron oxidation by anaerobic ammonium oxidation (anammox) bacteria. *Appl. Environ. Microbiol.* 79, 4087–4093.
- Pan, Y., Ni, B.J., Liu, Y., Guo, J., 2016. Modeling of the interaction among aerobic ammonium-oxidizing archaea/bacteria and anaerobic ammonium-oxidizing bacteria. *Chem. Eng. Sci.* 150, 35–40.
- Pellegrini, T.G., Ferreira, R.L., 2013. Structure and interactions in a cave guano-soil continuum community. *Eur. J. Soil Biol.* 57, 19–26.
- Pérez, J., Isanta, E., Carrera, J., 2015. Would a two-stage N-removal be a suitable technology to implement at full scale the use of anammox for sewage treatment? *Water Sci. Technol.* 72, 858–864.
- Pérez, J., Lotti, T., Kleerebezem, R., Picioreanu, C., van Loosdrecht, M.C.M., 2014. Outcompeting nitrite-oxidizing bacteria in single-stage nitrogen removal in sewage treatment plants: A model-based study. *Water Res.* 66, 208–218.
- Picioreanu, C., Van Loosdrecht, M.C.M., Heijnen, J.J., 1997. Modelling the effect of oxygen concentration on nitrite accumulation in a biofilm airlift suspension reactor, *Water Sci. Technol.* 36, 147-156.
- Pretel, R., Robles, A., Ruano, M. V., Seco, A., Ferrer, J., 2016. A plant-wide energy model for wastewater treatment plants: application to anaerobic membrane bioreactor technology. *Environ. Technol. (United Kingdom)* 37, 2298–2315.
- Puyol, D., Carvajal-Arroyo, J.M., Garcia, B., Sierra-Alvarez, R., Field, J.A., 2013. Kinetic characterization of *Brocadia* spp.-dominated anammox cultures. *Bioresour. Technol.* 139, 94–100.
- Rahman, M.M., Roberts, K.L., Grace, M.R., Kessler, A.J., Cook, P.L.M., 2019. Role of organic carbon, nitrate and ferrous iron on the partitioning between denitrification and DNRA in constructed stormwater urban wetlands. *Sci. Total Environ.* 666, 608–617.
- Ravishankara, A.R., Daniel, J.S., Portmann, R.W., 2009. Nitrous oxide (N₂O): The dominant ozone-depleting substance emitted in the 21st century. *Science.* 326, 123–125.
- Regmi, P., Miller, M.W., Holgate, B., Bunce, R., Park, H., Chandran, K., Wett, B., Murthy, S., Bott, C.B., 2014. Control of aeration, aerobic SRT and COD input for mainstream nitrification/denitrification. *Water Res.* 57, 162–171.
- Rehr, B., Klemme, J.H., 1989. Competition for nitrate between denitrifying *Pseudomonas stutzeri* and nitrate ammonifying enterobacteria. *FEMS Microbiol. Lett.* 62, 51–57.
- Reichert, P., 1994. Aquasim - A tool for simulation and data analysis of aquatic systems. *Water Sci. Technol.* 30, 21–30.
- Rittmann, B.E., McCarty, P.L., 2001. *Environmental biotechnology: principles and applications.* McGraw-Hill Book Co., New York.
- Robertson, L.A., Kuenen, J.G., 1990. Combined heterotrophic nitrification and aerobic denitrification in *Thiosphaera pantotropha* and other bacteria. *Antonie Van Leeuwenhoek* 57, 139–152.
- Roots, P., Wang, Y., Rosenthal, A.F., Griffin, J.S., Sabba, F., Petrovich, M., Yang, F., Kozak, J.A., Zhang, H., Wells, G.F., 2019. Comammox Nitrospira are the dominant ammonia oxidizers in a mainstream low dissolved oxygen nitrification reactor. *Water Res.* 157, 396–405.
- Rütting, T., Boeckx, P., Müller, C., Klemedtsson, L., 2011. Assessment of the importance of dissimilatory nitrate reduction to ammonium for the terrestrial nitrogen cycle. *Biogeosciences* 8, 1779–1791.
- Schaubroeck, T., De Clippeleir, H., Weissenbacher, N., Dewulf, J., Boeckx, P.,

- Vlaeminck, S.E., Wett, B., 2015. Environmental sustainability of an energy self-sufficient sewage treatment plant: Improvements through DEMON and co-digestion. *Water Res.* 74, 166–179.
- Schielke-Jenni, S., Villez, K., Morgenroth, E., Udert, K.M., 2015. Observability of anammox activity in single-stage nitritation/anammox reactors using mass balances. *Environ. Sci. Water Res. Technol.* 1, 523–534.
- Shu, D., He, Y., Yue, H., Zhu, L., Wang, Q., 2015. Metagenomic insights into the effects of volatile fatty acids on microbial community structures and functional genes in organotrophic anammox process. *Bioresour. Technol.* 196, 621–633.
- Siegrist, H., Salzgeber, D., Eugster, J., Joss, A., 2008. Anammox brings WWTP closer to energy autarky due to increased biogas production and reduced aeration energy for N-removal. *Water Sci. Technol.* 57, 383–388.
- Sliekers, A.O., Third, K.A., Abma, W., Kuenen, J.G., Jetten, M.S.M., 2003. CANON and Anammox in a gas-lift reactor. *FEMS Microbiol. Lett.* 218, 339–344.
- Smith, V.H., Graham, D.W., Cleland, D.D., 1998. Application of resource-ratio theory to hydrocarbon biodegradation. *Environ. Sci. Technol.* 32, 3386–3395.
- Smitshuijzen, J., Pérez, J., Duin, O., Loosdrecht, M.C.M. van., 2016. A simple model to describe the performance of highly-loaded aerobic COD removal reactors. *Biochem. Eng. J.* 112, 94–102.
- Solon, K., Volcke, E.I.P., Spérandio, M., Van Loosdrecht, M.C.M., 2019. Resource recovery and wastewater treatment modelling. *Environ. Sci. Water Res. Technol.* 5, 631–642.
- Sotta, E.D., Corre, M.D., Veldkamp, E., 2008. Differing N status and N retention processes of soils under old-growth lowland forest in Eastern Amazonia, Caxiuanã, Brazil. *Soil Biol. Biochem.* 40, 740–750.
- Spalding, R.F., Exner, M.E., 1993. Occurrence of nitrate in groundwater - A review. *J. Environ. Qual.* 22, 392–402.
- Straka, L.L., Summers, A., Stahl, D.A., Winkler, M.K.H., 2019a. Kinetic implication of moving warm side-stream Anaerobic ammonium oxidizing bacteria to cold mainstream wastewater. *Bioresour. Technol.* 288, 121534.
- Straka, L.L., Meinhardt, K.A., Bollmann, A., Stahl, D.A., Winkler, M.K.H., 2019b. Affinity informs environmental cooperation between ammonia-oxidizing archaea (AOA) and anaerobic ammonia-oxidizing (Anammox) bacteria. *ISME J.*
- Strohm, T.O., Griffin, B., Zumft, W.G., Schink, B., 2007. Growth yields in bacterial denitrification and nitrate ammonification. *Appl. Environ. Microbiol.* 73, 1420–1424.
- Strous, M., Heijnen, J.J., Kuenen, J.G., Jetten, M.S.M., 1998. The sequencing batch reactor as a powerful tool for the study of slowly growing anaerobic ammonium-oxidizing microorganisms. *Appl. Microbiol. Biotechnol.* 50, 589–596.
- Strous, M., Pelletier, E., Mangenot, S., Rattei, T., Lehner, A., Taylor, M.W., Horn, M., Daims, H., Bartol-Mavel, D., Wincker, P., Barbe, V., Fonknechten, N., Vallenet, D., Segurens, B., Schenowitz-Truong, C., Medigue, C., Collingro, A., Snel, B., Dutilh, B.E., Op den Camp, H.J., van der Drift, C., Cirpus, I., van de Pas-Schoonen, K.T., Harhangi, H.R., van Niftrik, L., Schmid, M., Keltjens, J., van de Vossenberg, J., Kartal, B., Meier, H., Frishman, D., Huynen, M.A., Mewes, H.W., Weissenbach, J., Jetten, M.S., Wagner, M., Le Paslier, D., 2006. Deciphering the evolution and metabolism of an anammox bacterium from a community genome. *Nature* 440, 790–794.
- Tang, C.J., Zheng, P., Wang, C.H., Mahmood, Q., Zhang, J.Q., Chen, X.G., Zhang, L., Chen, J.W., 2011. Performance of high-loaded ANAMMOX UASB reactors containing granular sludge. *Water Res.* 45, 135–144.

- Tao, Y., Huang, X., Gao, D., Wang, X., Chen, C., Liang, H., van Loosdrecht, M.C.M., 2019. NanoSIMS reveals unusual enrichment of acetate and propionate by an anammox consortium dominated by *Jettenia asiatica*. *Water Res.* 223–232.
- Tiedje, J.M., 1988. Ecology of denitrification and dissimilatory nitrate reduction to ammonium, in: Zehnder, A.J.B. (Ed.), *Environmental Microbiology of Anaerobes*. John Wiley Sons, New York, pp. 179–244.
- Tilman, D., 1980. Resources: A Graphical-Mechanistic Approach to Competition and Predation. *Am. Nat.* 116, 362–393.
- Tilman, D., 1977. Resource Competition between Plankton Algae: An Experimental and Theoretical Approach. *Ecology* 58, 338–348.
- Tilman, D., 1976. Ecological Competition Between Algae : Experimental Confirmation of Resource-Based Competition Theory. *Science* (80-.). 192, 463–465.
- Van De Graaf, A.A., De Bruijn, P., Robertson, L.A., Jetten, M.S.M., Kuenen, J.G., 1996. Autotrophic growth of anaerobic ammonium-oxidizing micro-organisms in a fluidized bed reactor. *Microbiology* 142, 2187–2196.
- van den Berg, E.M., Boleij, M., Kuenen, J.G., Kleerebezem, R., van Loosdrecht, M.C.M., 2016. DNRA and denitrification coexist over a broad range of acetate/N-NO₃⁻ ratios, in a chemostat enrichment culture. *Front. Microbiol.* 7, 1–12.
- van den Berg, E.M., Elisário, M.P., Kuenen, J.G., Kleerebezem, R., van Loosdrecht, M.C.M., 2017a. Fermentative bacteria influence the competition between denitrifiers and DNRA bacteria. *Front. Microbiol.* 8, 1684.
- van den Berg, E.M., Rombouts, J.L., Kuenen, J.G., Kleerebezem, R., van Loosdrecht, M.C.M., 2017b. Role of nitrite in the competition between denitrification and DNRA in a chemostat enrichment culture. *AMB Express* 7, 91.
- Van den Berg, E.M., Van Dongen, U., Abbas, B., Van Loosdrecht, M.C.M., 2015. Enrichment of DNRA bacteria in a continuous culture. *ISME J.* 9, 2153–2161.
- van der Star, W.R.L., Abma, W.R., Blommers, D., Mulder, J.W., Tokutomi, T., Strous, M., Picioreanu, C., van Loosdrecht, M.C.M., 2007. Startup of reactors for anoxic ammonium oxidation: Experiences from the first full-scale anammox reactor in Rotterdam. *Water Res.* 41, 4149–4163.
- Van Der Star, W.R.L., Miclea, A.I., Van Dongen, U.G.J.M., Muyzer, G., Picioreanu, C., Van Loosdrecht, M.C.M., 2008. The membrane bioreactor: A novel tool to grow anammox bacteria as free cells. *Biotechnol. Bioeng.* 101, 286–294.
- Van Dongen, U., Jetten, M.S.M., Van Loosdrecht, M.C.M., 2001. The SHARON®-Anammox® process for treatment of ammonium rich wastewater. *Water Sci. Technol.* 44, 153–160.
- Van Kessel, M.A.H.J., Speth, D.R., Albertsen, M., Nielsen, P.H., Op Den Camp, H.J.M., Kartal, B., Jetten, M.S.M., Lücker, S., 2015. Complete nitrification by a single microorganism. *Nature* 528, 555–559.
- Veldkamp, H., Kuenen, J.G., 1973. The Chemostat as a Model System for Ecological Studies. *Bull. Ecol. Res. Comm.* 17, 347–355.
- Verstraete, W., Vlaeminck, S.E., 2011. ZeroWasteWater: Short-cycling of wastewater resources for sustainable cities of the future. *Int. J. Sustain. Dev. World Ecol.* 18, 253–264.
- Vlaeminck, S.E., De Clippeleir, H., Verstraete, W., 2012. Microbial resource management of one-stage partial nitrification/anammox. *Microb. Biotechnol.* 5, 433–448.
- Vlaeminck, S.E., Terada, A., Smets, B.F., De Clippeleir, H., Schaubroeck, T., Bolea, S., Demeestere, L., Mast, J., Boon, N., Carballa, M., Verstraete, W., 2010. Aggregate size and architecture determine microbial activity balance for one-stage

- partial nitrification and anammox. *Appl. Environ. Microbiol.* 76, 900–909.
- Volcke, E.I.P., Gernaey, K. V., Vrecko, D., Jeppsson, U., Van Loosdrecht, M.C.M., Vanrolleghem, P.A., 2006. Plant-wide (BSM2) evaluation of reject water treatment with a SHARON-anammox process. *Water Sci. Technol.* 54, 93–100.
- Volcke, E.I.P., Loccufier, M., Vanrolleghem, P.A., Noldus, E.J.L., 2006. Existence, uniqueness and stability of the equilibrium points of a SHARON bioreactor model. *J. Process Control* 16, 1003–1012.
- Volcke, E.I.P., Picioreanu, C., De Baets, B., van Loosdrecht, M.C.M., 2012. The granule size distribution in an anammox-based granular sludge reactor affects the conversion-Implications for modeling. *Biotechnol. Bioeng.* 109, 1629–1636.
- Volcke, E.I.P., Picioreanu, C., De Baets, B., Van Loosdrecht, M.C.M., 2010. Effect of granule size on autotrophic nitrogen removal in a granular sludge reactor. *Environ. Technol.* 31, 1271–1280.
- Vuono, D.C., Read, R.W., Hemp, J., Sullivan, B.W., Arnone, J.A., Neveux, I., Blank, R.R., Loney, E., Miceli, D., Winkler, M.K.H., Chakraborty, R., Stahl, D.A., Grzymiski, J.J., 2019. Resource concentration modulates the fate of dissimilated nitrogen in a dual-pathway actinobacterium. *Front. Microbiol.* 10, 3.
- Wan, X., Baeten, J.E., Volcke, E.I.P., 2019. Effect of operating conditions on N₂O emissions from one-stage partial nitrification-anammox reactors. *Biochem. Eng. J.* 143, 24–33.
- Wang, Q., Duan, H., Wei, W., Ni, B.J., Laloo, A., Yuan, Z., 2017. Achieving Stable Mainstream Nitrogen Removal via the Nitrite Pathway by Sludge Treatment Using Free Ammonia. *Environ. Sci. Technol.* 51, 9800–9807.
- Wett, B., 2006. Solved upscaling problems for implementing deammonification of rejection water, in: *Water Science and Technology*. pp. 121–128.
- Wett, B., Omari, A., Podmirseg, S.M., Han, M., Akintayo, O., Gómez Brandón, M., Murthy, S., Bott, C., Hell, M., Takács, I., Nyhuis, G., O'Shaughnessy, M., 2013. Going for mainstream deammonification from bench to full scale for maximized resource efficiency. *Water Sci. Technol.* 68, 283–289.
- Wett, B., Podmirseg, S.M., Gómez-Brandón, M., Hell, M., Nyhuis, G., Bott, C., Murthy, S., 2015. Expanding DEMON Sidestream Deammonification Technology Towards Mainstream Application. *Water Environ. Res.* 87, 2084–2089.
- Wiesmann, U., 1994. Biological Nitrogen Removal from Wastewater. *Adv. Biochem. Eng. Biotechnol.* 51, 113–154.
- Williamson, K., McCarty, P.L., 1976. Verification studies of the biofilm model for bacterial substrate utilization. *J. Water Pollut. Control Fed.* 48, 281–296.
- Williamson, M., MacArthur, R.H., 1974. Geographical Ecology. Patterns in the Distribution of Species. *J. Anim. Ecol.* 43, 601.
- Winkler, M.K.H., Straka, L., 2019. New directions in biological nitrogen removal and recovery from wastewater. *Curr. Opin. Biotechnol.* 57, 50–55.
- Winkler, M.K.H., Bassin, J.P., Kleerebezem, R., de Bruin, L.M.M., van den Brand, T.P.H., Van Loosdrecht, M.C.M., 2011. Selective sludge removal in a segregated aerobic granular biomass system as a strategy to control PAO-GAO competition at high temperatures. *Water Res.* 45, 3291–3299.
- Winkler, M.K.H., Boets, P., Hahne, B., Goethals, P., Volcke, E.I.P., 2017. Effect of the dilution rate on microbial competition: R-strategist can win over kstrategist at low substrate concentration. *PLoS One* 12, e0172785.
- Winkler, M.K.H., Kleerebezem, R., Van Loosdrecht, M.C.M., 2012. Integration of anammox into the aerobic granular sludge process for main stream wastewater treatment at ambient temperatures. *Water Res.* 46, 136–144.

- Wu, D., Ekama, G.A., Chui, H.K., Wang, B., Cui, Y.X., Hao, T.W., van Loosdrecht, M.C.M., Chen, G.H., 2016. Large-scale demonstration of the sulfate reduction autotrophic denitrification nitrification integrated (SANI ®) process in saline sewage treatment. *Water Res.* 100, 496–507.
- Wu, J., 2017. Comparison of control strategies for single-stage partial nitrification-anammox. *Water Res.* 110, 1–12.
- Agrawal, S., Seuntjens, D., Cocker, P. De, Lackner, S., Vlaeminck, S.E., 2018. Success of mainstream partial nitritation/anammox demands integration of engineering, microbiome and modeling insights. *Curr. Opin. Biotechnol.* 50, 214–221.
- WWAP, 2017. The United Nations World Water Development Report 2017. Wastewater: The Untapped Resource. Paris.
- Xie, G.J., Cai, C., Hu, S., Yuan, Z., 2017. Complete Nitrogen Removal from Synthetic Anaerobic Sludge Digestion Liquor through Integrating Anammox and Denitrifying Anaerobic Methane Oxidation in a Membrane Biofilm Reactor. *Environ. Sci. Technol.* 51, 819–827.
- Yoon, S., Cruz-García, C., Sanford, R., Ritalahti, K.M., Löffler, F.E., 2015a. Denitrification versus respiratory ammonification: Environmental controls of two competing dissimilatory $\text{NO}_3^-/\text{NO}_2^-$ reduction pathways in *Shewanella loihica* strain PV-4. *ISME J.* 9, 1093–1104.
- Yoon, S., Sanford, R.A., Löffler, F.E., 2015b. Nitrite control over dissimilatory nitrate/nitrite reduction pathways in *Shewanella loihica* strain PV-4. *Appl. Environ. Microbiol.* 81, 3510–3517.
- Zhang, M., Wang, S., Ji, B., Liu, Y., 2019. Towards mainstream deammonification of municipal wastewater: Partial nitrification-anammox versus partial denitrification-anammox. *Sci. Total Environ.* 692, 393–401.
- Zhang, Y., Ma, H., Niu, Q., Chen, R., Hojo, T., Li, Y.Y., 2016. Effects of soluble microbial products (SMP) on the performance of an anammox attached film expanded bed (AAFEB) reactor: Synergistic interaction and toxic shock. *Bioresour. Technol.* 222, 261–269.
- Zumft, W.G., 1997. Cell biology and molecular basis of denitrification. *Microbiol. Mol. Biol. Rev.* 61, 533–616.

Curriculum Vitae

Mingsheng JIA

Nationality Chinese
E-mail Jiasheng360@Gmail.com
Address Coupure Rechts 662, 9000 Gent, Belgium

Education

2014 –2019 **Ph.D. in Applied Biological Science: Environmental Technology**
Ghent University, Belgium
Topic: Nitrogen conversions in wastewater: from microbial interaction to process evaluation
Promotors: Prof. dr. Eveline Volcke (Ghent University, Belgium)
 Prof. dr. Mari Winkler (University of Washington, USA)

2011 –2014 **Master in Environmental Engineering**
University of Chinese Academy of Sciences, China
Institute of Urban Environment, Chinese Academy of Sciences (CAS), China
Thesis: Temporal and spatial variability of greenhouse gases emission from landfills and leachate treatment
Promotor: Prof. dr. Shaohua CHEN, Institute of Urban Environment, CAS

2007 –2011 **Bachelor in Environmental Engineering**
Beijing University of Civil Engineering and Architecture, China

Work/Research experience

07/2012 – **Internship**
09/2012 Chinese Association of Environmental Protection Industry, China
Advisor: Mr. Lixue MA, Director of the Environmental Certification Center

02/2011 – **Thesis student**
06/2011 Research Center for Eco-Environmental Sciences, CAS, China
Thesis: Evaluation of reclaimed water treatment technologies by genotoxicity
Advisor: Prof. Yu ZHANG, Research Center for Eco-Environmental Sciences, CAS

Additional training

- **Doctoral Training Programme**, Ghent University, Belgium
- **Advance Course on Environmental Biotechnology**, Delft University of Technology, the Netherlands (9-19 June 2015)
- **qPCR-course**, Biogazelle, Ghent University, Belgium (2015)
- **Industrial water production and treatment**, Ghent University, Belgium (9 sessions, 2017)

Supervision of master thesis students

- 2016-2017. Harisankar Venugopal, International Master of Science in Environmental Technology and Engineering, Thesis title: 'Anammox-based treatment of municipal wastewater – a simulation study'.
- 2015-2016. Daan Vandeplassche, Master of Science in Bioscience Engineering: Environmental Technology, Thesis title: 'Modelling of high-rate activated sludge systems for sustainable municipal wastewater treatment'.

Journal papers

- **Jia, M.**, Solon, K., Vandeplassche, D., Venugopal, H. and Volcke, E.I.P. (2019) Model-based evaluation of an integrated high-rate activated sludge and mainstream anammox system. *Chemical Engineering Journal*, in press, <https://doi.org/10.1016/j.cej.2019.122878>
 - Solon, K., **Jia, M.** and Volcke, E.I.P. (2019). Process schemes for future energy-positive water resource recovery facilities. *Water Science and Technology*, 79(9), 1808-1820.
 - **Jia, M.**, Castro-Barros, C.M., Winkler, M.K.H. and Volcke, E.I.P. (2018) Effect of organic matter on the performance and N₂O emission of a granular sludge anammox reactor. *Environmental Science: Water Research & Technology* 4, 1035–1046. (*In Best Papers 2018 – Environmental Science: Water Research & Technology*)
 - Castro-Barros, C.M., **Jia, M.**, van Loosdrecht, M.C.M., Volcke, E.I.P. and Winkler, M.K.H. (2017) Evaluating the potential for dissimilatory nitrate reduction by anammox bacteria for municipal wastewater treatment. *Bioresource Technology* 233: 363-372
 - Wang, X., **Jia, M.**, Zhang, H., Pan, S., Kao, C.M. and Chen, S. (2017) Quantifying N₂O emissions and production pathways from fresh waste during the initial stage of disposal to a landfill. *Waste Management* 63, 3-10.
 - Wang, X., **Jia, M.**, Zhang, C., Chen, S. and Cai, Z. (2017) Leachate treatment in landfills is a significant N₂O source. *Science of The Total Environment* 596–597: 18-25.
 - Wang, X., **Jia, M.**, Lin, X., Xu, Y., Ye, X., Kao, C.M. and Chen, S. (2017) A comparison of CH₄, N₂O and CO₂ emissions from three different cover types in a municipal solid waste landfill. *J Air Waste Manag Assoc* 67(4): 507-515.
 - **Jia, M.**, Wang, X., Chen, S., Lin, X. and Xu, Y. (2015) Greenhouse gas emissions from an open dump of municipal solid waste. *Environmental Science & Technology* 38(3), 136-141 (in Chinese).
 - Wang, X., **Jia, M.**, Chen, X., Xu, Y., Lin, X., Kao, C.M. and Chen, S. (2014) Greenhouse gas emissions from landfill leachate treatment plants: a comparison of young and aged landfill. *Waste Management* 34(7): 1156-1164.
 - **Jia, M.**, Wang, X. and Chen, S. (2014) Nitrous oxide emissions from municipal solid waste landfills and its measuring methodology: A review. *Chinese Journal of Applied Ecology* 25(6), 1815-1824.
- In preparation:**
- **Jia, M.**, Winkler, M.K.H. and Volcke, E.I.P. Elucidating the competition between heterotrophic denitrification and DNRA using the resource-ratio theory. (doi: <https://doi.org/10.1101/852327>)

Conference contributions (* presenting author)

- Solon, K.*, **Jia, M.** and Volcke, E.I.P. (2019) Evaluation criteria for water resource recovery facilities. 10th IWA Symposium on Modelling and Integrated Assessment (Watermatex 2019), 1-4 September 2019, Copenhagen, Denmark. **Oral presentation**
- Solon, K.*, **Jia, M.** and Volcke, E.I.P. (2019) Effects of carbon redirection on anaerobic digester performance of water resource recovery facilities. 16th World Congress on Anaerobic Digestion, 23-27 June 2019, Delft, the Netherlands. **Oral presentation**
- **Jia, M.***, Castro-Barros, C.M., Winkler, M.K.H. and Volcke, E.I.P. (2018) Effect of organic matter on the performance and N₂O emission of a granular sludge anammox reactor. IWA World Water Congress & Exhibition 2018, 16-21 September 2018, Tokyo, Japan. **Oral presentation**
- Solon, K., **Jia, M.*** and Volcke, E.I.P. (2018) Process schemes for future energy-positive water resource recovery facilities. IWA World Water Congress & Exhibition 2018, 16-21 September 2018, Tokyo, Japan. **Poster presentation**
- **Jia, M.***, Castro-Barros, C.M., Winkler, M.K.H. and Volcke, E.I.P. (2018) Effect of organic matter on the performance and N₂O emission of a granular sludge anammox reactor. IWA Biofilm: Granular Sludge Conference 2018, 18-21 March 2018, Delft, the Netherlands. **Oral presentation**
- Solon, K.*, **Jia, M.** and Volcke, E.I.P. (2018) Process schemes for future energy-positive water resource recovery facilities. Water Resource Recovery Modelling Seminar (WRRmod 2018), 10-14 March 2018, Québec, Canada. **Poster presentation**
- Castro-Barros, C.M., **Jia, M.***, van Loosdrecht, M.C.M., Volcke, E.I.P. and Winkler, M.K.H. (2016) Evaluating the potential for nitrate reduction through DNRA by anammox bacteria for municipal wastewater treatment. 21st European Nitrogen Cycle Meeting (ENC21), 05-07 September 2016, Norwich, UK. **Oral presentation**

Peer review

Water Research, Waste Management, Process Biochemistry, Process Safety and Environmental Protection, Journal of Air Waste Management Association, IWA World Water Congress and Exhibition 2016 & 2018

Selected awards and honours

2019	Best Papers 2018 – Environmental Science: Water Research & Technology
2017	Certificate of Outstanding Contribution in Reviewing, Water Research
2016	Merit-based Special Research Fund (BOF), Ghent University, Belgium
2012	Outstanding Students, University of Chinese Academy of Sciences
2011	Outstanding Graduates of Beijing, Beijing Municipal Education Commission
2011	Excellent Thesis, Beijing University of Civil Engineering and Architecture
2010	National Scholarship, Ministry of Education of The People's Republic of China

Acknowledgement

*Two roads diverged in a wood, and I
I took the one less traveled by,
And that has made all the difference.*

-Robert Frost, The Road Not Taken

At this moment, I cannot help thinking about the moment when I was writing the acknowledgement for my master thesis in China. The sun was rising and bringing a new day. It felt like a perfect moment to end a journey and start a new one. Back then, I was not sure yet if I was coming to Belgium for my PhD study, my 'Journey to the West'. It has been a long journey, with all kinds of experiences. Now, I would really like to express my gratitude to those who have been with me and who have contributed to the thesis along the journey.

I had the privilege of having two excellent promotors. Eveline, you have brought me into the world of modelling. I have learned a lot during these years with you, from your amazing ability to put things into perspective to your dedication to the details and more. I am very thankful for the freedom, trust, and guidance you gave that allowed me to apply a wide range of approaches to address the research topic at different levels. I am especially grateful for your consideration and encouragement regarding personal matters. Mari, I think my first ever Skype interview was with you before I came to Ghent. I have been amazed by how you work. You are so efficient, and it seems you always have ideas to make things work. I have deeply enjoyed the scientific discussions with you. I feel so sad that you left the group and went to the US just a few months after my arrival. I will always be grateful for the talks beyond research and the 'crazy' everyday Skype meeting across the ocean when I needed your help the most.

During my PhD, I was lucky to have a few occasions to have small talks with Prof. Mark van Loosdrecht. You are such an inspiring researcher, and I am very grateful for your encouragement and feedback, especially when we were walking in the natural park in Gent. I told you that I was thinking of writing a popular science book about the history of nitrogen removal in the future. I hope I will make it, and I will definitely need to interview you for this.

I am very thankful to the jury members, Prof. Nico Boon, Prof. Dana Ofiteru, Prof. Diederik Rousseau, Prof. Mathieu Sperandio, Dr. Michele Laurenzi and Dr. Jose Maria Carvajal Arroyo, for your comments and efforts to improve the quality of this work.

Acknowledgement

Special thanks go to the friends and colleagues from our BioCo group. Luis, it is hard to find a better colleague than you. Quan, Luis and I have talked many times about how cool what you are working on, and you nailed it. You are always willing to share, and I am not just talking about the food in the office. Kim, I was lucky to have you in the group at the last stage of my PhD. It has been a great pleasure to work with you and to share with you and Quan a lot of talks in the small office. Janis, maybe you are just too young, so I often forget that you joined the group just one year after me. There are many things I really appreciate and would like to learn from you. Xinyu, you are the only colleague from our motherland, and I have witnessed how you move forward and dare to try things out. Annelies, you are such a kind and humble person, and I am sure you will find your way. Stijn, I think you enjoy physical activities more than any of us in this group, and you are a walking Wikipedia and always willing to help in the office or in the lab. It is also nice to talk about politics with you. Farhang, you are relatively new to the group, but we have talked a lot, and I thoroughly enjoyed them. Thiago, you are the only one ever who called me 'Ming', and it was a pity that I had never played football with you to see the so-called 'Brazilian excellence'. Laurence, it is amazing to see how you have brought new elements to our group in such a short time, and I look forward to seeing what you will achieve with four years ahead. I would like to extend my thanks to those who have left the group. Celia, you were my only lab mate here. I still remember that it was only until a few months after my arrival that you told me how you had thought I wanted to kill your precious anammox bacteria because of my confused 'yes or no' answers to your questions. Because of you and Luis, I think I get a wrong impression that all Spanish speaking people are interesting and have a great sense of humor. Caroline, Thomas, Kris, Salatu and Matthijs, I would like to thank you all for your help, especially at the beginning of my PhD, and for the nice moments and talks. Caroline, you have given the highest appreciation to the Cola Chicken Lingshan made. I would also like to thank Chris, Paula Lucie, Luis (Lopez), it is a great pleasure to know you and have small talks with you during your stay here. I am also grateful for having had the opportunity to tutor great master students. Daan and Hari, thank you for transmitting me your enthusiasm and motivation.

I am not going to forget my colleagues from TCCB, the former Department of Biosystems Engineering and other groups: Xiaogang, Zuoyi, Junfeng, Mehmet, Stef, Adriana, Przemyslaw, Qi, Nannan, Dilani, Lizet, Gerlinde, Marlies, Jonas, Jop, Güray,

Acknowledgement

Diego, Ligia, Robert, Neil, Jan and Frederik. Special thanks go to Dieter, Lut, Eddy, and John for all your help in the lab and in the office.

I have to mention the friends with whom I have had so much fun playing badminton. Lei Wang, Xin Tong, Zongchen Lin, Tian Tian, Way Cern Khor, Yayun Chen, Junwen Zhai, Zhoujian Diao, Weidong Li, Tingting Cui, Yang Li, Fei Xie, and many others. Together with you, we had played several badminton tournaments around Belgium and won from the fourth to the second prize. Playing badminton every Friday after work was among the happiest memories abroad that I will always cherish.

A dedicated thanks to my other friends in Ghent, Dongdong Zhang, Lin Ouyang, Jiawei Hu, Shiyu Ma, Chen Yang, Yunhan Zhang, Lei Guo, Yu Xue, Xu Zhang, Xiaojie Liu, and Huanyu Zhao. We have had so many wonderful experiences together, those trips, dinners, drinks, games, music (of which I know nothing), and most importantly those talks. You have deeply enriched my life here. Many thanks to Cuijie Feng and Peng Wei. It is amazing to see how our pathways have crossed in Xiamen, Netherlands and Italy. Who knows where is the next? I also want to thank Gang Liu for hosting me when I was in TU Delft. During these years, I have missed so many things that happened to my old friends in China. But we will be there for each other as it has been.

I know we do not say this that much in our culture, but I want to take this chance to say I love you to all my families. I have been far away from home ever since my bachelor studies. I moved to Beijing (650 km), Xiamen (1500 km) and Ghent (Google map could not calculate the distance). Words cannot convey my gratitude to your unconditional and endless support, especially to my grandmothers and my parents. My parents-in-law deserve the greatest appreciation. To me, they are the best in-laws one may get. I would also like to express my thanks to Lingshan's uncle and his family for always being there during the difficult times. Finally, to my wife, Lingshan Ma. We came as boyfriend and girlfriend, and now we have been married for more than one year. You have made my life much more colorful and easier. We have been through the most difficult times together, and I know we will stay and face everything together. Come what may.

Mingsheng
29 November 2019
Coupure Rechts 662, Gent